PHOTOCHEMICALLY INDUCED REACTIONS BETWEEN OZONE AND HALOGENATED SPECIES: A MATRIX ISOLATION STUDY

by

Loraine Johanna Foley

A thesis submitted in partial fulfillment of the requirements for the degree of Doctor of Philosophy

Christopher Ingold Laboratories
University College London
University of London

December 2000

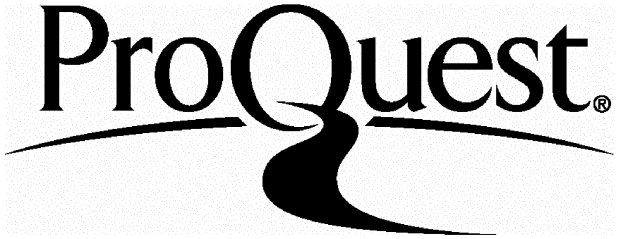

ABSTRACT

The main objective of this research was to study the photochemically induced reactions of ozone with some halogenated species in low temperature matrices, using Fourier-transform infrared spectroscopy, to observe and characterise novel intermediates and to determine pathways for such reactions. Ozone plays a significant role in the chemistry of both the stratosphere and troposphere and thus information concerning the photochemistry of halogenated species in the presence of ozone is of considerable atmospheric importance and is therefore relevant to gas phase atmospheric research.

The FT-IR matrix isolation technique is well suited to providing background information on gas phase atmospheric reactions since most atmospheric species exhibit infrared spectra, and the ability to isolate low concentrations of reactive chemical species in the matrix mimics the conditions of dilution in the atmosphere. Thus the results obtained from matrix isolation experiments can complement those obtained from gas phase studies. Since matrix-isolated species are held at very low temperatures, any thermal reactivity is quenched and reactions have to be initiated either photochemically or thermally. In these experiments the matrices are photolysed in order to initiate a reaction by using a range of wavelengths in the visible and UV regions. Any reactive or unstable species produced by irradiation at a particular wavelength are stabilised indefinitely for spectroscopic analysis, thus allowing the photochemical pathway to be revealed. In the matrix the species are held in close proximity to one another allowing secondary reactions to occur that would not have occurred in the gas phase; this has enabled a range of nearest-neighbour complexes to be generated *in situ* and detected in this study.

Of the halogenated species studied, the halogen cyanides, ICN and BrCN, were separately co-deposited with ozone and the photo-induced reactions are reported. Ozone is shown to form a complex with ICN but not with BrCN and so the photochemistry of ozone is altered in the O_3/ICN reaction, allowing the formation of several new species to be observed. Harsh UV irradiation is required to initiate a reaction in the O_3/BrCN matrix, as well as in the reactions between ozone and the

trihalomethanes ($CHBr_2Cl$ and $CHBrCl_2$) where several novel carbonyl···Lewis acid and carbon monoxide···Lewis acid complexes were detected. The co-deposition of ozone with each of the halogenated ethenes, BrCH=CHBr and ClCH=CHCl, led to the formation of a charge transfer complex which dissociates to form several new species including carbonyl and carbon monoxide species. Finally, the photo-induced reaction of ozone with some diiodo-species highlights the different photochemical behaviour of a molecule containing two iodine atoms as distinct from one in the presence of ozone.

In each case the photoproducts were identified by FT-IR spectroscopy and photochemical pathways proposed. In some instances nitrogen dioxide and solid oxygen matrices were used to provide alternative sources of O atoms for reaction.

ACKNOWLEDGEMENTS

There are many people who I would like to thank for contributing in one way or another towards the completion of this thesis. First I must thank Professor Robin Clark who over these last years has given me a considerable amount of support, encouragement, and knowledgeable advice, but most of all, his time. I also thank Dr Stephen Price for arranging the valuable and informative group meetings in the early stages and who was always there to give good advice when things were not going to plan.

Thanks go to Dr Ian Bell, who at the beginning gave me guidance, and later on, to Dr Steven Firth for listening and for always knowing the answers to my questions. I am also grateful to Dr Steven Firth for his constant help, while I was overseas, in the final production of this thesis. A special thanks goes to Jon Dann for teaching me the matrix isolation technique and who's own research gave inspiration towards some of the work in this thesis. Any mention of thanks with regard to Lab 132 would not be complete without thanking the rest of the Clark research group (Katherine, Amanda, Lucia, Joe, Marcia, and Paulina) for maintaining an interesting and fun environment to work in.

I must also take this opportunity in thanking Dr Andrea Sella for his help with the preparation of some of the samples used in these experiments and also for his advice concerning seminar presentations. An appreciative thanks goes to Dr Sean McGrady due to a problem concerning the cryogenic apparatus being resolved after a chance meeting. Regarding the maintenance of the equipment used in this thesis, I must convey my deepest appreciation to the members of the workshop, especially to John Hill, Dave Knapp, and Dick Waymark, without whom, there would have been no research and thus no thesis; I am truly indebted to each of them.

Last, but especially not least, so many 'thank yous' have to go to my family and friends. In particular, to my Mum and Dad for having always believed in me and giving me so much support, without them the past years would have been a lot harder and I truly thank them for everything. I thank the rest of my family, especially my nieces and nephews, for keeping things real and also all my friends for just being there and sharing the fun times with me. Finally an enormous amount of respect and affection goes to Marvin who is such a positive influence in all areas of my life, who understands and believes in me and who is such an abundant source of spiritual strength, but most of all, who makes me laugh, - thanks!

TABLE OF CONTENTS

LIST OF FIGURES

LIST OF TABLES

LIST OF SCHEMES

LIST OF ABBREVIATIONS

ν_a	antisymmetric stretching mode
δ	bending vibrational mode
γ	deformation
ρ	rocking mode
ν	stretching vibrational mode
τ	twisting mode
ω	wagging mode
λ	wavelength
ν_s	symmetric stretching mode
br	broad
ca.	circa
cf.	compare
cm^{-1}	wavenumber
FT	Fourier-transform
h	hour
i-p	in-plane
IR	infrared
K	Kelvin
m	medium
min	minutes
nm	nanometre
o-o-p	out-of-plane
s	strong
sh	shoulder
UV	ultraviolet
v	very
vis	visible
viz.	'in other words'
w	weak

Part of the work described in this thesis has been published:

A Matrix Isolation Study of the Photochemically Induced Reactions of Ozone with Iodine Cyanide and Bromine Cyanide; Clark, R. J. H.; Foley, L. J.; Price, S. D., *J. Phys. Chem. A* **2000**, *104*, 10675–10682.

Matrix Isolation Study of the Photochemically Induced Reaction of Ozone with Dibromochloromethane and Bromodichloromethane in Solid Argon at 14 K; Clark, R. J. H.; Dann, J. R.; Foley, L. J., *J. Chem. Soc. Dalton Trans.* **1999**, 73–78.

Chapter 1

Introduction

1.1 MATRIX ISOLATION

The examination of highly reactive molecules and intermediates can be achieved by using the matrix isolation technique. The species to be observed are trapped as isolated entities and their lifetimes are increased considerably enabling them to be studied at leisure using conventional spectroscopic methods (Fig. 1.1.1). The first matrix study was carried out by Lewis and Lipkin[1] in 1942 who studied the phosphorescence of aromatic molecules isolated in a rigid glassy medium at low temperatures. It was not until the 1950s that Norman and Porter[2] and also Pimentel *et al.*,[3,4] simultaneously developed argon and nitrogen matrix supports for the isolation of molecules and the photoproduction of free radicals. The early developments of the technique were largely pioneered by Pimentel and his associates such that they obtained the first infrared spectra of positively identified transient molecules, HNO[5] and HCO.[6] The subsequent development of new apparatus, particularly the development of closed-cycle cryogenic coolers,[7] enabled studies to be carried out reliably and systematically by many laboratories.

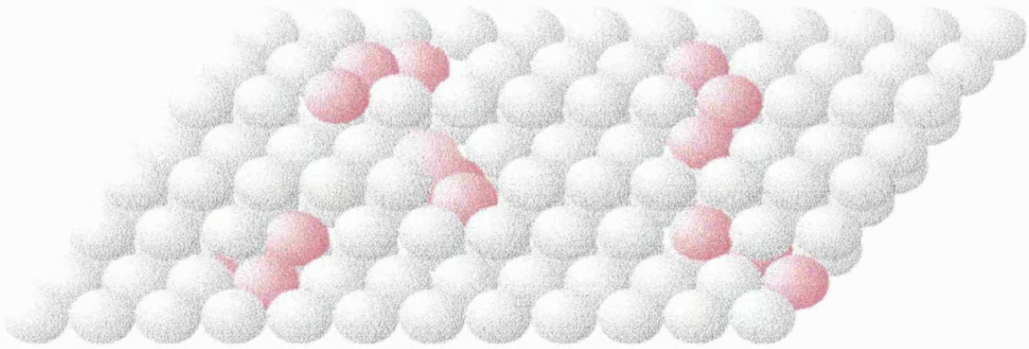

Figure 1.1.1. *A theoretical view of isolated molecules (red) embedded in a noble gas matrix (grey).*

Since the early studies of unstable intermediates and radicals, matrix isolation techniques have grown to be important and have been applied to a wide range of investigations including the spectroscopy of molecular ions, molecular complexes, vapourising molecules and metal clusters, the photochemistry of inorganic and

organometallic species, and also the spectroscopy of stable molecules. Matrix isolation has been combined with most types of spectroscopic method such as IR, ESR, UV-vis, Raman, and Mössbauer, although infrared spectral studies have been the most widely used. In this thesis, the matrix isolation technique is applied to the investigation of reactions occurring between atoms and stable molecules. Many workers have studied these types of reaction using various diatomic and triatomic species to generate the atoms (N, S, F, Cl, Br, and O etc.).[8] In some cases the atoms can diffuse through the matrix lattice gaps to encounter a reaction partner, whereas in other cases the reactions have to be photochemically induced to proceed. The results from these and many other matrix experiments have been well documented in a number of texts[7,9–12] and papers.[13–26]

1.2 AIMS OF RESEARCH

The idea behind this work was to study the photochemically induced reactions between ozone and various halogenated species in matrices, primarily to observe and characterise novel intermediates and to determine pathways for such reactions. In the last decade or so, ozone has been extensively studied because of its significant role in atmospheric processes. Therefore the reactions of ozone in the matrix, particularly with halogen containing species, may be relevant to processes occurring in the gas phase. Although reactions occurring in the solid matrix may not be the same as in the gas phase, the influence of concentration, diffusion of some species, cage recombination or rearrangement, photodegradation, internal structure, and the photochemical pathways displayed in matrices may be considered for gas phase modelling. In atmospheric models including physical, chemical, and transport processes, missing data could potentially be extrapolated from matrix laboratory experiments. Therefore many matrix isolation studies to date have been applied to atmospheric chemistry.[27–40]

Many matrix isolation studies have shown that ozone can interact and form weak complexes with small molecules, (CH_3I,[41] HF,[42] PH_3,[43] CF_3I,[44] ICl,[45] and C_2H_5I[46]) and then undergo interesting photochemically induced reactions. Weak ozone complexes have the potential to alter atmospheric reaction rates and/or

pathways whilst themselves being interesting subjects for experimental studies. It is the iodine-containing compounds that are of particular interest in this study as previous matrix studies have shown that ozone forms a complex with Z–I species upon deposition, but not with bromine- or chlorine-containing compounds. The experiments studied in this thesis have been chosen in order to establish which species form complexes with ozone and which do not, as well as to extend the number of known reactions of halogenated species with ozone in matrices.

1.2.1 CHOICE OF PRECURSORS

A brief discussion of each of the halogenated precursors studied in this thesis is given below. In all cases the photochemically induced reaction between the precursor and ozone in solid argon is probed and in some instances the reaction between the precursor and nitrogen dioxide is also reported to complement the ozone study. In some experiments the precursor is deposited in a solid oxygen matrix in order to provide upon photolysis an alternative source of oxygen atoms which can go on to react with the precursor.

Iodine Cyanide and Bromine Cyanide. The halogen cyanides are an interesting group of small molecules and may be considered analogous to diatomic interhalogen compounds due to the pseudo-halide character of the cyanide moiety, -CN. Ozone, iodine cyanide, and bromine cyanide together contain the atmospherically important elements C, N, O, Br, and I, and thus any photochemical reactions that occur between them may yield information relevant to the mechanisms of ozone depletion from the atmosphere and to interstellar chemistry. The O_3/ICN system was also chosen as an extension to the previously studied matrix reactions of ozone with other iodine-containing species to see whether an $O_3\cdots$ICN complex would form, and subsequently iodoso-, iodyl-, and hypoiodo-photoproducts.[41,44–46] However with ICN, it was not only the iodine atom that could interact with ozone, but also the nitrogen atom, which made this precursor all the more interesting to study in the presence of ozone. Bromine cyanide was chosen to react with ozone mainly to complement the iodine cyanide study so that the reactivities, photoproducts and reaction pathways could be compared, and also in an attempt to detect Br–O_x bonds.

Both ICN and BrCN were separately deposited with nitrogen dioxide, another atmospherically important species, to see whether the photochemically induced reactions behaved similarly to those with ozone.

Dibromochloromethane and Bromodichloromethane. The photochemically induced reactions of ozone with various mono- and di-bromo/chloromethanes in matrices have been studied[47,48] and a range of carbonyl···Lewis acid and carbon monoxide···Lewis acid complexes were detected. From the previous studies it is clear that bromine- and chlorine-containing alkanes do not form a complex with ozone upon deposition, unlike the iodine-containing alkanes, and require intense UV irradiation for many hours to initiate a reaction. The similar reactions of ozone with these tri-halomethanes ($CHBr_2Cl$ and $CHBrCl_2$) were chosen in order to extend the previous research by detecting differently arranged carbonyl···Lewis acid and carbon monoxide···Lewis acid complexes. Comparisons can then be made between the spectra of complexes having identical carbonyls but different Lewis acids and *vice versa*, and between the spectral shifts of the carbon monoxide complexes having different Lewis acid partners.

1,2-Dibromoethene and 1,2-Dichloroethene. The reaction of alkenes with ozone has considerable practical importance in organic chemistry and in photochemical smog problems and is also the main source of organic acids and hydroperoxides in the atmosphere. Due to the serious concern that some commonly used halocarbons affect the ozone concentration in the stratosphere, it is appropriate therefore to study the oxidation of the haloethenes (another class of halocarbon). Hence, BrCH=CHBr and ClCH=CHCl were chosen to react individually with ozone in solid argon in order to gain information about the photoproducts that form. Although it had been observed previously that bromine- and chlorine-containing alkanes did not form a complex with ozone,[47,48] the bromine- and chlorine-containing ethenes could possibly form a complex with ozone via the double bond of the molecule. Analogous π-type complexes with ozone have indeed been observed for other alkenes in matrices,[49] although the presence of halogen substituents in these precursors could affect whether or not an ozone···precursor complex could be formed; if so, which would be investigated.

Diiodomethane and 1,2-Diiodoethane. As mentioned before, the reactions between ozone and monoiodo-species are extensive but there is limited information available on the reaction between ozone and diiodo-species. Preliminary photolytic studies showed that diiodomethane behaved very differently towards ozone in matrices than did iodomethane, hence the motivation behind this particular study. It was also interesting to investigate the reaction between ozone and 1,2-diiodoethane, the purpose being whether the reaction would proceed in a similar manner to that between ozone and diiodomethane or between ozone and iodoethane.[46] Research into the photochemistry of iodine-containing systems was motivated by the fact that Solomon *et al.*[50] revealed that iodine chemistry could make a significant contribution to stratospheric ozone depletion. Research relating to ozone depletion has centred on chlorine and bromine chemistry although iodine, being the halogen of low electronegativity, forms very weak covalent bonds with carbon, hydrogen, nitrogen and, oxygen and in its various compound forms, is easily photodissociated in the near UV and visible regions. Iodine and its oxides were also shown to play an important role in the tropospheric photochemistry.[51]

1.3. THESIS OUTLINE

This thesis is divided into eight chapters, the first two providing the reader with an overview of this matrix study, the matrix isolation technique used, and a description of the equipment and experimental techniques involved (chapters 1 and 2). The final chapter gives a summary of the results obtained throughout the thesis, makes some general comments, and provides suggestions for further work to complement the research described (chapter 8). The remaining chapters 3–7 are mentioned in more detail below and each is self-contained in that all discussions, comparisons, conclusions, and references relevant to that study are given in the respective chapter.

Chapter 3. This chapter reports the photochemically induced reactions between iodine cyanide and ozone and iodine cyanide and nitrogen dioxide. The deposition of iodine cyanide in a solid oxygen matrix and the subsequent photolysis experiments are also reported. In each case the intermediates and/or photoproducts

produced are deduced from the recorded spectra and a mechanism for these reactions is proposed.

Chapter 4. This chapter describes the photochemically induced reactions of bromine cyanide with either ozone or nitrogen dioxide and compares the analogous reactions of iodine cyanide. A mechanism is proposed based on the species observed.

Chapter 5. This chapter extends the previous research completed on mono- and di-substituted bromo- and chloro-methanes by describing the photochemically induced reaction of ozone with two tri-substituted bromo- and chloro-methanes ($CHBr_2Cl$ and $CHBrCl_2$). The reaction of these species with ozone can also be compared to the behaviour of those discussed in chapters 3 and 4, *i.e.* the comparison of iodine- and non iodine-containing compounds with regard to the formation of complexes with ozone. A number of novel carbonyl and carbon monoxide···Lewis acid complexes are detected and the reaction pathways are shown to be time-dependent rather than wavelength-dependent.

Chapter 6. This chapter concentrates on the photochemistry of ozone with another class of halogenated species, the halogenated alkenes. The photochemically induced reactions of ozone with 1,2-dibromoethene and 1,2-dichloroethene are investigated. This chapter continues the line outlined in chapter 5 by examining other classes of bromine- and chlorine-containing compounds, the key difference being the ethene double bond. Thus whether an ozone···precursor complex is formed via the double bond on the haloethene is determined. Similar reactions with nitrogen dioxide instead of ozone are also reported.

Chapter 7. This chapter reports the effect of species containing two iodine atoms on their photochemically induced reactions with ozone, compared to that of species containing one iodine atom. The species under investigation are diiodomethane and 1,2-diiodoethane. Results obtained from these reactions can also be compared to those from dihalomethane/ozone and trihalomethane/ozone reactions studied elsewhere[47,48] and in this thesis (chapter 5), respectively.

1.4 REFERENCES

1. Lewis, G. N.; Lipkin, D., *J. Am. Chem. Soc.* **1942**, *64*, 2801–2808.
2. Norman, I.; Porter, G., *Nature*, **1954**, *174*, 508–509.
3. Whittle, E.; Dows, D. A.; Pimentel, G. C., *J. Chem. Phys.* **1954**, *22*, 1943–1948.
4. Becker, E D.; Pimentel, G. C., *J. Chem. Phys.* **1956**, *25*, 224–228.
5. Brown, H. C.; Pimentel, G. C., *J. Chem. Phys.* **1958**, *29*, 883–887.
6. Pimentel, G. C.; Ewing, G. E.; Thompson, W. E., *J. Chem. Phys.* **1960**, *32*, 927–930.
7. Andrews, L.; Moskovits, M., *Chemistry and Physics of Matrix-Isolated Species*; North Holland: Amsterdam; 1989.
8. Okabe, H., *Photochemistry of Small Molecules*; Wiley: NY; 1976.
9. Hallam, H. E., *Vibrational Spectroscopy of Trapped Species*; Wiley: NY; 1973.
10. Burnett, J. K.; Poliakoff, M.; Turner, J. J.; Dubost, H., *Advances in Infrared and Raman Spectroscopy*, Vol. 2; Eds: Clark, R. J. H.; Hester, R. E.; Heyden: London; 1976.
11. Downs, A. J.; Hawkins, M., *Advances in Infrared and Raman Spectroscopy*, Vol. 10; Eds: Clark, R. J. H.; Hester, R. E.; Heyden: London; 1983.
12. Almond, M. J.; Downs, A. J., *Advances in Infrared and Raman Spectroscopy*, Vol. 17; Eds: Clark, R. J. H.; Hester, R. E.; Wiley: Chichester; 1989.
13. Hawkins, M.; Almond, M. J.; Downs, A. J., *J. Phys. Chem.* **1985**, *89*, 3326–3334.
14. Zhang, L. N.; Dong, J.; Zhou, M. F., *J. Phys. Chem. A* **2000**, *104*, 8882–8886.
15. Greene, T. M.; Andrews, L.; Downs, A. J., *J. Am. Chem. Soc.* **1995**, *117*, 8180–8187.
16. Suzer, S.; Andrews, L., *Chem. Phys. Lett.* **1988**, *150*, 13–17.
17. Baskir, E. G.; Nefedov, O. M., *Russ. Chem. Bull.* **1996**, *45*, 99–106.

18. Maier, G.; Reisenauer, H. P.; Hu, J.; Schaad, L. J.; Andes Hess, B., *J. Am. Chem. Soc.* **1990**, *112*, 5117–5122.
19. Kornath, A.; Koper, I., *J. Raman Spect.* **1997**, *28*, 829–831.
20. Chertihin, G.; Andrews, L.; Rosi, M.; Bauschlicher, C., *J. Phys. Chem. A* **1997**, *101*, 9085–9091.
21. Thompson, W. E.; Jacox, M. E., *J. Chem. Phys.* **1999**, *111*, 4487–4496.
22. Bondybey, V. E.; English, J. H., *J. Phys. Chem. US* **1983**, *87*, 4647–4650.
23. McKinley, A. J.; Karakyriakos, E.; Knight, L. B.; Babb, R.; Williams, A., *J. Phys. Chem. A* **2000**, *104*, 3528–3536.
24. Momose, T.; Miki, M.; Uchida, M.; Shimizu, T.; Yoshizawa, I.; Shida, T., *J. Chem. Phys.* **1995**, *103*, 1400–1405.
25. Maier, J. P., *Mass Spectrom. Rev.* **1992**, *11*, 119–135.
26. Perutz, R. N., *Chem. Rev.* **1985**, *85*, 77–96.
27. Sander, S.; Pernice, H.; Willner, H., *Chem. A Eur. J.* **2000**, *6*, 3645–3653.
28. Givan, A.; Loewenschuss, A.; Nielsen, C. J., *J. Phys. Chem. A* **2000**, *104*, 3441–3445.
29. Dibben, M.; Szczepanski, J.; Wehlburg, C.; Vala, M., *J. Phys. Chem. A* **2000**, *104*, 3584–3592.
30. Hudgins, D. M.; Bauschlicher, C. W.; Allamandola, L. J.; Fetzer, J. C., *J. Phys. Chem. A* **2000**, *104*, 3655–3669.
31. Mihelcic, D.; Heitlinger, M.; Kley, D.; Musgen, P.; Volz-Thomas, A., *Chem. Phys. Lett.* **1999**, *301*, 559–564.
32. Tamburelli, I.; Chiavassa, T.; Borget, F.; Pourcin, J., *J. Phys. Chem. A* **1998**, *102*, 422–425.
33. Furlan, A.; Scheld, H. A.; Huber, J. R., *J. Chem. Phys.* **1997**, *106*, 6538–6547.
34. Bahou, M.; Schriver-Mazzuoli, L.; Schriver, A.; Chaquin, P., *Chem. Phys.* **1997**, *216*, 105–118.
35. Peterson, K. A.; Werner, H. J., *J. Chem. Phys.* **1996**, *105*, 9823–9832.
36. Graham, J. D.; Roberts, J. T.; Brown, L. A.; Vaida, V., *J. Phys. Chem.* **1996**, *100*, 3115–3120.

37. Pettersen, M. V.; Schriver-Mazzuoli, L.; Schriver, A.; Chaquin, P.; Lasson, E., *Chem. Phys.* **1996**, *204*, 115–127.
38. Grutter, M.; Freivogel, P.; Maier, J. P., *J. Phys. Chem. A* **1997**, *101*, 275–277.
39. Jaeger, K.; Weller, R.; Schrems, O., *Ber. Buns. Gesell. Phys. Chem.* **1992**, *96*, 485–488.
40. Müller, H. S. P.; Willner, H., *Inorg. Chem.* **1992**, *31*, 2527–2534.
41. Hawkins, M.; Andrews, L., *Inorg. Chem.* **1985**, *24*, 3285–3290.
42. Andrews, L.; Withnall, R.; Hunt, R., *J. Phys. Chem.* **1988**, *92*, 78–81.
43. Withnall, R.; Hawkins, M.; Andrews, L., *J. Phys. Chem.* **1986**, *90*, 575–579.
44. Andrews, L.; Hawkins, M.; Withnall, R., *Inorg. Chem.* **1985**, *24*, 4234–4239.
45. Hawkins, M.; Andrews, L.; Downs, A. J.; Drury, D., *J. Am. Chem. Soc.* **1984**, *106*, 3076–3082.
46. Clark, R. J. H.; Dann, J. R., *J. Phys. Chem.* **1996**, *100*, 532–538.
47. Lugez, C.; Schriver, A.; Schriver-Mazzuoli, L.; Lasson, E.; Nielsen, C. J., *J. Phys. Chem.* **1993**, *97*, 11617–11624.
48. Clark, R. J. H.; Dann, J. R., *J. Phys. Chem. A* **1997**, *101*, 2074–2082.
49. Singmaster, K. A.; Pimentel, G. C., *J. Phys. Chem.* **1990**, *94*, 5226–5229.
50. Solomon, S.; Garcia, R. R.; Ravishankara, A. R., *J. Geophys. Res.* **1994**, *99*, 20491–20499.
51. Chameides, W. L.; Davis, D. D., *J. Geophys. Res.* **1980**, *85*, 7383–7398.

Chapter 2

Experimental and Theory

2.1 INTRODUCTION

This chapter focuses on the description of the experimental methods employed to complete the research discussed in the later chapters. These range from the choice of matrix material, of spectroscopic technique, of preparation of the precursors, and of the experiments to be performed on the matrix. A description of the experimental apparatus used and, where appropriate, a description of the general theory behind the techniques are given.

2.2 PROPERTIES OF MATRIX MATERIALS

The main aim of the matrix isolation technique is to trap effectively and to isolate chosen precursors in an inert solid or matrix, so as to investigate their properties spectroscopically (Fig. 1.1.1). There are many substances that have the capability to be used as a matrix material, providing an inert, rigid, and spectroscopically transparent environment, but the suitability of the material also depends upon the limitations of the apparatus and the type of experiment envisaged. The main properties that a matrix material must have if it is to provide a successful matrix environment are discussed below.

Inertness. When choosing a matrix material to isolate the species being studied, it is of utmost importance that the matrix material does not react and interfere with the isolated precursors. Of course the presence of any impurities in the matrix material will affect its inertness and therefore it is necessary that the matrix material used be of the highest purity. The noble gases are regarded as inert for all species and in this study in particular, argon was used as the main matrix host. In some experiments oxygen was used as the matrix support so that upon photolysis the O–O bond would break to form O atoms, which could then react with the isolated precursor to form various products. It was hoped that the products formed would differ from those formed in the precursor/ozone/argon matrix experiments.

Rigidity. A matrix material that is rigid prevents the diffusion of species within the matrix; as such it prevents any bimolecular collisions from occurring and

increases the lifetime of any reactive species. The rigidity of a matrix is highly temperature dependent and as a rough guide matrix materials become sufficiently softened to allow diffusion at approximately half the melting point of the material.[1] In solid-state studies, Tammann's rule relates the temperature, T_d, at which diffusion first becomes appreciable, to the melting point, T_m, of salts, oxides, and covalent compounds ($T_d \approx 0.57T_m$, etc.). Therefore in this study, both argon and oxygen must be cooled to below 25 K, at least, to meet the rigidity requirements. Also operation at these very low temperatures prevents reactions with any significant activation energy from occurring. An additional advantage is that the rigid nature of the matrix allows the easy collection of spectra.

Spectroscopy. Many of the spectroscopic techniques available today can be applied to matrix isolation in order to gain a range of information about the matrix-isolated species and the induced chemical processes that occur. The spectroscopic technique used in this study is Fourier-transform infrared spectroscopy which allows the easy collection of spectra. Argon is spectroscopically transparent at the temperatures employed, in the IR vibrational region; the transparency of another noble gas, Xe, varies with temperature such that at 66 K it forms a reasonably transparent matrix whereas at 50 K, a highly scattering film results. The thickness of a matrix limits the degree of transparency such that as the solid layer gets thicker, more light from the IR source is scattered. This reflection loss therefore limits the total thickness of a matrix deposited and hence limits the dilution ratio. A slow rate of deposition may also reduce scattering as a smoother surface is achieved, whereas high rates can cause 'splash patterns' to be frozen in, inciting scattering.

Volatility. The mixing of the matrix material and the precursor in the gas phase at room temperature makes for easy preparation of a matrix because the mixture can be sprayed straight onto the cold window. The chosen matrix material should therefore be sufficiently volatile at room temperature to allow it to be handled in a vacuum line. A balance must be reached because the more volatile the matrix material the lower the temperature required to meet the rigidity requirements (see above). Argon, krypton, and xenon can all be used with a liquid hydrogen cryostat, while neon requires a liquid helium cryostat (4 K).

Thermal Properties. The thermodynamic properties of a matrix material (latent heat of fusion, lattice energy, and thermal conductivity) should be taken into account so as to minimise the heat produced upon matrix formation and to maximise the ability of the matrix to transfer heat. The latent heat of fusion is a measure of the amount of heat to be removed from the matrix area on condensation of the gaseous mixture. The amount of heat dissipated depends also upon the rate of deposition and must not exceed the cooling capacity of the cryostat, otherwise the temperature of the matrix area will rise allowing diffusion to occur. The lattice energy relates to the energy required to form a lattice at 0 K as well as to the energy required to remove a molecule from its position in the lattice, *i.e.* to diffuse in a lattice. A matrix material must have good thermal conductivity because during the deposition of the matrix, the gas phase material is at 295 K and condenses on the surface of a window held at 20 K. Upon condensation, the heat must be removed from the matrix area and, as the matrix grows, this conduction of heat through the layers becomes important (the better the conductivity, the faster the rate of deposition). Local heating occurs if the matrix material has poor thermal conductivity. Again the rates at which the matrices are deposited have a significant effect on the properties of the matrix material.

Crystal Structures. The noble gases are common matrix materials whose atoms are essentially spherical in shape and have a tendency to crystallise in one of the closest-packed structures. These achieve the maximum number of nearest neighbours and therefore the number of intermolecular van der Waals forces. Close-packed lattices can have three possible sites that the guest molecule can occupy: substitutional, in which the guest molecule replaces a host molecule, and two types of interstitial site which occur between the layers of close-packed spheres (either a tetrahedral hole or a octahedral hole). However, all crystals are not perfect and to some extent they deviate from the ideal crystal lattice, giving rise to additional trapping sites in the matrix which are known as dislocation sites. A species trapped in the matrix will therefore experience different degrees of perturbation from the matrix material, depending on which site it is occupying. In some cases matrix-isolated species give multiplet spectral features in the IR spectrum which are not due to rotation or aggregation but can be explained in terms of the multiple trapping sites.

Electrical Properties. The electrical properties of the matrix material (dielectric constant, polarisability, ionisation potentials, and electric multipole, dipole, and quadrupole moments) can have an effect on the recorded spectra and are discussed in further detail elsewhere.[1]

2.3 INFRARED SPECTROSCOPY

In order to characterise matrix-isolated species, common and convenient methods are infrared and UV-vis spectroscopy. Infrared spectroscopy has been used in this study to provide vibrational information about the species in the matrix so as to determine the identity of the species. The infrared spectra of matrix-isolated species usually show bands with very narrow widths at half-maximum and only exhibit bands attributable to vibrations of the ground electronic state of the molecule; any rotational component is removed because of the rigidity and low temperature of the matrix. The spectra usually agree very well with the gas phase spectra; the frequency shifts therefore being typically less than 0.5% for noble gas matrices. The narrow linewidths of the bands enable isotopic splitting to be resolved, including those due to heavy isotopes. The fact that the IR spectra of matrix-isolated species are less complicated than those of other phases eases the identification process. The analysis of matrix-isolated species using infrared and other forms of spectroscopy is covered in several texts.[1–7]

The remaining part of this section provides a basic description of the underlying theory concerning infrared spectroscopy,[8–13] as well as a description and discussion of the Fourier-transform spectrometer used in this study.

2.3.1 MOLECULAR VIBRATIONS

Molecular spectroscopy may be defined as the study of the interaction between incident electromagnetic radiation and the nuclear, molecular, or electronic changes of a molecule. It is only if there is a change in the dipole moment of the molecule that an interaction with the electric or magnetic fields associated with the radiation can occur, thereby giving rise to an observable spectrum. The energies and timescales of

nuclear, molecular, and electronic motions are sufficiently different that they can first be considered separately under the Born-Oppenheimer approximation. The Born-Oppenheimer approximation assumes that the total energy of a molecule's motion is the sum of the energies of the individual motions:

$$E_{total} = E_{elec.} + E_{vib.} + E_{rot.}$$

When the configuration of a molecule changes, in other words, when a molecule vibrates, a change in dipole moment may occur; if so, the molecule interacts with the infrared region of the electromagnetic spectrum, giving rise to an infrared (vibrational) spectrum. Starting with the simplest case of a diatomic molecule, the vibrational motions which give rise to an infrared spectrum are discussed. Note that vibrational spectra will be observable only in heteronuclear diatomics since homonuclear molecules have no dipole moment and therefore do not interact with radiation of IR wavelengths.

Vibrations of Diatomic Molecules

When two atoms combine to form a stable covalent molecule there is a balance of repulsive and attractive electronic forces, *i.e.* there is repulsion between the positively charged nuclei of both atoms and between their negative electron clouds, while there is an attraction between the nucleus of one atom and the electrons of the other, and vice versa. At equilibrium the potential energy of the system is at a minimum and the internuclear distance is referred to as the equilibrium distance ($r_{eq.}$), or bond length. So for a given potential $V(r_{eq.})$ the system is reduced to that of a single particle of mass moving in the same potential:

$$\mu = m_1 m_2/(m_1 + m_2) \quad \text{(reduced mass)}$$

Any attempt to increase or decrease the bond length requires an input of energy; thus the compression and extension of a bond may be compared classically to the behaviour of a linear spring and is assumed to obey Hooke's law:

$$f = -k(r - r_{eq.})$$

where f is the restoring force, k is the force constant, and r is the internuclear distance. The potential energy curve is parabolic with respect to displacement and has the form,

$$V = \tfrac{1}{2}\, k(r - r_{eq.})^2$$

which describes the vibrations of a harmonic oscillator. The frequency, ν_0, at which the system oscillates is found from the equation of motion for the system, in terms of reduced mass, μ,

$$\mu d^2r/dt^2 = -k(r - r_{eq.})$$

to give

$$\nu_0 = \tfrac{1}{2}\, \pi(k/\mu)^{1/2}$$

The vibration of a diatomic molecule can be treated quantum mechanically. Like all other molecular energies, vibrational energies are quantised and the allowed vibrational energies for any particular system may be calculated from the Schrödinger equation. For a vibrating molecule in terms of an harmonic oscillator these become:

$$E_v = (v + \tfrac{1}{2})h\nu_0 \qquad (v = 0, 1, 2, \ldots)$$

where v is the vibrational quantum number. Converting to wavenumber units, cm^{-1}, the equation becomes:

$$E_v = (v + \tfrac{1}{2})hc\bar{\nu}_0 \qquad (v = 0, 1, 2, \ldots)$$

where c is the speed of light. It is important to note that the diatomic molecule can never have zero vibrational energy; the molecule must always vibrate to some extent. Thus:

$$E_0 = \tfrac{1}{2}\, h\nu_0$$

However the harmonic oscillator model is insufficient to describe the vibrations of a diatomic molecule as it has a constant separation of $h\nu_0$ between vibrational levels, allowing transitions between any two neighbouring states to give the same energy change: in a real diatomic molecule, this separation decreases. The Morse function gives a better approximation to the potential energy curve of a real diatomic molecule:

$$V = D_e[1 - \exp\{a(r_{eq.} - r)\}]^2$$

where a is a constant for a particular molecule and D_e is the dissociation energy of the molecule. Solving the Schrödinger equation with this potential function yields a new pattern of the allowed vibrational levels:

$$E_v = (v + \tfrac{1}{2})hc\omega_e - (v + \tfrac{1}{2})^2 hc\omega_e\chi_e + \ldots \qquad (v = 0, 1, 2, \ldots)$$

where ω_e is an oscillation frequency and χ_e is the corresponding anharmonicity constant. For bond stretching vibrations χ_e is always small and positive ($\approx +0.01$) so as v increases, the vibrational levels crowd more closely together. For the harmonic oscillator only $\Delta v = +1$ transitions are allowed, but in the anharmonic case, transitions involving $\Delta v = +1, +2, +3, +4, \ldots$ are allowed. The frequency of $v = 0 \leftrightarrow 1$ is called the fundamental frequency while $v = 0 \leftrightarrow >1$ are called overtones. Transitions occurring from states that are excited, $v = 1 \leftrightarrow >1$, are called hot bands. As a consequence of the Boltzmann distribution, the fundamental transition occurs with most probability. In a matrix environment, probably all the transitions are of the $v = 0 \leftrightarrow 1$ type. A more detailed discussion of classical and quantum methods is discussed elsewhere.[8–13]

Vibrations of Polyatomic Molecules

The positions and motions of a molecule containing N atoms can be described by specifying $3N$ coordinates (the x, y, and z Cartesian coordinates). Thus the total number of coordinates is $3N$ and the molecule is said to have $3N$ degrees of freedom. The coordinates describing the translational movement along the axes and the rotations about the axes can be neglected since they do not affect the vibrations of the

molecule. Therefore a polyatomic molecule is left with $3N - 6$ degrees of freedom since translation and rotation each require three degrees of freedom. The only other motion allowed is internal vibration, thus a non-linear N-atomic molecule can have $3N - 6$ fundamental vibrational frequencies. Linear polyatomic molecules have no rotation about the bond axis; hence only two degrees of freedom are required, leaving $3N - 5$ degrees of vibrational freedom. The fact that linear and non-linear molecules have $N - 1$ bonds means that of the vibrations, $N - 1$ are bond-stretching ones and $2N - 4$ (linear) or $2N - 5$ (non-linear), are bending ones. For a diatomic molecule, $N = 2$, so $3N - 5 = 1$, thus there is only one fundamental vibration, which depends upon the nuclear separation.

Considering the linear triatomic molecule CO_2 as an example, the fundamental vibrations, also referred to as normal vibrations, are shown in Figure 2.3.1. Here $N = 3$ and so four normal vibrations are expected ($3N - 5 = 4$). For this molecule there are two different sets of symmetry axes (C_2 and C_∞) and it should be noticed that the symmetric stretch produces no change in the dipole moment and therefore is infrared inactive and the pair of vibrations labelled ν_2 are doubly degenerate, *i.e.* they have the same frequency and differ only in the direction of vibration.

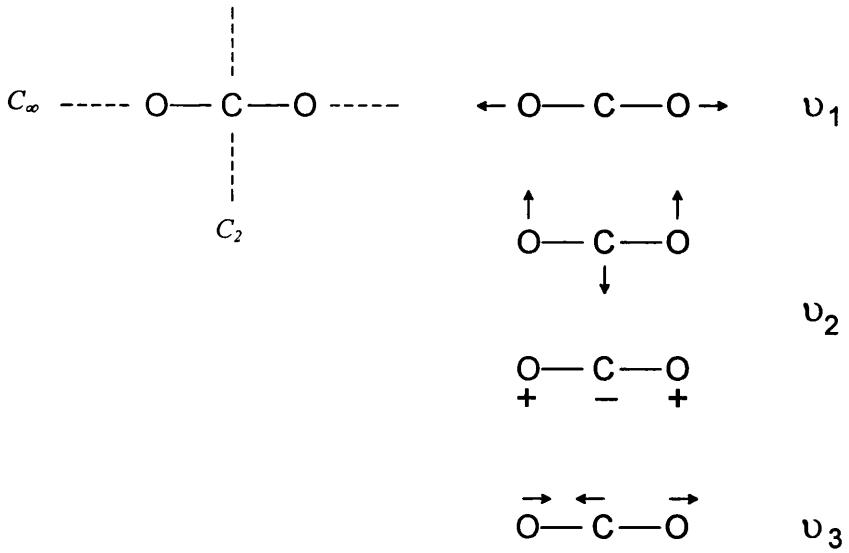

Figure 2.3.1. *The symmetry and fundamental vibrations of the carbon monoxide molecule.*

The fact that polyatomic molecules have several internuclear distances, several force constants, several dissociation energies and so on makes the situation a lot more complicated than for diatomics. However if the molecule possesses some symmetry, the normal vibrations will also have certain symmetry properties and thus the situation can be simplified somewhat. Therefore in all IR analyses of polyatomic molecules the symmetry of the molecule must be considered.

2.3.2 INSTRUMENTATION

In these experiments a Bruker IFS 113v Fourier-transform infrared (FT-IR) spectrometer was used. A FT-IR instrument consists of four main components, the source, the interferometer, the sample compartment, and the detector. The source is always some form of filament that is maintained at red- or white-heat by an electric current. Two common sources are the Nernst filament and the Globar filament, the latter being used in this work to supply infrared radiation over the range 4500–400 cm^{-1}. The Fourier-transform interferometer device is discussed in greater detail below and is described in a number of texts.[14–17] The sample chamber is located after the interferometer and before the detector and can be evacuated, using a mechanical vacuum pump, to remove atmospheric constituents so that any water and carbon dioxide absorptions are prevented from interfering with the sample spectrum. Detectors in common use are either ones that sense the heating effect of the radiation or ones that depend on photoconductivity. A mercury-cadmium-telluride (MCT) detector is an example of a photoconductive detector and is used in this work. The MCT detector operates at liquid nitrogen temperatures, which reduces noise, and tends to have a fast response time and high sensitivity in the mid-IR region. The pyroelectric detector, deuterated triglycine sulphate (DTGS), is a common alternative to the MCT detector, although it is not as sensitive; it has the advantage that it can be used at room temperature and is sensitive across the whole infrared range.

FT Interferometer

A typical Michelson interferometer consists of a beam splitter B and two mirrors M_1 and M_2 (Fig. 2.3.2). Initially a parallel beam of radiation is directed from the source

to the beam splitter, which is a plate of transparent material that is coated so as to reflect only 50% of the radiation; thus half the radiation is reflected onto the mirror M_1 and half is transmitted to the moving mirror M_2. The radiation then returns from both of these mirrors and recombines to a single beam at the beam splitter, which is again reflected and transmitted. Upon recombination the beam leaving B shows constructive or destructive interference, depending on the path lengths B to M_1 and B to M_2. If the path lengths are identical or the path difference is an integral number of wavelengths, $n\lambda$, then constructive interference gives a bright beam leaving B, whereas if the path difference is a half-integral number of wavelengths, $(n + ½)\lambda$, destructive interference causes the beams to cancel at B. Therefore as M_2 is moved smoothly towards or away from B, a detector sees radiation alternating in intensity. The following equation shows that the intensity of the transmitted beam, $I(\lambda)$, is a function of the optical path difference, x (cm); this is called the interferogram

$$I(x) = 0.5\, I(\lambda)\{1 + \cos(2\pi x/\lambda)\}$$

rearranging in terms of wavenumbers, $\bar{\nu}$ ($\bar{\nu} = 1/\lambda$),

$$I(x) = 0.5\, I(\bar{\nu}) \cos(2\pi x \bar{\nu})$$

As the amplitude is directly proportional to the intensity of the transmitted beam, $I(\bar{\nu})$, and the wavelength is directly proportional to the wavelength of the source, spectral information can therefore be obtained from the interferogram. Using a continuous source in the required spectral range, the interferogram is the integral of the contributions from all the wavelengths emitted from the source.

The Bruker IFS 113v FT-IR spectrometer used in this study has a Genzel interferometer rather than a Michelson interferometer; the difference is that the Genzel type has two stationary mirrors M_1 and M_2 that are coplanar with a moving mirror M_3 positioned between them (Fig. 2.3.3). The advantage of this optical arrangement is that, for a mirror displacement of x, the optical retardation changes by $4x$, compared with $2x$ for a standard Michelson interferometer, due to light being reflected from both sides of M_3.

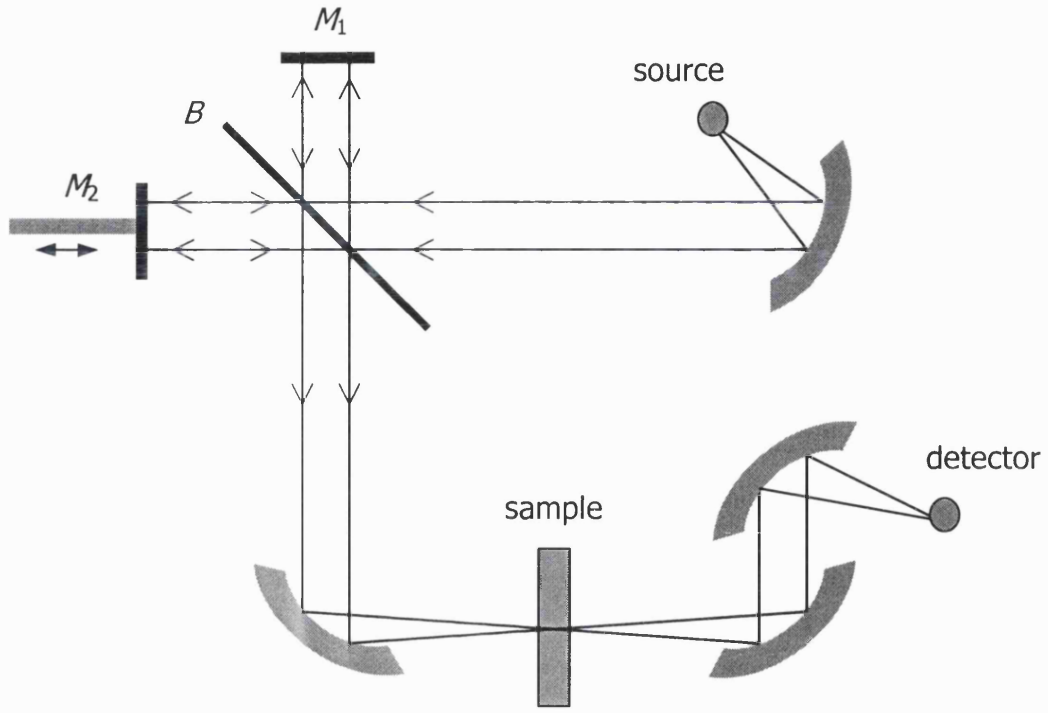

Figure 2.3.2. *Schematic diagram of a Michelson Fourier-transform IR spectrometer.*

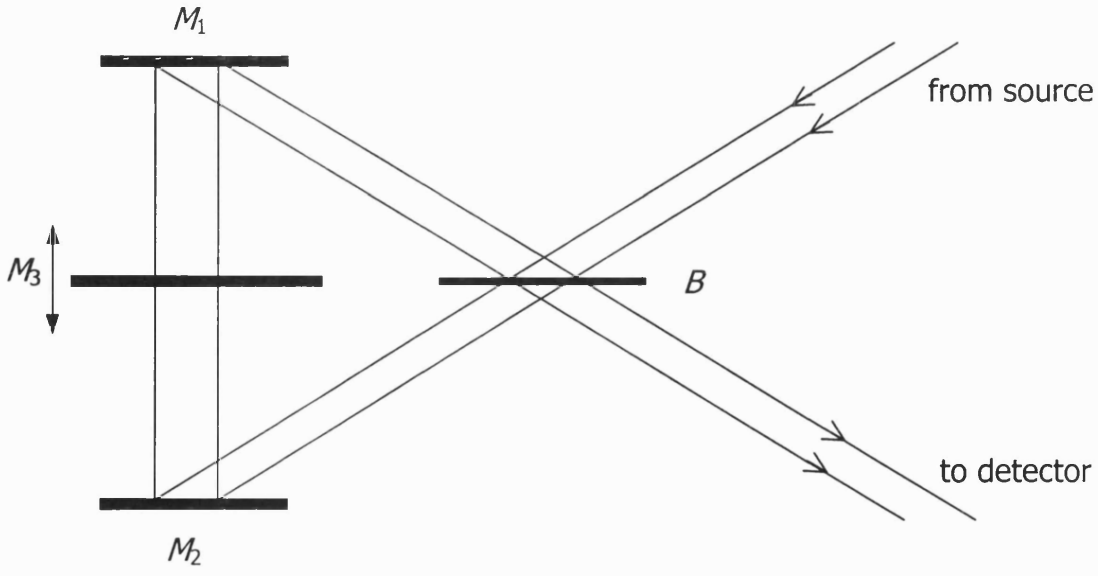

Figure 2.3.3. *Schematic diagram of a Genzel interferometer.*

Advantages of FT-IR

Fourier-transform infrared spectroscopy has a number of important advantages over dispersive infrared spectroscopy and they are listed below.

1. Jacquinot's advantage, or the throughput advantage, is a measure of how much more throughput an interferometer gives due to the aperture being larger than the slits of a dispersive spectrometer. For example, in a dispersive instrument the radiation is brought to a focus on a slit and the narrower the slit, the better the resolving power, although the total amount of energy passing through is extremely limited. In a FT instrument, however, parallel beams are used and there is no need to bring the radiation to a focus on a slit and as a consequence *all* the source energy passes through the instrument. FT instruments are especially suited for use in the energy-limited far infrared region.

2. Fellgett's advantage, or the multiplex advantage, arises because the scanning time required by a FT instrument is considerably less than that required to produce a dispersive spectrum of equal signal-to-noise ratio, resolution and sensitivity. Hence for a dispersive spectrometer each resolution element is scanned consecutively and the total scan time is labelled T and the time taken to record one resolution element is labelled t, so $t = T/n$ where n is the number of resolution elements. In FT-IR the entire frequency range is scanned within a time T. Moreover, considering the signal-to-noise ratio, S/N, it is found that S is proportional to t and N is proportional to $t^{1/2}$ therefore S/N $\propto t^{1/2}$

   thus $(S/N)_{FT} = T^{1/2}$, $(S/N)_{DISP.} = (T/n)^{1/2}$ or $(S/N)_{FT}/(S/N)_{DISP.} = n^{1/2}$

   Thus for equal data acquisition times the signal-to-noise ratio of measurements taken on a FT instrument will be $n^{1/2}$ times better than on a dispersive instrument, or alternatively, to record a spectrum of equal signal-to-noise, the dispersive instrument will take $n^{1/2}$ times longer.

3. The Connes advantage relates to the ability of the helium-neon laser to make extremely accurate measurements of the moving mirror, which subsequently allows very accurate measurements of the frequency. Therefore the transmittance or absorbance spectrum of a sample can be calculated more accurately and repeatably with reference to the background spectrum, enabling band wavenumbers to be determined with confidence.

4. The resolving power of a FT-IR spectrometer is related to the optical path difference between the moving and fixed mirrors by:

$$\Delta\bar{\nu} = 1/\delta$$

where $\Delta\bar{\nu}$ is the resolution and δ is the maximum travel of the mirror. Thus for a resolution of 1 cm^{-1}, the maximum distance travelled by the mirror must be 1 cm, while for a resolution of 0.01 cm^{-1}, 100 cm must be travelled. By comparison the dispersive spectrometer uses more dispersive gratings, or a series of gratings, to achieve a higher resolution although these modifications reduce the efficiency of the spectrometer. The resolving power of a FT instrument is also constant over the whole spectrum whereas for a dispersive spectrometer the resolving power varies with frequency.

5. For FT-IR spectrometers, the entire spectrum is obtained across the whole frequency range at once, whereas for dispersive IR spectrometers, usually more than one type of grating is needed to cover the whole frequency range because one grating is usually unable to function sufficiently throughout.

2.4 EXPERIMENT AND PROCEDURE

A description of the various pieces of equipment used to carry out these matrix isolation experiments is given in the following sections as well as a summary of the experimental procedure.

2.4.1 APPARATUS

In order to generate matrix-isolated species and to record any products resulting from their photo-induced reactions, a variety of equipment is needed. This consists of three main types: gas handling and cryogenic apparatus, photolysis apparatus, and spectroscopic apparatus.

Gas Handling and Cryogenic Apparatus

The chosen precursors ready to be studied are isolated in the chosen matrix material and these matrices are prepared using the gas handling and cryogenic apparatus.

The gas mixtures, containing the precursors and the matrix material argon, are deposited onto the cold window via metered deposition lines. These are part of two gas handling stainless steel manifolds which are used to prepare and to mix the gases prior to matrix isolation. The manifolds are arranged as shown in Figure 2.4.1 and consist of various valves and connectors which enable evacuation of the manifolds by a mechanical pump, the gaseous mixing of the desired S/Ar (species-to-argon) ratios, and finally the controlled deposition of the gaseous mixtures onto the cold window. The different types of vacuum apparatus are well reported[18] and, a number of manufacturers provide very useful manuals[19] to aid in the design of an apparatus suitable for matrix experiments.[20] The cold window is the centrepiece of the matrix equipment because this is where the matrix is formed, photolysed, and probed spectroscopically. The cold window is housed within a vacuum shroud and is cooled to temperatures around 14 K by a closed-cycle helium refrigerator (an Air Products Displex DE 202 S closed-cycle He refrigerator); the different types of refrigerators are described elsewhere.[5] The vacuum shroud is connected to an Edwards 63 mm

Diffstak diffusion pump backed by an Edwards mechanical pump which could reach pressures of ~ 2 x 10^{-6} Torr. The cold window is made of caesium iodide, CsI, due to its spectral transparency (UV to far-IR) and thermal properties (it has good thermal conductivity and is resistant to thermal shock). The CsI window and cryostat are arranged vertically within the vacuum shroud and can be rotated in order to be placed in correct alignment with the deposition line outlets, the photolysis window, and the IR transmission/absorbance beam for spectral collection (Fig. 2.4.2). The shroud therefore has two KBr windows for spectroscopic analysis and a third made of quartz for the photolysis studies. The vacuum shroud and cryostat are reasonably compact and can fit easily inside the sample chamber of the spectrometer.

Photolysis Apparatus

Photolysis of the matrices was carried out using an Oriel medium pressure xenon arc lamp which operates in the wavelength range 220–1000 nm. By placing a cut-off transmission filter in front of the quartz window on the vacuum shroud, the desired wavelength of radiation could be achieved. The following transmission filters were available for use in this study: 8 mm thick deep red (λ > 650 nm), 2 mm thick green (λ > 410 nm), Corning 7 mm thick blue/green (550 > λ > 350 nm), Pyrex (λ > 290 nm), and quartz (λ > 240 nm). The filters were checked by the use of a Shimadzu UV-vis spectrometer over the range 200–1000 nm. A 5 cm thick water filter was placed between the lamp and the sample to reduce the infrared output of the lamp so as not to warm the matrix.

Photolysis of the matrix is believed to excite the molecule causing either rearrangement or dissociation of the molecule; these processes are discussed further elsewhere.[21–23]

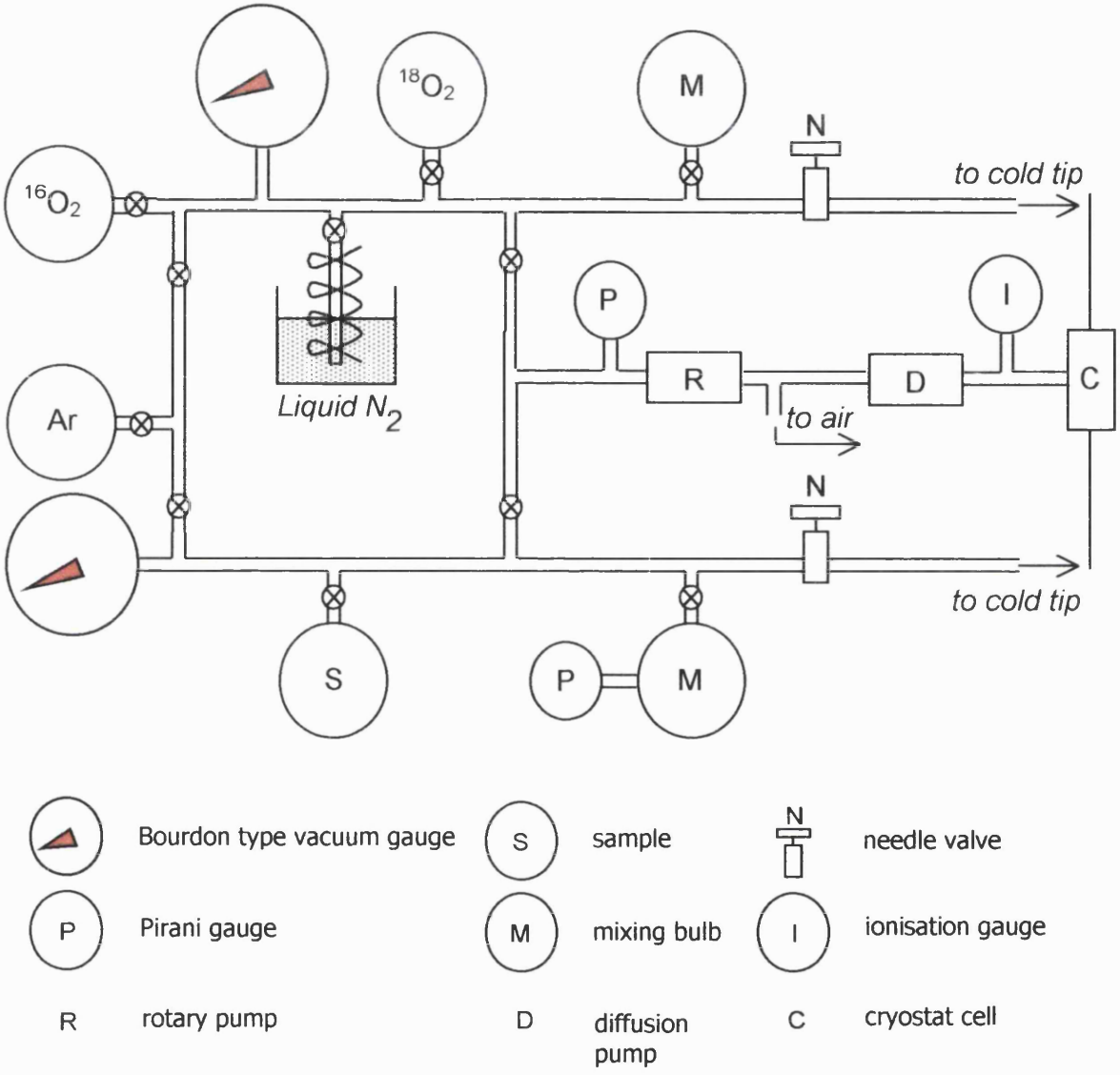

Figure 2.4.1. *Schematic diagram of the gas handling manifolds, the top one being used to make ozone which is then mixed with argon and the bottom one being used to mix the chosen precursor with argon; both mixtures are separately deposited onto the cold window at a controlled rate.*

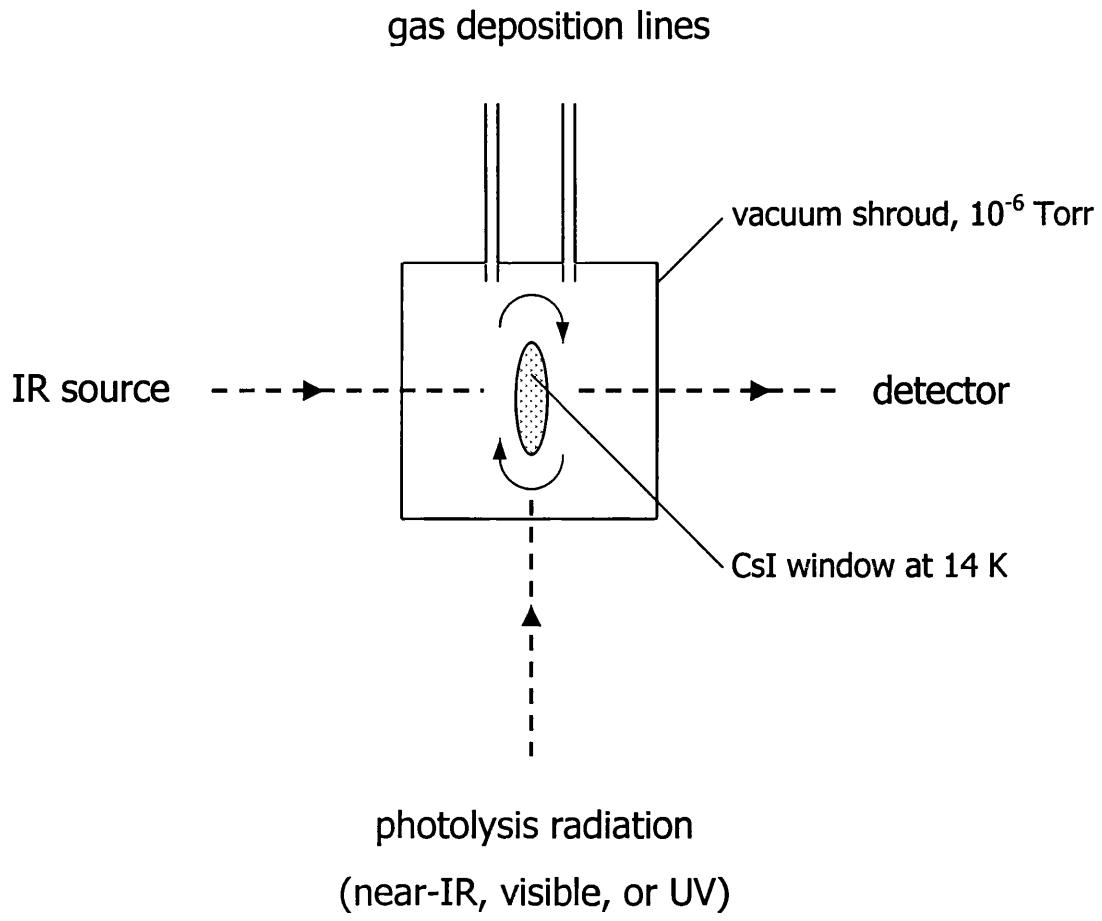

Figure 2.4.2. *Schematic diagram of the cryogenic cold window and the respective deposition, photolysis, and spectral paths.*

Spectroscopic Apparatus

The matrices were examined spectroscopically using a Bruker IFS 113v Fourier-transform infrared spectrometer. As mentioned earlier, the vacuum shroud containing the cryostat is mounted in the sample chamber of the spectrometer so that radiation can be transmitted through the shroud windows and the cold CsI window. The spectrometer was evacuated prior to spectrum acquisition in order reduce contributions from water and carbon dioxide vibrations to the spectrum. Infrared spectra were recorded after deposition and after each photolysis or warming cycle so as to observe any changes caused by these processes. The spectrometer was operated over the range 500–4000 cm^{-1} at a resolution of 0.5 cm^{-1} using a germanium-coated KBr beam splitter and a MCT detector cooled with liquid nitrogen and over the range

400–600 cm^{-1} at a resolution of 1 cm^{-1} using a 3.5-μm Mylar beam splitter and a DTGS detector (higher resolutions up to 0.25 cm^{-1} can be attained although the amount of time taken is a significant deterrent). The matrices were scanned between 500 and 1000 times and the interferograms were added and converted to a single beam spectrum by a fast Fourier-transform algorithm[16] using a zero filling factor of times two or four and the Happ-Genzel apodization function.[24] The spectra were then converted to double beam absorbance spectra using the reference spectra of the cold window before deposition. The band wavenumbers observed are accurate to ±0.2 cm^{-1}.

2.4.2 EXPERIMENTAL PROCEDURE

A number of experimental techniques and procedures are described for the benefit of future workers in this laboratory, ranging from those used to prepare the precursors prior to deposition to the analysis of the photoinduced reactions performed on the matrix-isolated samples.

Equipment Set up. Before an experiment commences, the gas handling manifolds and cryogenic equipment must be evacuated and the cold window must be clear of any deposits remaining from any previous experiment. The cooling of the matrix window takes up to an hour to reach 14 K so the cryostat is switched on at the earliest opportunity. This is also an appropriate time to start cooling the MCT detector in the IR spectrometer with liquid nitrogen.

Preparation of the Precursors. This study has focussed on the photochemical reactions of ozone and various halogen-containing species. All of the halogenated species were purchased commercially, either from Aldrich or Lancaster, at the highest purity possible (often better than 99.9% pure). Before use, the halogenated compound was transferred to a suitable Pyrex storage flask fitted with a Youngs tap and Quickfit B14 ground glass socket. Only in the case of iodine cyanide was purification necessary; ICN had to be sublimed in order to obtain it in the form of pure white needle-like crystals. The selected precursor was then degassed by repeated freeze-thaw cycles at liquid nitrogen temperatures and was ready to be diluted and

mixed with the matrix material. Ozone, on the other hand, was produced in situ; it is generated by passing normal oxygen, oxygen-18, or a 1:1 mixture of each through a Tesla coil discharge surrounding a 10 cm Pyrex finger immersed in liquid nitrogen (Fig. 2.4.1). The ozone was collected on the Pyrex finger in a condensed blue form and was purified by a freeze-thaw cycle to remove any residual oxygen. British Oxygen Company supplied the research-grade oxygen (>99.9%), while oxygen-18 (>97.7%) was supplied by Enritech Enrichment Technologies Ltd. Both precursors (ozone and the halogenated species) were then diluted separately with argon (the matrix material) in two different manifolds (Fig. 2.4.1) at species-to-argon (S/Ar) ratios in the range of 1:1000–1:6000 determined by standard manometric procedures at room temperatures. Precursors such as iodine cyanide and diiodoethane were in solid form but had sufficient vapour pressure to be able to mix with argon in the gas phase. The gases were left to mix in 2 L mixing bulbs before being deposited onto the cold CsI window (14 K). Research-grade argon was supplied also by British Oxygen Company. In some experiments nitrogen dioxide was used instead of ozone and oxygen instead of argon, in which cases the matrices were prepared in the same way as described above by simply replacing the appropriate gas cylinder; nitrogen dioxide was used as supplied by Argo.

Deposition. Once the window has reached 14 K, an IR reference spectrum is recorded so that absorptions due to the matrix-isolated species can be identified. Only then can deposition commence. The matrix is formed by depositing the ozone/Ar and precursor/Ar mixtures at an average rate of 3 mmol h^{-1} for 6–12 h. As deposition is proceeding the backing pressure reduces and requires the metering needle valves to be opened gradually during the deposition process. It was found that good quality spectra were obtained from matrices in which the initial deposition rate of 1 mmol h^{-1} is increased gradually over the following two hours. The increase in pressure in the vacuum chamber and the rate at which the pressure in the manifold reduces indicate the speed of deposition. The valves were opened further at reduced intervals over the next hour until a flow rate of ~ 5–6 mmol h^{-1} was obtained, and left running for a further 3–9 h. This last flow rate would decrease over the course of the deposition giving the required average flow rate of 3 mmol h^{-1}.

Species-to-Ar Ratios. In these studies the S/Ar ratio was usually chosen so as to produce clear spectra with the precursors in reasonable concentrations so that reactions could occur. Generally, the stoichiometric ratios of the reactants is an integral part of the understanding of any reaction but, in low temperature matrices, high concentrations of the isolated species result in aggregation giving rise to complicated but interesting spectra.[1–7,25–28] True isolation is achieved only at very low S/Ar ratios, usually smaller than 1/1000. Varying the S/Ar ratio sometimes helped with the assignment of IR bands, *i.e.* increasing the concentration of one of the precursors would lead to an increase in the intensity of bands that belonged to a related intermediate.

Isotopic Substitution. In this particular study, isotopic substitution proved to be a very valuable tool in determining the assignments of many new bands. Essentially substitution of $^{16}O_2$ by $^{18}O_2$ in the preparation of ozone ($^{18}O_3$ and $^{16}O_{3-x}{}^{18}O_x$) was carried out, since many of the new product species contained an O atom. After ^{18}O substitution a band assignable to a molecular vibration that contains an O atom should shift to a lower wavenumber from that belonging to the ^{16}O isotopomer. A shift of this sort indicates that the band can be assigned to a mode that contains some contribution from an O atom. The number of shifted bands and the magnitude of the shift can provide more information as to the mode to which the band can be assigned. The substitution of an atom in a bond by one of a different mass results in a specific change of frequency because the force constant of the bond remains the same in the harmonic approximation. Wavenumber shifts for various species and the relevant calculations are discussed elsewhere.[10–13]

Photolysis and Warming Studies. Photolysis was required to initiate a reaction between ozone and the halogenated species in all the reactions studied in this thesis. Wavelength-dependent photolysis provides information regarding the actual threshold wavelength required to initiate a reaction, thus establishing the wavelength selectivity of the product distribution. Therefore by shortening the wavelength of the radiation a series of reaction intermediates may be observed, as well as the threshold at which they form. For example irradiating a matrix successively with the following visible and UV radiation for 30 min each cycle, ($\lambda > 650$ nm), ($\lambda > 410$ nm), ($550 > \lambda$

> 350 nm), (λ > 290 nm), and (λ > 240 nm), may enable the step-wise photochemical pathway of a reaction to be deduced. Time-dependent photolysis studies were also carried out; this is where the matrix is photolysed at a fixed wavelength for increasing time periods. The time-dependent photolysis studies can provide kinetic information concerning the formation and destruction of certain species in the reaction. Therefore both wavelength- and time-dependent photolysis studies provide a great deal of information with regard to the grouping of new bands that have similar photolytic behaviour. Once the IR bands are grouped, the species responsible can be identified.

Warming the matrix reduces its rigidity slightly and allows some of the species in the matrix to diffuse in order to encounter a reaction partner or simply to rearrange to a more stable geometry. The temperature control is achieved by using a variable voltage heater wound around the cold head of the cryostat and the temperature is monitored by both a chromel vs. gold (0.07% Fe) thermocouple and a hydrogen vapour pressure bulb. Both argon and oxygen matrices were warmed up to 25–30 K for 20 min in these studies, although in some instances argon had to be warmed up to 35 K before evaporation of the matrix became significant.

Spectral Collection. An infrared spectrum of the cold window before deposition is recorded for each new experiment and is used as the reference spectrum for all the subsequent spectra recorded during that experiment. Infrared spectra are also recorded after deposition of the matrix and after each photolysis or warming cycle and are converted to double beam absorbance spectra using the pre-recorded reference spectrum. Before each spectrum is collected the spectrometer is evacuated by a mechanical pump in order to remove the atmospheric gases. The spectra were examined using the program Opus 2.2 and are represented graphically in this thesis using the program Origin 4.0. Collection of the spectra at resolutions exceeding 0.25 cm^{-1} with 1000 scans required a huge amount of processing time, typically about 1.5 h, whereas reducing the number of scans to 500 and the resolution to 0.5 cm^{-1} reduced the collection time to 25 min with no detrimental effect on the identification of spectral features. In some cases infrared spectra were collected over 100 scans at a resolution of 1 cm^{-1} and the time taken would be only 5 minutes. Time was therefore an important factor, considering the number of spectra that could yield useful

information, considering all the photolysis and warming cycles which might be investigated. Additionally, the Genzel-type arrangement of the interferometer enabled the spectra to be collected in approximately half the time of a Michelson FT-IR interferometer.

End of an Experiment. At the end of an experiment the cryostat is switched off and the matrix slowly evaporates and is pumped away. Once the window has reached room temperature the cryostat is removed from the vacuum shroud and the window is cleaned with methanol. The CsI window is polished from time to time. The equipment is then made ready for the next experiment. The spectra in the meantime are processed and analysed.

2.5 REFERENCES

1. Hallam, H. E., *Vibrational Spectroscopy of Trapped Species*; Wiley: NY; 1973.
2. Burnett, J. K.; Poliakoff, M.; Turner, J. J.; Dubost, H., *Advances in Infrared and Raman Spectroscopy*, Vol. 2; Eds: Clark, R. J. H.; Hester, R. E.; Heyden: London; 1976.
3. Downs, A. J.; Hawkins, M., *Advances in Infrared and Raman Spectroscopy*, Vol. 10; Eds: Clark, R. J. H.; Hester, R. E.; Heyden: London; 1983.
4. Almond, M. J.; Downs, A. J., *Advances in Infrared and Raman Spectroscopy*, Vol. 17; Eds: Clark, R. J. H.; Hester, R. E.; Wiley: Chichester; 1989.
5. Andrews, L.; Moskovits, M., *Chemistry and Physics of Matrix Isolated Species*; North-Holland: Amsterdam; 1989.
6. Moskovits, M.; Ozin, G. A., *Cryochemistry*; Wiley: NY; 1976.
7. Durig, J. R., *Analytical Applications of FT-IR to Molecular and Biological Systems*; Reidel: Boston; 1980.
8. Banwell, C. N.; McCash, E. M., *Fundamentals of Molecular Spectroscopy*, 4th Ed.; McGraw-Hill: London; 1994.
9. Herzberg, G., *Spectra of Diatomic Molecules*; Van Nostrand: NY; 1939.

10. Herzberg, G., *Infrared and Raman Spectra of Polyatomic Molecules*; Van Nostrand: NY; 1945.
11. Wilson, E. B.; Decius, J. C.; Cross, P. C., *Molecular Vibrations: The Theory of Infrared and Raman Vibrational Spectra*; McGraw-Hill; 1955.
12. Nakamoto, K., *Infrared and Raman Spectra of Inorganic and Coordination Compounds*; Wiley: NY; 1986.
13. Woodward, L. A., *Introduction to the Theory of Molecular Vibrations and Vibrational Spectroscopy*; Clarendon Press: Oxford; 1972.
14. Martin, A. E., *Infrared Instrumentation and Techniques*; Elsevier; 1966.
15. Bell, R. J., *Introductory Fourier Transform Spectroscopy*; Academic Press: NY; 1972.
16. Griffiths, P. R., *Transform Techniques in Chemistry*; Plenum: NY; 1978.
17. Griffiths, P. R., *Chemical Infrared Fourier Transform Spectroscopy*; Wiley: NY; 1975.
18. Shriver, D. F.; Drezdzon, M. A., *The Manipulation of Air-Sensitive Compounds*; Wiley: NY; 1986.
19. VAT Switzerland; Swagelock; Hoke; Edwards; Leybold-Heraeus; Gyrolock; ITL; Nor-Cal Products Inc.
20. Dunkin, I. R., *Matrix-Isolation Techniques: A Practical Approach*; Oxford University Press; 1998.
21. Calvert, J. G.; Pitts, J. N. Jr., *Photochemistry*; Wiley: NY; 1966.
22. Wayne, R. P., *Principles of Photochemistry*; Oxford University Press; 1988.
23. Wayne, R. P., *Photochemistry of Atmospheres*; Oxford University Press; 1990.
24. Bruker IFS User's Manual, version 4/89, 1987.
25. Jacox, M. E., *J. Phys. Chem. Ref. Data* **1984**, *13*, 945–1068.
26. Jacox, M. E., *J. Phys. Chem. Ref. Data* **1988**, *17*, 269–511.
27. Perutz, R. N., *Chem. Rev.* **1985**, *85*, 77–96.
28. Perutz, R. N., *Chem. Rev.* **1985**, *85*, 97–127.

Chapter 3

Photochemically Induced Reactions of Iodine Cyanide

3.1 INTRODUCTION

The photochemically induced reactions of iodine cyanide, ICN, with either ozone (section 3.2) or nitrogen dioxide (3.3) are studied in this chapter, the idea being to detect any products that form after photolysis and consequently to compare not only the photochemistry but the type and nature of the photoproducts formed. Additionally, by studying the reaction of ICN with either ozone or nitrogen dioxide, the question of whether a precursor complex ($O_3\cdots$ICN or $NO_2\cdots$ICN) is present will be explored.

Previous matrix isolation studies have already shown that ozone can interact with small molecules (CH_3I,[1] HF,[2] PH_3,[3] CF_3I,[4] ICl,[5] and C_2H_5I[6]) to form a molecular complex. This charge-transfer complex sufficiently changes the photochemical behaviour of ozone in the matrix, allowing oxygen–oxygen bond cleavage to occur with visible radiation and hence the transfer of an oxygen atom to the precursor molecule. By contrast isolated ozone will only photodissociate effectively after ultraviolet absorption in the intense Hartley continuum (200–310 nm) which results in the formation of molecular oxygen and atomic oxygen in the excited state, $O(^1D)$. Therefore, for many ozone and precursor reactions, where no complex is formed upon deposition, shorter wavelength radiation ($\lambda < 310$ nm) is required to initiate a reaction.

With compounds containing iodine (Z–I)[1,4–8] it has been possible to form previously unknown inorganic monomeric iodoso- (Z–IO), iodyl- ($Z–IO_2$) and hypoiodo-species (Z–OI) by photolysis of the ozone$\cdots$precursor complex. Previous to the matrix isolation experiments there were only a very few known inorganic, aliphatic and aromatic compounds of these types. It is therefore of interest as to whether ozone forms a complex with ICN (an iodine-containing compound) upon deposition and if the subsequent photochemical reactions will produce similar intermediates. It is also of interest as to whether nitrogen dioxide will behave similarly to ozone in the identical reaction with ICN, *i.e.* to act as an oxygen atom donor.

3.2 IODINE CYANIDE AND OZONE

The study of the photochemically induced reaction of ICN and ozone in argon matrices was chosen in order to extend the number of known reactions of ozone with iodine-containing compounds (CH_3I,[1] ICl,[5] C_2H_5I,[6] C_2F_5I,[7] and CHClI[8]). The main aim is to establish whether a weak $O_3\cdots$ICN complex is present upon deposition and whether the ICN/O_3 photo-induced reaction produces similar intermediates analogous to those detected in the previous Z–I reactions, such as iodoso- (OI–CN), iodyl- (O_2I–CN), and hypoiodo-species (IO–CN). Moreover, the matrix isolation technique is especially well suited for the determination of the type of complex present *e.g.* $O_3\cdots$ICN or $O_3\cdots$NCI. Additionally, other intermediates and products are also expected due to the presence of a nitrogen atom.

3.2.1 RESULTS AND DISCUSSION

Deposition of the Precursors, ICN and O_3

The infrared spectra of ICN isolated separately in argon matrices (ICN/Ar = 1:1500 to 1:8000) and in oxygen matrices (ICN/O_2 = 1:6000) have been recorded (Table 3.2.1). The ICN band wavenumbers were found to be in close agreement with those reported elsewhere for this species in the gas phase[9–11] and in various matrices.[12,13] Increasing the concentration of ICN resulted in the appearance of additional bands; some were slightly blue-shifted from the band attributed to the C≡N stretch while others appeared on either side of that attributed to the X–C stretch. These concentration-dependent bands are due to small aggregates of the halogen cyanide, sustained by the conditions of the matrix. Only at species-to-argon ratios in the region of 1:10,000 was it possible to detect solely ICN monomer bands (Fig. 3.2.1). Ultraviolet ($\lambda > 240$ nm) photolysis of an Ar matrix containing ICN produced a new band appearing at 2057.2 cm^{-1} with a shoulder at 2059.0 cm^{-1} (Fig. 3.2.1). These bands have also been observed by Fraenkel *et al.*,[12] who assigned them to $\nu_{C\equiv N}$ of INC, the photoisomer of ICN. The fact that $\nu_{C\equiv N}$ of ICN is ~120 cm^{-1} higher than that of INC suggests that the C≡N bond

in ICN has more triple bond character than that in INC. This is also typical of other XCN-XNC pairs.[14]

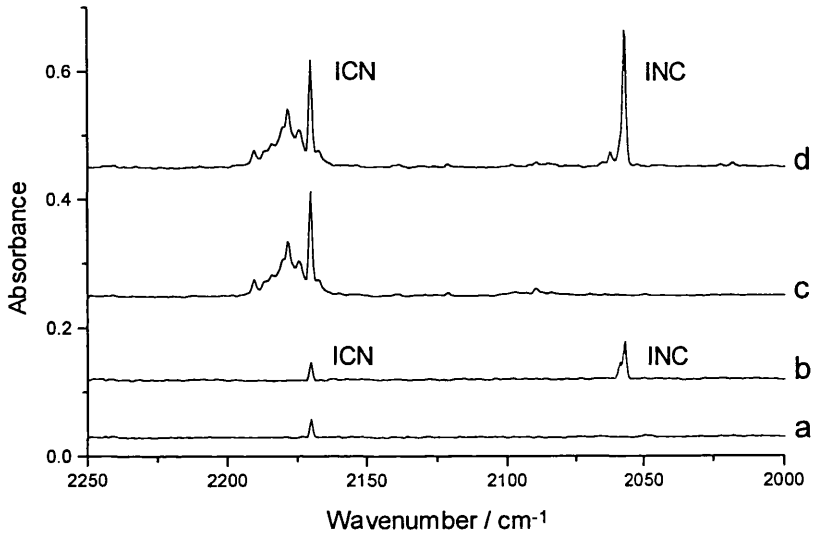

Figure 3.2.1. *Infrared spectra of argon matrices containing ICN after (a) deposition (ICN/Ar = 1:10000), (b) UV photolysis ($\lambda > 240$ nm) for 30 min (ICN/Ar = 1:10000), (c) deposition (ICN/Ar = 1:1500), and (d) UV photolysis ($\lambda > 240$ nm) for 30 min (ICN/Ar = 1:1500). The spectra show bands assigned to $\nu_{C\equiv N}$ of ICN and to $\nu_{C\equiv N}$ of INC formed after photolysis.*

The infrared spectrum of ICN co-deposited with ozone in solid argon ($ICN/O_3/Ar$ = 1:2:8000) exhibited bands that resembled those detected in the infrared spectra of ICN or ozone[15,16] isolated separately in argon (Table 3.2.1). However weak bands with small wavenumber shifts from the ozone fundamental bands appeared at 1033.9, 1028.6, 706.9 and 698.7 cm^{-1}, and were destroyed by visible irradiation ($\lambda >$ 650 nm and $\lambda > 410$ nm). These weak, shifted bands are attributed to the molecular complex $O_3\cdots ICN$ since they are comparable with those reported for other ozone$\cdots$I–Z complexes detected elsewhere[1,4–8] and since, upon irradiation with visible light, bands belonging to OI–CN are observed. Although the complex could alternatively be of the type $ICN\cdots O_3$, the lack of shifts in $\nu_{C\equiv N}$ and of any new bands that could be attributed to ICNO, militates against this possibility. This interaction between ozone and ICN in the matrix is sufficient to change the photochemical

behaviour of ozone, allowing oxygen–oxygen bond cleavage to occur with visible radiation. By contrast isolated ozone will only photodissociate effectively after ultraviolet irradiation (200–310 nm). In addition to the precursor bands, others attributable to small quantities of matrix-isolated water and carbon dioxide were also detected.

Isotopic ozone, $^{18}O_3$, and mixed isotopic ozone, $^{16}O_{3-x}{}^{18}O_x$, samples have also been condensed with iodine cyanide in argon matrices and the appropriate spectroscopic data are listed in Tables 3.2.1 and 3.2.2. An important feature to note is that in the mixed ozone experiments there was a sextet of ν_3 bands for complexed ozone that matched in intensity distribution that of isolated ozone (1:2:1:1:2:1) indicating that the ozone submolecule in the complex has the same symmetry as ozone itself. In other words the terminal oxygen atoms are equivalent and therefore ozone binds to ICN via the central oxygen atom (see Appendix A1).

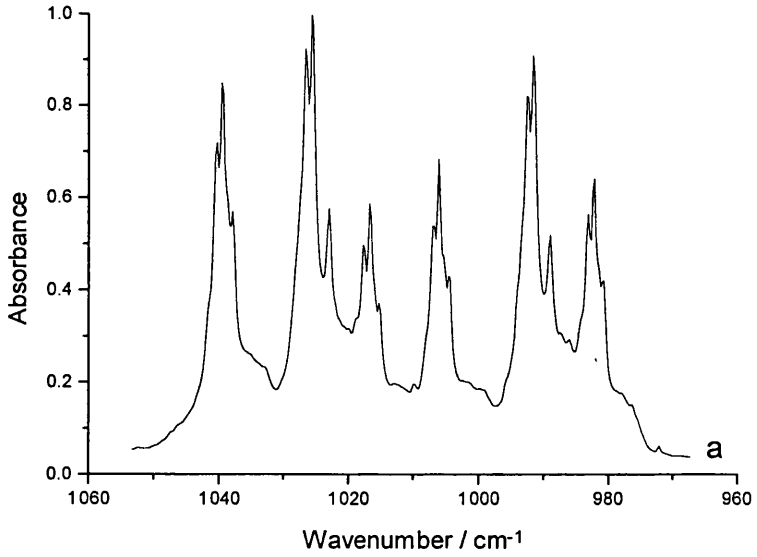

Figure 3.2.2. *Infrared spectrum recorded after (a) deposition of an ICN/$^{16}O_{3-x}{}^{18}O_x$/Ar matrix, showing complex bands alongside those belonging to ozone isotopomers.*

Photolysis of ICN/O_3 Matrices

Deposition of argon matrices containing ICN and ozone and their subsequent photolysis cycles using radiation of different wavelengths created a number of new species, as made evident by the emergence of new bands. Different photoproducts resulted depending upon the threshold wavelength for formation; these are grouped below.

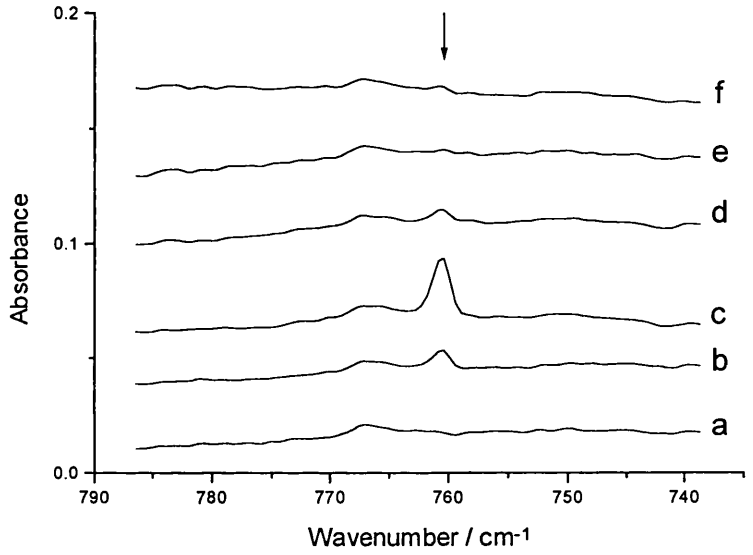

Figure 3.2.3. *Infrared spectra showing the ν_{I-O} region for an argon matrix containing ICN and ozone, taken after (a) deposition, (b) $\lambda > 650$ nm photolysis, (c) $\lambda > 410$ nm photolysis, (d) $\lambda > 350$ nm photolysis, (e) Pyrex-filtered ($\lambda > 290$ nm) photolysis, and (f) quartz-filtered ($\lambda > 240$ nm) photolysis.*

OICN. The first new band detected, at 760.6 cm^{-1}, was weak and formed after visible irradiation ($\lambda > 650$ nm) (Table 3.2.3). The band intensified upon filtered photolysis at $\lambda > 410$ nm, but was destroyed on UV-vis ($\lambda > 350$ nm) irradiation (Fig. 3.2.3). In the ^{18}O-enriched ozone spectrum, $\nu_{I-^{16}O}$ occurs at 760.2 cm^{-1} and $\nu_{I-^{18}O}$ at 722.2 cm^{-1}, an isotopic shift of 38.0 cm^{-1}. Bands in this region are therefore assigned to the I–O stretch of the iodoso-species OI–CN, based on the band wavenumbers and the ^{18}O isotopic shift, both of which compare well with those obtained for other iodoso-species isolated in argon, viz. CH_3–IO (723.7 cm^{-1}, ^{18}O-shift of 35.6 cm^{-1}),[1]

CF_3–IO (732.3 cm^{-1}, ^{18}O-shift of 26.3 cm^{-1}),[4] and Cl–IO (779.1 cm^{-1}, ^{18}O-shift of 27.8 cm^{-1}).[5] The predicted isotopic shift for an harmonic I–O vibration is 37.4 cm^{-1}, suggesting that ν_{I-O} of OI–CN is essentially uncoupled to any nearby vibrational modes. Note that ν_{I-O} of OI–CN (760.6 cm^{-1}) falls between that of the fluorine- and chlorine-containing iodoso-species, illustrating the point that the CN group behaves as a pseudohalide with properties in between those of F and Cl. A doublet of bands belonging to the ^{16}O and ^{18}O isotopomers of OI–CN was detected in the mixed ozone experiment; no intermediate components were observed, thus confirming that there is a contribution from only a single oxygen atom to the vibrational mode. There was no detectable shift to any of the $\nu_{C\equiv N}$ bands, nor were any new bands detected which could be indicative of the formation of either free IO or free CN.

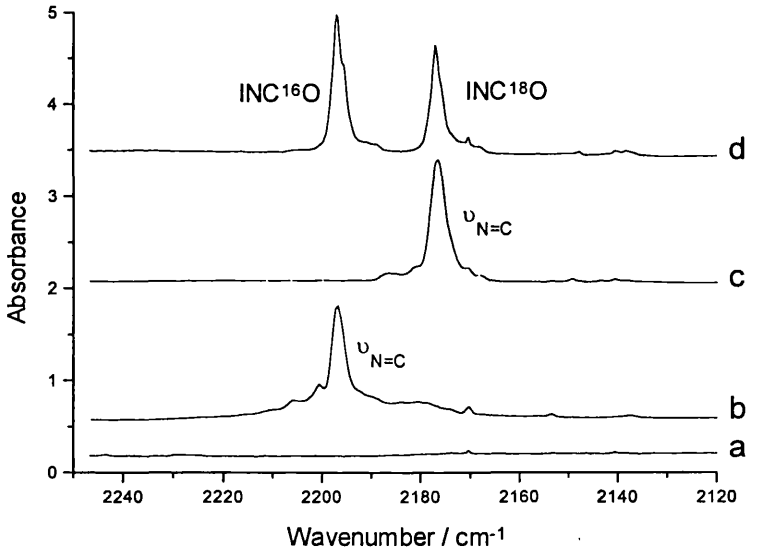

Figure 3.2.4. *Infrared spectra of argon matrices containing ICN and ozone after (a) deposition, (b) λ > 350 nm photolysis (ICN/$^{16}O_3$/Ar), (c) λ > 350 nm photolysis (ICN/$^{18}O_3$/Ar), and (d) λ > 350 nm photolysis (ICN/$^{16}O_{3-x}{}^{18}O_x$/Ar).*

INCO. A group of bands started to appear after irradiation at wavelengths longer than 410 nm and continued to grow upon UV-vis (λ > 350 nm) and UV irradiation (λ > 290 nm and 240 nm); they were attributed to iodoisocyanate INCO (Table 3.2.4), the bands at 2196.9, 1273.2, and 591.6 cm^{-1} being assigned to the N=C stretch, C=O stretch, and the –NCO out-of-plane bend, respectively. The I–N stretch

escaped detection but should have appeared just below 500 cm^{-1}; it should thus occur beyond the range of the MCT detector but may have been too weak to be detected in the range of the DTGS detector. Extra bands also appeared alongside the fundamentals owing either to additional sites in the matrix or to aggregates of INCO. Analogous bands at lower wavenumbers appeared in the spectra of $ICN/^{18}O_3/Ar$ matrices under identical photolytic conditions, and were attributed to the formation of $INC^{18}O$. When $^{18}O_3$ is replaced by a $^{16}O_3/^{18}O_3$ mixture many doublets appear which incorporate the ^{16}O and ^{18}O isotopomer bands detected in the experiments with pure isotopic ozone ($^{16}O_3$ and $^{18}O_3$) (Table 3.2.4 and Fig. 3.2.4). These features suggest that only a single oxygen atom is present in the photoproduct, which further supports the attribution of bands to an INCO species. The wavenumbers of the INCO bands obtained here compare extremely well with those obtained for halogen isocyanate molecules, XNCO (X = Cl, Br, or I) in the vapour state.[17] The ^{18}O-shift observed for $\nu_{N=C}$ (of the –NCO moiety) of BrNCO vapour[18] is 22.1 cm^{-1} and clearly relates to that observed in this work for INCO, viz. $\nu_{N=C}$ = 2196.9 cm^{-1} ($INC^{16}O$), $\nu_{N=C}$ = 2177.0 cm^{-1} ($INC^{18}O$), ^{18}O-shift = 19.9 cm^{-1}. The wavenumbers of the –NCO group vibrations are very similar for each of the halogen isocyanates and hence changing the halogen atom, X, does not significantly change the electronic structure. The formation of $\nu_{N=C}$ bands at the expense of ozone bands can be seen in Figure 3.2.5.

The wavenumbers of the fundamentals of halogen nitrile oxides have been determined previously;[19,20] thus $\nu_{C\equiv N}$, ν_{N-O}, and δ_{CNO} occur between ~2260–2220, ~1345–1305, and ~465–420 cm^{-1}, respectively. The formation of iodonitrile oxide (I–C≡N→O) upon photolysis might also have been expected but no bands attributable to this species were detected in the IR spectra. However, it is possible that ICNO could exist in the matrix as a transition-state intermediate, leading to the formation of the more stable iodoisocyanate INCO (this is discussed further in section 3.2.2).

IC(O)NCO. Further photolysis of ICN/O_3 matrices with Pyrex-filtered radiation ($\lambda > 290$ nm) gave rise to new bands appearing in the carbonyl region of the infrared spectrum (Table 3.2.5), the intensities of which continued to increase after subsequent quartz-filtered ($\lambda > 240$ nm) irradiation (Fig. 3.2.6). In fact several very weak and weak bands assigned to $\nu_{C=O}$ appeared in the spectrum between 1787.9 and

1779.3 cm^{-1}, and are due to different carbonyl species occupying different matrix sites. Upon ^{18}O substitution many carbonyl bands appeared between 1742.2 and 1736.9 cm^{-1} with ^{18}O isotopic shifts of c. 42 cm^{-1}. In the mixed-ozone experiment, both sets of bands were detected, indicating that only one ^{16}O atom or one ^{18}O atom is present in the molecule. The majority of these $\nu_{C=O}$ bands are attributed to an iodocarbonyl isocyanate species, IC(O)NCO, based on similarities with analogous fluorocarbonyl isocyanate, chlorocarbonyl isocyanate, and bromocarbonyl isocyanate species studied elsewhere.[21–24] Comparing the $\nu_{C=O}$ values obtained here (Table 3.2.5) for IC(O)NCO (1787.9–1779.3 cm^{-1}) with the gas-phase values obtained for trans-FC(O)NCO (1879 cm^{-1}),[21] trans-ClC(O)NCO (1817 cm^{-1}),[21] and matrix isolated trans-BrC(O)NCO (1813 cm^{-1}),[24] it can be seen that the wavenumbers of $\nu_{C=O}$ bands for XC(O)NCO species decrease in the following order: X = F > Cl > Br > I. Halogen carbonyl isocyanates exist in either a cisoid or a transoid conformation whereby the –NCO group adopts either a cis or trans orientation with respect to the carbonyl group. The $\nu_{C=O}$ vibration of the known cisoid conformers occurs 20-30 cm^{-1} below that of transoid ones. The work presented here shows evidence for the presence of but one isomer in the matrix, namely the transoid. However in one experiment ($ICN/^{16}O_{3-x}{}^{18}O_x/Ar$) prolonged quartz irradiation for 12 h led to the appearance of bands around 1723–1717 cm^{-1} showing a ~ 20 cm^{-1} shift from those of the transoid conformer and are thus attributed to the cisoid conformer (Table 3.2.6 and Fig. 3.2.6). Durig *et al.* showed that the transoid conformer is the more stable of the two,[22,23] a conclusion which is consistent with the formation and assignment of bands in these experiments. The bands at 2200.5 and 1278.3 cm^{-1} are assigned to $\nu_{N=C}$ and $\nu_{C=O}$ (–NCO), respectively, of IC(O)NCO since, as photolysis times increase, they continue to grow relative to those at 2196.9 and 1273.2 cm^{-1}, respectively, of INCO (Table 3.2.5 and Fig. 3.2.7). The ^{18}O counterparts for $\nu_{N=C}$ and $\nu_{C=O}$ of –NCO, attributed to $IC(^{18}O)NC^{18}O$, appeared at 2180.9 and 1230.6 cm^{-1}, respectively. These NCO bands first appeared after Pyrex-filtered photolysis and continued to grow upon quartz-filtered irradiation. The characteristic ν_{C-N} band of IC(O)NCO could not be detected in these experiments owing to the fact that strongly absorbing ozone bands appear in the same region. Warming the matrix caused the intensities of some $\nu_{C=O}$ bands of IC(O)NCO to increase slightly at the expense of the $\nu_{N=C}$ bands of INCO, indicating a thermally induced route from the isocyanate to the carbonyl isocyanate.

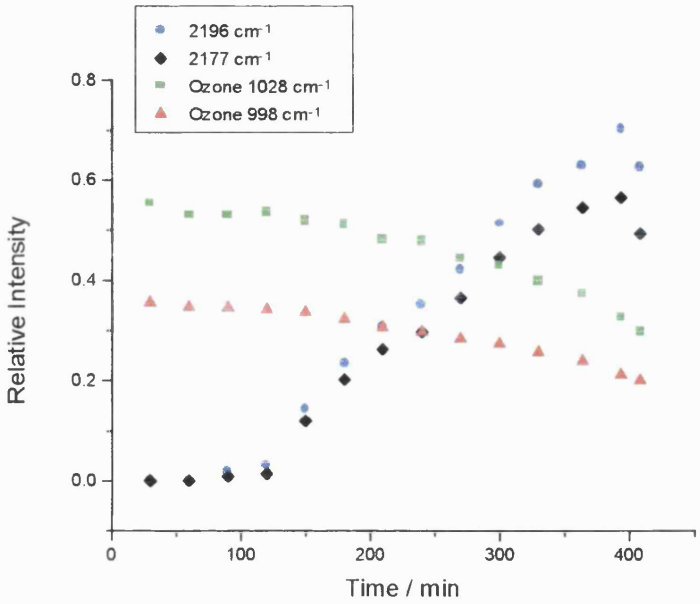

Figure 3.2.5. *IR absorbance for the new $\nu_{N\equiv C}$ bands of $INC^{16}O$ and $INC^{18}O$ at 2196 and 2177 cm^{-1}, respectively, and for the depleting ozone (ν_3) bands at 1028 and 998 cm^{-1} as a function of photolysis time.*

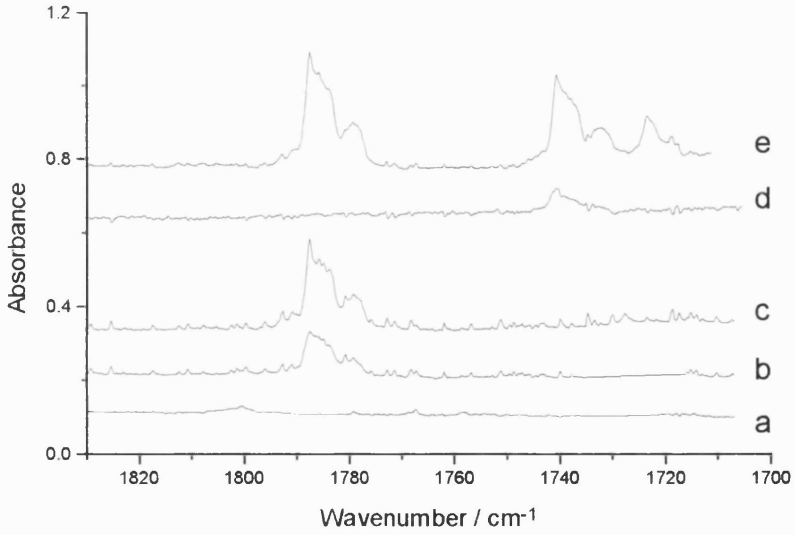

Figure 3.2.6. *Infrared spectra of the carbonyl region of argon matrices containing ICN and ozone after (a) deposition, (b) $\lambda > 240$ nm photolysis for 30 min ($ICN/^{16}O_3/Ar$), (c) $\lambda > 240$ nm photolysis for 12 h ($ICN/^{16}O_3/Ar$), (d) $\lambda > 240$ nm photolysis for 30 min ($ICN/^{18}O_3/Ar$), and (e) $\lambda > 240$ nm photolysis for 12 h ($ICN/^{16}O_{3-x}{}^{18}O_x/Ar$).*

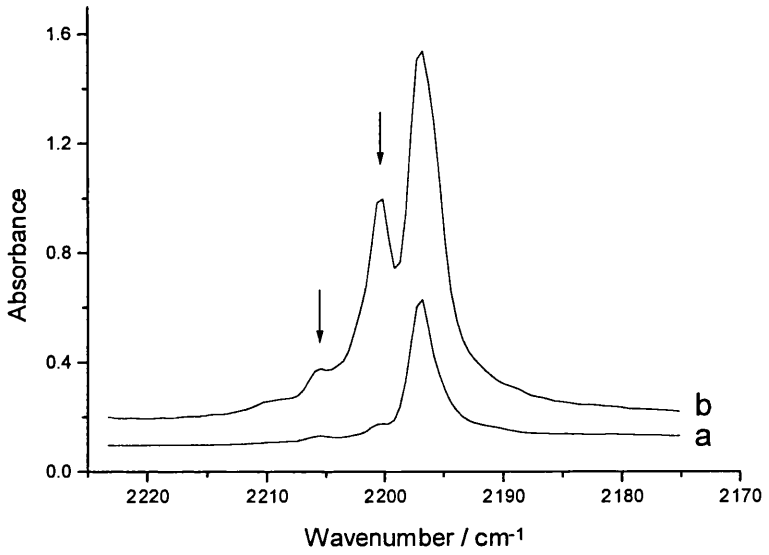

Figure 3.2.7. *Infrared spectra of an ICN/$^{16}O_3$/Ar matrix after (a) $\lambda > 350$ nm photolysis showing the $\nu_{N=C}$ band of INCO and (b) $\lambda > 240$ nm photolysis showing the appearance of other $\nu_{N=C}$ bands, this time belonging to IC(O)NCO.*

Other Species. Other new bands growing in very slowly after Pyrex-filtered irradiation, and much more rapidly after quartz-filtered irradiation, were situated between 833.3 and 777.8 cm^{-1} ($^{16}O_3$ experiments) and between 804.6 and 784.0 cm^{-1} ($^{18}O_3$ experiments) (Table 3.2.5). Those occurring very weakly at 814.8 and 813.4 cm^{-1} are assigned to the antisymmetric -IO_2 stretch of an iodyl species, Z–IO_2; the ^{18}O counterparts occurred between 787.6 and 784.0 cm^{-1}. There is good agreement between the wavenumbers of ν_{IO_2} bands detected here and those detected for other iodyl species.[1,4–7] Moreover, a triplet of bands in a 1:2:1 ratio appeared in the 1:1 mixed ozone experiment, which indicates that two symmetrically placed oxygen atoms contribute to ν_{IO_2} (Fig. 3.2.8). Bands belonging to the symmetric stretch of the –IO_2 unit were too weak to be detected in the ^{18}O experiments. Although it is possible that the bands in this region could alternatively belong to the -C(O)I deformation of IC(O)NCO, cf. fluorocarbonyl isocyanate[22] and chlorocarbonyl isocyanate,[23] the presence of a 1:2:1 triplet in the ICN/$^{16}O_{3-x}{}^{18}O_x$ experiment and the fact that no such bands appear in this region for BrCN/O_3 experiments, makes such an

assignment unlikely. Extremely weak bands appearing between 833.3 and 825.5 cm^{-1} are tentatively assigned to the NC stretch (NCN) of carbonyl diisocyanate $CO(NCO)_2$, cf. gas-phase values (831 and 827 cm^{-1}) and as a liquid (824 cm^{-1}).[25] Furthermore ν_{NC} (NCN) bands could also arise from the dimer $I_2NC(O)NCO$, once produced by Birkenbach *et al.* as a result of INCO polymerisation.[26] These bands also appeared in the mixed ozone experiment but were too weak for detection in the $^{18}O_3$ experiments. The presence of $CO(NCO)_2$ or $I_2NC(O)NCO$ could be responsible for some of the many carbonyl bands detected in the IR spectra ($\nu_{C=O}$ of $CO(NCO)_2$ occurs at 1772 cm^{-1}).[25]

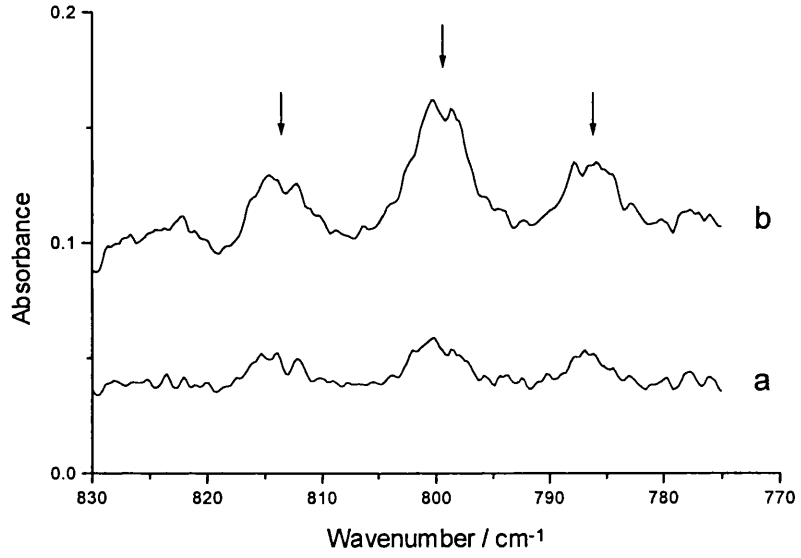

Figure 3.2.8. *Infrared spectra of an ICN/$^{16}O_{3-x}{}^{18}O_x$/Ar matrix after (a) Pyrex-filtered photolysis ($\lambda > 290$ nm) and (b) quartz-filtered photolysis ($\lambda > 240$ nm), showing ν_{IO_2} isotopomer bands in a 1:2:1 ratio.*

In cases where the concentration of ICN was high, a weak band situated at 2059.1 cm^{-1} was formed after prolonged UV photolysis and assigned to $\nu_{C\equiv N}$ of INC (Table 3.2.6). Thus, any uncomplexed ICN in ICN/O_3 matrices will photoisomerise to form INC in the same way as does ICN isolated in argon (Fig. 3.2.1).

Solid Oxygen Matrices. Prolonged quartz-filtered ($\lambda > 240$ nm) photolysis of ICN deposited in solid oxygen rather than ozone/Ar matrices was required before any

new bands were formed (Table 3.2.6 and Fig. 6.2.9) and the latter were assigned on the basis of their resemblance to those detected in the ICN/O_3 experiments. The oxygen matrix like the ozone/Ar matrix consequently acts as an oxygen atom source but, unlike the situation with ozone, no complex is formed; thus very harsh photolysis conditions are required to form INCO, IC(O)NCO and O_2ICN.

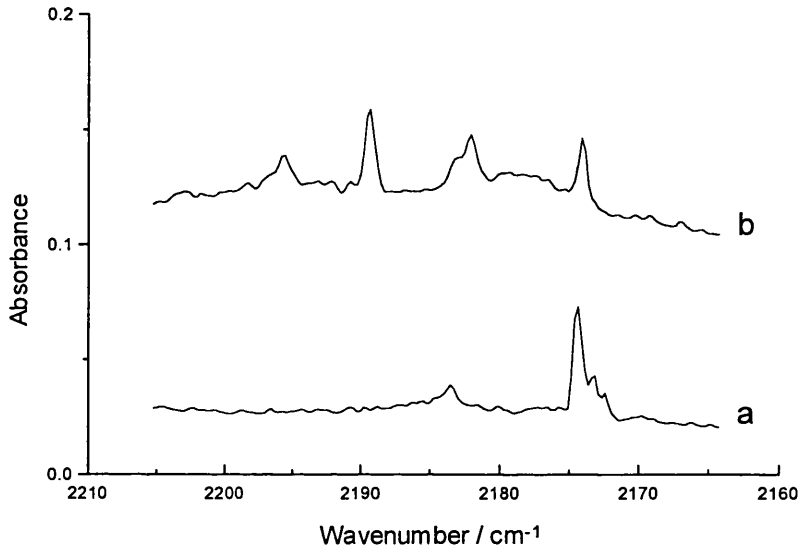

Figure 6.2.9. *Infrared spectra of an ICN/O_2 matrix after (a) deposition and (b) prolonged photolysis ($\lambda > 240$ nm).*

3.2.2 PHOTOCHEMICAL PATHWAY

The first step in the photochemical pathway (Scheme 3.2.1a) is the formation of a weak complex between ICN and ozone after co-deposition of the two precursors in solid argon; this complex dramatically changes the photochemistry of ozone allowing dissociation to occur at longer wavelengths than those required for uncomplexed ozone. The complex is of the type $O_3\cdots ICN$, as an I–O bond forms first; after irradiation ($\lambda > 650$ nm) via a charge-transfer type intermediate the iodoso species OI–CN is produced. Photolysis with shorter wavelength radiation ($\lambda > 350$ nm) results in the destruction of OI–CN and, at the same time, the formation of INCO, thus demonstrating a link between these two species. The photo-induced conversion

of OI–CN into INCO is considered to take place by the formation of a cyclic intermediate to form the N–O bond of the ICNO intermediate which then readily isomerises into the isocyanate INCO. Such rearrangements can go via the conversion of the nitrile oxide to form an oxazirene, which converts into an acylnitrene and then rearranges to the isocyanate.[20] Other possible mechanisms are discussed elsewhere.[27] Previous studies,[20,27,28] and the work presented here, have been unable to generate –CNO in concentrations sufficient for infrared detection due to the efficient photoisomerisation process in matrices; the same radiation that produces –CNO results in the isomerisation of the latter to –NCO.

Further Pyrex-filtered (λ > 290 nm) and quartz-filtered (λ > 240 nm) photolysis produced carbonyl bands belonging to the transoid conformer of iodocarbonyl isocyanate, IC(O)NCO (Scheme 3.2.1b). Only the transoid conformer is observed due to its greater stability than the cisoid (cisoid bands were only observed after prolonged quartz-filtered irradiation in a single experiment). Upon photolysis of INCO, the reaction mechanism is believed to proceed by a series of radical interconversions,[29,30] forming other products such as N_2, I_2, and CO on route; these could complex with the carbonyl group and contribute to the large number of $\nu_{C=O}$ bands detected. The detection of CO in the matrix after photolysis is consistent with the proposed mechanism. There is a possibility that the dimer, $I_2NC(O)NCO$, is formed since bands are detected which tentatively may be assigned to ν_{NC} (NCN); these bands could also belong to carbonyl diisocyanate $CO(NCO)_2$. At this stage no evidence is available to distinguish between the two possibilities, although it is certain that more than one species is responsible for the many $\nu_{C=O}$ bands detected.

Production of the iodyl bands (ν_{IO_2}) after Pyrex-filtered irradiation (λ > 290 nm) is believed to occur via the reaction between isolated ICN and excited molecular oxygen to form O_2ICN (Scheme 3.2.1c). Molecular oxygen could also react with INCO (formed after λ > 350 nm irradiation) to form O_2INCO, although the intensities of INCO bands were seen to increase after Pyrex-filtered photolysis rather than decrease, as would be the case if this reaction had occurred.

Scheme 3.2.1

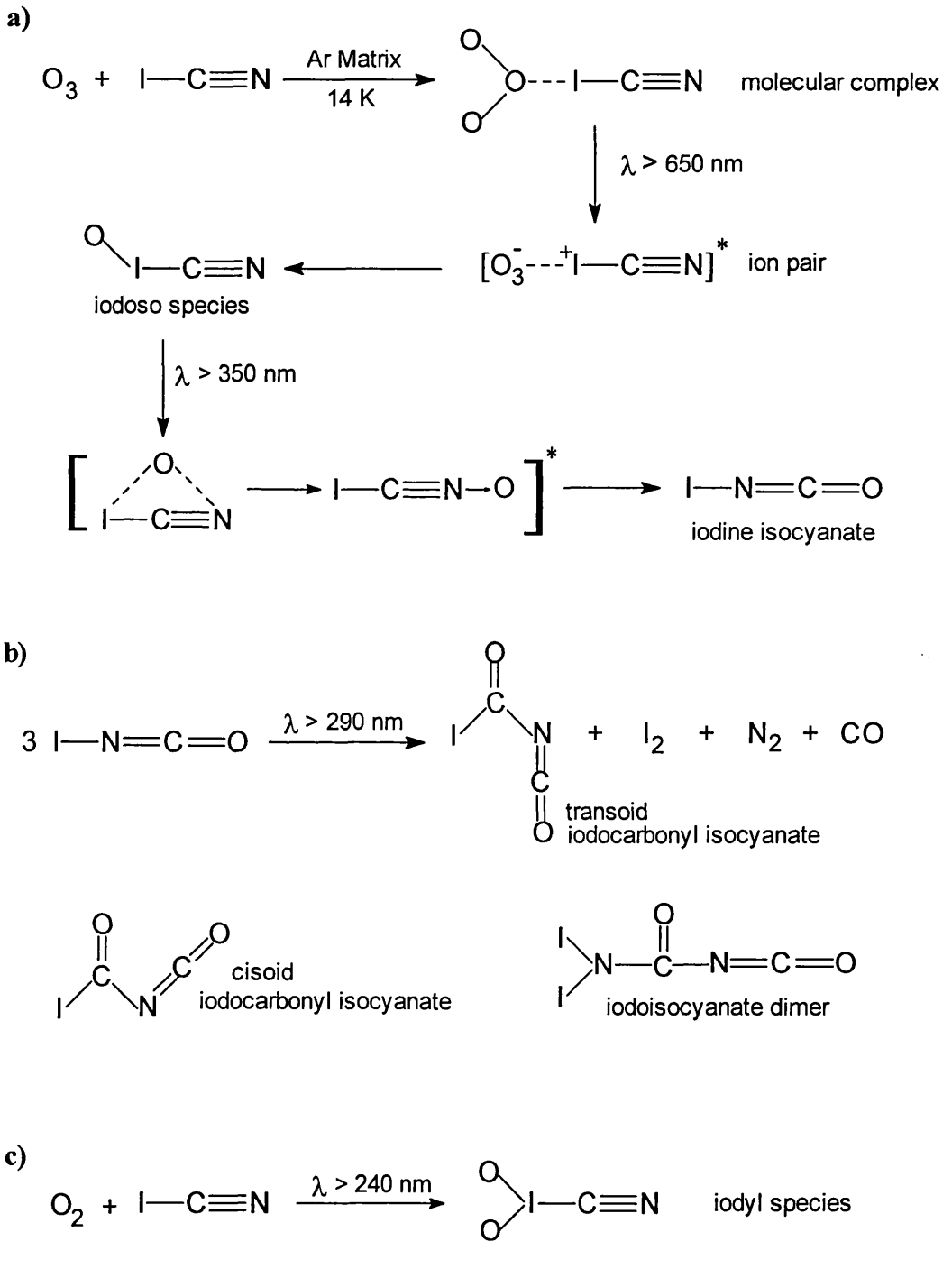
a)
Ar Matrix
14 K
molecular complex
λ > 650 nm
ion pair
iodoso species
λ > 350 nm
iodine isocyanate
b)
λ > 290 nm
transoid
iodocarbonyl isocyanate
cisoid
iodocarbonyl isocyanate
iodoisocyanate dimer
c)
λ > 240 nm
iodyl species

Table 3.2.1. *Infrared bands/cm^{-1} of iodine cyanide, ICN, trapped in a variety of matrices at 14 K*

Ar	O_2	$^{16}O_3$/Ar	$^{18}O_3$/Ar	Assignment
2190.5vw, sh[a]		2189.9vw[a]		
2178.4w, sh[a]	2183.5vw[a]	2183.4vw[a]	2178.5vw[a]	
2174.5vw, sh[a]	2174.4vw[a]	2180.5w[a]	2174.1vw[a]	
	2173.2vw[a]	2178.1w[a]		
		2174.8vw[a]		
2170.3w	2172.5vvw	2170.4w	2170.4vw	$\nu_{C\equiv N}$
		2153.5w[d]		
			2149.2vw	$\nu_1 + \nu_3$ ($^{16}O_3$)
		2111.0vw[d]		
		2108.5vw		$3\nu_2$ ($^{16}O_3$)
			1996.4vw[d]	
			1993.7vw	$3\nu_2$ ($^{18}O_3$)
		1109.4vw		ν_1 ($^{16}O_3$)
			1043.2w	ν_1 ($^{18}O_3$)
		1039.6mw		ν_3 ($^{16}O_3$)
		1033.9w, sh[b]		
		1028.6w[b]		
			998.9vw[b]	
			989.6vw[d]	
			983.2ms	ν_3 ($^{18}O_3$)
			972.7vw, sh[b]	
	725.2vw			?
		706.9vvw[b]		
		704.9mw		ν_2 ($^{16}O_3$)
		698.7w[b]		
			664.2mw	ν_2 ($^{18}O_3$)
			653.7w[b]	
506.1w[a]				
486.5w	*c*	486.5vw	*c*	ν_{I-C}
485.1w[d]				
460.1ms[a]				
456.1ms[a]				

[a] Bands of ICN aggregates. [b] Complex bands of O_3. [c] Bands are too weak to detect. [d] Bands due to matrix site effects.

Table 3.2.2. *Infrared bands/cm^{-1} assigned to ozone isotopomers after deposition of mixed ozone ($^{16}O_{3-x}{}^{18}O_x$) and ICN in argon at 14 K*

ν_1	ν_2	ν_3	$3\nu_2$	Assignment[a]
1106.5vw, sh[b]		1040.3m, sh[b]	2111.1vw[b]	
1103.8vw	705.1vw	1039.5ms	2108.6vw	16-16-16
	704.3vw, sh[b]	1037.9m[b]	2102.2vw, sh[c]	
	703.5vw ,sh[c]	1035.0mw, sh[c]		
		1032.8mw, sh[c]		
		1026.5ms, sh[b]	2090.0vw	
1091.7w	688.8w	1025.5ms	2087.7vw	16-16-18
1090.2w[b]	688.1w, sh[b]	1022.9m[b]	2083.9vw, sh[c]	
		1020.0mw, sh[c]		
		1018.8mw ,sh[b]		
		1017.5m, sh[b]	2060.1vw[b]	
d	672.1vw	1016.6m	2057.6vw	18-16-18
	671.4vw, sh[b]	1015.2mw, sh[b]	2055.9vw, sh[c]	
		1012.8w, sh[c]		
		1009.8w, sh[c]		
1077.2vw[b]	698.8vw[b]	1006.9m, sh[b]	2049.8vw, sh[b]	
1075.5vw	697.4vw	1006.1m	2047.4vw	16-18-16
	695.8vw[c]	1005.4m, sh[b]	2045.1vw, sh[c]	
		1004.5m, sh[b]		
		1001.5mw, sh[c]		
		999.1mw, sh[c]		
1063.3vw, sh[b]		992.4ms, sh[b]	2027.4vw[b]	
1061.9vw	681.5w	991.5ms	2024.9vw	18-18-16
1060.5vw, sh[b]	680.7w, sh[b]	989.0m[b]	2021.4vw, sh[c]	
		987.5mw, sh[c]		
		986.1mw, sh[c]		
		983.2m, sh[b]	1996.3vw[b]	
e	*f*	982.3m	1993.7vw	18-18-18
		980.9m, sh[b]	1990.1vw, sh[c]	
		977.8w, sh[c]		
		976.5w, sh[c]		

[a] Represents the isotopomer arrangement of ozone. [b] Bands due to matrix site effects. [c] Complex bands of O_3. [d] Bands are too weak to be detected. [e] Bands are obscured by ν_3 bands of O_3. [f] Bands are obscured by CO_2 (663 cm^{-1}).

Table 3.2.3. *Infrared bands/cm^{-1} formed after visible (λ > 650 nm) irradiation of matrices containing ICN and ozone, and attributed to OICN*

$^{16}O_3$/Ar	$^{18}O_3$/Ar	$^{16}O_{3-x}{}^{18}O_x$/Ar	Assignment
760.6w		760.2vw	ν_1-^{16}O
	727.6w[a]		
	726.2vw[a]		
	721.0w	722.2vw	ν_1-^{18}O

[a] Bands due to matrix site effects.

Table 3.2.4. *Infrared bands/cm^{-1} detected after photolysis ($\lambda > 350$ nm) of matrices containing ICN and ozone, and attributed to INCO*

$^{16}O_3$/Ar	$^{18}O_3$/Ar	$^{16}O_{3-x}{}^{18}O_x$/Ar	Assignment
		2198.0ms, sh[a]	
2196.9ms		2197.1s	$\nu_{N=C}$ (–NC^{16}O)
2192.5mw, sh[a]		2195.5ms, sh[a]	
		2178.1mw, sh[a]	
	2177.0mw	2177.0ms	$\nu_{N=C}$ (–NC^{18}O)
	2175.6w[a]	2175.5mw, sh[a]	
	2148.3vw		?
2149.0vw	2147.7vw	2147.7vw	?
1275.1vvw, sh[a]		1277.6vvw[a]	
		1274.5vvw[a]	
1273.2vw		1272.9vw	$\nu_{C=O}$ (–NC^{16}O)
		1250.8vw[a]	
		1249.0vvw[a]	
		1247.2vw[a]	
		1245.0vvw[a]	
	1226.8vw[a]	1226.6vvw[a]	
	1226.0vw[a]	1225.8vvw[a]	
	1224.7vw	1224.7vw	$\nu_{C=O}$ (–NC^{18}O)
596.1vw[a]			
593.9vw[a]			
591.6w			$\delta_{NC^{16}O}$ (o-o-p)[b]
586.3vw[a]			
583.0vw[a]			
580.4vw[a]		578.7vw, sh[a]	
577.0w[a]		577.5vw, sh[a]	
		576.8vw[a]	
		576.6vw, sh[a]	
		575.6vw, sh[a]	
	572.8vw[a]	572.5vw, sh[a]	
	571.9vw	571.6vw	$\delta_{NC^{18}O}$ (o-o-p)
	567.7vw[a]		
	561.8vw[a]		

[a] Bands due to matrix site effects or aggregates. [b] $\delta_{NC^{16}O}$ (i-p) and $\delta_{NC^{18}O}$ (^{18}O) (i-p) bands are obscured by CO_2 impurity bands at c. 667 cm^{-1}.

Table 3.2.5. *Infrared bands/cm^{-1} formed after Pyrex-filtered ($\lambda > 290$ nm) photolysis of ICN/O_3 matrices at 14 K*

$^{16}O_3$/Ar	$^{18}O_3$/Ar	$^{16}O_{3-x}{}^{18}O_x$/Ar	Assignment
2205.6w		2205.6vw	
		2202.3vw	
2200.5ms		2200.9mw	$\nu_{N=C}$ (–NC^{16}O)
		2182.8vw	
	2180.9mw	2181.3w	$\nu_{N=C}$ (–NC^{18}O)
2137.6vw			$\nu_{C\equiv O}$ (CO)
1787.9w		1787.9w	}
1786.1w, sh			}
1785.0vw, sh		1785.8mw	} $\nu_{C=^{16}O}{}^{a}$
1783.7vw, sh		1784.2w	}
1780.8vw		1780.8vw	}
1779.3w		1779.3vw	}
	1742.2vw, sh	1741.0w, sh	}
	1741.2vw	1740.0w	}
	1740.2vw, sh	1739.0vw, sh	}
	1739.0vw	1737.9vw, sh	} $\nu_{C=^{18}O}{}^{a}$
	1738.1vvw	1736.9vw, sh	}
	1736.9vw	1734.6vw	}
		1733.5vw	}
		1279.6vw, sh	
1278.3w		1278.4vw	$\nu_{C=O}$ (–NC^{16}O)
	1230.6vw	1231.0vvw	$\nu_{C=O}$ (–NC^{18}O)
833.3vw			}
832.5vvw, sh			}
828.0vvw		828.3vvw	} ν_{NC} (NCN) ?
825.5vvw		825.3vvw	}
		823.8vvw	}
		822.0vvw	}
		815.6vw, sh	}
814.8vw		814.8vw, sh	} $\nu_{a\ I^{16}O_2}{}^{b}$
813.4vw		813.8vw	}
		812.5vw	}
		804.0vvw	}
		801.7vw, sh	}
		800.6vw	} $\nu_{a\ I^{16}O^{18}O}{}^{b}$
		798.8vw, sh	}
		798.0vw, sh	
	787.6vw		}
	786.2vw, sh		} $\nu_{a\ I^{18}O_2}{}^{b}$
	784.0vw		}

continued

Table 3.2.5 continued.

$^{16}O_3$/Ar	$^{18}O_3$/Ar	$^{16}O_{3-x}{}^{18}O_x$/Ar	Assignment
777.8vvw			$\nu_a\, I^{16}O_2$

[a] Carbonyl bands attributable to either IC(O)NCO, $I_2NC(O)NCO$, $CO(NCO)_2$ or to $-C{=}O\cdots I_2$ complexes. [b] Bands attributed to O_2ICN; such bands arise from matrix site effects and/or the formation of aggregates.

Table 3.2.6. *Infrared bands/cm^{-1} detected after prolonged quartz-filtered (λ > 240 nm) irradiation of ICN/O_3 matrices at 14 K*

$^{16}O_3$/Ar	$^{16}O_{3-x}{}^{18}O_x$/Ar	O_2	Assignment
		2195.7vw	$\nu_{N=C}$ (IC(O)NCO)
		2189.4vw	$\nu_{N=C}$ (INCO)
		2138.7w	$\nu_{C\equiv O}$ (CO)
2064.8vvw, sh[a] 2062.7vw[a] 2059.1w 2057.2w[a]	*b*	2061.3vw	$\nu_{C\equiv N}$ (INC)
		1808.7vw 1807.6w 1806.5vw 1804.3vw	$\nu_{C=^{16}O}$[c]
	1723.6w 1722.4w 1718.9vw 1717.6vw	1793.0vw 1789.4vw 1784.5vw, sh 1781.6vw 1775.6vw	$\nu_{C=^{16}O}$[d]
		1273.4vw	$\nu_{C=O}$ ($-NC^{16}O$) (IC(O)NCO)
		1272.3wm 1268.6vw[a]	$\nu_{C=O}$ ($-NC^{16}O$) (INCO)
		843.6vw 841.8vvw 840.0vw 834.2vw	$\nu_a\, I^{16}O_2$ (O_2ICN)

[a] Bands due to matrix site effects. [b] Bands in this region are obscured by precursor bands. [c] Carbonyl bands attributable to either IC(O)NCO, $I_2NC(O)NCO$, $CO(NCO)_2$ or to $-C{=}O\cdots I_2$ complexes. [d] Bands are due to the cisoid conformer of IC(O)NCO.

3.3 IODINE CYANIDE AND NITROGEN DIOXIDE

The photochemically induced reaction of ICN with nitrogen dioxide was studied in order compare its reaction intermediates and products, as well as the photochemical pathway, with those determined in the ICN/O_3 reaction studied in the first part of this chapter. Nitrogen dioxide has a number of similarities with ozone not to mention some dissimilarities. For example, O_3 and NO_2 both have C_{2v} symmetry with the same angular structure with terminal oxygen atoms and both show some degree of delocalisation, while NO_2 unlike O_3, is an odd electron molecule that can form a stable dimer.

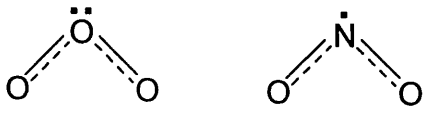

Therefore NO_2 could react with ICN in the same way as O_3 does, forming in part the same species and following the same pathway, or alternatively could react completely differently.

3.3.1 RESULTS AND DISCUSSION

Deposition of the Precursors, ICN and NO_2

The infrared spectra of ICN isolated separately in argon matrices have been recorded and are reported earlier in this chapter (section 3.2.1); the band wavenumbers closely match those reported elsewhere for ICN in the gas phase[9–11] and in various matrices.[12,13] The infrared spectra recorded for NO_2 isolated in solid argon contain bands that agree well with those reported for NO_2 in the gas phase.[9] As expected, infrared absorptions of the dimer, dinitrogen tetroxide (N_2O_4), were also observed and agree with those detected elsewhere.[9,31–33] The spectroscopic data are listed in Appendix A2. Ultraviolet photolysis of NO_2 in an argon matrix produced no new bands, only the intensities of the bands belonging to the NO_2/N_2O_4 equilibrium varied slightly.

On co-deposition of ICN/Ar and NO_2/Ar samples (ICN/NO_2/Ar = 1:0.5:3000), the infrared spectrum exhibited bands that resembled those detected in the infrared spectra of ICN or nitrogen dioxide isolated separately in argon (Table 3.3.1). No bands could be assigned to a complex formed between ICN and nitrogen dioxide, unlike the situation with ICN and ozone discussed in section 3.2.1. Moreover, it was found that harsh UV irradiation (λ > 240 nm) of ICN/NO_2/Ar matrices was required before any new bands were formed.

Photolysis of ICN/NO_2 Matrices

Deposition of ICN/NO_2/Ar matrices and their subsequent photolysis cycles using quartz-filtered radiation for varying periods of time created a number of new bands which are grouped according to the chemical species to which they refer.

INCO. The iodine isocyanate bands were first formed after quartz-filtered photolysis (λ > 240 nm) for 1 h of ICN/NO_2/Ar matrices and their intensities continued to increase upon further irradiation (Table 3.3.2). The weak band detected at 2198.2 cm^{-1} is assigned to $\nu_{N=C}$ of the –NCO unit (Fig. 3.3.1), while a weak, broad band occurring at 570 cm^{-1} is assigned to the –NCO out-of-plane bend. These bands are attributed to an INCO species on the basis that a –NCO group has been identified and also because the wavenumbers compare extremely well with those detected for halogen isocyanate molecules, XNCO (X = Cl, Br, or I) in the vapour state,[17] viz. $\nu_{N=C}$ = 2212.2 cm^{-1} (ClNCO), $\nu_{N=C}$ = 2198.0 cm^{-1} (BrNCO), and $\nu_{N=C}$ = 2201.1 cm^{-1} (INCO). The $\nu_{C=O}$ band of INCO was expected to occur near 1273 cm^{-1}, as in the ICN/O_3 experiment, but the N_2O_4 precursor bands occurring in the range 1282.8–1257.0 cm^{-1}, obscured this band. Additional bands appeared alongside the INCO fundamental bands and, after concentration and annealing experiments, were found to belong to INCO occupying different sites in the matrix. The formation of $\nu_{N=C}$ bands at the expense of nitrogen dioxide bands can be seen in Fig. 3.3.2.

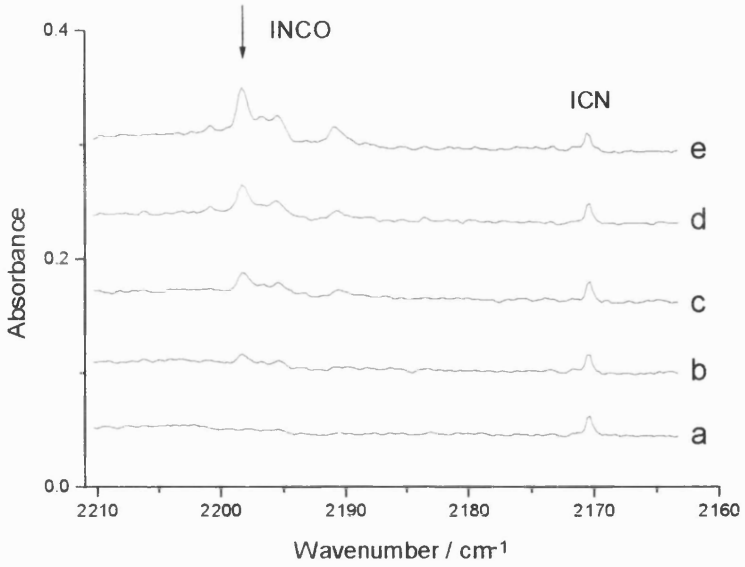

Figure 3.3.1. *Infrared spectra of an ICN/NO_2/Ar matrix after (a) deposition, (b) quartz-filtered ($\lambda > 240$ nm) photolysis for 1 h, (c) $\lambda > 240$ nm photolysis for 5 h, (d) $\lambda > 240$ nm for 9 h, and (e) $\lambda > 240$ nm for 30 h. Spectra show the $\nu_{C\equiv N}$ band of ICN and the growth of the $\nu_{N=C}$ band attributed to INCO.*

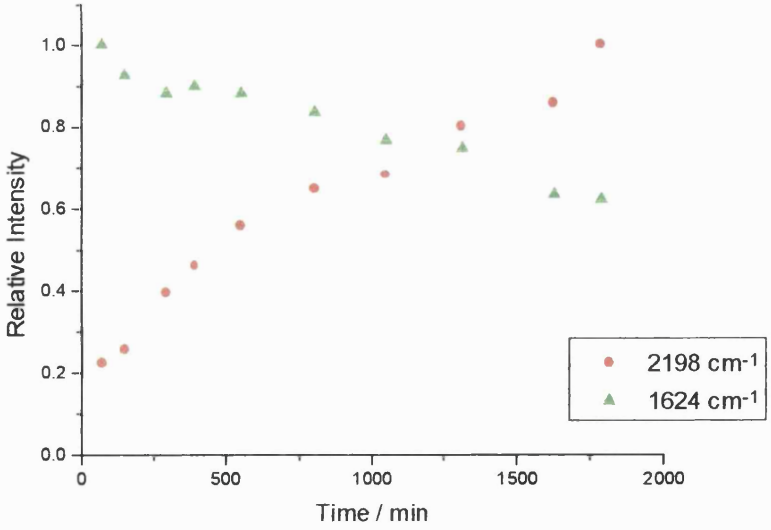

Figure 3.3.2. *IR absorbance for the new $\nu_{N=C}$ band of INCO at 2198 cm^{-1} and for the depleting nitrogen dioxide (ν_1) band at 1624 cm^{-1} as a function of photolysis time.*

No bands attributable to iodonitrile oxide (I–C≡N→O) were detected in the infrared spectra after photolysis, just as in the case of ICN and ozone, therefore the isocyanate seems to be the favoured photoproduct once again. Warming of the matrix caused the intensities of the bands situated at 2198.2, 2196.7, and 2195.4 cm^{-1} all to increase slightly while that of the 2190.9 cm^{-1} band to decrease slightly.

Other Species. Again a band assigned to $\nu_{C\equiv N}$ of the photoisomer INC was formed after UV photolysis (Table 3.3.2). This band, occurring at 2057.2 cm^{-1}, is detected when the concentration of ICN in the matrix is high, or alternatively when the concentration of the NO_2 reagent is low, *i.e.* any unreacted ICN in the ICN/NO_2 matrix will photoisomerise to form INC in the same way as does ICN isolated in argon (Fig. 3.2.1).[12] In the other system investigated, ICN/O_3, bands attributable to OICN, O_2ICN and IC(O)NCO were produced upon photolysis, although in the ICN/NO_2 experiment no species of this type were detected. Photolysis of isolated NO_2/Ar matrices showed that all other new bands appearing after photolysis of ICN/NO_2/Ar matrices are due to the photodissociation of NO_2/N_2O_4 and the subsequent chemistry of the fragments NO and $(NO)_2$[34,35] (Table 3.3.2).

3.3.2 PHOTOCHEMICAL PATHWAY

The photochemically induced reactions of ICN with nitrogen dioxide are schematically shown in Scheme 3.3.1. Unlike the reaction between ICN and ozone, in which irradiation using different wavelengths (λ > 650–240 nm) created a number of new species, that between ICN and NO_2 required harsh quartz-filtered (λ > 240 nm) irradiation before any new species at all could form. However, the main photoproduct detected was INCO in both reactions even though the photochemical pathways differ. Therefore nitrogen dioxide acts as an oxygen atom source but, unlike the situation with ozone, does not form a complex. NO_2 has two terminal oxygen atoms, which are comparable to those of ozone, and so could presumably form a complex with ICN. However, as discussed in section 3.2.1, it is not the terminal atoms of ozone that are involved in the complexation with ICN but the central one. It is the central atom of O_3 and NO_2 that is the major difference between these two compounds; the oxygen atom has the higher electronegativity and therefore O_3 favours the formation of a

charge-transfer complex ($O_2O^{-}\cdots{}^{+}ICN$) while NO_2 does not. Also NO_2 is an odd electron molecule preferring to form its stable dimer N_2O_4.

Initially, UV irradiation causes NO_2 to dissociate, releasing oxygen atoms which then react with ICN to form the intermediate ICNO. As discussed previously (section 3.2.2) photoisomerisation occurs at the same time as oxidation[20,27,28] and hence INCO is detected.

Scheme 3.3.1

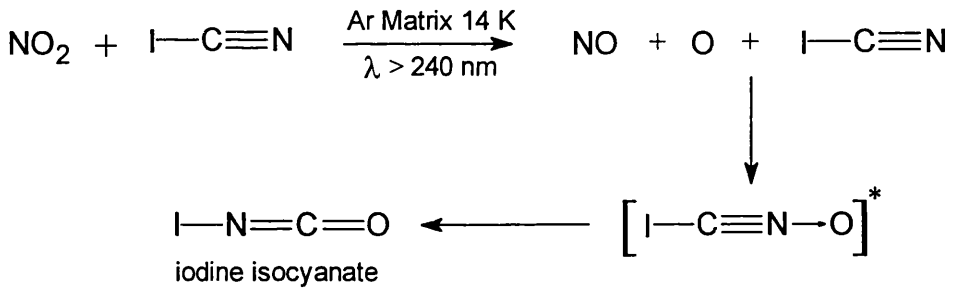

Table 3.3.1. *Infrared bands/cm^{-1} detected after deposition of ICN and NO_2 in an Ar matrix at 14 K*

Absorptions	Assignment[a]
3573.8mw	$\nu_1+\nu_2+\nu_3$ (NO_2)
2904.2mw	
2902.2m	$\nu_1+\nu_3$ (NO_2)[b]
2893.4vw	
2218.6w	$\nu_2+\nu_3$ (NO_2)
2170.4w	$\nu_{C\equiv N}$
1893.8vw	ν_1 (N_2O_2)
1829.2w, sh	ν_1 (*a*-N_2O_3)[b]
1827.9mw	
1826.1vw, sh	
1779.2vw	ν_5 (N_2O_2)
1699.4mw	ν_1 (*s*-N_2O_3)[b]
1694.6vw	
1688.3vw	
1683.8vw	
1644.5m	ν_2 (*a*-N_2O_3)[b]
1642.3mw	
1624.0s	
1321.4mw	ν_1 (NO_2)[b]
1308.4vw	
1304.5vw	
1291.2w, sh	
1290.3w	
1287.3w	
1282.8vw	
1278.1vw	
1269.9vw	
1265.8vw	ν_{11} (N_2O_4)[b]
1263.8vw	
1260.1vw	
1257.0vw	
903.5vw	
896.9vw	
786.9w	ν_4 (*a*-N_2O_3)
756.2vw	
753.7vw	ν_2 (NO_2)[b]
751.4vw	
748.8vw	
746.1vw	ν_{12} (N_2O_4)[b]
720.8w	
640.4w	ν_8 (N_2O_4)[b]
638.4w	
636.7w	
528vw, br	ν_6 (N_2O_4)

[a] See Appendix A2 for reference to the band assignments used for the oxides of nitrogen. [b] The number of bands are due to matrix site effects or to aggregates.

Table 3.3.2. *Infrared bands/cm^{-1} detected after quartz-filtered photolysis ($\lambda > 240$ nm) of ICN/NO_2/Ar matrices at 14 K*

Absorptions	Assignment
2824.6vw 2822.5vw	
2200.8vw 2198.2w 2196.7vw 2195.4vw 2190.9vw	$\nu_{N=C}$ (INCO)[a]
2057.2vw	$\nu_{C\equiv N}$ (INC)
1871.9vw 1870.4vw, sh	ν_{NO} (NO)[a]
1863.5vw	*cis*-(*s*-$NO)_2$[b]
1776.2mw	*cis*-(*a*-$NO)_2$[b]
1757.4vw	*trans*-(*a*-$NO)_2$[b]
570w, br	δ_{NCO} (o-o-p) (INCO)
520w, br	

[a] The number of bands are due to matrix site effects or to aggregates.
[b] *a* - asymmetric arrangement of $(NO)_2$, *s* – symmetric arrangement of $(NO)_2$.

3.4 CONCLUDING REMARKS

Iodine cyanide has been co-deposited with ozone and, separately, with nitrogen dioxide in argon matrices at 14 K. The photochemically induced reactions of each system have been examined. Iodine isocyanate (INCO) is the major product detected in both reactions; in fact it is the only product in the ICN/NO_2 system. Although bands attributed to this species are detected when ICN reacts with either O_3 or NO_2, the photochemical pathway for the ICN/NO_2 reaction differs considerably from that for ICN/O_3 reaction (Schemes 3.2.1 and 3.3.1).

In the case of ICN/O_3, ICN does indeed react with ozone similarly to other iodine-containing precursors such that an ozone···precursor complex was detected upon deposition as well as an iodoso- and an iodyl-species being detected after photolysis. However no bands belonging to a hypoiodo-species were detected due to the fact that the presence of a nitrogen atom in ICN allowed other reactions and rearrangements to take place.

Several intermediates and species observed in this chapter are characterised by their infrared absorption bands and their photochemical behaviour. These species are compared with those produced by the analogous photochemically induced reactions of $BrCN/O_3$ and $BrCN/NO_2$, both to confirm the identification of the species and to note any trends in the spectra (chapter 4).

3.5 REFERENCES

(1) Hawkins, M.; Andrews, L., *Inorg. Chem.* **1985**, *24*, 3285–3290.

(2) Andrews, L.; Withnall, R.; Hunt, R., *J. Phys. Chem.* **1988**, *92*, 78–81.

(3) Withnall, R.; Hawkins, M.; Andrews, L., *J. Phys. Chem.* **1986**, *90*, 575–579.

(4) Andrews, L.; Hawkins, M.; Withnall, R., *Inorg. Chem.* **1985**, *24*, 4234–4239.

(5) Hawkins, M.; Andrews, L.; Downs, A. J.; Drury, D., *J. Am. Chem. Soc.* **1984**, *106*, 3076–3082.

(6) Clark, R. J. H.; Dann, J. R., *J. Phys Chem.* **1996**, *100*, 532–538.

(7) Clark, R. J. H.; Dann, J. R.; Foley, L. J., *J. Phys. Chem. A* **1997**, *101*, 9260–9271.

(8) Clark, R. J. H.; Dann, J. R., *J. Phys. Chem. A* **1997**, *101*, 2074–2082.

(9) Herzberg, G. *Infrared and Raman Spectra of Polyatomic Molecules*; Van Nostrand: NY; 1945.

(10) Thompson, G.; Maki, A. G., *J. Mol. Spectrosc.* **1993**, *160*, 73–83.

(11) Hemple, S.; Nixon, E. R., *J. Chem. Phys.* **1967**, *47*, 4273–4274.

(12) Fraenkel, R.; Haas, Y., *Chem. Phys. Lett.* **1993**, *214*, 234–240.

(13) Grzybowski, J. M.; Carr, B. R.; Chadwick, B. M.; Cobbold, D. G.; Long, D. A., *J. Raman Spectrosc.* **1976**, *4*, 421–429.

(14) Milligan, D. E.; Jacox, M. E., *J. Chem. Phys.* **1967**, *47*, 278–285.

(15) Brosset, P.; Dahoo, R.; Gauthier-Roy, B.; Abouaf-Marguin, L.; Lakhlifi, A. L., *Chem. Phys.* **1993**, *172*, 315–324.

(16) Dimitrov, A.; Seppelt, K.; Scheffler, D.; Willner, H., *J. Am. Chem. Soc.* **1998**, *120*, 8711–8714.

(17) Devore, T. C., *J. Mol. Struct.* **1987**, *162*, 287–304.

(18) Gerke, M.; Schatte, G.; Willner, H., *J. Mol. Spectrosc.* **1989**, *135*, 359–369.

(19) Pasinszki, T.; Westwood, N. P. C., *J. Phys. Chem. A.* **1998**, *102*, 4939–4947.

(20) Maier, G.; Teles, J. H., *Angew. Chem., Int. Ed. Engl.* **1987**, *26*, 155–156.

(21) Klapstein, D.; Nau, W. M., *Spectrochim. Acta* **1994**, *50A*, 307–316.

(22) Durig, J. R.; Guirgis, G. A.; Krutules, K. A.; Phan, H.; Stidham, H. D., *J. Raman Spectrosc.* **1994**, *25*, 221–232.

(23) Sullivan, J. F.; Nandy, S. K.; Lee, M. J.; Durig, J. R., *J. Raman Spectrosc.* **1992**, *23*, 51–60.

(24) Della Védova, C. O., *Spectrochim. Acta* **1992**, *48A*, 1179–1185.

(25) Balfour, W.J.; Fougere, S. G.; Klapstein, D.; Nau, W. M., *Spectrochim. Acta* **1994**, *50A*, 1039–1046.

(26) Birckenbach, L.; Linhard, M., *Ber. Dt. Chem. Ges.* **1930**, *63*, 2544–2558.

(27) Taylor, G. A., *J. Chem. Soc., Perkin Trans. 1* **1985**, 1181–1184.

(28) Bondybey, V. E.; English, J. H.; Matthews, C. W.; Contolini, R. J., *Chem. Phys. Lett.* **1981**, *82*, 208–212.

(29) Gottardi, W.; Henn, D., *Monatsh. Chem.* **1970**, *101*, 11–18.

(30) Gorbatenko, V. I., *Tetrahedron* **1993**, *49*, 3227–3257.

(31) Begun, G. M.; Fletcher, W. H., *J. Mol. Spectrosc.* **1960**, *4*, 388–397.

(32) Andrews, B.; Anderson, A., *J. Chem. Phys.* **1981**, *74*, 1534–1537.

(33) Bibart, C. H.; Ewing, G. E., *J. Chem. Phys.* **1974**, *61*, 1284–1292.

(34) Fitzmaurice, D. J.; Frei, H., *J. Phys. Chem.* **1992**, *96*, 10308–10315.

(35) Laane, J.; Ohlsen, J. R., *Prog. Inorg. Chem.* **1980**, *27, 465*–513.

Chapter 4

Photochemically Induced Reactions of Bromine Cyanide

4.1 INTRODUCTION

The photochemically induced reactions of low-temperature argon matrices containing either bromine cyanide/ozone or bromine cyanide/nitrogen dioxide have been studied by FTIR spectroscopy and are reported in this chapter. The aim of this study is to extend the number of known reactions of halogen cyanides with either O_3 or NO_2 in argon matrices in order to compare the photoproducts and photochemical pathways with those produced by the ICN/O_3 and ICN/NO_2 reactions (chapter 3). Any similarities between these ICN and BrCN reactions will help to confirm the identification of the proposed photoproducts as well as generating trends in the spectra.

It is of interest whether BrCN will form a complex with ozone upon deposition, like ICN did, or whether BrCN will behave like other bromine-containing compounds, studied later in this thesis and elsewhere[1,2] by not complexing with ozone. Therefore, the question of whether or not ozone only forms a complex with a halogenated compound if the halogen is iodine will be answered.

4.2 BROMINE CYANIDE AND OZONE

Since the photochemically induced reaction of ICN with ozone in argon matrices yielded an array of intermediates and products, the same reaction with another halogen cyanide, BrCN, is chosen for investigation. It is expected that photoproducts analogous to the ones formed by the ICN/O_3 reaction will be detected, such as OBrCN, BrNCO, and BrC(O)NCO etc.. However, there is a strong possibility that a different photochemical pathway may occur based on the fact that the iodoalkane/O_3 reaction pathway differs from that of the bromoalkane/O_3 reaction pathway.[1-3]

4.2.1 RESULTS AND DISCUSSION

Deposition of the Precursors, BrCN and O_3

The infrared spectra of BrCN isolated separately in argon matrices (BrCN/Ar = 1:4000 to 1:8000) and in oxygen matrices ($BrCN/O_2$ = 1:5000) have been recorded (Table 4.2.1 and Fig. 4.2.1). The BrCN band wavenumbers were found to be in close agreement with those reported elsewhere for these species in the gas phase[4] and in various matrices.[5,6] Increasing the concentration of BrCN resulted in the appearance of additional bands appearing alongside the fundamental bands. These concentration-dependent bands are due to small aggregates of BrCN, sustained by the conditions of the matrix. Ultraviolet (λ > 240 nm) photolysis of Ar matrices containing BrCN produced no new bands, compared to the situation with ICN in which a new band belonging to INC was formed upon photolysis. Hence BrCN differs from ICN upon photolysis such that BrCN does not photoisomerise in the matrix.

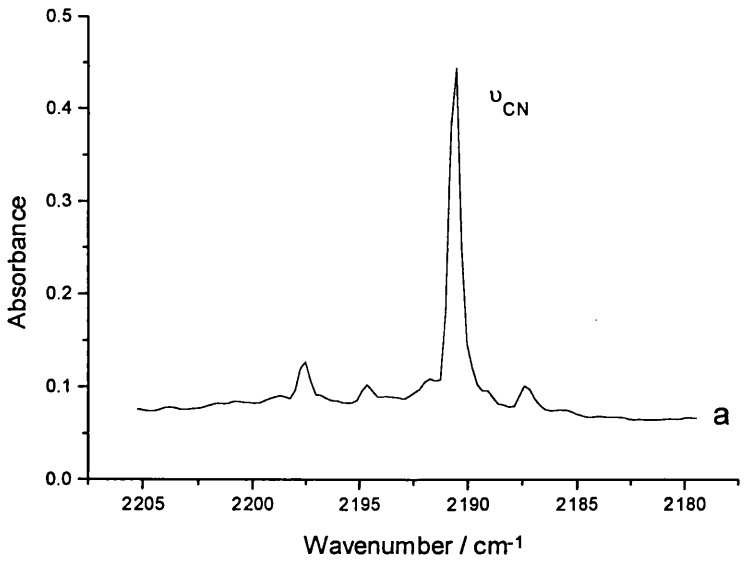

Figure 4.2.1. *Infrared spectrum of an argon matrix containing BrCN after (a) deposition. The spectrum shows the* $\nu_{C\equiv N}$ *band of BrCN and its aggregates.*

The infrared spectra of BrCN co-deposited with ozone in argon matrices ($BrCN/O_3/Ar$ = 1:1.5:8000) exhibited bands that resembled those detected in the

infrared spectra of BrCN and ozone[7,8] isolated separately in argon (Table 4.2.1). Some weak bands with small wavenumber shifts from the ozone fundamental bands were also detected and are attributed to ozone molecules occupying different sites in the matrix rather than to an $O_3\cdots$BrCN complex. This is because the intensities of these shifted ozone bands were unaffected by photolysis with radiation of wavelengths longer than 290 nm, contrary to the ICN/O_3 case in which similar bands were destroyed by visible irradiation ($\lambda > 650$ nm) and so were attributed to an $O_3\cdots$ICN complex. In other experiments in which ozone has been deposited with a bromine-containing compound there was likewise no evidence for complex formation[1,2] (chapter 5). In addition to the precursor bands, others attributable to small quantities of matrix-isolated water and carbon dioxide were also detected.

Isotopic ozone, $^{18}O_3$, and mixed isotopic ozone, $^{16}O_{3-x}{}^{18}O_x$, samples have also been condensed with BrCN in solid argon and the appropriate spectroscopic data are listed in Table 4.2.1.

Photolysis of BrCN/O_3 Matrices

Deposition of argon matrices containing BrCN and ozone and their subsequent photolysis cycles using quartz-filtered radiation created a number of new species which are grouped below.

BrNCO. Photolysis of argon matrices containing BrCN and ozone, using radiation with varying wavelengths ($\lambda > 650$ nm, $\lambda > 410$ nm, $\lambda > 350$ nm, and $\lambda > 290$ nm) did not produce any new bands; only after quartz-filtered irradiation ($\lambda > 240$ nm) for longer than 60 min were any produced (Table 4.2.2). Of these the medium bands detected at 2191.9 cm^{-1} with $^{16}O_3$ and at 2170.3 cm^{-1} with $^{18}O_3$ were assigned to $\nu_{N=C}$ of BrN$C^{16}O$ and BrN$C^{18}O$, respectively. Furthermore, only two bromoisocyanate isotopomer bands appeared in this region in the mixed ozone ($^{16}O_{3-x}{}^{18}O_x$) experiment, thus confirming the contribution of only one oxygen atom to the vibrational mode, $\nu_{N=C}$, of –NCO (Figs. 4.2.2, 4.2.3, and 4.2.4). The observed ^{18}O-shift of 21.6 cm^{-1} is in good agreement with that calculated for BrN$C^{16/18}O$ (22 ± 2 cm^{-1}).[9] The $\nu_{N=C}$ value for BrN$C^{16}O$ compares well with that for BrNCO in the gas phase (2198.0 cm^{-1}),[10]

(2199 cm^{-1}),[9] in a neon matrix (2196.0 cm^{-1}),[9] in an argon matrix (2191.9 cm^{-1}),[9] and condensed on a KBr disk (2164 cm^{-1}).[11] In these cases, bromoisocyanate was prepared either by the reaction of bromine vapour with silver isocyanate, AgNCO,[11] or by vacuum pyrolysis of tribromoisocyanuric acid, $(BrNCO)_3$.[12] Hence, the work presented here demonstrates for the first time the formation of BrNCO in solid matrices using the photochemical reaction between ozone and bromine cyanide, BrCN.

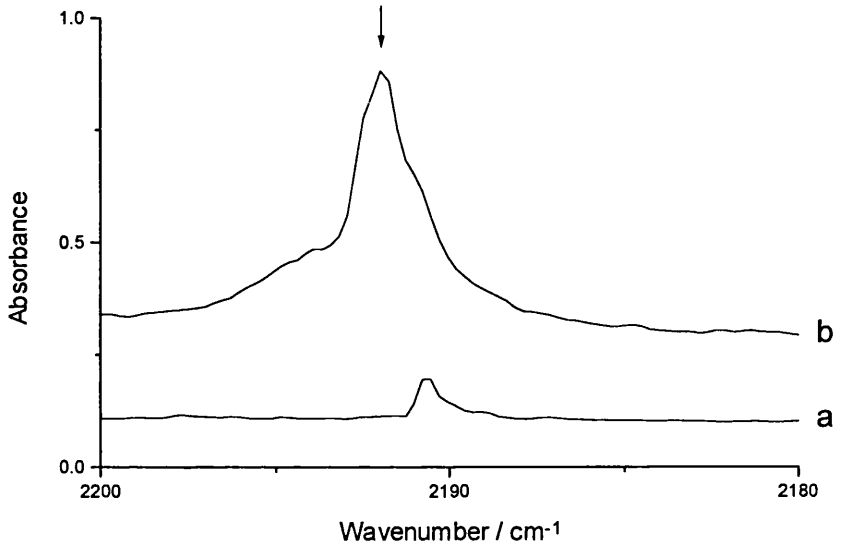

Figure 4.2.2. *Infrared spectra of a BrCN/$^{16}O_3$/Ar matrix after (a) deposition and (b) $\lambda > 240$ nm photolysis for 24 h. The spectra show new bands assigned to $\nu_{N=C}$ of BrNC^{16}O.*

Other bands that were detected after quartz-filtered photolysis of the matrix could also be attributed to BrNCO. These include very weak to weak-medium bands situated between 1299.4 and 1272.8 cm^{-1} (the ^{18}O counterparts occurring at 1252.5 and 1231.2 cm^{-1}) and assigned to the C=O stretch of BrNCO; the large number of such bands is due to the presence of different matrix sites and possible aggregates of bromoisocyanate (Table 4.2.2). Very weak bands detected around 591.2 cm^{-1} are assigned to the out-of-plane bend, δ_{NCO}; these bands compare well with those detected elsewhere for BrNCO.[9-11] However in the $^{18}O_3$ and $^{16}O_{3-x}{}^{18}O_x$ experiments, δ_{NCO}

bands were too weak to be detected. The Br–N stretch, ν_{Br-N}, expected to occur at ~500 cm^{-1}, was too weak to be detected.

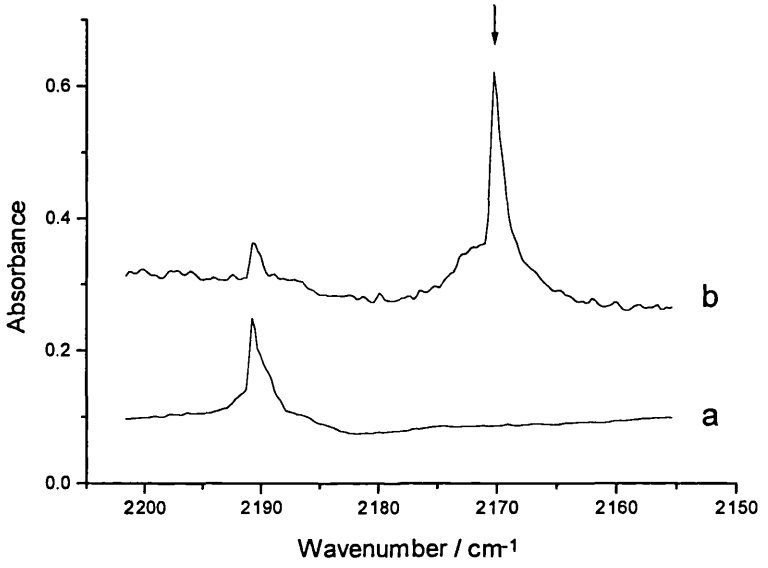

Figure 4.2.3. *Infrared spectra of a BrCN/$^{18}O_3$/Ar matrix after (a) deposition and (b) $\lambda > 240$ nm photolysis for 12 h. The spectra show new bands assigned to $\nu_{N=C}$ of BrNC^{18}O.*

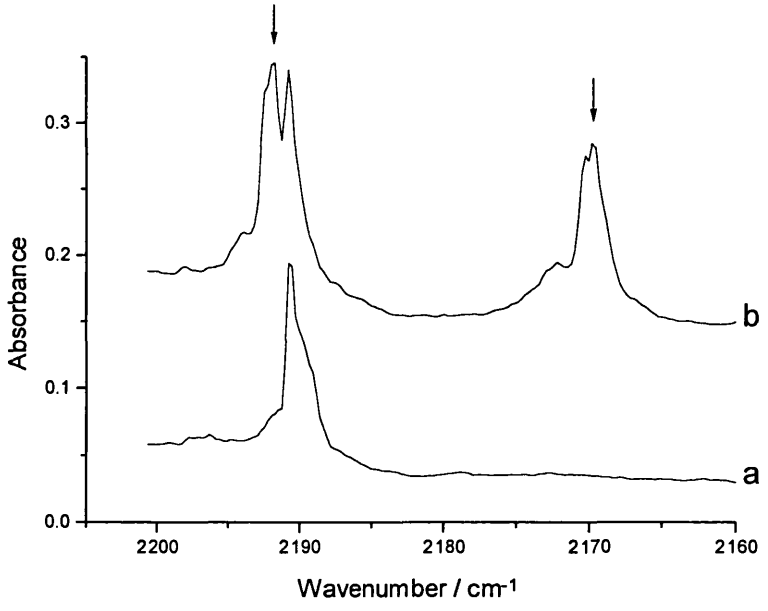

Figure 4.2.4. *Infrared spectra of a BrCN/$^{16}O_{3-x}{}^{18}O_x$/Ar matrix after (a) deposition and (b) $\lambda > 240$ nm photolysis for 8 h. The spectra show new bands assigned to $\nu_{N=C}$ of BrNC^{16}O and BrNC^{18}O.*

In a mixed-ozone experiment, a very weak band at 2223.9 cm^{-1} is cautiously assigned to $\nu_{C\equiv N}$ of the bromonitrile oxide isomer, BrCNO, based on the value of $\nu_{C\equiv N}$ detected for BrCNO elsewhere.[13,14] Its weakness and the fact that no other fundamentals were detected nor did the band appear in the other spectra suggest that the photo-induced formation of the isocyanate is the favoured pathway.

BrC(O)NCO. Like the ICN/O_3 system (chapter 3), new bands also appeared in the carbonyl region after UV irradiation of $BrCN/O_3/Ar$ matrices. In this case the $\nu_{C=O}$ bands occurred between 1817.7 and 1807.4 cm^{-1} (Table 4.2.2 and Fig. 4.2.5) and are attributed to the stable transoid conformer of bromocarbonyl isocyanate BrC(O)NCO. In the $^{18}O_3$ experiments the $\nu_{C=O}$ band for the isotopomer $BrC(^{18}O)NC^{18}O$ appeared at 1723.3 cm^{-1} while in the mixed ozone experiment both isotopomer bands were present, at 1807.4 and 1723.3 cm^{-1}. The $\nu_{C=O}$ values obtained for BrC(O)NCO compare well with those detected for IC(O)NCO discussed earlier in chapter 3, and for analogous species in the vapour phase studied elsewhere, viz. FC(O)NCO,[15,16] ClC(O)NCO,[15,16] and BrC(O)NCO.[17,18] Some new $\nu_{N=C}$ bands were detected at 2194.5 and 2193.9 cm^{-1} and are also attributed to BrC(O)NCO. These and analogous bands appearing in the ^{18}O-enriched matrices and are listed in Table 4.2.2. No bands could be assigned to the characteristic C–N stretch of the halogen carbonyl isocyanate due to the presence of ozone bands in the expected region. In one experiment extremely weak bands were detected at 800.9 and 784.7 cm^{-1} and are tentatively assigned to the Br–C stretch of BrC(O)NCO, due to their resemblance to the ν_{Br-C} band at 775 cm^{-1} for BrC(O)NCO in the gas phase[18] (none of the ν_{Br-C} bands showed evidence for bromine isotopic structure). Alternatively it is possible the bands in this region could also arise from a Br–O stretch (ν_{Br-O}), cf. spectra of Br–O bonded species in argon matrices detected elsewhere (804 cm^{-1}).[19,20] However, no bands attributed to other isocyanates were detected nor were any clearly identifiable bands found belonging to Z–BrO or $Z–BrO_2$ species, unlike the case with ICN and ozone. Furthermore, unlike the case with ICN and ozone, BrCN did not form a complex with ozone. Consequently, the $BrCN/O_3$ matrices required intense UV irradiation for many hours before the precursors would react. Warming the matrix caused the intensities of $\nu_{N=C}$ bands of BrNCO to decrease slightly while those of $\nu_{C=O}$ bands of BrC(O)NCO to increase slightly.

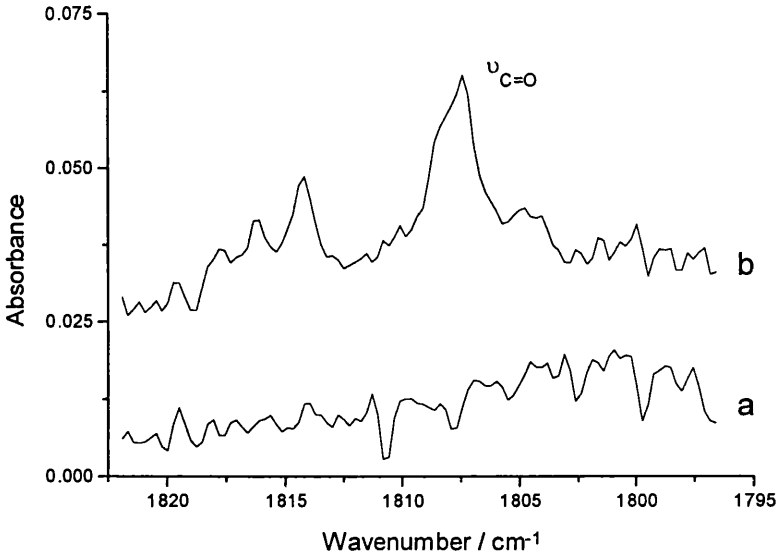

Figure 4.2.5. *Infrared spectra of a BrCN/$^{16}O_3$/Ar matrix after (a) deposition and (b) quartz-filtered ($\lambda > 240$ nm) photolysis showing new bands appearing in the carbonyl region.*

Solid Oxygen Matrices. Photolysis of BrCN in solid oxygen matrices did not result in reaction, even after tens of hours of intense UV irradiation. However, solid oxygen matrices are not very transparent, thus adding to the difficulty of observing any possible new bands.

4.2.2 PHOTOCHEMICAL PATHWAY

Unlike the reaction between ICN and ozone (chapter 3), which is wavelength-dependent, that between BrCN and ozone is time-dependent (Scheme 4.2.1). There was no evidence for the formation of a complex between BrCN and ozone nor any to suggest that any Br–O bonds are formed. Extreme photolysis conditions ($\lambda > 240$ nm for a few hours) were required to produce any new bands, those that eventually formed belonging to bromoisocyanate BrNCO. Initially, UV irradiation causes ozone to dissociate, forming oxygen atoms which then react with BrCN to form the intermediate BrCNO. Again photoisomerisation occurs at the same time as oxidation, and hence only BrNCO is detected.[14,33,34] Alternatively, cleavage of the Br–C bond

could occur and so O, Br, and CN could recombine in the matrix cage forming either BrCNO or BrNCO, the former then photoisomerising to the isocyanate. However, the fact that no bands assignable to either BrOCN or BrONC were detected makes this pathway seem unlikely.

Carbonyl bands were also detected and are attributed to the stable transoid conformer of bromocarbonyl isocyanate, BrC(O)NCO, on the basis that a similar photo-induced reaction has been performed elsewhere[12] and that chlorocarbonyl isocyanate ClC(O)NCO is formed after photolysis ($\lambda > 280$ nm) of chloroisocyanate ClNCO.[23,24] The reaction mechanism is considered to go via a sequence of radical interconversions with the formation of other products such as N_2, Br_2 and CO (bands attributed to CO were detected in some experiments). The carbonyl bands could also belong to the dimer of bromoisocyanate, $Br_2NC(O)NCO$, which has been identified earlier by Gottardi[12] after polymerisation of BrNCO. However, the fact that carbon monoxide was observed suggests that the formation of BrC(O)NCO is the favoured product.

Scheme 4.2.1

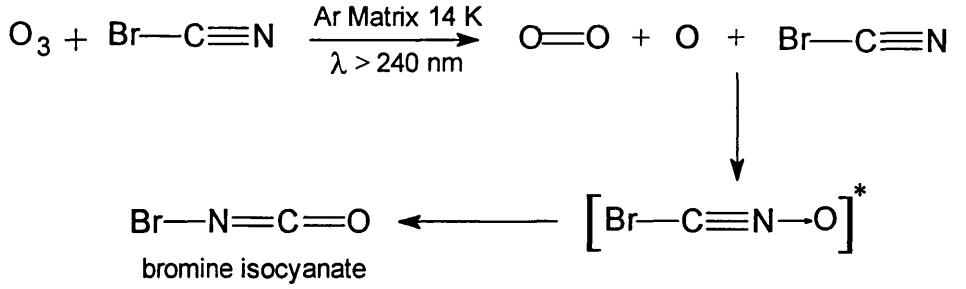
O3 + Br—C≡N
Ar Matrix 14 K
λ > 240 nm
O=O + O + Br—C≡N
[Br—C≡N→O]*
Br—N=C=O
bromine isocyanate

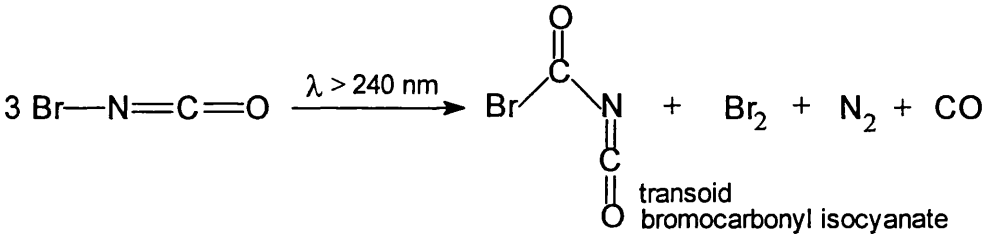
3 Br—N=C=O
λ > 240 nm
Br
N
C
O
+ Br2 + N2 + CO
transoid
bromocarbonyl isocyanate

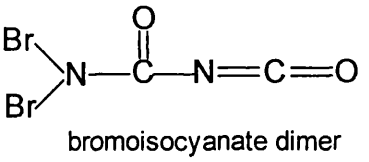
Br
Br
N—C—N=C=O
O
bromoisocyanate dimer

Table 4.2.1. *Infrared bands/cm^{-1} of bromine cyanide, BrCN, trapped in a variety of matrices at 14 K*

Ar	O_2	$^{16}O_3$/Ar	$^{18}O_3$/Ar	Assignment
2763.4w				$\nu_{Br-C} + \nu_{C\equiv N}$ [a]
2761.7w				
2536.0vw				$\delta_{BrCN} + \nu_{C\equiv N}$ [a]
2533.3w				
2211.2w[b]				
2208.8w[b]				
2197.6w[b]		2196.3vw[b]		
2190.6mw	2194.4wm	2190.7mw	2190.7wm	$\nu_{C\equiv N}$
2187.4vw[c]	2192.7w[c]			
		2149.1w		$\nu_1 + \nu_3$ ($^{16}O_3$)
		2110.7ms[c]		
		2108.6ms		$3\nu_2$ ($^{16}O_3$)
			1996.1ms[c]	
			1993.9ms, sh	$3\nu_2$ ($^{18}O_3$)
		1106.2wm		ν_1 ($^{16}O_3$)
			1043.7wm	ν_1 ($^{18}O_3$)
		1045.1vs		ν_3 ($^{16}O_3$)
		1037.7vs[c]		
		1035.9s[c]		
		1034.7 s[c]		
			973.6vs, br	ν_3 ($^{18}O_3$)
		704.2ms		ν_2 ($^{16}O_3$)
			665.4ms	ν_2 ($^{18}O_3$)
			652.4vw[c]	
576.8vvw[b]				
575.0vw	*d*	*d*	*d*	ν_{Br-C}
573.4vw[b]				

[a] BrCN in the gas phase[4] has fundamentals at 580, 368 and 2187 cm^{-1}, ν_{Br-C}, δ_{BrCN} and $\nu_{C\equiv N}$ respectively. [b] Bands of BrCN aggregates. [c] Bands due to matrix site effects. [d] Bands too weak to detect.

Table 4.2.2. *Infrared bands/cm^{-1} formed after quartz-filtered (λ > 240 nm) irradiation of BrCN/O_3 matrices at 14 K*

$^{16}O_3$/Ar	$^{18}O_3$/Ar	$^{16}O_{3-x}{}^{18}O_x$/Ar	Assignment
		2223.9vw	$\nu_{C\equiv N}$ (BrCNO) ?
		2202.7vw[a]	
2194.5w, sh		2194.0vw, sh	$\nu_{N=C}$ (–NC^{16}O) (BrC(O)NCO)
2193.9mw, sh[a]			
2192.4m, sh[a]		2192.4w, sh[a]	
2191.9m		2191.9wm	$\nu_{N=C}$ (–NC^{16}O) (BrNCO)
	2172.9w, sh[a]		
	2171.6w	2172.2w	$\nu_{N=C}$ (–NC^{18}O) (BrC(O)NCO)
	2170.3m	2170.4wm	$\nu_{N=C}$ (–NC^{18}O) (BrNCO)
	2169.6mw, sh[a]	2169.7wm[a]	
2138.6vw			$\nu_{C\equiv O}$ (CO)
1817.7vvw[a]			
1816.2vw[a]			
1814.2vw[a]			
1808.3vw, sh[a]			
1807.4w		1807.4vw	$\nu_{C=^{16}O}$ (BrC(O)NCO)
	1723.3vw	1723.3vw	$\nu_{C=^{18}O}$ (BrC(O)NCO)
1299.4vw[a]		1303.1vw[a]	
1292.6vw[a]			
1290.8wm		1291.0vw	$\nu_{C=O}$ (–NC^{16}O) (BrC(O)NCO)
1280.1wm[a]		1278.6vw[a]	
1272.8w		1272.8w	$\nu_{C=O}$ (–NC^{16}O) (BrNCO)
	1252.5w	1255.6vw	$\nu_{C=O}$ (–NC^{18}O) (BrC(O)NCO)
	1231.2w	1232.1vw	$\nu_{C=O}$ (–NC^{18}O) (BrNCO)
800.9vvw			ν_{Br-C} (BrC(O)NCO) ?
784.7vvw[a]			
592.2vw[a]			
591.2vw	*b*	*b*	δ_{NCO} o-o-p[c] (BrNCO)
587.0vw[a]			

[a] Bands are due to matrix site effects or to aggregates. [b] Bands are too weak to detect.

[c] $\delta_{NC^{16}O}$ (i-p) and $\delta_{NC^{18}O}$ (i-p) bands are obscured by CO_2 impurity bands at c. 667 cm^{-1}.

4.3 BROMINE CYANIDE AND NITROGEN DIOXIDE

The photochemically induced reaction of BrCN with nitrogen dioxide was studied in order compare its reaction intermediates and products, as well as the photochemical pathway, with those determined in the $BrCN/O_3$ reaction (section 4.2.1) and in the ICN/NO_2 reaction (chapter 3). It has already been shown in the ICN/NO_2 reaction that NO_2 acts as an oxygen atom donor enabling INCO to form, which is also formed, among others, in the ICN/O_3 reaction. Therefore the reaction of BrCN with NO_2 is expected to form the BrNCO as did the reaction of BrCN with O_3. Moreover, the photochemical pathways are expected to be the same since there was no evidence to support complex formation in the $BrCN/O_3$ system.

4.3.1 RESULTS AND DISCUSSION

Deposition of the Precursors, BrCN and NO_2

The infrared spectra of BrCN isolated separately in argon matrices have been recorded and are reported earlier in this chapter (section 4.2.1); the band wavenumbers closely match those reported elsewhere for BrCN in the gas phase[4] and in various matrices.[5,6] The infrared spectra recorded for NO_2/N_2O_4 isolated in solid argon contain bands that agree well with those reported for NO_2 and N_2O_4 in the gas phase.[4,25–27] The spectroscopic data are listed in Appendix A2. Ultraviolet photolysis of NO_2 in an argon matrix produced no new bands, only the intensities of the bands belonging to the NO_2/N_2O_4 equilibrium varied slightly.

The infrared spectra of BrCN co-deposited with NO_2 in solid argon at 14 K ($BrCN/NO_2/Ar$ = 1:2:4500) showed bands that resembled those detected in the infrared spectra of BrCN or NO_2 isolated separately in argon (Table 4.3.1). There was no evidence to suggest that a complex between BrCN and NO_2 was present, plus harsh quartz-filtered ($\lambda > 240$ nm) irradiation was required for many hours before any new bands were formed.

Photolysis of $BrCN/NO_2$ Matrices

Deposition of $BrCN/NO_2/Ar$ matrices and their subsequent photolysis cycles using quartz-filtered radiation for varying periods of time created a new species which is discussed below.

BrNCO. A familiar isocyanate band appeared weakly at 2192.0 cm^{-1} after a few hours of UV irradiation of a $BrCN/NO_2/Ar$ matrix and is thus assigned to $\nu_{N=C}$ of BrNCO (Table 4.3.2 and Fig. 4.3.1). This assignment is made on the basis that this value agrees extremely well with the $\nu_{N=C}$ value obtained for BrNCO elsewhere and from analogous systems studied in this thesis, viz. $\nu_{N=C}$ = 2198.0 cm^{-1} (BrNCO in the gas phase),[10] $\nu_{N=C}$ = 2196.0 cm^{-1} (BrNCO in a neon matrix),[9] $\nu_{N=C}$ = 2191.9 cm^{-1} (BrNCO in an argon matrix),[9] $\nu_{N=C}$ = 2191.9 cm^{-1} (BrNCO in an argon matrix, section 4.2.1), and $\nu_{N=C}$ = 2196.9 cm^{-1} (INCO in an argon matrix, chapter 3).

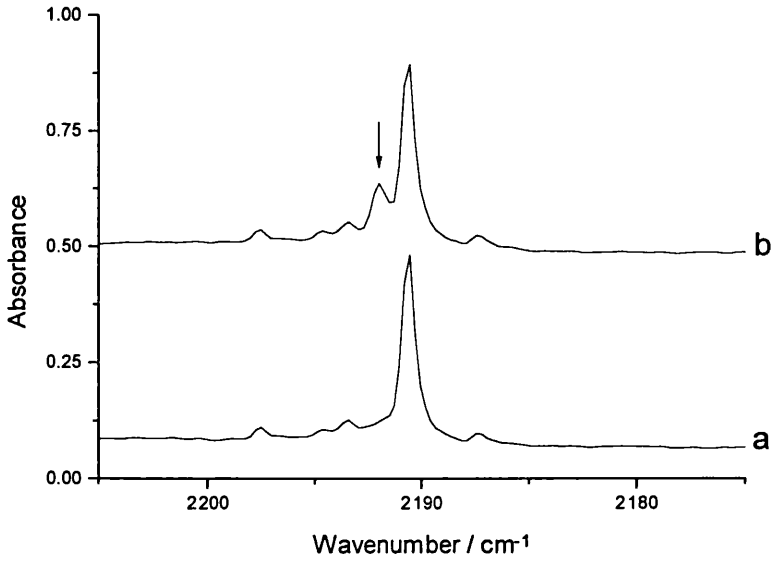

Figure 4.3.1. *Infrared spectra of an argon matrix containing BrCN and NO_2 after (a) deposition and (b) quartz-filtered photolysis ($\lambda > 240$ nm) showing the new $\nu_{N=C}$ band of BrNCO growing alongside $\nu_{C\equiv N}$ of the precursor BrCN.*

The $\nu_{N=C}$ band is the most diagnostic feature as no $\nu_{C=O}$ bands were detected due to the N_2O_4 precursor bands occurring in the same region (~1290 cm^{-1}), while the γ_{NCO} bands were too weak to be recorded. Nevertheless, the $\nu_{N=C}$ band is sufficient to ascertain that BrNCO is present due to the remarkable likeness with photoproducts produced in analogous experiments studied earlier (ICN/O_3, ICN/NO_2 and $BrCN/O_3$).

Other Species. The other systems investigated in this thesis (ICN/O_3, and $BrCN/O_3$) produced halogen carbonyl isocyanate species, XC(O)NCO upon photolysis, although in this experiment ($BrCN/NO_2$) no species of this type were detected. In fact the $\nu_{N=C}$ band of BrNCO was the only new band to appear in the IR spectrum after UV photolysis. Other bands appearing in the spectrum after UV photolysis of a $BrCN/NO_2/Ar$ matrix can be attributed to the fragments NO and $(NO)_2$[28,29] formed from the photodissociation of NO_2/N_2O_4 (Table 4.3.2).

4.3.2 PHOTOCHEMICAL PATHWAY

The photochemically induced reaction between BrCN and NO_2 requires harsh quartz-filtered photolysis before any new features form in the spectrum, just like in the situation with $BrCN/O_3$ (section 4.2.1). Extreme photolysis conditions ($\lambda > 240$ nm for many hours) eventually formed a band belonging to BrNCO in which the irradiation caused NO_2 to dissociate, forming oxygen atoms, which react with BrCN to form the undetectable intermediate BrCNO. As reported previously, photoisomerisation occurs at the same time as oxidation and hence only BrNCO is detected. The fact that such harsh photolysis conditions for such long periods of time were needed to produce any bromoisocyanate species answers the question as to why no other species (BrC(O)NCO, etc.) were formed; the low reaction rate produced insufficient quantities of BrNCO to go on and react further. The photochemical pathway is schematically shown in Scheme 4.3.1.

Scheme 4.3.1

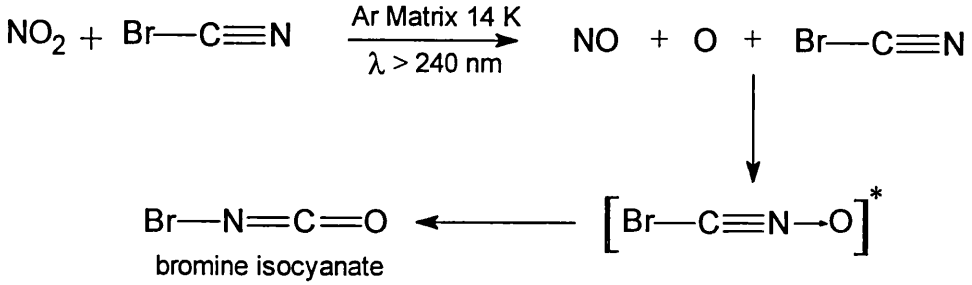
NO2 + Br—C≡N
Ar Matrix 14 K
λ > 240 nm
NO + O + Br—C≡N
[Br—C≡N→O]*
Br—N=C=O
bromine isocyanate

Table 4.3.1. *Infrared bands/cm^{-1} detected after deposition of BrCN and NO_2 in an argon matrix at 14 K*

Absorptions	Assignment[a]
2904.2m	$\nu_1+\nu_3$ (NO_2)[b]
2902.3ms	
2893.5w	
2763.4w	
2761.7w	
2218.6w	$\nu_2+\nu_3$ (NO_2)
2211.2vw	
2208.7vw	
2197.5vw	
2193.4vw	
2190.6m	$\nu_{C\equiv N}$[b]
2187.3vw	
1893.9vw	ν_1 (N_2O_2)[b]
1872.0vw	
1868.0vw	
1866.6vw	
1844.3vw	ν_1 $(a\text{-}N_2O_3)$[b]
1828.0ms	
1779.2vw	ν_5 (N_2O_2)[b]
1767.2vw	
1748.8vw	ν_9 (N_2O_4)[b]
1734.6vw	
1704.5vw	
1699.3m	
1695.8w	
1688.4w	ν_1 $(s\text{-}N_2O_3)$[b]
1684.9vw	
1675.4vw	
1669.3vw	
1653.4w	
1652.5w	
1644.4s	ν_2 $(a\text{-}N_2O_3)$[b]
1642.4ms, sh	
1624.1ms	ν_3 (NO_2)
1296.2vw	ν_1 (NO_2)[b]
1290.3m	
1287.2mw	
1282.8vw	
1277.9w	
1270.1w	
1265.8w	
1256.3w	ν_{11} (N_2O_4)[b]
985.6vw	
977.7vw	
918.1vw	
903.5mw	
896.9w	
889.6vw	
884.6vw	ν_2 $(s\text{-}N_2O_3)$[b]
873.5vw	
853.0vw	
850.3vw	
836.3vw	
796.5vw	
786.9mw	
781.6w, sh	ν_4 $(a\text{-}N_2O_3)$[b]
764.3vw	
756.3vw	
753.6w	
751.0w	ν_2 (NO_2)[b]
748.9w	
746.1vw	ν_{12} (N_2O_4)
720.9vw	
707.0w	
699.6vw	
640.3mw	ν_8 (N_2O_4)[b]
637.3mw, sh	
636.4mw	

[a] See Appendix A2 for reference to the band assignments used for the oxides of nitrogen. [b] The number of bands are due to matrix site effects or to aggregates.

Table 4.3.2. *Infrared bands/cm^{-1} formed after quartz-filtered ($\lambda > 240$ nm) photolysis of BrCN/NO_2/Ar matrices at 14 K*

Absorptions	Assignment[a]
2192.0w	$\nu_{N=C}$ (BrNCO)
1872.7vw	ν_{NO} (NO)
1863.6w	*cis*-(*s*-$NO)_2$
1776.3w	*cis*(*a*-$NO)_2$

[a] *a* – asymmetric arrangement of $(NO)_2$, *s* – symmetric arrangement of $(NO)_2$.

4.4 CONCLUDING REMARKS

Quartz-filtered (λ > 240 nm) photolysis of either $BrCN/O_3$ or $BrCN/NO_2$ in argon matrices at 14 K has been shown by FTIR spectroscopy to lead to the formation of bromine isocyanate, BrNCO. This was the only species to be detected in the $BrCN/NO_2$ reaction, unlike the situation with $BrCN/O_3$ in which bands attributed to the carbonyl isocyanate species, BrC(O)NCO, were also detected. The presence of BrC(O)NCO is supported by the fact that bands belonging to the analogous species IC(O)NCO were detected after photolytic reactions of ICN with O_3 (chapter 3).

In summary, the photochemically induced reaction between ICN and O_3 produces the same main photoproducts as that of BrCN with O_3 (XNCO and XC(O)NCO) except the photochemical pathways for each reaction differ greatly (Schemes 3.2.1 and 4.2.1). Also other intermediates such as OXCN and O_2XCN are detected in the ICN/O_3 reaction but not in the $BrCN/O_3$ reaction. The photochemically induced reaction between ICN and NO_2 produces the same photoproduct (XNCO) as that between BrCN and NO_2, via the same photochemical pathway (Schemes 3.3.1 and 4.3.1). It has been noted that the wavenumbers of the –NCO group vibrations are very similar for either INCO or BrNCO and hence changing the halogen atom does not significantly change the electronic structure of X–N=C=O. This property thus enabled the analogous species to be identified with ease.

It has been deduced from these experiments studied in chapter 3 and 4, that a halogen isocyanate species XNCO is the main photoproduct formed after photolysis of an argon matrix containing a halogen cyanide (ICN or BrCN) co-deposited with either O_3 or NO_2.

4.5 REFERENCES

(1) Clark, R. J. H.; Dann, J. R., *J. Phys. Chem. A* **1997**, *101*, 2074–2082.

(2) Clark, R. J. H.; Dann, J. R.; Foley, L. J., *Chem. Soc., Daton Trans.* **1999**, 73–78.

(3) Clark, R. J. H.; Dann, J. R., *J. Phys Chem.* **1996**, *100*, 532–538.

(4) Herzberg, G. *Infrared and Raman Spectra of Polyatomic Molecules*; Van Nostrand: NY; 1945.

(5) Jacobs, J.; Willner, H.; Pawelke, G., *J. Phys. Chem.* **1992**, *96*, 5793–5796.

(6) Milligan, D. E.; Jacox, M. E., *J. Chem. Phys.* **1967**, *47*, 278–285.

(7) Brosset, P.; Dahoo, R.; Gauthier-Roy, B.; Abouaf-Marguin, L.; Lakhlifi, A. L., *Chem. Phys.* **1993**, *172*, 315–324.

(8) Dimitrov, A.; Seppelt, K.; Scheffler, D.; Willner, H., *J. Am. Chem. Soc.* **1998**, *120*, 8711–8714.

(9) Gerke, M.; Schatte, G.; Willner, H., *J. Mol. Spectrosc.* **1989**, *135*, 359–369.

(10) Devore, T. C., *J. Mol. Struct.* **1987**, *162*, 287–304.

(11) Gottardi, W., *Angew. Chem., Int. Ed.* **1971**, *10*, 416–416.

(12) Gottardi, W., *Monatsh. Chem.* **1972**, *103*, 1150–1157.

(13) Pasinszki, T.; Westwood, N. P. C., *J. Phys. Chem. A.* **1998**, *102*, 4939–4947.

(14) Maier, G.; Teles, J. H., *Angew. Chem., Int. Ed. Engl.* **1987**, *26*, 155–156.

(15) Klapstein, D.; Nau, W. M., *Spectrochim. Acta* **1994**, *50A*, 307–316.

(16) Durig, J. R.; Guirgis, G. A.; Krutules, K. A.; Phan, H.; Stidham, H. D., *J. Raman Spectrosc.* **1994**, *25*, 221–232.

(17) Della Védova, C. O., *Spectrochim. Acta* **1992**, *48A*, 1179–1185.

(18) Durig. J. R.; Guirgis, G. A.; Krutules, K. A., *J. Mol. Struct.* **1995**, *354*, 1–14.

(19) Kölm, J.; Schrems, O.; Beichert, P., *J. Phys. Chem. A* **1998**, *102*, 1083–1089.

(20) Tevault, D. E.; Walker, N.; Smardzewski, R. R.; Fox, W. B., *J. Phys. Chem.* **1978**, *82*, 2733–2736.

(21) Taylor, G. A., *J. Chem. Soc., Perkin Trans. 1* **1985**, 1181–1184.

(22) Bondybey, V. E.; English, J. H.; Matthews, C. W.; Contolini, R. J., *Chem. Phys. Lett.* **1981**, *82*, 208–212.

(23) Gottardi, W.; Henn, D., *Monatsh. Chem.* **1970**, *101*, 11–18.

(24) Gorbatenko, V. I., *Tetrahedron* **1993**, *49*, 3227–3257.

(25) Begun, G. M.; Fletcher, W. H., *J. Mol. Spectrosc.* **1960**, *4*, 388–397.

(26) Andrews, B.; Anderson, A., *J. Chem. Phys.* **1981**, *74*, 1534–1537.

(27) Bibart, C. H.; Ewing, G. E., *J. Chem. Phys.* **1974**, *61*, 1284–1292.

(28) Laane, J.; Ohlsen, J. R., *Prog. Inorg. Chem.* **1980**, *27*, 465–513.

(29) Fitzmaurice, D. J.; Frei, H., *J. Phys. Chem.* **1992**, *96*, 10308–10315.

Chapter 5

Photochemically Induced Reactions of Dibromochloromethane and Bromodichloromethane

5.1 INTRODUCTION

Previous studies have shown that the photolysis of ozone with CH_3I,[1] CH_2X_2 (X = Br or Cl),[2] $CHCl_3$,[3] CH_2ClI,[4] or CH_2BrCl[4] produces novel carbonyl···Lewis acid complexes, for example $H_2C(O)\cdots HI$,[1] from iodomethane and ozone. The infrared spectra of such complexes differ slightly from those of isolated species on account of perturbation by the Lewis acids. The dihalomethanes CH_2XY (X and Y = Br or Cl, X and Y ≠ I) react with ozone, first via hydrogen halide abstraction to form the carbonyl complex HXC(O)···HY, etc. and then, on further photolysis, to form various carbon monoxide complexes (OC)(HX)(HY).[2,4] By varying X and Y of the halogenoalkane, comparisons can be made between the spectra of complexes having identical carbonyls but different Lewis acids and *vice versa*, and between the spectral shifts of the carbon monoxide complexes having different Lewis acid partners.

The photochemically induced reaction of ozone with a halogenated alkane containing an iodine atom (CH_3I,[1] CH_2ClI,[4] or C_2H_5I,[5]) still produces a carbonyl···Lewis acid complex like the one with CH_2XY (X and Y = Br or Cl) but the photochemical pathways differ. For example, the iodine-containing alkane forms a complex with ozone upon deposition and requires only near-infrared or visible irradiation for 30 min before a reaction takes place to form an I–O bond which goes on to produce a carbonyl complex.[1,4,5] Conversely, no ozone complex is formed with a CH_2XY (X and Y ≠ I) species and harsh UV irradiation is required for many hours before any new bands belonging to a carbonyl complex are formed. Also the carbonyl complexes dissociate to form the carbon monoxide complexes; this is not observed when iodine is present in the precursor. Other iodine- and non-iodine-containing species studied in this thesis have also shown a range of similarities and differences (ICN and BrCN, chapters 3 and 4, respectively).

This chapter is concerned with the study of the photochemically induced reaction of some trihalomethanes ($CHBr_2Cl$ and $CHBrCl_2$) with ozone, an extension of the well-documented dihalomethane/ozone reactions,[2,4] and to detect a range of new carbonyl and carbon monoxide complexes for which comparisons can be made

between the spectral shifts of the complexes having different Lewis acid partners. The possible photochemical pathways will also be considered.

5.2 DIBROMOCHLOROMETHANE AND OZONE

The photochemically induced reaction of dibromochloromethane ($CHBr_2Cl$) with ozone is expected to produce a variety of carbonyl···Lewis acid complexes which dissociate to form a variety of carbon monoxide···Lewis acid complexes. Both of these types of complex can be compared with those detected after the reaction of oxygen atoms with dibromomethane (CH_2Br_2),[2] dichloromethane (CH_2Cl_2),[2] and bromochloromethane (CH_2BrCl),[4] *e.g.* the complexes of HC(O)Br with either HBr[2] or HCl[4] or BrCl (this chapter) may be compared so as to note the effect of the different Lewis acids on the same carbonyl species.

5.2.1 RESULTS AND DISCUSSION

Deposition of the Precursors, $CHBr_2Cl$ and O_3

The infrared spectra of $CHBr_2Cl$ isolated in an argon matrix ($CHBr_2Cl$/Ar = 1:450) and in an oxygen matrix ($CHBr_2Cl/O_2$ = 1:150) have been recorded (Table 5.2.1). The bands are assigned using as guides the assignments of bands for CH_2BrCl[6,7] and other halogenomethanes in the gas phase. Ultraviolet (λ > 240 nm) photolysis of $CHBr_2Cl$ in Ar matrices produced no new bands.

The infrared spectra of $CHBr_2Cl$ co-deposited with ozone in argon matrices ($CHBr_2Cl/O_3$/Ar = 1:2:400) exhibited bands that resembled those detected in the spectra of $CHBr_2Cl$ or ozone[8,9] isolated separately in argon (Table 5.2.1). No bands could be assigned to a complex formed between the two precursors; indeed even after photolysis with UV-Vis irradiation (λ > 350 nm) no new bands appeared. This situation is different from that for a monoiodoalkane co-deposited with ozone,[1,5,10] for which the spectroscopic evidence indicates that a molecular complex is formed immediately after deposition and in turn breaks up after just ~10–20 min of photolysis (λ > 800 nm or λ >650 nm). Thus the presence of an iodine atom, as opposed to a

bromine or chlorine atom, in a halogenocarbon dramatically changes the photochemistry of ozone. Irradiation of the $CHBr_2Cl/O_3/Ar$ matrix with Pyrex- ($\lambda >$ 290 nm) or quartz-filtered radiation ($\lambda >$ 240 nm) for tens of hours was required before any new bands were produced; for similar photolysis times the Pyrex-filtered irradiation cycles produced weaker bands than those detected after quartz-filtered photolysis. Various matrix experiments were performed in order to increase the intensities of the product bands; the first, varying the deposition ratio $CHBr_2Cl/O_3/Ar$, made no difference to the photochemistry, only to the intensities of the precursor bands, due simply to the reduced or increased concentrations of precursors. The most informative experiments proved to be ones in which the matrices were photolysed at fixed wavelengths (quartz-filtered) for different periods of time.

Photolysis of $CHBr_2Cl/O_3$ matrices

Photolysis of the $CHBr_2Cl/O_3/Ar$ matrix with UV radiation ($\lambda >$ 240 nm) for tens of hours led to the formation of many new bands in the infrared spectrum. For clarity they are grouped according to the product species to which they can be attributed.

Carbonyl Complexes. Of the many new bands detected after UV irradiation, several of these are attributed to different carbonyl···Lewis acids complexes. In all cases the carbonyl stretching bands are the most diagnostic.

BrC(O)Cl···HBr. Bands attributable to carbonyl bromide chloride were detected after photolysis of $CHBr_2Cl/O_3/Ar$ matrices with quartz-filtered radiation (Table 5.2.2 and Fig. 5.2.1) and were found to be at similar wavenumbers to those detected for BrC(O)Cl in the gas phase.[11] The intensities of the bands increased as the photolysis times increased up to ~50 h, at which point they began to decrease. The weak bands situated at 1824.6, 1820.3 and 1817.4 cm^{-1} are assigned to carbonyl stretches, $\nu_{C=O}$, as are the medium-weak and medium bands occurring between 1813.5 and 1794.7 cm^{-1}. Those between 1824.6 and 1817.4 cm^{-1} are attributed to BrC(O)Cl isolated in argon, the least perturbing environment; *cf.* the closely similar values found for BrC(O)Cl, in the gas phase (1828 cm^{-1}).[11] The other $\nu_{C=O}$ bands were shifted to lower wavenumbers as a result of perturbation by the remainder of the

precursor, HBr, and are considered to arise from the complex BrC(O)Cl···HBr, the shifts being of a similar magnitude to those reported for other carbonyls perturbed by the Lewis acid HBr.[2,4] However, the three weak bands at 1824.6, 1820.3, and 1817.4 cm^{-1}, detected after 25 h of photolysis ($\lambda > 240$ nm) could, alternatively, be assigned to the perturbed $\nu_{C=O}$ of BrC(O)Br···HCl since the $\nu_{C=O}$ band of BrC(O)Br in the gas phase[12] occurs at 1828 cm^{-1}. Nevertheless formation of this complex seems unlikely, as breakage of the two strongest bonds (C–H and C–Cl) would be required while the weaker C–Br bond would need to remain intact.

A set of medium-weak and medium bands between 824.1 and 791.2 cm^{-1} were recorded and are assigned to C–Cl stretches of BrC(O)Cl, however, no bands assigned to ν_{C-Br} were detected due to their being either too weak or their obscured by the $CHBr_2Cl$ precursor bands. The large number of bands assigned to ν_{C-Cl} may be a result of chlorine isotopic splitting or due to the fact that further species or more than one distinct environment are present.

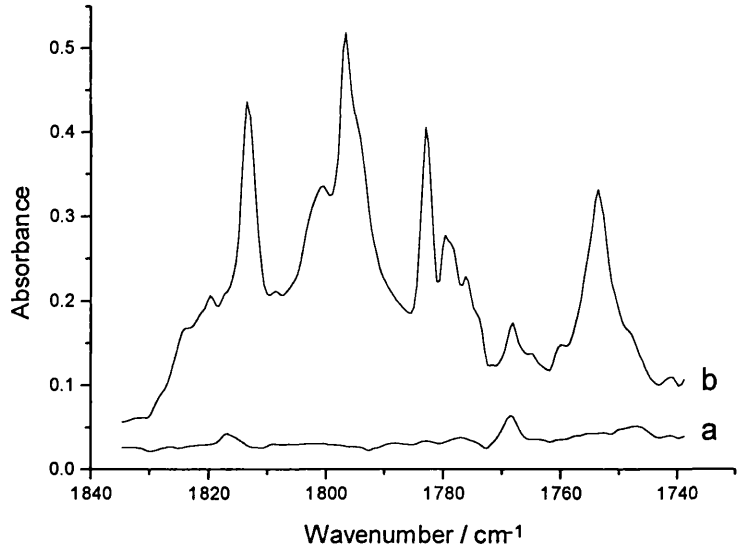

Figure 5.2.1. *Infrared spectra of a $CHBr_2Cl/O_3/Ar$ matrix after (a) deposition and (b) quartz-filtered photolysis ($\lambda > 240$ nm) for ~50 h, showing the growth of new bands assigned to $\nu_{C=O}$ of different carbonyl···Lewis acid complexes.*

HC(O)Br···BrCl. Formyl bromide bands are formed after UV irradiation of argon matrices containing $CHBr_2Cl$ and ozone (Table 5.2.2 and Fig. 5.2.1). Like the BrC(O)Cl bands, their intensities increased progressively until after ~50 h of irradiation, whereupon some of the bands began to weaken. A medium band situated at 1783.1 cm^{-1} is assigned to $\nu_{C=O}$ of a HC(O)Br···BrCl complex, which exhibits a wavenumber shift of 18.4 cm^{-1} from that (at 1801.5 cm^{-1})[4] of isolated HC(O)Br. For comparison, greater wavenumber shifts are observed for the $\nu_{C=O}$ bands of the HC(O)Br···HBr complex (at 1756.3 and 1754.9 cm^{-1}, wavenumber shifts of 45.2 and 46.6 cm^{-1}, respectively)[2] thus highlighting the fact that HBr is a stronger perturbing Lewis acid than BrCl. The wavenumbers of the $\nu_{C=O}$ bands of HC(O)Br complexes are compared in Table 5.2.3. Bands assigned to δ_{C-H} were also detected and occurred at 1285.9, 1279.7 and 1273.1 cm^{-1} while a weak band at 642.0 cm^{-1} is assigned to ν_{C-Br}.

HC(O)Cl···Br₂. Quartz-filtered (λ > 240 nm) photolysis of $CHBr_2Cl/O_3/Ar$ matrices gave rise to bands attributable to formyl chloride (Table 5.2.2 and Fig. 5.2.1) which behave similarly, after photolysis, to those of BrC(O)Cl and HC(O)Br. This group of bands is assigned as follows: the bands at 1779.7, 1776.3 and 1753.7 cm^{-1} are assigned to $\nu_{C=O}$. Weak bands at 1307.9, 1302.8 and 1298.5 cm^{-1} are assigned to δ_{C-H} while weak bands at 716.9 and 712.7 cm^{-1} are assigned to C–Cl stretches.

Again the most diagnostic bands for a complex of this type occur in the carbonyl stretching region. The medium-weak band at 1779.7 cm^{-1} is assigned to $\nu_{C=O}$ of HC(O)Cl isolated in argon.[13] The slightly red-shifted band from this is assigned to $\nu_{C=O}$ of HC(O)Cl in a greater perturbing environment, *i.e.* complexed with a Lewis acid (the remaining moiety of the precursor), HC(O)Cl···Br_2. Moreover, the other carbonyl band detected at 1753.7 cm^{-1} (a wavenumber shift of 26 cm^{-1}) is attributed to HC(O)Cl strongly perturbed by two hydrogen halides. The wavenumbers of the $\nu_{C=O}$ bands of HC(O)Cl complexes are compared in Table 5.2.4. Warming the matrix led to either the growth or destruction of some $\nu_{C=O}$ bands; this further supports the idea that more than one formyl chloride species must be present.

Carbon Monoxide Complexes. The following bands, attributed to several carbon monoxide···Lewis acid complexes (Table 5.2.5), appeared after UV photolysis and their intensities increased with photolysis time while those of the carbonyl complexes decreased. Therefore a mechanism in which the carbonyl···Lewis acid complex photodissociates to form the carbon monoxide complex is proposed. Warming the matrices did not cause any of the intensities of the bands to change, indicating that these carbon monoxide complexes are thermally stable.

(OC)(Br$_2$)(HCl). After prolonged UV photolysis (120 h) of $CHBr_2Cl/O_3/Ar$ matrices, bands detected at 2150.7 and 2153.1 cm^{-1} are assigned to C≡O stretches, while those detected between 2813.5 and 2791.4 cm^{-1} are assigned to H–Cl stretches (Table 5.2.5). The shifts of $\nu_{C\equiv O}$ bands to higher wavenumbers from that of isolated CO (~2138 cm^{-1})[14,15] suggest that carbon monoxide is perturbed by different species to form more that one complex (Fig. 5.2.2). Similarly the large number of bands detected in the ν_{H-Cl} region indicates that HCl forms part of more than one complex present in the matrix (HCl in solid argon absorbs at 2888.0, 2869 and 2853.3 cm^{-1})[4,14,16] (Fig. 5.2.3).

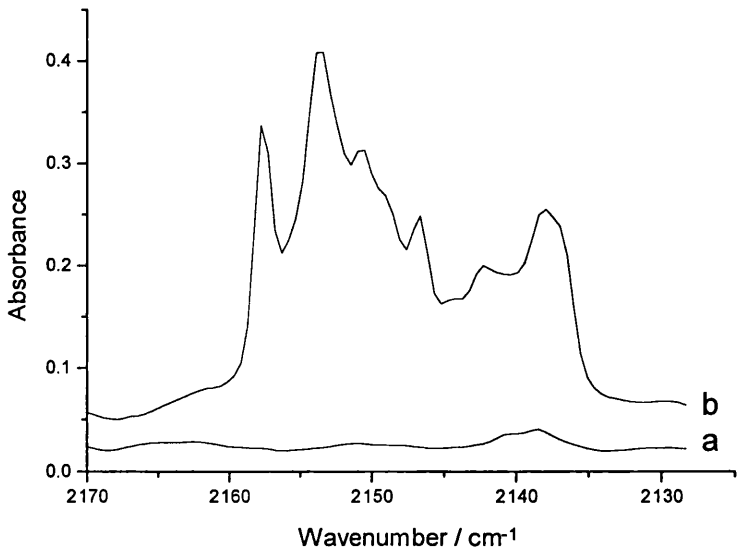

Figure 5.2.2. *Infrared spectra recorded after (a) deposition and (b) ~120 h of quartz-filtered photolysis (λ > 240 nm) of a $CHBr_2Cl/O_3/Ar$ matrix, showing new bands assigned to $\nu_{C\equiv O}$ of different carbon monoxide···Lewis acid complexes.*

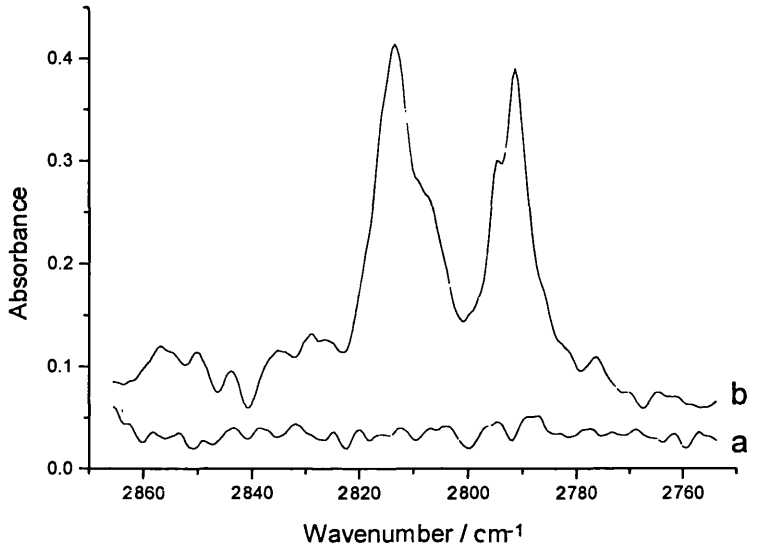

Figure 5.2.3. *Infrared spectra of an argon matrix containing $CHBr_2Cl$ and O_3 after (a) deposition and (b) quartz-filtered irradiation ($\lambda > 240$ nm) for ~120 h. Spectrum (b) shows new bands in the ν_{H-Cl} region attributed to different carbon monoxide complexes.*

In previous studies [4,14] the position of HX at either *a* or *b* in complexes such as $OC\cdots HX^a\cdots HX^b$ could be distinguished by the wavenumber of the ν_{H-Cl} band. In the complex $OC\cdots HCl^a\cdots HCl^b$ for example, the HCl in the *a* position absorbs between 2791.3 and 2780.5 cm^{-1}, and in the *b* position between 2811.2 and 2803.0 cm^{-1}. Thus in the $CHBr_2Cl/O_3$ experiment the complex $OC\cdots Br_2\cdots HCl$ could be identified by the ν_{H-Cl} values of 2813.5 and 2807.6 cm^{-1}. A second group of similar bands was detected and attributed to another complex whose ν_{H-Cl} values (2794.6 and 2791.4 cm^{-1}) are typical of that of HCl in the *a* position; $OC\cdots HCl\cdots Br_2$. Also the wavenumbers of the $\nu_{C\equiv O}$ bands detected for both complexes compare reasonably well with those of related carbon monoxide complexes, *i.e.* $OC\cdots(HCl)_2$ (2157.2 cm^{-1},[14,17,18] 2156.7 and 2155.6 cm^{-1},[2]), $OC\cdots HCl\cdots HBr$ (2154.9 cm^{-1}),[4] $OC\cdots HCl\cdots HI$ (2151.5 and 2141.4 cm^{-1}),[4] and $OC\cdots HCl$ (2151 cm^{-1}).[16–18] The bands of complexes $OC\cdots Br_2\cdots HCl$ and $OC\cdots HCl\cdots Br_2$ have similar intensities and, since it is unfavourable that the $BrC(O)Br\cdots HCl$ complex forms, it is believed that they form

from photodissociated HC(O)Cl···Br_2. The two structures exist because, unlike the complex OC···HCl···HBr,[4] bromine does not form a sufficiently strong hydrogen bond for one type of arrangement to dominate.

(OC)(BrCl)(HBr). Once more bands attributed to perturbed fundamentals, $\nu_{C\equiv O}$ and ν_{H-Br}, could be detected after prolonged UV photolysis of $CHBr_2Cl/O_3$ in argon matrices and are attributed to various carbon monoxide complexes (Table 5.2.5 and Figs. 5.2.2 and 5.2.4).

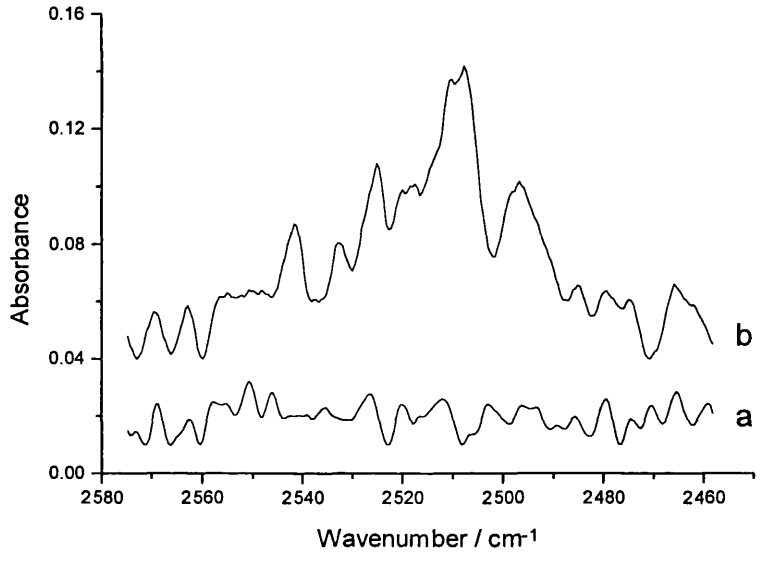

Figure 5.2.4. *Infrared spectra recorded after (a) deposition and (b) ~120 h of quartz-filtered photolysis of a $CHBr_2Cl/O_3/Ar$ matrix, showing new bands assigned to ν_{H-Br} of different carbon monoxide complexes.*

Bands detected at 2510.4 and 2507.8 cm^{-1} are assigned to ν_{H-Br} in the complex OC···BrCl···HBr on the basis that HBr in the *b* position of the complex OC···HBr^a···HBr^b absorbs at ~2509.7 cm^{-1}.[2,19] Also the value of ν_{H-Br} compares well with those of other carbon monoxide···HBr complexes studied elsewhere.[2,14,16–19] Other bands detected at 2496.7 and 2146.6 cm^{-1} are assigned to ν_{H-Br} and $\nu_{C\equiv O}$, respectively, for the complex BrCl···OC···HBr. Here the value of ν_{H-Br} is close to the value of HBr in the *a* position which has been found to absorb at ~2484.8 cm^{-1} in

the OC···HBr^a···HBr^b complex.[2,19] The small discrepancy between the HBr^a values arises in view of the fact that there is no Lewis acid in the *b* position of the complex BrCl···OC···HBr to perturb HBr^a. These complexes are formed only weakly, probably from the photodissociation of the carbonyl complexes HC(O)Br···BrCl or BrC(O)Cl···HBr. Note that HBr isolated in argon absorbs at 2568.4 and 2549.6 cm^{-1}.[14]

Other carbon monoxide complexes. The remaining HBr and CO bands are attributed to other carbon monoxide complexes present in the matrix (Table 5.2.5). The medium-weak band at 2157.6 cm^{-1} is assigned to a strongly perturbed $\nu_{C\equiv O}$ band, which is probably attributable to the complex OC···$(HCl)_2$,[2,14,17,18] where HCl is the strongest Lewis acid present in the matrix. The medium-weak band at 2138.0 cm^{-1} is assigned to $\nu_{C\equiv O}$ belonging to carbon monoxide isolated in the matrix based on similar values detected elsewhere for CO in solid argon (~2138 cm^{-1}).[14,15] The very weak and weak bands at 2525.2 and 2142.3 cm^{-1} are assigned to ν_{H-Br} and $\nu_{C\equiv O}$, respectively, and are attributed to a complex of the type $(CO)_m(HBr)_n$ where *m* is most likely equal to 2. The final band at 2541.6 cm^{-1} is assigned to ν_{H-Br} and is attributed to HBr isolated in the matrix on the basis that HBr isolated in argon absorbs at 2568.4 and 2549.6 cm^{-1}.

Solid Oxygen Matrices. Photolysis of $CHBr_2Cl$ in solid oxygen matrices did not result in reaction even after many hours of UV irradiation. The fact that 25–120 h was required to see any new products form from the reaction of $CHBr_2Cl$ with ozone indicates that the same reaction with less reactive O_2 would require much longer photolysis times.

5.2.2 PHOTOCHEMICAL PATHWAY

The photochemically induced reaction between ozone and $CHBr_2Cl$ is a time-dependent one and after 25 h of quartz-filtered irradiation carbonyl complexes are formed and the intensities of their bands continue to increase with photolysis time (Scheme 5.2.1). The carbonyl complexes then decay to form carbon monoxide

complexes after photolysis times in the region of 50–120 h. There was no evidence for the formation of species having C–Br–O or C–O–Br bonds. Although other mechanisms have been considered for the formation of carbonyl products,[2,4,20] the favoured one in this study and elsewhere[20] involves the insertion of an O atom (from ozone or oxygen) into either the C–H, C–Br, or C–Cl bond of $CHBr_2Cl$. This subsequently results in the abstraction of either a hydrogen halide (HBr or HCl) or a halogen (Br_2 or BrCl) which can weakly interact with the carbonyl O atom. All the possible products have, in fact, been detected (Scheme 5.2.1).

Alternatively, photodissociation of a C–Br bond could occur resulting in CHBrCl and Br atoms to react with O atoms forming either HC(O)Cl or BrC(O)Cl. However, the lack of detection of bands attributable to BrO[21] makes this mechanism seem unlikely. Equally possible is the suggestion that an O atom could add directly to the C atom of $CHBr_2Cl$ to form a five-centered intermediate, which could rearrange to form a variety of products. This possibility has not been considered in any great detail due to the broad range of previous studies in which insertion into the C–X bond (X = H or halogen) seems to be the prevalent mechanism. For the previous reaction of either CH_2Br_2 or CH_2Cl_2 with oxygen atoms,[2] *ab initio* calculations predicted that the carbonyl complex HXC(O)···HX would be favoured over the alternative complexes $X_2C(O)\cdots H_2$ and $H_2C(O)\cdots X_2$.

After prolonged periods of photolysis the band intensities of the carbonyl products decreased while new bands attributed to several carbon monoxide complexes were detected. This supports the idea that the carbonyl complexes dissociate via elimination of molecular CO and Lewis acids to form the carbon monoxide···Lewis acid complexes (Scheme 5.2 1).

Scheme 5.2.1

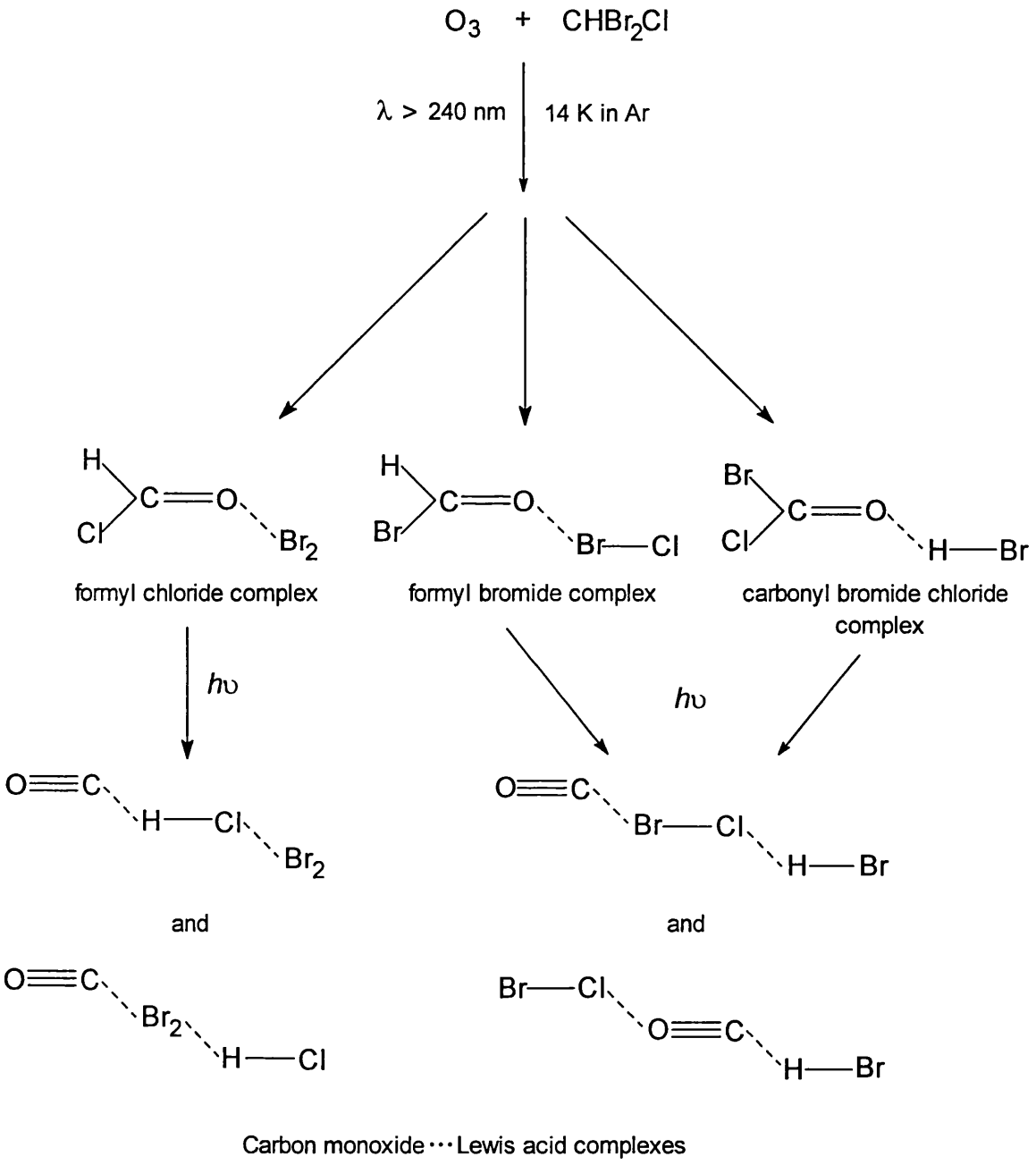
O3 + CHBr2Cl
λ > 240 nm
14 K in Ar
formyl chloride complex
formyl bromide complex
carbonyl bromide chloride complex
hυ
hυ
and
and
Carbon monoxide···Lewis acid complexes

Table 5.2.1. *Infrared bands/cm^{-1} detected for $CHBr_2Cl$ after deposition in an argon matrix and in a solid oxygen matrix at 14 K*

Ar	O_2	Assignment
3070.5w	3057.2mw	ν_{C-H}
3058.9m		
3040.1w		
1361.2mw	1360.9w	$\delta_{a\,C-H}$
1353.9w		
1321.2w		
1308.6mw		
1217.0wm	1216.3w	
1198.7ms	1197.9m	$\delta_{s\,C-H}$
1160.1m	1154.1m	
1155.3ms		
1147.1w, sh		
751.7s	751.0s	ν_{C-Cl}
737.1s	737.0s	
730.0w		
670.7vs	669.9s	ν_{C-Br}
647.6w		
573.3s	572.1ms	
529.5w		

Table 5.2.2. *Infrared bands/cm^{-1} assigned to the carbonyl products detected after photolysis ($\lambda > 240$ nm) of a mixture of O_3/Ar and $CHBr_2Cl$/Ar at 14 K*

Complex	$\nu_{C=O}$	δ_{C-H}	ν_{C-Cl}	ν_{C-Br}	other
BrC(O)Cl···Ar	1824.6w				
	1820.3w				
	1817.4w, sh				
			824.1mw		626.8vw[a]
BrC(O)Cl···HBr	1813.5m		820.7m		
	1801.4mw		814.9m		
	1796.1m		812.0m	*b*	
	1794.7m, sh		805.7m		
			797.0mw		
			791.2mw		
HC(O)Br···BrCl	1783.1m	1285.9w		642.0w	1073.8vw[c]
		1279.7w		*b*	
		1273.1mw			
HC(O)Cl···Ar	1779.7mw		*d*		
HC(O)Cl···Br_2	1776.3w	1307.9w	*d*		
HC(O)Cl···$(HX)_2$[e]	1753.7m	1302.8w	716.9w		1147.1m[f]
		1298.5w	712.7w		

[a] combination $\nu_{C=O} + \delta_{C-Br-Cl}$; [b] ν_{C-Br} bands of BrC(O)Cl or HC(O)Br are obscured by those of $CHBr_2Cl$ at 670.7 cm^{-1}; [c] combination $\nu_{C-Br} + \nu_5$; [d] ν_{C-Cl} bands obscured by those of $CHBr_2Cl$ at 751.7 cm^{-1}; [e] HX of the nearest neighbour; [f] combination $\nu_{C-Cl} + \nu_5$.

Table 5.2.3. *Infrared bands/cm^{-1} assigned to the carbonyl stretch of the HC(O)Br moiety in several complexes*

Complex[a]	$\nu_{C=O}$
HC(O)Br···Ar	1801.5[4]
	1799.5[2]
HC(O)Br···BrCl	1783.1[b]
HC(O)Br···Cl_2	1778.6[b]
	1776.5[b]
HC(O)Br···HBr	1756.3[2]
HC(O)Br···HCl	1753.0[4]

[a] The complexes are listed in order of increasing pertubation. [b] This work.

Table 5.2.4. *Infrared bands/cm^{-1} assigned to the carbonyl stretch of the HC(O)Cl moiety in several complexes*

Complex[a]	$\nu_{C=O}$
HC(O)Cl···Ar	1785.0[b]
	1783.5[13]
	1781.5[4]
HC(O)Cl···Br_2	1776.3[b]
HC(O)Cl···BrCl	1774.8[b]
	1772.9[b]
HC(O)Cl···HBr	1761.8[4]
	1756.6[4]
HC(O)Cl···HCl	1754.6[2]
	1753.0[4]
	1751.3[2]

[a] The complexes are listed in order of increasing perturbation. [b]This work.

Table 5.2.5. *Infrared bands/cm^{-1} assigned to ν_{H-Cl}, ν_{H-Br} and $\nu_{C\equiv O}$ of carbon monoxide complexes detected after UV photolysis ($\lambda > 240$ nm) of a mixture of O_3/Ar and $CHBr_2Cl$/Ar at 14 K*

Complex	$\nu_{C\equiv O}$	ν_{H-Br}	ν_{H-Cl}
OC···$(HCl)_2$	2157.6mw		
OC···Br_2···HCl	2150.7mw		2813.5m
			2807.6mw, sh
OC···HCl···Br_2	2153.1m		2794.6mw
			2791.4m
HBr···Ar		2541.6vw	
$(HBr)_n(CO)_m$	2142.3w	2525.2vw	
OC···BrCl···HBr		2510.4w	
		2507.8w	
BrCl···CO···HBr	2146.6mw	2496.7w	
CO···Ar	2138.0mw		

5.3 BROMODICHLOROMETHANE AND OZONE

The photochemically induced reaction of bromodichloromethane ($CHBrCl_2$) with ozone in argon matrices has been studied by FTIR spectroscopy. The reaction is expected to produce both carbonyl··· and carbon monoxide···Lewis acid complexes, as in the case of $CHBr_2Cl$ (section 5.2.1), CH_2Br_2,[2] CH_2Cl_2,[2] and CH_2BrCl.[4]

5.3.1 RESULTS AND DISCUSSION

Deposition of the Precursors, $CHBrCl_2$ and O_3

The spectra of $CHBrCl_2$ isolated in an argon matrix ($CHBrCl_2$/Ar = 1:500) and in an oxygen matrix ($CHBrCl_2/O_2$ = 1:150) are assigned using the assignments of bands for CH_2BrCl and other halogenomethanes in the gas phase as guides (Table 5.3.1). Quartz-filtered photolysis (λ > 240 nm) of $CHBrCl_2$ in an argon matrix produced no new bands.

The spectra recorded after co-deposition of $CHBrCl_2$ and ozone in argon matrices ($CHBrCl_2/O_3$/Ar = 1:3:600) exhibited bands that could be assigned to either precursor (Table 5.3.1). Thus unlike the situation with precursors containing a single iodine atom[1,4,5,8,22,23] (chapter 3), no initial complex with ozone was formed on deposition. UV-vis (λ > 350 nm) photolysis of these matrices for 60 min produced no detectable bands, while Pyrex-filtered (λ > 290 nm) photolysis for many hours, produced only weak bands. Quartz-filtered irradiation, for similar periods, doubled the intensities of the bands. The most diagnostic experiments were ones which employed fixed wavelength (λ > 240 nm) photolysis for different periods of time upon the matrices.

Photolysis of $CHBrCl_2/O_3$ matrices

Quartz-filtered (λ > 240 nm) photolysis of $CHBrCl_2/O_3$/Ar matrices gave rise to new bands appearing in the IR spectrum which are listed in Tables 5.3.2 and 5.3.3. The bands detected are grouped as reported below.

Carbonyl complexes. Bands attributable to several carbonyl···Lewis acid complexes were detected after prolonged UV irradiation of argon matrices containing $CHBrCl_2$ and ozone. In each case the carbonyl stretching bands are the most diagnostic and the various carbonyl···Lewis acid complexes are discussed.

BrC(O)Cl···HCl. The carbonyl bromide chloride bands (Table 5.3.2 and Fig. 5.3.1) were detected after UV photolysis of argon matrices containing $CHBrCl_2$ and O_3. The bands increased in intensity as the photolysis times increased up to ~50 h, beyond which they began to decrease, just like in the $CHBr_2Cl/O_3$ experiments mentioned in section 5.2.1. The new bands were found to be at similar wavenumbers to those detected for BrC(O)Cl in the gas phase.[11] Again the most diagnostic bands are those assigned to the carbonyl stretch, in particular the medium-strong $\nu_{C=O}$ bands at 1794.3 and 1792.6 cm^{-1} are attributed to the complex BrC(O)Cl···HCl. The shift in $\nu_{C=O}$ from its value for the uncomplexed carbonyl (1817.3 cm^{-1})[4] increases with the Lewis acid strength. As a comparison, the corresponding $\nu_{C=O}$ shifts for BrC(O)Cl···HBr and BrC(O)Cl···HCl are ~20 and 25 cm^{-1}, respectively, thus the complex BrC(O)Cl···HCl exhibits highly perturbed carbonyl bands. The $\nu_{C=O}$ shifts determined in this work are of a similar magnitude to those reported for other carbonyls perturbed by HCl and HBr.[2,4] Other bands occurring at 823.3 and 821.1 cm^{-1} are assigned to the C–Cl stretch.

ClC(O)Cl···HBr. Bands attributable to this species were detected after UV photolysis of an argon matrix containing $CHBrCl_2$ and ozone and behave similarly, after photolysis, to those of BrC(O)Cl (Table 5.3.2). A medium-weak band occurring at 1813.5 cm^{-1} is assigned to $\nu_{C=O}$ of isolated ClC(O)Cl on the basis that its wavenumber is similar to those detected previously for carbonyl chloride in the gas phase[24] and in solid argon.[25] The other $\nu_{C=O}$ bands attributed to ClC(O)Cl were red-shifted to 1806.0, 1804.1, and 1802.4 cm^{-1} suggesting that a complex of the form ClC(O)Cl···HBr is present, *i.e.* carbonyl chloride exists in a perturbing environment (Fig. 5.3.1). A medium band at 849.9 cm^{-1} also appeared and is assigned to the C–Cl stretch.

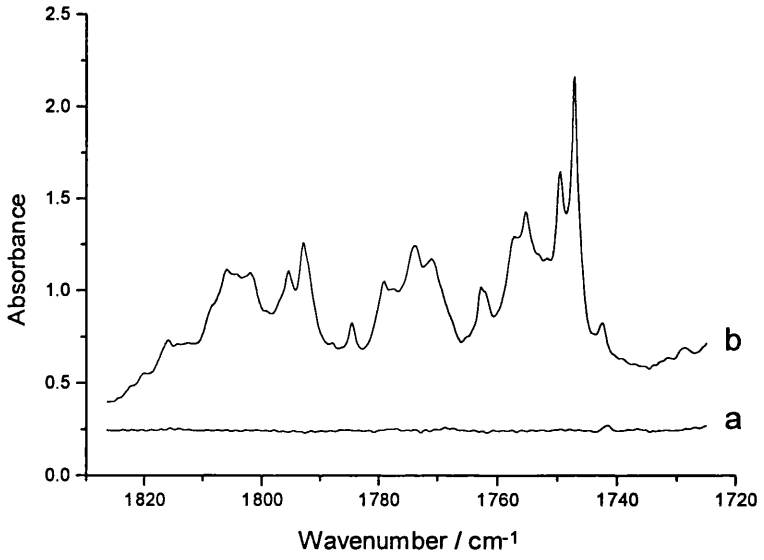

Figure 5.3.1. *Infrared spectra of a $CHBrCl_2/O_3/Ar$ matrix after (a) deposition and (b) quartz-filtered photolysis ($\lambda > 240$ nm) for ~50 h. Spectrum (b) shows new bands assigned to $\nu_{C=O}$ of different carbonyl···Lewis acid complexes.*

HC(O)Br···Cl₂. The infrared spectrum recorded after quartz-filtered photolysis of $CHBrCl_2/O_3/Ar$ matrices gave rise to bands attributed to formyl bromide (Table 5.3.2 and Fig. 5.3.1). Once again the band intensities are observed to increase with photolysis times and to then decrease after ~50 h. The medium bands situated at 1778.6 and 1777.4 cm^{-1} are assigned to $\nu_{C=O}$, while those occurring weakly at 1286.2 and 1279.7 cm^{-1} are assigned to δ_{C-H}. Bands assigned to ν_{C-Br} are also detected and are found at 662.3, 661.6, and 658.8 cm^{-1} with medium intensity. Of these, the carbonyl bands proved to be the most diagnostic so much so that the presence of the complex $HC(O)Br\cdots Cl_2$ was identified. The $\nu_{C=O}$ bands detected at 1778.6 and 1777.4 cm^{-1} give wavenumber shifts of 22.9 and 24.1 cm^{-1}, respectively, from that for isolated HC(O)Br (1801.5 cm^{-1})[4] thus suggesting that $HC(O)Br\cdots Cl_2$ is indeed present in the matrix. For comparison, the corresponding shifts for $HC(O)Cl\cdots Cl_2$[3] and $HC(O)Cl\cdots Br_2$ are 23.5 and 7.2 cm^{-1}, respectively.

HC(O)Cl···BrCl. Formyl chloride bands, formed after UV photolysis of $CHBrCl_2/O_3$/Ar matrices, behave, after irradiation, in a manner similar to those of BrC(O)Cl, ClC(O)Cl, and HC(O)Br referred to above. Bands detected between 1785.0 and 1742.5 cm^{-1} displaying a range of intensities, are assigned to carbonyl stretches of HC(O)Cl; the number of such bands suggests that HC(O)Cl complexes or distinct environments are present (Fig. 5.3.1). Weak bands situated at 1315.4 and 1303.1 cm^{-1} are assigned to δ_{C-H}, while ν_{C-Cl} bands were obscured by the broad precursor bands at 767.9 and 726.8 cm^{-1} (Table 5.3.2). The carbonyl bands are again used to identify which carbonyl complexes are present. The $\nu_{C=O}$ band at 1785.0 cm^{-1} is attributed to HC(O)Cl isolated in argon while those bands slightly red shifted to 1774.8 and 1772.9 cm^{-1} are assigned to $\nu_{C=O}$ of HC(O)Cl in perturbing environments, *i.e.* complexed with a Lewis acid (the remainder of the precursor), HC(O)Cl···BrCl. Furthermore, carbonyl bands experiencing very large wavenumber shifts were detected between 1762.0 and 1742.5 cm^{-1} and are attributed to HC(O)Cl strongly perturbed by one or two hydrogen halides of a nearest neighbour in the matrix; the hydrogen halides being the strongest Lewis acids present in the matrix.

Carbon monoxide comlpexes. The bands in this group are attributed to several carbon monoxide···Lewis acid complexes (Table 5.3.3) and appear to increase in intensity with increase in photolysis time at the expense of those attributed to the carbonyl···Lewis acid complexes discussed above. Warming the matrices appeared to have no effect on any of these bands indicating that the complexes are formed in a thermally stable environment.

(OC)(HCl)(BrCl). In the $CHBrCl_2/O_3$ experiment, bands attributed to CO and HCl were detected after prolonged UV irradiation and their intensities continued to increase throughout the entire photolysis period of 120 h (Table 5.3.3 and Figs. 5.3.2 and 5.3.3). Bands are attributed to carbon monoxide species on the basis that their wavenumbers are near to that of carbon monoxide in the gas phase (~2138 cm^{-1}) and in solid argon matrices (2138.3 cm^{-1}).[14,15] Shifts of $\nu_{C\equiv O}$ to higher wavenumbers (a blue-shift) suggests that carbon monoxide is perturbed by different species to form more than one complex (Table 5.3.3). Also the large quantity of bands detected in the

ν_{H-Cl} region indicates that HCl forms more than one complex. It is important to note that HCl alone in solid argon absorbs at 2888.0, 2869, and 2853.3 cm^{-1}.[4,14,16]

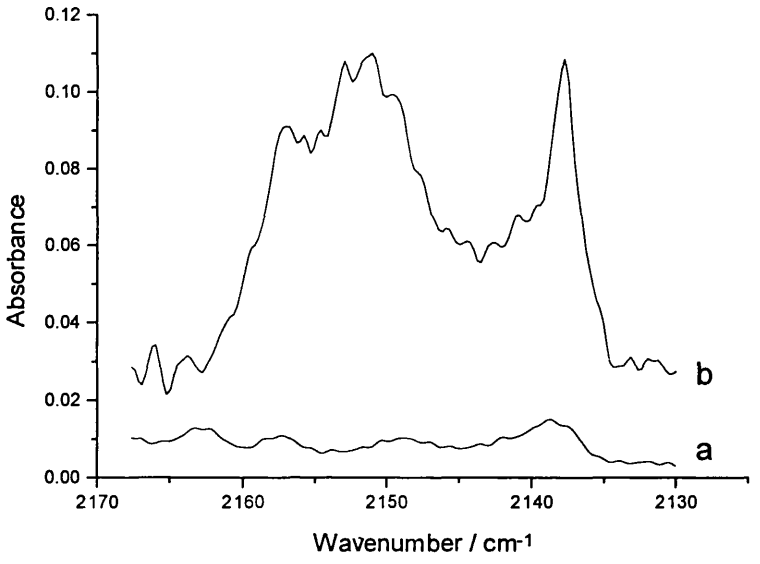

Figure 5.3.2. *Infrared spectra in the $\nu_{C\equiv O}$ region of a $CHBrCl_2/O_3/Ar$ matrix after (a) deposition and (b) quartz-filtered irradiation ($\lambda > 240$ nm) for ~120 h. Spectrum (b) shows new bands attributed to different carbon monoxide···Lewis acid complexes.*

As mentioned earlier in this chapter, the position of HCl in complexes such as OC···HCl^a···HCl^b can be distinguished by the wavenumber of ν_{H-Cl}. As a reminder, the critical values for ν_{H-Cl} when HCl is in the *a* position are between 2791.3 and 2780.5 cm^{-1} and in the *b* position between 2811.2 and 2803.0 cm^{-1}. Therefore the bands at 2823.8 and 2836.9 cm^{-1} are attributed to the complexes OC···HCl···BrCl and OC···BrCl···HCl, respectively. Both of these values for ν_{H-Cl} occur higher than those referred to for the OC···HCl^a···HCl^b complex because BrCl is a much weaker Lewis acid than HCl and thus has less effect on the shift of ν_{H-Cl} from its value for the isolated molecule. These (OC)(HCl)(BrCl) complexes most likely form from the photodissociation of the initial carbonyl complexes, HC(O)Cl···BrCl and BrC(O)Cl···HCl.

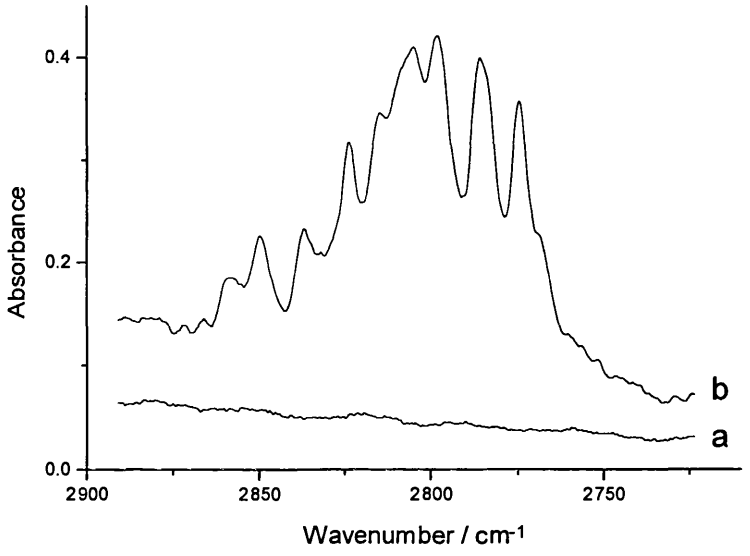

Figure 5.3.3. *Infrared spectra of an argon matrix containing $CHBrCl_2$ and O_3 after (a) deposition and (b) quartz-filtered photolysis (λ > 240 nm) for ~120 h, showing new bands in the ν_{H-Cl} region attributed to different carbon monoxide complexes.*

(OC)(HBr)(Cl_2). Once again bands assigned to $\nu_{C\equiv O}$, as well as ν_{H-Br}, could be detected after prolonged quartz-filtered photolysis of $CHBrCl_2$ and ozone in argon matrices and are attributed to carbon monoxide complexes, OC···HBr···Cl_2 and OC···Cl_2···HBr (Table 5.3.3 and Figs. 5.3.2 and 5.3.4). The band at 2494.7 cm^{-1} is close to the value obtained when HBr is located in the *a* position, while those detected between 2509.3 and 2506.3 cm^{-1} are typical of HBr in the *b* position (OC···HBr^a···HBr^b, HBr^a absorbs at ~2484.8 cm^{-1} and HBr^b absorbs at ~2509.7 cm^{-1}). The blue-shift in $\nu_{C\equiv O}$ from its value for the uncomplexed CO in solid argon (2138.3 cm^{-1})[14] increases with the Lewis acid strength. This is due to the degree of removal of electron density from the antibonding orbital of CO (located primarily on the C atom),[26] leading to an increase in bond strength and therefore of $\nu_{C\equiv O}$, *cf.* the values of $\nu_{C\equiv O}$ in the related complexes OC···$(HBr)_2$ (2153.1 cm^{-1})[2] and OC···HBr (2152.4 cm^{-1},[14] 2150 cm^{-1},[20]).

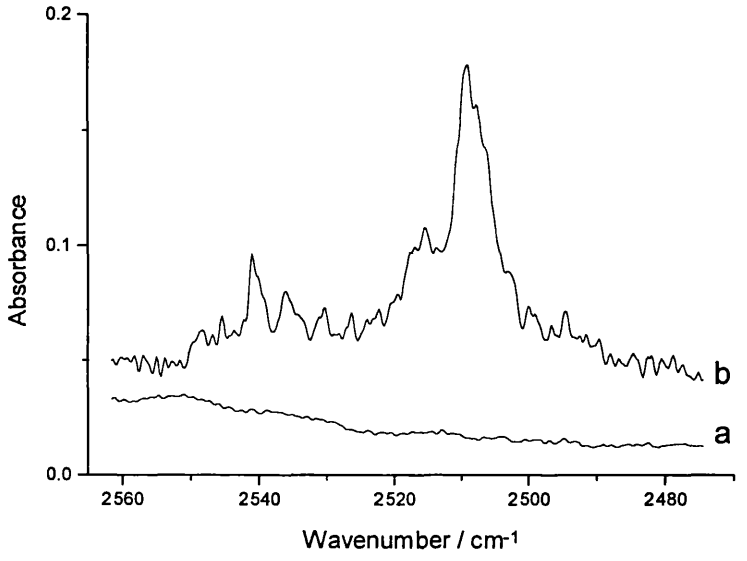

Figure 5.3.4. *Infrared spectra recorded after (a) deposition and (b) ~120 h of quartz-filtered photolysis of a $CHBrCl_2/O_3/Ar$ matrix. New bands assigned to ν_{H-Br} of different carbon monoxide complexes.*

Other carbon monoxide complexes. Bands attributed to other CO complexes were also detected (Table 5.3.3). The band situated at 2159.7 cm^{-1} is assigned to $\nu_{C\equiv O}$ while those at 2797.7 and 2786.3 cm^{-1} to ν_{H-Cl}; these bands are attributed to the OC···$(HCl)_2$ complex, due to the highly shifted bands. Bands attributed to OC···HCl[17,18] were also detected and occurred at 2154 .4, 2153.0, and 2850.0 cm^{-1}. The weak bands at 2152.1 and 2515.8 cm^{-1} are assigned to $\nu_{C\equiv O}$ and ν_{H-Br}, respectively, and belong to the complex OC···HBr.[14] The $\nu_{C\equiv O}$ band at 2137.9 cm^{-1} is attributed to CO isolated in argon,[14,15] while the $\nu_{C\equiv O}$ band slightly shifted to 2140.6 cm^{-1} is assigned to the weakly perturbed $\nu_{C\equiv O}$ of OC···Ar···Cl_2.

Solid Oxygen Matrices. Photolysis of $CHBrCl_2$ in solid oxygen matrices did not result in reaction, even after tens of hours of intense UV irradiation. The fact that solid oxygen matrices are not very transparent may add to the difficulty of observing new bands.

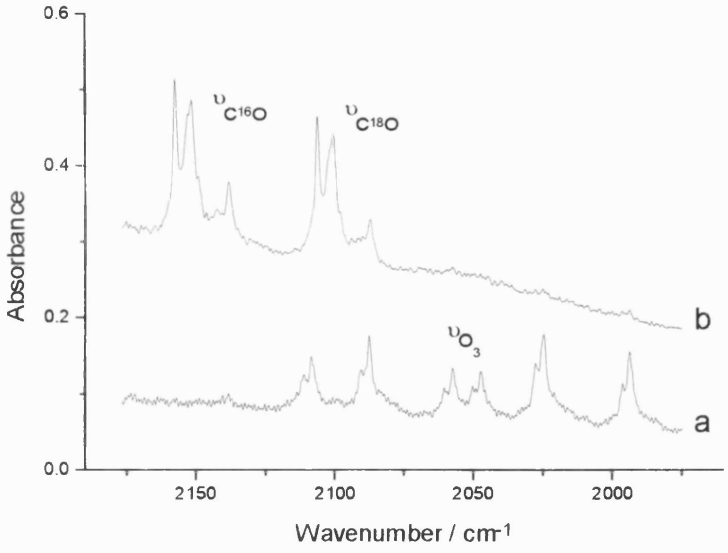

Figure 5.3.5. *Infrared spectra recorded after (a) deposition and (b) prolonged quartz-filtered photolysis of a $CHBrCl_2/^{16}O_{3-x}{}^{18}O_x/Ar$ matrix. New bands assigned to the $\nu_{C\equiv O}$ isotopomers of different carbon monoxide complexes.*

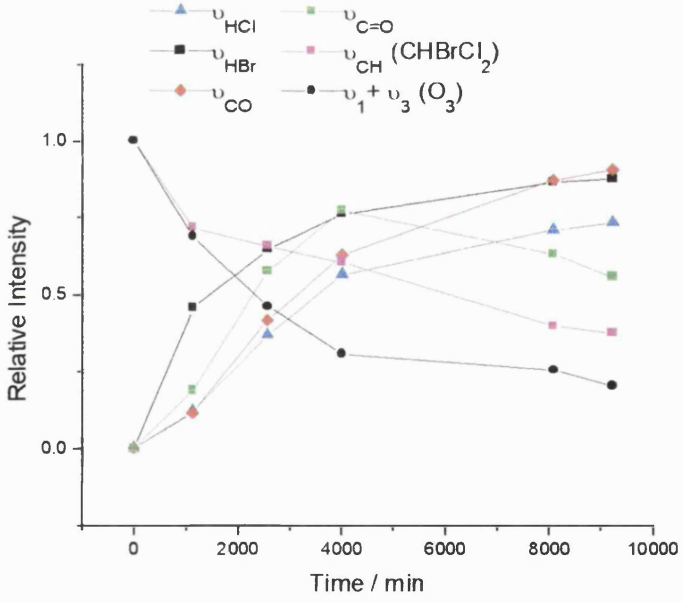

Figure 5.3.6. *IR absorbance for the new ν_{H-Cl}, ν_{H-Br}, $\nu_{C=O}$, and $\nu_{C\equiv O}$ bands, and for the depleting ozone ($\nu_1 + \nu_3$) and $CHBrCl_2$ (ν_{C-H}) bands as a function of photolysis time.*

5.3.2 PHOTOCHEMICAL PATHWAY

Like the reaction between ozone and $CHBr_2Cl$, that with ozone and $CHBrCl_2$ is also time dependent such that up to 50 h of quartz-filtered photolysis was required to form new bands. These initial bands are also attributed to carbonyl complexes which are most likely to be formed by insertion of an O atom (ozone or oxygen) into either bond of $CHBrCl_2$ followed by either HBr, HCl, or Cl_2 abstraction. Once again carbonyl complex bands are seen to deplete upon prolonged UV irradiation (50–120 h) while bands attributed to carbon monoxide complexes grow. This confirms that each of the carbonyl complexes dissociates via elimination of molecular CO and HX to form its related carbon monoxide···Lewis acid complex (Fig. 5.3.6 and Scheme 5.3.1).

Scheme 5.3.1

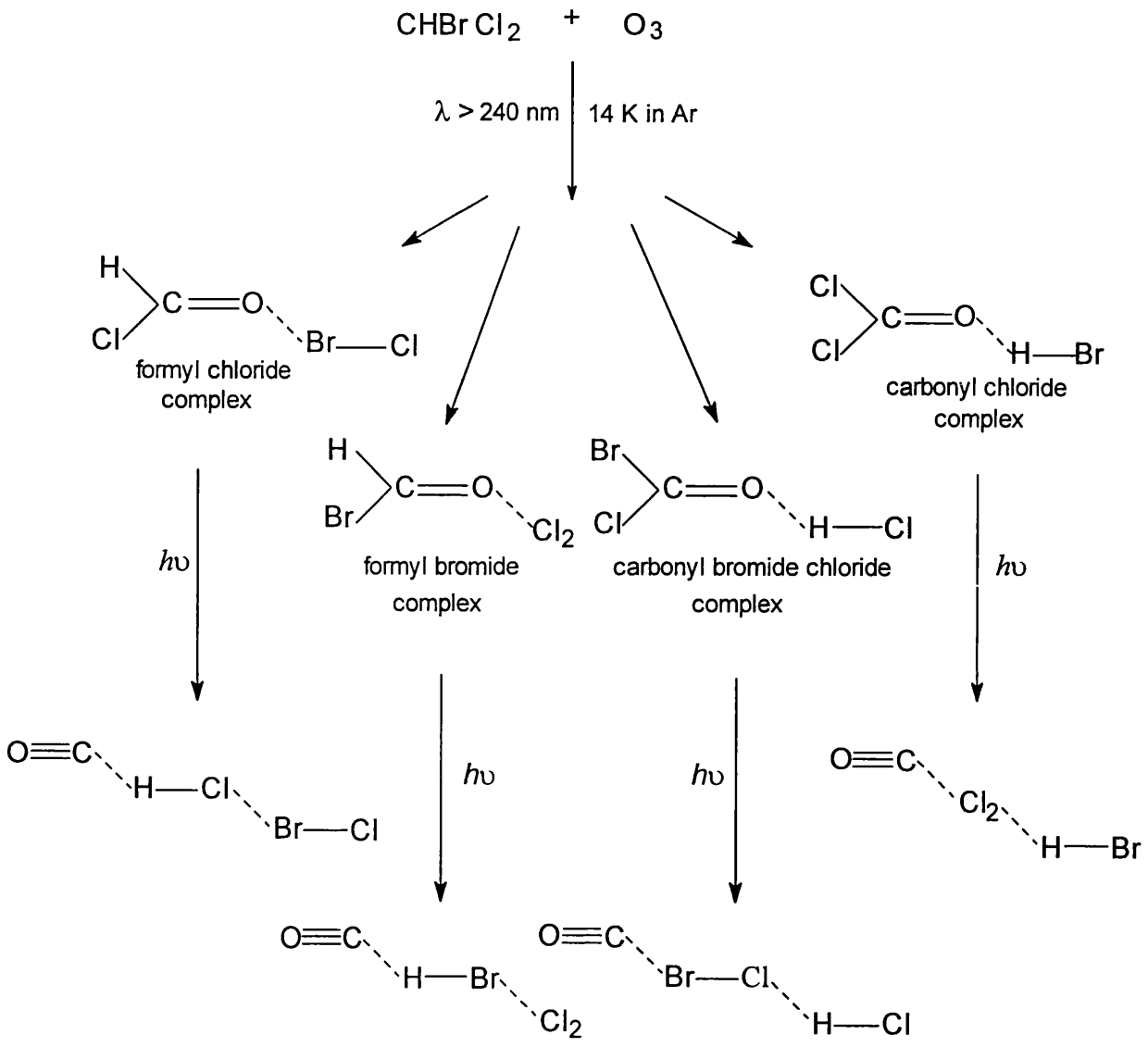
CHBr Cl2 + O3
λ > 240 nm
14 K in Ar
formyl chloride complex
carbonyl chloride complex
formyl bromide complex
carbonyl bromide chloride complex
hυ
hυ
hυ
hυ
Carbon monoxide ··· Lewis acid complexes

Table 5.3.1. *Infrared bands/cm^{-1} detected after deposition of $CHBrCl_2$ in an argon matrix and in a solid oxygen matrix at 14 K*

Ar	O_2	Assignment
3058.4s	3016.0m	ν_{C-H}
3055.5m		
3040.6w		
1362.9vw, sh		$\delta_{a\ C-H}$
1361.5w		
1354.0vw		
1320.9w		
1315.3w		
1307.8w		
1288.8w		
1266.5w		
1220.3mw	1211.6m	
1179.7w		$\delta_{s\ C-H}$
1173.9w	1169.4m	
1118.9w		
1117.5w		
821.4mw		ν_{C-Cl}
820.6mw		
767.9vs, br	772.2sh	
763.0vs	757.5vs, br	
744.1mw		
726.8vs, br		
723.0vs	720.3vs, br	
696.3vw	698.6w	ν_{C-Br}
691.4vw		
687.7mw		
662.8mw		
661.4mw		
658.5mw		
607.9vs, br	603.9s	
588.7w	586.2vw	
529.8mw		

Table 5.3.2. *Infrared bands/cm^{-1} assigned to carbonyl products detected after photolysis ($\lambda > 240$ nm) of a mixture of O_3/Ar and $CHBrCl_2$/Ar at 14 K*

Complex	$\nu_{C=O}$	δ_{C-H}	ν_{C-Cl}	ν_{C-Br}
	1820.2w, sh			
BrC(O)Cl···Ar	1815.9mw			
ClC(O)Cl···Ar	1813.5mw, sh		849.9m	
ClC(O)Cl···HBr	1806.0ms			
	1804.1ms, sh			
	1802.4ms			
BrC(O)Cl···HCl	1794.3ms		823.3m, sh	
	1792.6ms		821.1m	
HC(O)Cl···Ar	1785.0m	1315.4w	*a*	
HC(O)Br···Cl_2	1778.6m	1286.2w		662.3m
	1777.4m, sh	1279.7w		661.6m
				658.8m
HC(O)Cl···BrCl	1774.8ms			
	1772.9ms			
HC(O)Cl···HX[b]	1762.0m			
	1757.3ms, sh		*a*	
	1755.3s			
HC(O)Cl···$(HX)_2$[b]	1749.2s	1303.1w		
	1747.5vs			
	1742.5m			

[a] Obscured by a broad precursor band. [b] HX of the nearest neighbour.

Table 5.3.3. *Infrared bands/cm^{-1} detected after photolysis (λ > 240 nm) of a $CHBrCl_2/^{16}O_{3-x}{}^{18}O_x/Ar$ matrix showing bands belonging to both ^{16}O and ^{18}O isotopomers*[a]

^{16}O Absorption	^{18}O Absorption	Assignment
1762.8m	1723.4m, sh	$\nu_{C=O}$ (HC(O)Cl···HX)[b]
1762.0m, sh	1721.9m	
1757.4ms	1716.1m, sh	
1755.4s	1714.7m	
1749.7s	1708.2s	$\nu_{C=O}$ (HC(O)Cl···$(HX)_2$)[b]
1747.3vs	1706.1vs	
2157.4mw	2106.1mw	$\nu_{C\equiv O}$ (OC···HCl···BrCl)
2152.8mw, sh	2101.5w, sh	$\nu_{C\equiv O}$ (OC···HBr)
2151.7mw	2100.4mw	$\nu_{C\equiv O}$ (OC···BrCl···HCl)
2149.3w	2097.9w, sh	$\nu_{C\equiv O}$ (OC···HBr···Cl_2)
2142.2vw	2093.5vw	$\nu_{C\equiv O}$ (OC···Cl_2···HBr)
2138.0w	2087.0w	$\nu_{C\equiv O}$ (CO···Ar)

[a] $\nu_{C=^{18}O}$ bands occurring above 1723 cm^{-1} are obscured by the $\nu_{C=^{16}O}$ bands occurring between 1820 and 1747 cm^{-1}. [b] HX of the nearest neighbour.

Table 5.3.4. *Infrared bands/cm^{-1} assigned to carbon monoxide complexes detected after UV photolysis ($\lambda > 240$ nm) of a mixture of O_3/Ar and $CHBrCl_2$/Ar at 14 K*

Complex	$\nu_{C\equiv O}$	ν_{H-Cl}	ν_{H-Br}
OC···$(HCl)_2$[a]	2159.7w,sh	2797.7w	
		2786.3w	
		2774.9w[b]	
OC···HCl···BrCl	2156.7w	2823.8w	
OC···HCl	2154.4w	2850.0w	
	2153.0w		
OC···HBr	2152.1w,sh		2540.8w[c]
			2515.8w
OC···BrCl···HCl	2151.3w	2836.9w	
OC···HBr···Cl_2	2149.5w		2494.7vw
OC···Cl_2···HBr	2143.1w		2509.3w
	2142.1w		2507.7w
			2506.3w
OC···Ar···Cl_2 ?	2140.6w		
CO···Ar	2137.9w		

[a] HX of the nearest neighbour. [b] $(OC)_m(HCl)_n$. [c] HBr···Ar.

5.4 CONCLUDING REMARKS

The photochemically induced reactions between ozone and either $CHBr_2Cl$ or $CHBrCl_2$ in solid argon have been examined using FTIR spectroscopy. It has been shown that harsh photolysis conditions were required to produce an array of carbonyl···Lewis acid complexes which subsequently dissociate upon further irradiation to form an array of carbon monoxide···Lewis acid complexes. Some of the complexes detected are novel and can be compared with similar complexes formed from analogous reactions.[2–4]

5.5 REFERENCES

(1) Hawkins, M.; Andrews, L., *Inorg. Chem.* **1985**, *24*, 3285–3290.

(2) Lugez, C.; Schriver, A.; Schriver-Mazzouli, L.; Lasson, E.; Nielsen, C. J., *J. Phys. Chem.* **1993**, *97*, 11617–11624.

(3) Schriver, L.; Gauthier-Roy, B.; Carrere, D.; Schriver, A.; Abouaf-Marguin, L., *Chem. Phys.* **1992**, *163*, 357–370.

(4) Clark, R. J. H.; Dann, J. R., *J. Phys. Chem.* **1997**, *101*, 2074–2082.

(5) Clark, R. J. H.; Dann, J. R., *J. Phys. Chem.* **1996**, *100*, 532–538.

(6) Giorgianni, S.; DeCarli, B.; Visinoni, R.; Ghersetti, S., *Spectrosc. Lett.* **1986**, *19*, 1207–1214.

(7) Weber, A.; Meister, A. G.; Cleveland, F. F., *J. Chem. Phys.* **1953**, *21*, 930–933.

(8) Brosset, P.; Dahoo, R.; Gauthier-Roy, B.; Abouaf-Marguin, L., *Chem. Phys.* **1993**, *172*, 315–324.

(9) Dimitrov, A.; Seppelt, K.; Scheffler, D.; Willner, H., J. Am. Chem. Soc. **1998**, *120*, 8711–8714.

(10) Clark, R. J. H.; Dann, J. R.; Foley, L. J., *J. Phys. Chem. A* **1997**, *101*, 9260–9271.

(11) Overend, J.; Evans, J. C., *Trans. Faraday Soc.* **1960**, *55*, 1817–1825.

(12) Kwiatkowski, J. S.; Leszczynski, J., *J. Mol. Phys.* **1994**, *81*, 119–.

(13) Strandman-Long, L.; Nelander, B.; Nord, L., *J. Mol. Struct.* **1984**, *117*, 217–233.

(14) Andrews, L.; Arlinghaus, R. T.; Johnson, G. L., *J. Chem. Phys.* **1983**, *78*, 6347–6352.

(15) Dubost, H.; Abouaf-Marguin, L., *Chem. Phys. Lett.* **1972**, *17*, 269–273.

(16) Barnes, A. J.; Hallam, H. E.; Schrimshaw, G. F., *Trans. Faraday Soc.* **1969**, *65*, 3150–3158.

(17) Barnes, A. J.; Hallam, H. E.; Schrimshaw, G. F., *Trans. Faraday Soc.* **1969**, *65*, 3159–3171.

(18) Barnes, A. J.; Hallam, H. E.; Schrimshaw, G. F., *Trans. Faraday Soc.* **1969**, *65*, 3172–3178.

(19) Perchard, J. P.; Cipriani, J.; Silvi, B.; Maillard, D., *J. Mol. Struct.* **1983**, *100*, 317–339.

(20) Lasson, E.; Nielsen, C. J., *Acta Chem. Scand.* **1997**, *51*, 1–7.

(21) Tevault, D. E.; Walker, N.; Smardzewski, R. R.; Fox, W. B., *J. Phys. Chem.* **1978**, *82*, 2733–2736.

(22) Andrews. L.; Hawkins, M.; Withnall, R., *Inorg. Chem.* **1985**, *24*, 4234–4239.

(23) Hawkins, M.; Andrews, L.; Downs, A. J.; Drury, D., *J. Am. Chem. Soc.* **1984**, *106*, 3076–3082.

(24) Catalano, E.; Pitzer, K. S., *J. Am. Chem. Soc.* **1958**, *80*, 1054–1057.

(25) Bouteiller, Y.; Abdelaoui, O.; Schriver, A.; Schriver-Mazzuoli, L., *J. Chem. Phys.* **1995**, *102*, 1731–1739.

(26) Huo, W. M., *J. Chem. Phys.* **1965**, *43*, 624–.

Chapter 6

Photochemically Induced Reactions of 1,2-Dibromoethene and 1,2-Dichloroethene

6.1 INTRODUCTION

The gas phase reaction of ozone with alkenes has attracted considerable attention over the years,[1-10] especially in the last few, due to its importance in atmospheric chemistry.[7,11-13] The mechanism of the ozonolysis of alkenes, first proposed by Criegee in 1951,[14] has received substantial experimental support and is the accepted mechanism. The reaction leads to the oxidative cleavage of the double bond and the formation of aldehydes and/or ketones or their peroxidic derivatives. The three-step mechanism involves three intermediates, the primary ozonide (1,2,3-trioxolane, POZ), a carbonyl oxide (Criegee intermediate, CI) and carbonyl compound, and the secondary ozonide (1,2,4-trioxolane, SOZ) (Fig. 6.1.1). The Criegee intermediate can also undergo different decomposition and isomerisation pathways in the gas phase leading to a variety of oxygenated organic products. Later work revealed the presence of an ozone···alkene charge-transfer complex[9,15-18] which is presumably the precursor of the POZ.

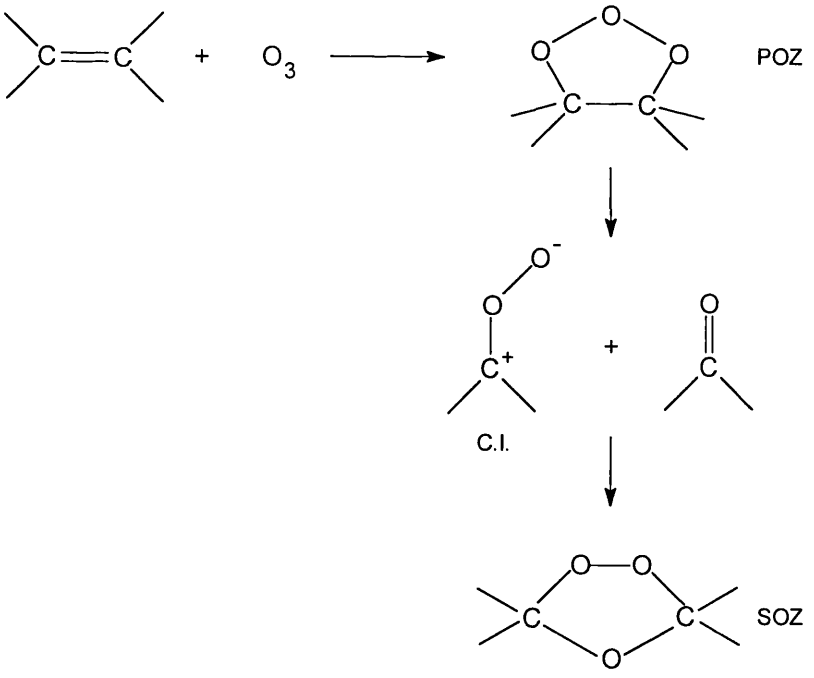

Figure 6.1.1. *The Criegee mechanism of alkene ozonolysis.*

Matrix isolation studies of the ozone/alkene reaction enabled the full characterisation the POZ and SOZ intermediates by infrared spectroscopy.[2,3,6,9] However to initiate

the reaction, the matrices had to be warmed to relatively high temperatures (77 K for a N_2 matrix,[3] 80–100 K for a Xe matrix,[6] 25 K for an amorphous CO_2 matrix,[9] and 77 K for a crystalline CO_2 matrix[9]), although no reaction took place at any temperature below the softening onset of an argon matrix.[9]

Besides ozonolysis, other studies have looked at the oxidation of halogenated alkenes with $O(^3P)$ atoms[19,20] or O_2,[21,22] which afforded a range of oxygenated organic products as well as the elimination of small molecules such as CO, CO_2, and X_2. Furthermore some studies have observed the elimination of HCl from chlorinated alkenes upon photolysis to yield an alkyne species. [23–25]

This chapter aims to analyse the photochemically induced reactions of halogenated alkenes (1,2-dibromoethene and 1,2-dichloroethene) with ozone in argon matrices; this is an extension of the simple alkene/ozone reactions studied previously in the gas phase as well as an extension of the halogenated alkane/ozone reactions studied previously in chapter 5. It is of interest as to whether irradiation can initiate ozonolysis in the argon matrix via the Criegee mechanism and whether the halogen substituents have any effect on the reaction mechanism. Oxygen atom oxidation may occur instead of ozonolysis resulting in the decomposition of the halogenoethene. The question of whether an ozone···CHXCHX (X = Br or Cl) charge-transfer complex will form is also of interest.

6.2 1,2-DIBROMOETHENE

The study of the photochemically induced reaction of 1,2-dibromoethene (BrCH=CHBr) with ozone in argon matrices has been chosen in order to compare any photoproducts and the reaction pathway with those characterised for the C_2H_4/O_3 reaction reported elsewhere, *i.e.* whether a POZ, a carbonyl compound, or a SOZ can be detected.[14] Hence the $BrCH=CHBr/O_3$ reaction is expected to produce the HC(O)Br carbonyl compound. Additional products might be detected as a result of the dissociation and isomerisation of the Criegee intermediate (carbonyl oxide) as well as the dissociation of HC(O)Br (as seen in chapter 5 for analogous carbonyl

species). The possible elimination of CO, CO_2, HBr, and Br_2, after O atom oxidation of BrCH=CHBr, may also add to the list of additional products.

6.2.1 RESULTS AND DISCUSSION

Deposition of the Precursors, BrCH=CHBr and O_3

The infrared spectra of *cis*- and *trans*-1,2-dibromoethene, BrCH=CHBr, isolated in an argon matrix (BrCH=CHBr/Ar = 1:3000) and in an oxygen matrix (BrCH=CHBr/O_2 = 1:2500) were recorded (Table 6.2.1), and the band wavenumbers were assigned using as guides the assignments of bands for ethene[26–28] and other halogenoethenes[23–25] in matrices. Ultraviolet photolysis (λ > 240 nm) of BrCH=CHBr deposited in an argon matrix produced no new bands. This differs from the situation in which dichloroethenes photolysed (λ > ~240 nm) in krypton and xenon matrices undergo elimination of Cl_2 or HCl to produce an alkyne complex, $C_2H_2\cdots Cl_2$ or $C_2HCl\cdots HCl$.[24,25]

The infrared spectrum of BrCH=CHBr co-deposited with ozone in an argon matrix (BrCH=CHBr/O_3/Ar = 1:3:2000) exhibited bands that resembled those detected in the infrared spectra of BrCH=CHBr or ozone[29–31] isolated separately in argon (Tables 6.2.1 and 6.2.2). As seen in the ICN and ozone experiments (chapter 3), additional weak bands with small wavenumber shifts from the ozone fundamental bands were detected in these BrCH=CHBr/O_3 experiments and are attributed to an ozone···precursor complex. This initial interaction between ozone and the halogenoethene occurs at the double bond of the alkene (an electron-donating area) forming a charge-transfer complex. The appearance in the infrared spectra of $\nu_{C=C}$ bands weakly shifted from those detected for isolated BrCH=CHBr provides further evidence that such a complex is present. The bands attributed to the ozone···BrCH=CHBr charge-transfer complex began to deplete upon UV-vis irradiation (λ > 350 nm) while those belonging to new species began to grow. The formation and characterisation of ozone complexes with other carbon π systems have been explored elsewhere.[8,9,15–18]

Varying the deposition ratios of BrCH=CHBr/O_3/Ar made no difference to the photochemistry but caused the intensities of the precursor bands to increase or decrease according to whether the concentrations were increased or decreased. Moreover, increasing the precursor bands resulted in the intensities of the complex bands to increase. In addition to the precursor bands, small quantities of matrix-isolated water and carbon dioxide were detected. Isotopic ozone, $^{18}O_3$, and mixed-ozone, $^{16}O_{3-x}{}^{18}O_x$, samples have also been condensed with 1,2-dibromoethene in argon matrices (Tables 6.2.1 and 6.2.2). The sextet of bands for each vibrational mode of the six isotopomers of ozone was detected (Table 6.2.2 and Fig. 6.2.1) and their wavenumbers agree with those of isolated ozone detected elsewhere[29–31] (Appendix A1). The bands for complexed ozone could also be detected alongside those of isolated ozone.

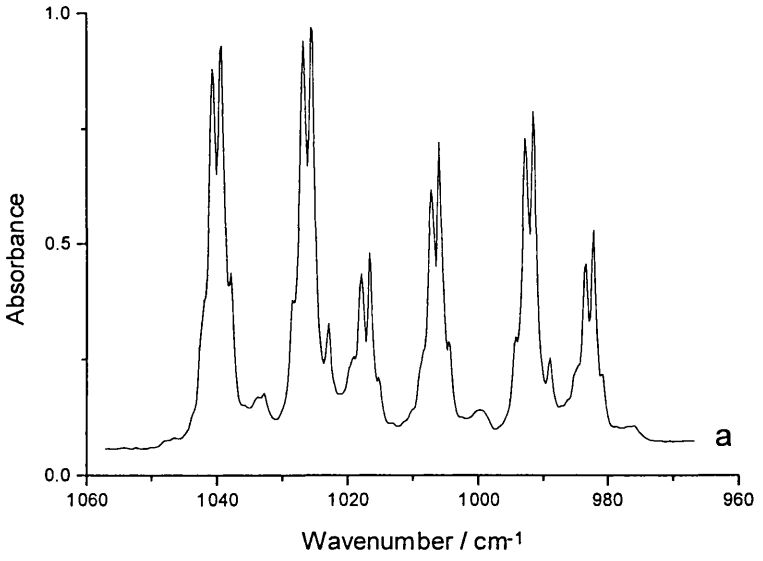

Figure 6.2.1. *Infrared spectrum of a $^{16}O_{3-x}{}^{18}O_x$/Ar matrix recorded after (a) deposition showing the ν_3 bands of the six isotopomers of ozone with the complex bands appearing alongside.*

Photolysis of BrCH=CHBr/O_3 Matrices

Photolysis of argon matrices containing BrCH=CHBr/O_3 led to the formation new bands which are grouped according to the species to which they refer.

Carbonyl Species. Many new bands in the carbonyl stretching region were detected after UV-vis irradiation (λ > 350 nm) and their intensities increased very slightly upon Pyrex- (λ > 290 nm) and quartz-filtered (λ > 240 nm) irradiation. As seen in chapter 5, the carbonyl bands are the most diagnostic and thus many of the $\nu_{C=O}$ bands observed here are attributed to carbonyl···Lewis acid complexes.

HC(O)Br. A group of new bands occurred in the carbonyl region of the infrared spectrum and some of these are assigned to $\nu_{C=O}$ of formyl bromide in different environments (Table 6.2.3 and Fig. 6.2.2). For example the very weak and weak bands situated at 1804.5 and 1801.1 cm^{-1}, respectively, are indicative of HC(O)Br isolated in argon ($\nu_{C=O}$ = 1799 cm^{-1},[32] and 1801.5 cm^{-1},[33]), while those detected weakly between 1756.7 and 1747.9 cm^{-1} are indicative of HC(O)Br perturbed by the Lewis acid, HBr ($\nu_{C=O}$ = 1756.3 cm^{-1}).[34] Bands detected between 1734.6 and 1730.0 cm^{-1} are assigned to $\nu_{C=O}$ in an even greater perturbing environment such as HC(O)Br···$(HBr)_2$. In the ^{18}O-enriched matrices, the $\nu_{C=O}$ band belonging to the formyl bromide isotopomer HC(^{18}O)Br was expected to occur at ~1742 cm^{-1} (^{18}O-shift of ~57 cm^{-1}),[34] while $\nu_{C=O}$ of HC(^{18}O)Br···HBr was expected to occur at ~1715 cm^{-1}.[34] Neither of these species could be detected in the BrCH=CHBr/$^{18}O_3$ or BrCH=CHBr/$^{16}O_{3-x}{}^{18}O_x$ experiments, although they could be, albeit weakly, in the BrCH=CHBr/$^{16}O_3$ experiment. However a set of bands occurring at lower wavenumbers than expected for $\nu_{C=O}$ of HC(^{18}O)Br···HBr, appeared between 1709.6 and 1706.7 cm^{-1} and could possibly belong to HC(^{18}O)Br in a greater perturbing environment, *i.e.* HC(^{18}O)Br···$(HBr)_2$. Another band attributed to formyl bromide was detected at 637.2 cm^{-1} (at 636.9 and 631.9 cm^{-1} in the $^{18}O_3$ experiment) and is assigned to ν_{C-Br}.

HC(O)H. The band occurring in the carbonyl stretching region at 1740.1 cm^{-1} possibly belongs to isolated formaldehyde, HC(O)H, on the basis that its wavenumber agrees well with that detected for HC(O)H in the gas phase (1746.1 cm^{-1})[35] (1743.6 cm^{-1}),[36] in nitrogen matrices (1739.9 cm^{-1})[35] (1740.3 cm^{-1}),[37] and in argon matrices (1742.0 cm^{-1})[35] (1742.5 cm^{-1}).[34] A band attributed to HC(^{18}O)H appeared in the ^{18}O-enriched ozone experiments and occurred at 1704.1 cm^{-1}, along with shoulders at 1703.9 and 1703.4 cm^{-1} (Fig. 6.2.3). The ^{18}O-shift of 36.0 cm^{-1} is consistent with that observed for the HC(^{16}O)H/HC(^{18}O)H pair studied elsewhere (34.2 cm^{-1}).[34] Other $\nu_{C=O}$ bands, red-shifted to 1726.6 and 1721.0 cm^{-1}, are attributed to the carbonyl···Lewis acid complex HC(O)H···HBr ($\nu_{C=O}$ = 1727.9 cm^{-1} for HC(O)H···HBr in solid argon)[38] while the ^{18}O isotopomer bands occurred at 1698.7 and 1696.2 cm^{-1} (Table 6.2.3).

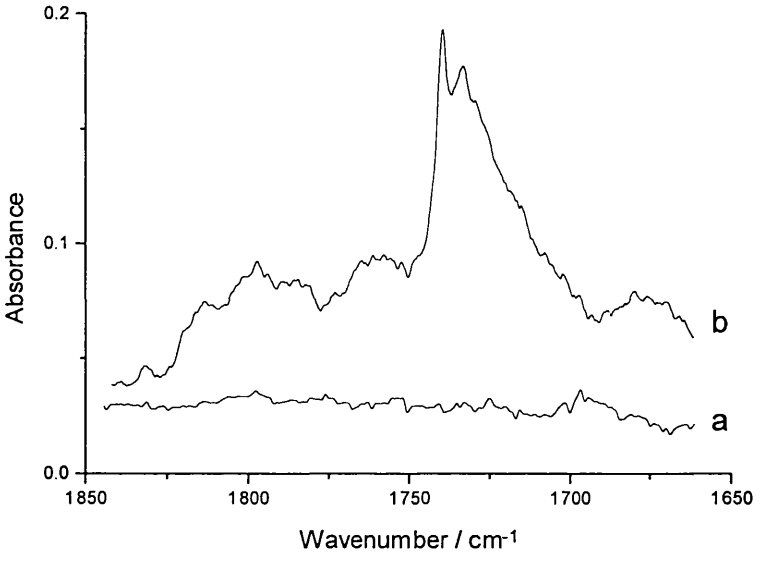

Figure 6.2.2. *Infrared spectra of a BrCH=CHBr/$^{16}O_3$/Ar matrix after (a) deposition and (b) quartz-filtered photolysis ($\lambda > 240$ nm). The spectra show bands assigned to $\nu_{C=O}$ of new species.*

These carbonyl species form from the photochemically induced reaction of BrCH=CHBr with ozone. As mentioned earlier, the gas phase reaction of ozone with alkenes (ozonolysis) is well documented.[1-14,39] Ozone reacts vigorously with alkenes

to form unstable compounds called primary ozonides (POZ), which cleave to form a carbonyl oxide and aldehyde or ketone type species which then rearrange spontaneously to form compounds known as secondary ozonides (SOZ) (Fig. 6.1.1). However, the conditions of the matrix prevent this reaction from occurring such that photolytic or thermal conditions[3,6,9] are required for initiation and control. Therefore it is possible to isolate the intermediate aldehyde and/or ketone species. In the case of 1,2-dibromoethene reacting with ozone, oxidative cleavage of the primary ozonide would produce the aldehyde, HC(O)Br, which is indeed observed. However, the wavenumbers of some $\nu_{C=O}$ bands suggest that formaldehyde species are present; but it is unclear how HC(O)H can form from the cleavage of a primary ozonide formed by ozonolysis of 1,2-dibromoethene as the H atoms are on opposite C atoms (unless rearrangement to 1,1-dibromoethene occurs so that the H atoms are on the same C atom). The liquid phase oxidation of analogous 1,2-dichloroethene with oxygen, studied by Griesbaum *et al.*,[21] afforded the inorganic products HCl, CO, CO_2, and phosgene, ClC(O)Cl. This highlights the fact that the halogenated alkene/ozone reaction in the matrix could follow an alternative pathway to ozonolysis whereby O atoms (from dissociated ozone) react instead, causing the elimination of small molecules (CO, CO_2, and HX) from the halogenated alkene. It is therefore possible that, after oxidation of BrCH=CHBr, various rearrangements and recombinations could occur, especially in a matrix environment, allowing species such as HC(O)H to form. In the infrared spectrum after photolysis, bands belonging to CO_2 do indeed grow and, as discussed below, so do bands belonging to CO. Nevertheless, the attribution of bands to HC(O)H species remains speculative. Warming experiments caused little change to the intensities of the $\nu_{C=O}$ bands; however bands attributed to HC(^{16}O)H···HBr intensified slightly while those attributed to HC(^{18}O)Br···HBr and HC(^{18}O)H increased markedly.

Some of the many carbonyl bands detected in the $^{16}O_3$ experiment (Table 6.2.3) could belong to an acyl halide species such as $CH_2BrC(O)Br$, the carbonyl vibrations of which are expected to absorb in the region 1815–1770 cm^{-1}.[26] However the lack of other bands associated with this molecule suggests that its presence is uncertain.

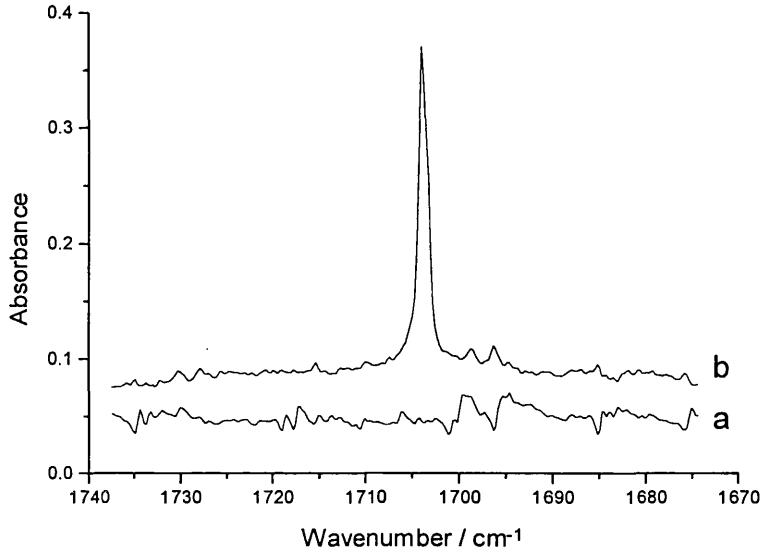

Figure 6.2.3. *Infrared spectra of a BrCH=CHBr/$^{18}O_3$/Ar matrix after (a) deposition and (b) quartz-filtered photolysis (λ > 240 nm) showing new bands appearing in the $\nu_{C\equiv O}$ region.*

Carbon Monoxide Species. Bands appearing in the $\nu_{C\equiv O}$ region were first detected after UV-vis irradiation (λ > 350 nm) and their intensities increased dramatically upon Pyrex- (λ > 290 nm) and quartz-filtered (λ > 240 nm) irradiation. As seen in chapter 5, carbon monoxide can form an array of Lewis acid complexes, giving rise to many bands in the $\nu_{C\equiv O}$ region.

OC···HBr. After photolysis of BrCH=CHBr/O_3/Ar matrices, weak bands detected at 2153.0 and 2150.8 cm^{-1} are assigned to $\nu_{C\equiv O}$ (Table 6.2.4 and Fig. 6.2.4), while a very weak band detected at 2504.4 cm^{-1} is assigned to ν_{H-Br} (Table 6.2.5). The fact that $\nu_{C\equiv O}$ is shifted to higher wavenumber than that of isolated CO (~2138 cm^{-1})[40–42] suggests that carbon monoxide is present in a perturbing environment. Similarly the shift of ν_{H-Br} to lower wavenumber from that of isolated HBr (2568.4, 2559.6, 2549.6, and 2540.8 cm^{-1})[41,43,44] suggests that HBr is also part of a perturbing environment. Therefore these bands are attributed to the OC···HBr carbon monoxide···Lewis acid complex based on the band wavenumbers reported elsewhere

for OC···HBr,[32] viz. $\nu_{C\equiv O}$ = 2152 cm^{-1} and ν_{H-Br} = 2518–2502 cm^{-1}. Bands belonging to the isotopic counterpart, ^{18}OC···HBr could be detected in the ^{18}O enriched experiments; here $\nu_{C\equiv O}$ occurred at 2106.1 and 2100.8 cm^{-1} giving an isotopic shift of ~50 cm^{-1} ($\nu_{C\equiv{}^{16}O}$ = 2138 cm^{-1}, $\nu_{C\equiv{}^{18}O}$ = 2087 cm^{-1}, ^{18}O-shift = 51 cm^{-1})[32] (Fig. 6.2.4). Greater wavenumber shifts are observed for the $\nu_{C\equiv O}$ and ν_{H-Br} bands of the OC···(HBr)$_2$ complex (Tables 6.2.4 and 6.2.5), and the values closely match those observed for OC···(HBr)$_2$ studied elsewhere.[32,34] The bands for ^{18}OC···(HBr)$_2$ are listed in Tables 6.2.4 and 6.2.5. Warming of the matrix caused the intensity of some bands belonging to OC···(HBr)$_2$ to decrease while some new bands, probably belonging to OC···(HBr)$_x$ ($x > 2$) appeared.

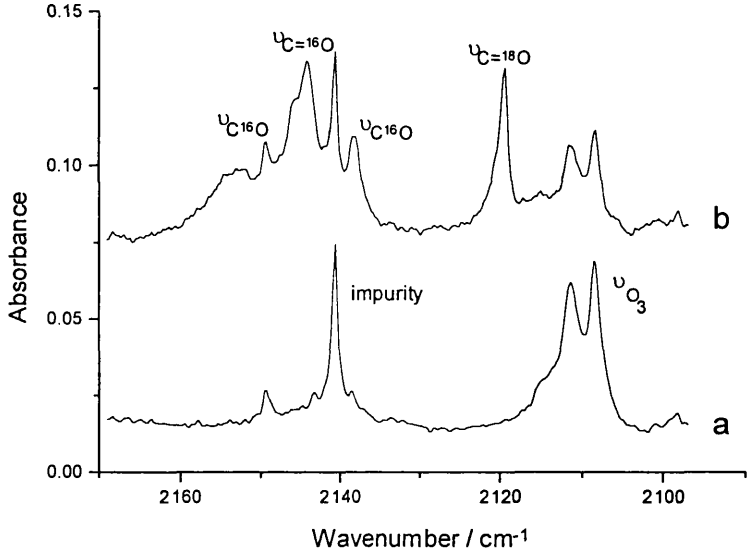

Figure 6.2.4. *Infrared spectra of a BrCH=CHBr/$^{16}O_{3-x}{}^{18}O_x$/Ar matrix after (a) deposition and (b) quartz-filtered photolysis ($\lambda > 240$ nm). The spectra show the growth of new bands assigned to $\nu_{C\equiv O}$ and $\nu_{C=O}$ (BrHC=C=O).*

These observations can be rationalised by the removal of electron density from the 5σ orbital of CO to the Lewis acid, HBr. The 5σ orbital of CO has been shown to be weakly antibonding and, located on the C atom, removal of electron density results in an increase in bond strength and $\nu_{C\equiv O}$.[41,45] Complete ionisation raises $\nu_{C\equiv O}$ from 2143 cm^{-1} ($CO_{(g)}$) to 2184 cm^{-1} ($CO^+_{(g)}$).[41,46] Subsequently, the electron density

transfer from the 5σ orbital of CO to the σ* HBr orbital (antibonding) causes the H–Br bond to weaken and ν_{H-Br} to drop in wavenumber from that of the value for isolated HBr.

Other carbon monoxide species. Remaining $\nu_{C\equiv O}$ bands are listed in Table 6.2.4 and those situated at 2138.6 and 2138.1 cm^{-1} ($C^{18}O$ at 2087.5 and 2086.9 cm^{-1}) are indicative of CO isolated in argon (Fig. 6.2.4).[32,42] Those at 2140.5 and 2139.3 cm^{-1} are attributed to the CO dimer based on similar bands observed elsewhere for $(CO)_2$.[40] The band situated at 2145.6 cm^{-1} is tentatively attributed to carbon monoxide perturbed by the impurity H_2O, or could be due to higher aggregates of CO.[40,42] Warming of the matrix did not result in any significant changes to the intensities of these bands.

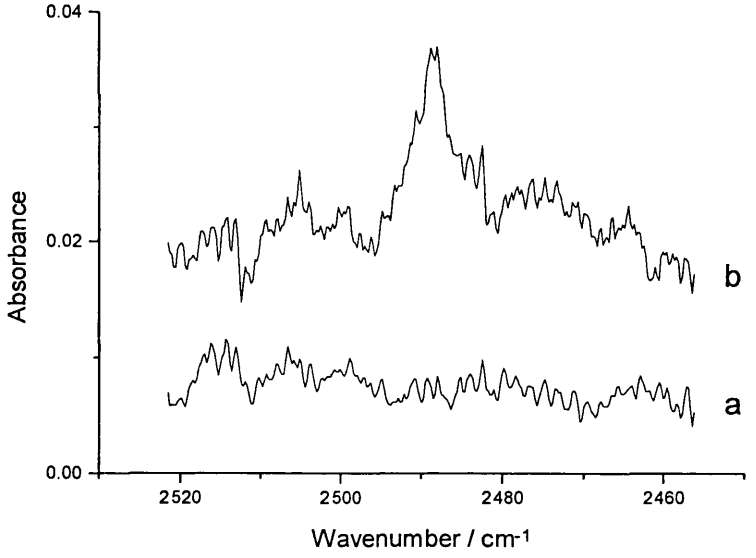

Figure 6.2.5. *Infrared spectra of a BrCH=CHBr/$^{16}O_{3-x}{}^{18}O_x$/Ar matrix after (a) deposition and (b) quartz-filtered photolysis (λ > 240 nm) showing new bands assigned to ν_{H-Br} of different species.*

These carbon monoxide species probably arise from the dissociation of the carbonyl complexes which formed from the cleavage of a primary ozonide. For example HC(O)Br···HBr was detected and could therefore dissociate to form either

OC···HBr or OC···$(HBr)_2$; the dissociation of carbonyl complexes to form carbon monoxide complexes has also been observed in chapter 5 and elsewhere.[33,34,44] Alternatively the oxidation of BrCH=CHBr could result in the elimination of CO and HBr, forming these OC···HBr species.

Ketene. Bands attributable to a ketene type species BrHC=C=O, were first detected after UV-vis irradiation and their intensities continued to increase after Pyrex- and quartz-filtered irradiation (Table 6.2.5 and Fig. 6.2.4). The medium weak bands at 2143.6 and 2142.0 cm^{-1} are assigned to $\nu_{C=O}$ of BrHC=C=O while bands detected in the $^{18}O_3$ experiment occurred between 2120.4 and 2113.2 cm^{-1} and are assigned to $\nu_{C=O}$ of the isotopomer BrHC=C=^{18}O. Both sets of bands were detected in the mixed-ozone experiment highlighting the contribution from one O atom to the vibrational mode $\nu_{C=O}$. The C=C stretch of BrHC=C=O occurred at 1107.0 and 1111.9 cm^{-1} in the $^{18}O_3$ and $^{16}O_{3-x}{}^{18}O_x$ experiments, respectively. For comparison the $\nu_{C=O}$ and $\nu_{C=C}$ bands detected elsewhere for the ketene species H_2C=C=O appeared at 2142.2 cm^{-1} (^{18}O at 2115.4 cm^{-1})[47,48] and 1111.4 cm^{-1} (^{18}O at 1108.0 cm^{-1}),[47,48] respectively. The absorptions of the other vibrational modes of BrHC=C=O were either too weak to be detected or were hidden by precursor or product bands.

Ozonide. A number of new bands appeared after prolonged photolysis cycles (24 h) using quartz-filtered (λ > 240 nm) radiation of BrCH=CHBr/O_3/Ar matrices. Of these, the very weak bands detected at 1218.1, 1200.3, and 1197.8 cm^{-1} are assigned to a CHBr bending mode. More bands between 1145.4 and 1130.9 cm^{-1} are tentatively assigned to another CHBr bending mode. Bands assigned to a C–O stretch occurred at 1260.6 and 1260.0 cm^{-1} for the ^{16}O isotopomer and at 1042.7 cm^{-1} for the ^{18}O one. The very weak band at 799.6 cm^{-1} is assigned to an O–O stretch (the band at 765.2 cm^{-1} is assigned to the ^{18}O–^{18}O stretch), although no bands were detected that could be assigned to the ^{16}O–^{18}O species in the mixed-ozone experiment. These bands could therefore possibly belong to an epoxide species. This group of bands suggests that a secondary ozonide (SOZ) is present (Table 6.2.5) as bands at similar wavenumbers were obtained for 1,2,4-trioxolane (SOZ) detected in the CH_2=CH_2/O_3 experiments (Fig. 6.1.1).[2,20] The ν_{C-H} and ν_{C-Br} bands of the SOZ are probably

hidden by those belonging to the precursor. Warming of the matrix did not lead to any changes in the intensities of these bands.

Other Species. Some of the bands already discussed could alternatively belong to other species. For example, ethene oxide has been studied by a number of groups[26,36,49] who have associated bands at 1265, 1165, 865 cm^{-1} with the epoxy group. Bands detected at 1264.1 and near 1145.4 cm^{-1}, attributed to a HC(O)H and a SOZ species, respectively, could also be attributed to an epoxy group of an epoxide species formed after photolysis of $BrCH{=}CHBr/O_3/Ar$ matrices, although no bands appeared close to 865 cm^{-1} (Table 6.2.5). Other studies of halogenoethene reactions[19,20] proposed that cyclopropane could form, but the characteristic ring bending mode absorbing near 1020–1000 cm^{-1},[26] was not detected in these experiments. Carboxylic acids have also been detected amongst the many reaction products of alkene/O_3 reactions, but again there was no evidence to suggest that any carboxylic acids formed in these experiments, as no ν_{O-H} bands were detected.

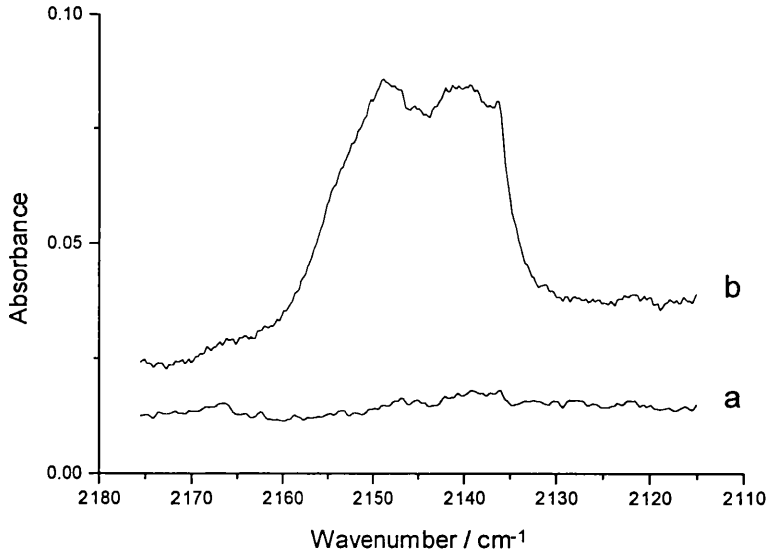

Figure 6.2.6. *Infrared spectra of a $BrCH{=}HBr/O_2$ matrix after (a) deposition and (b) quartz-filtered photolysis ($\lambda > 240$ nm) for many hours showing bands appearing in the $\nu_{C\equiv O}$ and $\nu_{C=O}$ (BrHC=C=O) region.*

Solid Oxygen Matrices. Prolonged quartz-filtered ($\lambda > 240$ nm) irradiation of BrCH=CHBr deposited in solid oxygen matrices produced similar bands to those produced in the BrCH=CHBr/O_3 experiments and are assigned on this basis (Tables 6.2.3 and 6.2.4 and Fig. 6.2.6). No complex is formed and so long photolysis periods were required to initiate the reaction. The oxygen matrix acts as an oxygen atom source to produce the oxygenated products (C=O, C≡O, and BrHC=C=O species) but, unlike the situation with ozone, no bands could be attributed to the SOZ species; this is obviously due to the fact that SOZ is produced from the ozonolysis of BrCH=CHBr. These oxygen matrix experiments therefore highlight the fact that the carbonyl and carbon monoxide species are produced via an alternative pathway to the Criegee one. Warming experiments led to an increase in intensity of $\nu_{C\equiv O}$ bands between 2154.7 and 2145.0 cm^{-1} at the expense of those between 2140.6 and 2136.2 cm^{-1} indicating a preference towards the formation of carbon monoxide complexes (Table 6.2.4).

BrCH=CHBr and NO_2 Matrices

The photochemically induced reaction of 1,2-dibromoethene with nitrogen dioxide has also been studied in order to establish whether the transfer of an oxygen atom occurs, producing similar photoproducts to those detected in the BrCH=CHBr/O_3 reaction discussed above. The infrared spectrum of BrCH=CHBr co-deposited with NO_2 in solid argon was obtained and the band wavenumbers closely matched either those detected in the infrared spectra of BrCH=CHBr recorded previously or those recorded for NO_2 in the gas phase[36,50] (Appendix A2) (Table 6.2.6). Traces of N_2O_4 and other nitrogen oxides were inevitably present in the matrix. No infrared absorptions belonging to a precursor complex were observed, unlike the situation with ozone. An infrared spectrum recorded after UV photolysis ($\lambda > 240$ nm) led to the appearance of new bands (Table 6.2.7). Of these the very-weak bands detected at 2146.8, 2145.4, 2140.8, and 2138.5 cm^{-1} are indicative of those assigned to a C≡O stretch of carbon monoxide isolated in various environments,[32,40–42] while those at 2144.2 and 2142.2 cm^{-1} result from a C=O stretch of the ketene BrHC=C=O, viz. $\nu_{C=O}$ = 2142.2 cm^{-1} ($H_2C=C=O$).[47,48] This species has been observed elsewhere as a product formed from the analogous reaction of ethene with NO_2.[51,52] Several bands

appeared in the carbonyl stretching region and are thus assigned to $\nu_{C=O}$ of either HC(O)Br or HC(O)H, some of these were overlapped by N_2O_4 bands.[53–55] Photolysis of isolated NO_2/Ar matrices showed that all other new bands appearing after UV irradiation of BrCH=CHBr/NO_2/Ar matrices are due to photodissociation of NO_2/N_2O_4 and the subsequent chemistry of the fragments NO and $(NO)_2$.[51, 56–58]

6.2.2 PHOTOCHEMICAL PATHWAY

The first step in the photochemical pathway (Scheme 6.2.1) is the formation of a charge-transfer complex between ozone and the π system of BrCH=CHBr after co-deposition of each precursor in solid argon. The detection of other charge-transfer complexes between ozone and sp^2 systems has been reported in several studies.[8,15–18] The complex could be of a σ–type which favours the formation of an epoxide via O_2 loss, although bands tentatively attributed to an epoxide appeared after prolonged UV irradiation, suggesting first the dissociation of ozone followed by the addition of an $O(^1D)$ atom to form the epoxide (Scheme 6.2.2). The π charge-transfer complex allows ozone to photodissociate at wavelengths longer than those required to dissociate isolated ozone (UV irradiation into the Hartley band (200–310 nm) forms excited-state atomic oxygen, $O(^1D)$, and molecular oxygen). Hence, photolysis with radiation of wavelengths > 350 nm caused new bands to form at the expense of bands of the complex; these new bands are attributed to $\nu_{C=O}$ and $\nu_{C\equiv O}$ in different carbonyl···Lewis acid and carbon monoxide···Lewis acid complexes, respectively. By contrast, the lack of ozone complexation in the halogenated alkane/ozone reactions (chapter 5) meant that quartz-filtered irradiation (λ > 240 nm) for tens of hours was necessary before new $\nu_{C=O}$ and $\nu_{C\equiv O}$ bands could form.

The carbonyl compounds have also been formed in the analogous gas and liquid phase alkene/ozone reactions as intermediates in the ozonolysis reaction via the Criegee mechanism (Fig. 6.1.1). Thus the alkene/ozone reaction here is believed to follow the same pathway such that the π complex undergoes a 1,3-dipolar cycloaddition to form the five-membered ring of the POZ. The POZ then cleaves to form the carbonyl oxide (Criegee intermediate) and the aldehyde, HC(O)Br. The

rearrangement of 1,2- to 1,1-dibromoethene, followed by ozonolysis, could occur as bands attributed to HC(O)H were detected. However this rearrangement would have to occur upon deposition, *i.e.* without photolysis, which seems very unlikely. No bands belonging to the POZ or carbonyl oxide[59] could be detected, indicating that these must be transient species which immediately dissociate. The infrared study of the low-temperature ozonolysis of CH_2CCl_2[20] also showed no formation of the POZ even though the reactions were taking place as evidenced by the appearance of the infrared bands of ClC(O)Cl. As reported in chapter 5, carbonyl complexes photodissociate to form carbon monoxide complexes, likewise HC(O)Br in these experiments photodissociates to form the carbon monoxide complex OC···HBr. The formation of HC(O)Br and its subsequent dissociation to form OC···HBr occurs at the same time, *i.e.* after $\lambda > 350$ nm filtered irradiation. The relative intensities of bands belonging to HC(O)Br remained approximately constant upon shorter wavelength photolysis while the relative intensities of bands belonging to OC···HBr increased dramatically under the same photolytic conditions, indicating that a much higher percentage of the newly formed HC(O)Br dissociates upon UV photolysis. This greater concentration of carbon monoxide species could also result from the simultaneous dissociation of the carbonyl oxide intermediate resulting in the elimination of CO_2, CO and HBr.[7,11] Prolonged quartz-filtered photolysis produced bands that resembled those of a SOZ. Following the Criegee mechanism, the SOZ forms from the recombination of the undissociated carbonyl oxide and aldehyde HC(O)Br (Scheme 6.2.1).

From these experiments it is clear that an independent reaction pathway is being followed to give the same carbonyl and carbon monoxide products; it is one that involves the reaction of O atoms, (^{3}P) and (^{1}D), rather than the whole O_3 molecule, with BrCH=CHBr (Scheme 6.2.2). This is indeed the case for the reaction occurring in the solid oxygen matrix and in the NO_2/Ar matrix whereby $\nu_{C=O}$ and $\nu_{C\equiv O}$ bands are also detected. However there are many feasible routes that the reaction can proceed by[20,51,60–62] (Scheme 6.2.2 (i)–(vi)), which give rise to intermediates that can react further; thus the exact pathway responsible for the observed photoproducts is difficult to elucidate. Formyl bromide, HC(O)Br, and OC···HBr could occur from reaction pathways (i) and (ii), respectively. The excited species CHBrCHBrO* represents

several possible excited structures, including that of the epoxide (iii) which has been tentatively identified in these experiments and elsewhere.[60] The detection of bands attributable to a ketene species suggests that BrHC=C=O is produced, probably by the 1,1-elimination of HBr from CHBrCHBrO* (iii). Bands attributed to formaldehyde HC(O)H were detected but it is unclear how this species could form from BrCH=CHBr, unless it is via rearrangements and recombination of fragments such as those in pathway (iv). For HC(O)H to form via ozonolysis 1,2-dibromoethene would first have to isomerise to form 1,1-dibromoethene without any photolysis, or alternatively 1,1-dibromoethene could be present as an impurity. The fairly intense $\nu_{C=O}$ bands detected for HC(O)H makes these explanations doubtful. Another possibility is that photolysis of complexed BrCH=CHBr in the matrix could result in the elimination of H_2 or Br_2 to form the alkynes BrC≡CBr or HC≡CH, respectively, allowing H_2 to combine with CO to form HC(O)H.[24,25] The presence of HC(O)H therefore remains uncertain. Some of the $\nu_{C=O}$ bands could also belong to an acyl bromide, $CH_2BrC(O)Br$, formed from reaction pathway (v). At this stage there is not enough evidence available to identify an acyl bromide, although it is certain that more than one species is responsible for the large number of $\nu_{C=O}$ bands detected. The diradical species formed in reaction (i) and (ii) could react with each other to form an alkane or add to BrCH=CHBr to form a cyclopropane (vi), although there was no evidence to confirm the presence of these species.

The reaction mechanism of BrCH=CHBr with O_3 is not straightforward as BrCH=CHBr can react with either O_3 or O atoms via different pathways. It is very probable that both pathways are followed in these experiments as each contributes to the production of the observed photoproducts.

Scheme 6.2.1

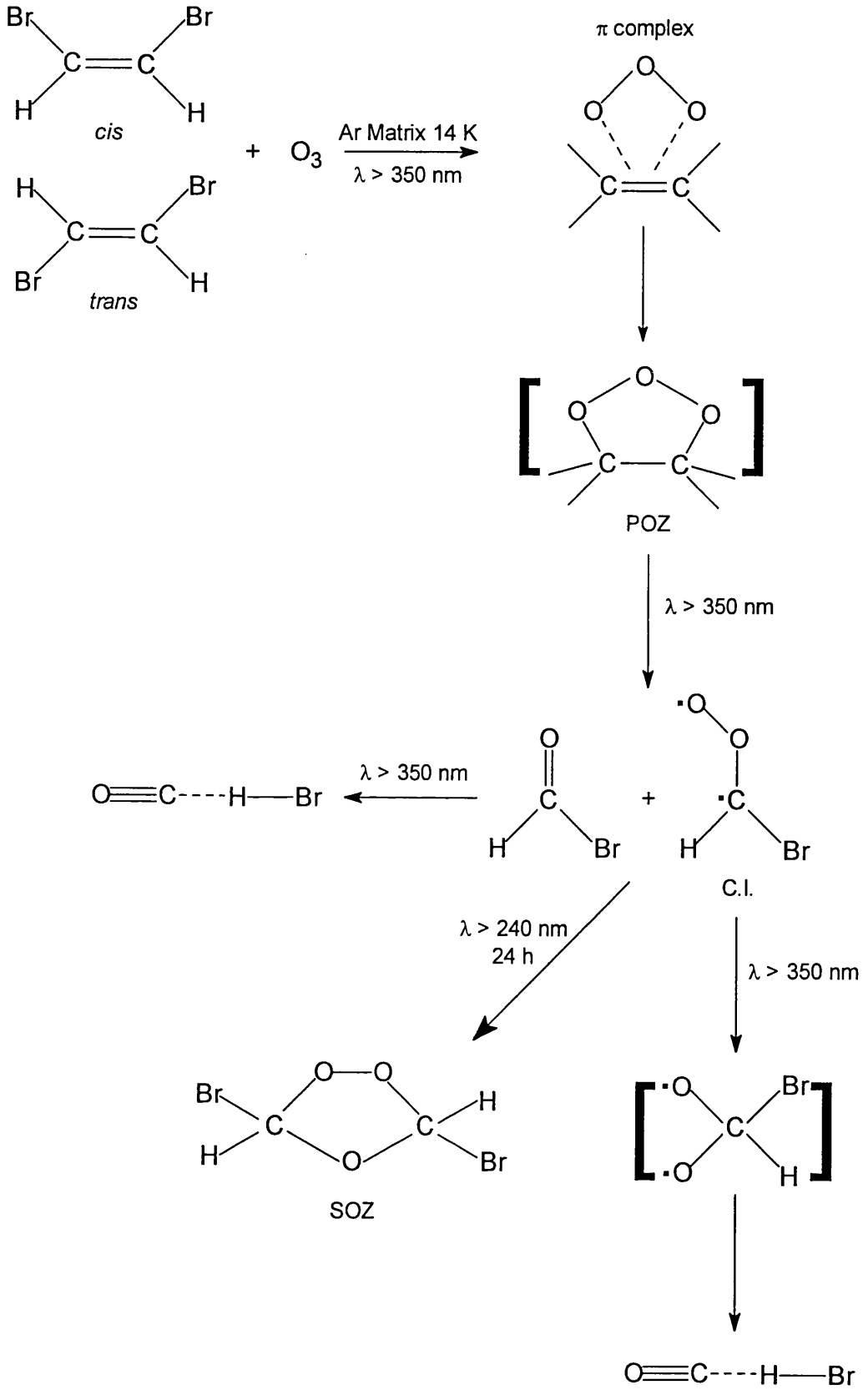
cis
trans
+ O3
Ar Matrix 14 K
λ > 350 nm
π complex
POZ
λ > 350 nm
λ > 350 nm
C.I.
λ > 240 nm
24 h
λ > 350 nm
SOZ

Scheme 6.2.2

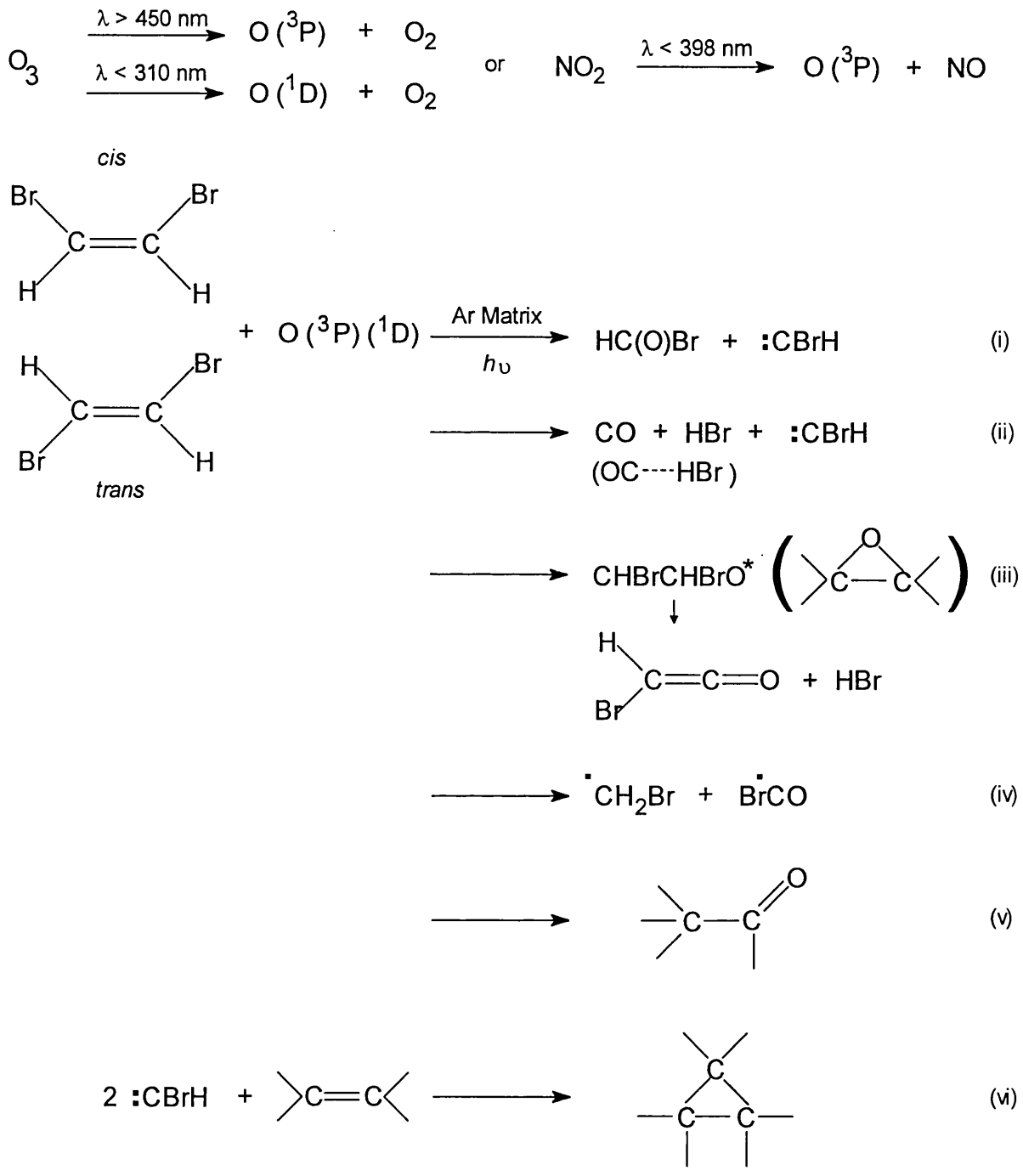
λ > 450 nm
λ < 310 nm
O (3P) + O2
O (1D) + O2
or
NO2
λ < 398 nm
O (3P) + NO
cis
trans
+ O (3P) (1D)
Ar Matrix
hυ
HC(O)Br + :CBrH
(i)
CO + HBr + :CBrH
(OC----HBr)
(ii)
CHBrCHBrO*
(iii)
HBr
CH2Br + BrCO
(iv)
(v)
2 :CBrH +
(vi)

Table 6.2.1. *Infrared bands/cm^{-1} recorded after deposition of cis- and trans-BrCH=CHBr in a variety of matrices at 14 K*

Ar	O_2[a]	$^{16}O_3$/Ar	$^{18}O_3$/Ar	Assignment
3107.9w	3100.8w		3107.6mw	$\nu_{a\ C-H}$
	3089.1w[b]			
3076.1vw, sh	3077.9w	3074ms, br	3075.9w	$\nu_{s\ C-H}$
3073.7w[b]	3072.0w[b]		3073.6mw[b]	
		2140.7vw	2140.7vw	$(CO\cdots H_2O)$?
		2110.8w[b]	1996.5vw[b]	
		2108.3w	1993.6mw	$3\nu_2\ (O_3)$
		2103.7w[c]		
1592.7w[b]			1593.1w[b]	
1590.3mw	1589.8m	1589.6s, sh	1590.2mw	$\nu_{C=C}$[d]
		1588.1s[c]	1588.4w, sh[c]	
	1549.7w	1541.4mw	1541.8w	?
1536.9w	1548.32	1536.9mw	1536.8w	
1494.5vw	1497.2vw	1494.3w	1494.4vw	$2\nu_{a\ C-Br}$
		1493.1w[b]	1492.8vw[b]	
1261.1w[b]			1261.1w[b]	
1259.4mw	1259.9mw		1259.4m	δ_{CHBr} (i-p)[d]
1258.9w,sh[b]		1255ms, br		
1162.2mw	1164.4mw	1161.9s	1162.0m	δ_{CHBr} (i-p)[e]
1161.4w,sh		1159.1s		
1151.0vw	1151.3vw	1149.2mw	1151.0w	
		1040.5ms[b]	984.6ms, sh[b]	
		1039.3s	983.4s	$\nu_3\ (O_3)$
		1037.9ms[b]	982.3s[b]	
		1033.5ms[c]	980.8ms[b]	
		1031.8m, sh[c]	978.9mw[c]	
			976.9mw[c]	
914.5vw			914.2mw	
912.4mw		912.0m	912.2m	
908.5w	906.1m		908.4w	
900.2vw	904.3mw, sh	901s, br		δ_{CHBr} (o-o-p)[e]
898.9vw, sh				
897.3vw				
753.2m	754.8ms		753.1ms	$\nu_{a\ C-Br}$
752.2mw, sh		752.4vs	752.3ms	
		751.5vs		
		750.8vs, sh		
		703.0w, br	665.2w	$\nu_2\ (O_3)$
694.5mw	689.5m	694.0mw	694.3m	δ_{CHBr} (o-o-p)[d]
690.2vw	685.2m	685.9vs		
		684.5vs		
		683.4vs		
	679.1mw, sh	681.6vs		

continued

Table 6.2.1 continued

Ar	O_2[a]	$^{16}O_3$/Ar	$^{18}O_3$/Ar	Assignment
675.1mw	676.5mw	675.2s	675.1m	δ_{CHBr} (o-o-p)[d]
673.4w			673.4mw	
672.0mw		672.2s	672.0mw	
587.8w	588.3w	585.1m	587.5w	γ_{CHBr}[d]

[a] Bands slightly shifted in the O_2 matrix. [b] Bands due to matrix site effects. [c] Bands of complex. [d] Bands attributed to *cis*-BrCH=CHBr only. [e] Bands attributed to *trans*-BrCH=CHBr only.

Table 6.2.2. *Infrared bands/cm^{-1} attributed to ozone isotopomers after deposition of mixed-ozone ($^{16}O_{3-x}{}^{18}O_x$) and cis- and trans-BrCH=CHBr in argon at 14 K*

ν_1	ν_2	ν_3	$3\nu_2$	Assignment[a]
	704.9vw[b]	1040.7ms[b]	2111.4w[b]	
1104.5vw	704.2vw	1039.4ms	2108.5w	16-16-16
		1033.9w, sh[c]		
		1032.8w[c]		
1093.0vw, sh[b]			2090.5w, sh[b]	
1091.5vw[b]		1026.8ms[b]	2089.7w[b]	
1090.0vw	688.6vw	1025.5ms	2087.6w	16-16-18
	687.9vw[b]	1022.9mw[b]		
		1019.2mw, sh[c]		
d	673.4vw[c]	1017.9m[b]	2060.4vw[b]	
	672.0w	1016.6m	2057.5vw	18-16-18
		1008.9mw, sh[c]		
	696.5vw, sh[b]	1007.3m[b]	2050.1vw[b]	
1074.7vvw	694.3w	1006.1ms	2047.3vw	16-18-16
	692.3vw, sh[c]	1004.5mw[b]		
1063.5vw, sh[b]		994.3mw, sh[c]		
1061.9vw		992.8ms[b]	2027.7vw[b]	
1060.3vw[b]	681.4vw	991.5ms	2024.9vw	18-18-16
	680.6vw[b]	989.0mw[b]		
	675.1w[c]			
1048.0vw, sh[b]	668.0vw[b]	983.5m[b]	1996.4vw[b]	
1046.6vw, sh	*e*	982.2m	1993.6vw	18-18-18
		980.8mw[b]		
		976.1w[c]		

[a] Represents the isotopomer arrangement of ozone. [b] Bands due to matrix site effects. [c] Bands of complexed O_3. [d] Bands are too weak to be detected. [e] Bands are obscured by CO_2 bands (663 cm^{-1}).

Table 6.2.3. *Infrared bands/cm^{-1} assigned to $\nu_{C=O}$ and detected after quartz-filtered (λ > 240 nm) photolysis of a variety of matrices containing cis- and trans-BrCH=CHBr at 14 K*[a]

$^{16}O_3$/Ar	$^{18}O_3$/Ar	$^{16}O_{3-x}{}^{18}O_x$/Ar	O_2	Species
1831.8vvw				
1819.4vw, sh				
1814.2vw, sh				$CH_2BrC(O)Br$?
1812.4vw				
1809.6vw, sh				
1804.5vw, sh				
1801.1w, sh				$HC(^{16}O)Br$
1797.0w				
1795.3w, sh				
1793.4w, sh				?
1788.2w, sh				
1785.3w				
1783.2w, sh				
1772.4w, sh				$HC(^{16}O)Br\cdots Br_2$?
1767.8w, sh				
1765.2w, sh				$(HC(O)Br)_2$?
1763.8w				
1759.0w, sh				
1756.7w				$HC(^{16}O)Br\cdots HBr^b$
1755.5w, sh				
1753.5w				
1747.9w, sh				
1740.1mw		1740.0vw	1740.1vw	$HC(^{16}O)H$?
1734.6mw, sh		1734.7vw	1734.2vw	
1733.4mw		1733.6vw, sh		$HC(^{16}O)Br\cdots(HBr)_2{}^b$
1730.0w, sh		1730.1vw		
1726.6w, sh		1723.3w, sh	1724.5vw	$HC(^{16}O)H\cdots HBr^b$?
1721.0w, sh		1722.0w	1721.1vw	
		1719.0vw	1719.6vw, sh	
1716.0w, sh		1717.6vw, sh	1718.8vw	
		1709.6vw, sh		
		1708.0vw		$HC(^{18}O)Br\cdots(HBr)_2{}^b$?
		1706.7vw		
	1704.1mw	1704.0w		$HC(^{18}O)H$?
	1703.9mw, sh			
	1703.4mw, sh			
		1700.9w, sh		
	1698.7vw	1699.1mw		$HC(^{18}O)H\cdots HBr^b$?
	1696.2vw	1696.2w, sh		
		1694.6w		
		1685.3vw		

continued

Table 6.2.3 continued

[a] The large number of bands may be due to aggregates or to matrix site effects. [b] Lewis acid HBr of the nearest neighbour.

Table 6.2.4. *Infrared bands/cm^{-1} assigned to $\nu_{C\equiv O}$ and detected after quartz-filtered (λ > 240 nm) irradiation of a variety of matrices containing cis- and trans-BrCH=CHBr at 14 K*

$^{16}O_3$/Ar	$^{18}O_3$/Ar	$^{16}O_{3-x}{}^{18}O_x$/Ar	O_2	Species
		2156.4vw, sh[a]		
		2154.5vw, sh	2154.7vw, sh	$^{16}OC\cdots(HBr)_2$[b]
		2153.9 vw, sh[a]		
2153.0w, sh[a]		2153.1vw[a]	2152.5vw, sh[a]	
2150.8w, sh		2151.6vw, sh	2150.4w, sh	$^{16}OC\cdots HBr$[b]
			2148.9w[a]	
		2147.6vw, sh	2147.7w, sh	$^{16}OC\cdots H_2O$[c]
		2146.0vw, sh	2146.8w, sh	$^{16}OC\cdots H_2O$[c] or
2145.6mw, sh			2145.5w	$(C^{16}O)_x$
			2145.0w, sh	
2140.5mw[a]			2140.6w, sh[a]	
2139.3mw, sh			2139.3w	$(C^{16}O)_2$
2138.6mw, sh[a]			2138.7w, sh[a]	
2138.1mw		2138.1vw	2138.0w, sh	$C^{16}O$
			2137.2w, sh[a]	
2136.7mw, sh[a]			2136.2w[a]	
	2131.3w[a]			
	2128.2w			$^{18}OC\cdots(HBr)_2$[b]
	2106.1vw	*d*		$^{18}OC\cdots(HBr)$[b]
	2100.8vw[a]			
	2087.5vw	*d*		$C^{18}O$
	2086.9vw, sh[a]			

[a] Bands due to aggregates or to matrix site effects. [b] HBr of the nearest neighbour. [c] H_2O impurity. [d] Obscured by O_3 precursor bands.

Table 6.2.5. *Infrared bands/cm^{-1} detected after photolysis ($\lambda > 240$ nm) of cis- and trans-BrCH=CHBr in a variety of matrices at 14 K*

$^{16}O_3$/Ar	$^{18}O_3$/Ar	$^{16}O_{3-x}{}^{18}O_x$/Ar	Assignment
2504.4vw	2505.2vw	2505.1vw	ν_{H-Br}[a] (OC···HBr)
	2499.1vw, sh[b]		or (OC···**HBr**···HBr)
	2490.7vw[b]	2490.7vw[b]	
2488.3w, sh	2488.6w	2488.8vw	ν_{H-Br}[c]
2479.6w, sh[b]	2487.4vw, sh[b]	2488.0vw[b]	(OC···HBr···**HBr**)
2471.7w[b]		2474.8vw[b]	
2464.2w[b]		2464.4vw[b]	
2457.1w[b]			
2446.0w, sh[b]			
2424.7w[b]			
2143.6mw		2144.1w	$\nu_{C=}{}^{16}{}_O$ (BrHC=C=O)
2142.0mw, sh[b]			
	2120.4mw, sh[b]	2120.5w, sh[b]	
	2119.5m	2119.7w	$\nu_{C=}{}^{18}{}_O$ (BrHC=C=O)
	2116.6w, sh[b]		
	2113.2w, sh[b]		
	1267.0w[b]		δ_{CH} (HC(O)H) ?
1264.1w, sh	1265.2w	1265.2w	or epoxy group ?
1218.1vw[b]		1218.5vw[b]	
	1210.8vw[b]		
1200.3vw	1200.8vw		δ_{CHBr} (SOZ)
	1199.3vw, sh[b]		
1197.8vw[b]	1198.6vw[b]	1198.7vw	
1145.4mw, sh			}
1142.0mw		1142.1vw	}
1140.8mw, sh			} δ_{CHBr}[b] (SOZ) ?
1130.9w			} or epoxy group ?
	1125.4vw	1126.3vw	}
	1122.2w		}
	1107.0vw	1111.9vw	$\nu_{C=C}$ (BrHC=C=O)
1060.6vw		1060.5vw[d]	$\nu_{C-}{}^{16}{}_O$ (SOZ)
1060.0vw, sh			
	1042.7vw	*d*	$\nu_{C-}{}^{18}{}_O$ (SOZ)
799.6vw	801.1vw[e]	799.7vw	$\nu^{16}{}_{O-}{}^{16}{}_O$ (SOZ)[f] or
	771.6vw[e]		Ring bend (SOZ) ?
	766.8vw, sh[b]		
	765.2w	765.6vw	$\nu^{18}{}_{O-}{}^{18}{}_O$ (SOZ)[f] or
	760.8, sh[b]		Ring bend (SOZ)
637.2vw	636.9w		ν_{C-Br} (HC(O)Br) or
	631.9vw*b*		Ring bend (SOZ) ?

continued

Table 6.2.5 continued

[a] A very weak band detected at 2502.3 cm^{-1} in the O_2 matrix is assigned to ν_{H-Br} (OC···HBr). [b] Bands due to aggregates or to matrix site effects. [c] A very weak band detected at 2497.7 cm^{-1} in the O_2 matrix is assigned to ν_{H-Br} (OC···$(HBr)_2$). [d] Bands obscured by O_3 bands. [e] ^{16}O impurity? [f] No $^{16}O^{18}O$ isotopomer band detected.

Table 6.2.6. *Infrared bands/cm^{-1} detected after deposition of cis- and trans-BrCH=CHBr and NO_2 in argon at 14 K*

Absorptions	Assignment[a]
3107.5mw	$\nu_{a\ C-H}$
3075.8mw	$\nu_{s\ C-H}$
3073.6m	
3053.4w	
2903.6m	$\nu_1 + \nu_3$ (NO_2)
2902.1s	
2897.6mw	
2863.9vw	
2837.5vw	
2218.6w	$\nu_2 + \nu_3$ (NO_2)
1844.6m	ν_1 (*a*-N_2O_3)
1837.3m	
1828.3vs	
1750.3mw	
1740.1mw	ν_9 (N_2O_4)
1692.3vw, sh	
1688.8w	ν_1 (*s*-N_2O_3)
1644.1 vs	ν_2 (*a*-N_2O_3)
1642.2 vs,sh	
1639.8s, sh	
1633.2 m	
1630.2 m	
1616vs, br	
1610vs, br	ν_3 (NO_2)
1541.8w	
1539.0w	?
1536.9w	
1534.2vw	
1494.5w	$2\nu_{a\ C-Br}$
1492.8w	
1298.7mw, sh	ν_1 (NO_2)
1296.3m	
1290.9vs	
1287.2ms	
1281.0mw	
1277.3m	
1270.5m	
1265.3m	ν_{11} (N_2O_4)
1259.4vs	δ_{CHBr} (i-p)[b]
1162.0ms	δ_{CHBr} (i-p)[c]
1151.0w	
912.0s	
908.3mw	δ_{CHBr} (o-o-p)[c]
903.4m	
786.7s	ν_4 (*a*-N_2O_3)
781.6m, sh	
753.2s	$\nu_{a\ C-Br}$
752.3s, sh	ν_2 (NO_2)
746.0mw	ν_{12} (N_2O_4)
694.2s	δ_{CHBr} (o-o-p)[b]
684.2mw	
675.1ms	
673.4m	
672.0ms	
640.1ms	ν_8 (N_2O_4)
637.3m	
587.7mw	γ_{CHBr}[b]

[a] See Appendix A2 for reference to the band assignments used for the oxides of nitrogen. [b] Bands attributed to *cis*-BrCH=CHBr only. [c] Bands attributed to *trans*-BrCH=CHBr only.

Table 6.2.7. *Infrared bands/cm^{-1} recorded after quartz-filtered (λ > 240 nm) photolysis of cis- and trans-BrCH=CHBr and NO_2 in argon at 14 K*

Absorptions	Assignment
2146.8vw, sh 2145.4vw, sh 2140.8vw 2138.5vw	$\nu_{C\equiv O}$[a]
2144.2vw 2142.2vw	$\nu_{C=O}$ (BrHC=C=O)[a]
1872.1vw	ν_{NO} (NO)
1863.5w	*cis*-(*s*-NO)$_2$
1777.0w, sh 1776.1mw 1771.0w 1770.1w, sh 1769.6w 1768.3w	*cis*-(*a*-NO)$_2$[a]
1758.4mw, sh	*trans*-(*a*-NO)$_2$
1757.0mw, sh 1751.6m	$\nu_{C=O}$ (HC(O)Br···HBr)[a]
1740.2m 1739.2m 1731.6mw, sh	$\nu_{C=O}$ HC(O)H[a]
1242.9w	δ_{C-H} (HC(O)H)[b]
764.3vw	
737.4mw	
568.7vw	

[a] Bands due to aggregates or matrix site effects. [b] Bands belonging to δ_{C-H} (HC(O)Br) hidden by precursor bands.

6.3 1,2-DICHLOROETHENE

Since the photochemically induced reactions of 1,2-dibromoethene with ozone and atomic oxygen in a matrix environment produced a selection of intermediates and products (section 6.2.1), this chapter has been extended to investigate the analogous reactions of another halogenated alkene, 1,2-dichloroethene. Many previous laboratory studies into the oxidation of chlorinated alkenes have been undertaken in order to investigate their significance in tropospheric chemistry.[19–22] It is expected that the photochemical pathway in the matrix will be complicated by secondary reactions as indicated by the available data for chlorinated alkenes in the gas and liquid phase.[7,19–22]

6.3.1 RESULTS AND DISCUSSION

Deposition of the Precursors, ClCH=CHCl and O_3

The infrared spectra of *trans*-1,2-dichloroethene, ClCH=CHCl, isolated in solid argon (ClCH=CHCl/Ar = 1:1000) and in solid oxygen (ClCH=CHCl/O_2 = 1:1000) have been recorded (Table 6.3.1) and the ClCH=CHCl band wavenumbers were found to be in close agreement with those reported for this species in various matrices.[23–25] Ultraviolet photolysis ($\lambda > 240$ nm) of ClCH=CHCl in Ar matrices produced no new bands whereas in solid oxygen matrices, many new bands were observed upon prolonged UV photolysis.

On co-deposition of ClCH=CHCl/Ar and O_3/Ar samples (ClCH=CHCl/O_3/Ar = 1:2.5:2500), the infrared spectrum exhibited bands that resembled those detected in the infrared spectra of ClCH=CHCl or ozone[29–31] isolated separately in argon (Tables 6.3.1 and 6.3.2 and Appendix A1). Additional weak bands with small wavenumber shifts from the ozone fundamental bands and $\nu_{C=C}$ bands were detected in these ClCH=CHCl/O_3 experiments and are attributed to the O_3···ClCH=CHCl charge-transfer π complex. These bands began to deplete upon UV-vis irradiation ($\lambda > 350$ nm) while those belonging to new species began to grow. The formation and

characterisation of ozone complexes with other carbon π systems have been reported elsewhere.[8,9,15–18]

Varying the deposition ratios of ClCH=CHCl/O_3/Ar just caused the intensities of the precursor bands to increase or decrease according to whether the concentrations were increased or decreased. In addition to the precursor bands, small quantities of matrix-isolated water and carbon dioxide were detected. Isotopic ozone, $^{18}O_3$, and mixed-ozone, $^{16}O_{3-x}{}^{18}O_x$, samples were also condensed with 1,2-dichloroethene in argon matrices (Tables 6.3.1 and 6.3.2) and the sextet of bands for each vibrational mode of the six isotopomers of ozone was detected. The wavenumbers agree with those of isolated mixed-ozone detected elsewhere (Appendix A1).[31]

Photolysis of ClCH=CHCl/O_3 Matrices

Deposition of ClCH=CHCl and O_3 in argon matrices and the subsequent photolysis cycles led to the formation of new infrared bands which are grouped according to the chemical species to which they refer.

Carbonyl Species. New bands appeared in the carbonyl-stretching region of the infrared spectra after UV-vis photolysis (λ > 350 nm) of ClCH=CHCl/O_3/Ar matrices and their intensities increased only slightly after subsequent Pyrex- (λ > 290 nm) and quartz-filtered (λ > 240 nm) photolysis. The carbonyl bands are the most diagnostic for identifying the different carbonyl···Lewis acid complexes present in a matrix.

HC(O)Cl. Bands assigned to $\nu_{C=O}$ were detected between 1761.8 and 1751.5 cm^{-1} and are attributed to formyl chloride HC(O)Cl perturbed by a Lewis acid, namely HCl (Figs. 6.3.1 and 6.3.2). Bands belonging to the unperturbed species were expected to occur around ~1780 cm^{-1}[1,33,63] but in this case were too weak to be detected, although they were detected in the mixed-ozone experiment. The shift produced in $\nu_{C=O}$ of HC(O)Cl···HCl from that of isolated HC(O)Cl compares well with those observed for other carbonyl···HCl complexes.[33,34] In the $^{18}O_3$ experiments, bands occurring between 1751.5 and 1739.9 cm^{-1} are assigned to $\nu_{C=O}$ of HC(^{18}O)Cl

isolated in argon, based on the similar ^{18}O shift of ~40 cm^{-1} for the $HC(^{16/18}O)Cl\cdots HCl$ pair reported elsewhere.[34] The attribution of medium-weak bands, detected between 1715.1 and 1710.0 cm^{-1}, to $HC(^{18}O)Cl\cdots HCl$ is made on the basis that the ^{18}O shift for the $HC(^{16/18}O)Cl\cdots HCl$ pair[34] is similar to that observed in these experiments. Both sets of isotopomer bands were detected in the mixed-ozone experiment indicating that only one ^{16}O or ^{18}O atom is present in the molecule (Fig. 6.3.2); these and the other assignments are listed in Table 6.3.3.

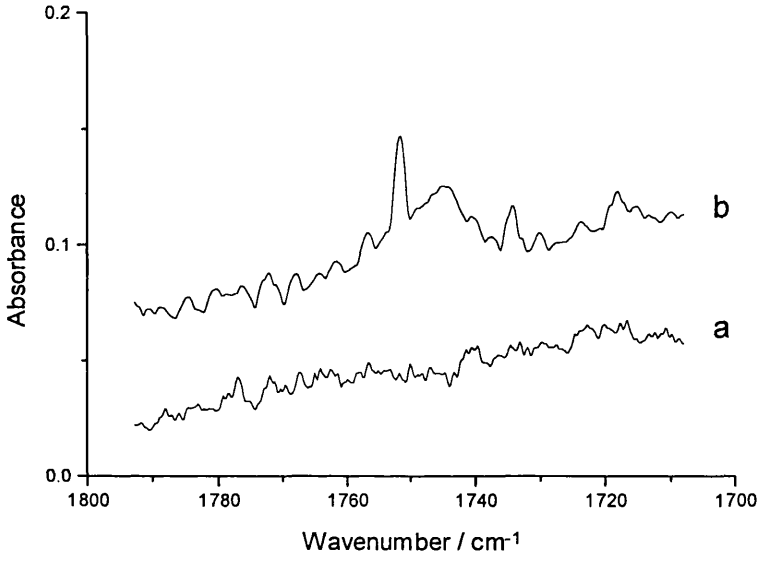

Figure 6.3.1. *Infrared spectra of a ClCH=CHCl/$^{16}O_3$/Ar matrix after (a) deposition and (b) quartz-filtered irradiation (λ > 240 nm), showing the growth of new bands assigned to $\nu_{C=O}$ of different species.*

HC(O)H. Like the dibromoethene and ozone experiments, bands characteristic of formaldehyde, HC(O)H, were detected after UV-vis irradiation of $ClCH=CHCl/O_3$ matrices (Table 6.3.3 and Figs. 6.3.1 and 6.3.2). For instance, those occurring at 1746.5, 1744.7, and 1741.6 cm^{-1} are assigned to $\nu_{C=O}$ of HC(O)H, *cf.* $\nu_{C=O}$ = 1746.1 cm^{-1} (HC(O)H in the gas phase),[35] $\nu_{C=O}$ = 1742.0 cm^{-1} (HC(O)H in an argon matrix).[35] Bands belonging to the ^{18}O isotopic counterpart appeared at 1708.5, 1706.5, and 1704.4 cm^{-1} showing an ^{18}O-shift of 33.1 cm^{-1} (^{18}O-shift = 34.2 for $HC(^{16}O)H/HC(^{18}O)H$).[34] Very weak bands situated at 1718.4, 1717.2, and 1715.8 cm^{-1}

are assigned to $\nu_{C=O}$ and tentatively attributed to HC(O)H strongly perturbed by two hydrogen halides of the nearest neighbour in the matrix, *e.g.* HC(O)H···$(HCl)_2$. In the $^{18}O_3$ experiment, bands attributed to HC(^{18}O)H···HCl were detected between 1700.0 and 1696.0 cm^{-1}.

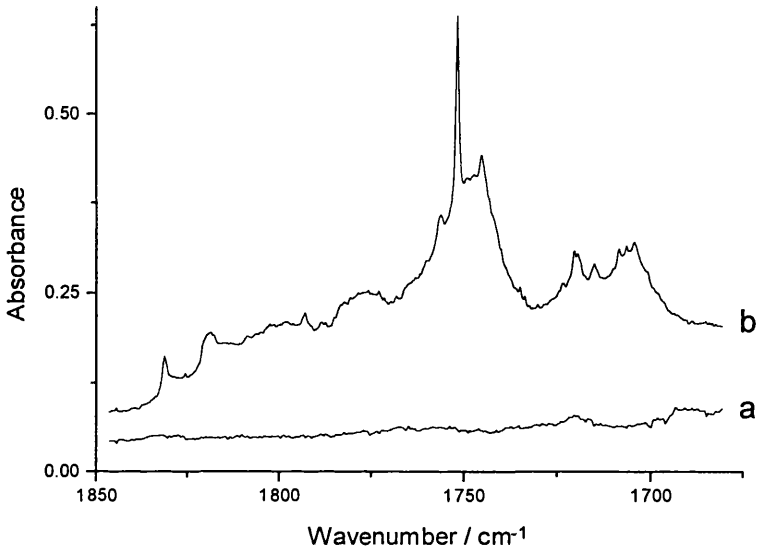

Figure 6.3.2. *Infrared spectra of a ClCH=CHCl/$^{16}O_{3-x}{}^{18}O_x$/Ar matrix after (a) deposition and (b) quartz-filtered irradiation ($\lambda > 240$ nm), showing the appearance of new bands in the $\nu_{C=O}$ region.*

Analogous carbonyl species to the ones detected here were detected in the photochemically induced reaction of BrCH=CHBr with ozone (section 6.2.1). As mentioned previously, aldehyde intermediates form during the ozonolysis reaction of alkenes (Fig. 6.1.1), therefore in the case of ClCH=CHCl with ozone the expected aldehyde HC(O)Cl is in fact detected. The other carbonyl species HC(O)H could form from the ozonolysis reaction, although the rearrangement of 1,2-dichloroethene to 1,1-dichloroethene would have to occur first. The alternative reaction where O atoms instead of ozone react with ClCH=CHCl could result in the formation of HC(O)H. In other studies[19–22] the oxidation of chloroethenes has led to the elimination of small molecules such as CO, CO_2, HCl and H_2, and thus recombination of say CO and H_2 could give rise to HC(O)H. Warming experiments made no

significant change to the intensities of the $\nu_{C=O}$ bands. Of the many carbonyl bands detected, some could belong to an acyl chloride species $CH_2ClC(O)Cl$, although no other bands indicative of this species were detected.

Carbon Monoxide Species. Bands attributable to C≡O species were first detected after UV-vis photolysis ($\lambda > 350$ nm) and their intensities increased upon Pyrex- and quartz-filtered photolysis, ($\lambda > 290$ nm) and ($\lambda > 240$ nm), respectively. The infrared bands detected are discussed below.

OC···HCl. A band detected after photolysis and occurring at 2151.1 cm^{-1} is assigned to the perturbed C≡O stretch of the complex OC···HCl. The ν_{H-Cl} bands associated with this complex occurred at 2809.4 cm^{-1} (isolated HCl in solid argon absorbs between 2888.0 and 2853.3 cm^{-1})[41,43,64] (Tables 6.3.4 and 6.3.5). For comparison, $\nu_{C\equiv O}$ bands occurred at 2154.2 and 2152.2 cm^{-1} and ν_{H-Cl} bands occurred at 2815.3 and 2810.2 cm^{-1} for OC···HCl studied elsewhere.[41,63,65] Bands belonging to the ^{18}OC···HCl isotopomer were detected around 2097.3 cm^{-1}. Some $\nu_{C\equiv O}$ bands were strongly perturbed as they experienced large wavenumber shifts to 2160.2 and 2157.7 cm^{-1} from that of isolated CO (~2138 cm^{-1});[40–42] they are thus attributed to $OC\cdots(HCl)_2$ based on the fact that $\nu_{C\equiv O}$ bands of similar wavenumber were obtained for this complex elsewhere.[34,41] The ν_{H-Cl} bands of $OC\cdots(HCl)_2$ appeared around 2788.0 cm^{-1} (ν_{H-Cl} = 2788.2 cm^{-1} for $OC\cdots(HCl)_2$).[43] The $\nu_{C\equiv O}$ bands for the $^{18}OC\cdots(HCl)_2$ isotopomer are referred to in Table 6.3.4 and resemble those detected for elsewhere[34] $^{18}OC\cdots(HCl)_2$. A weak shoulder situated at 2155.5 cm^{-1} and a weak band at 2800.5 cm^{-1} are assigned to $\nu_{C\equiv O}$ and ν_{H-Cl}, respectively, of HCl···OC···HCl as these wavenumbers are intermediate between those of $OC\cdots(HCl)_2$ and OC···HCl (Figures 6.3.3–6.3.5). No significant changes to the $\nu_{C\equiv O}$ bands were observed upon warming experiments except in the $^{18}O_3$ experiment where the intensities of bands attributed to $OC\cdots(HCl)_2$ decreased. A slight decrease in the intensities of ν_{H-Cl} bands belonging to $OC\cdots(HCl)_2$ was also observed.

Other carbon monoxide species. A very weak band attributable to CO isolated in argon was detected at 2138.5 cm^{-1} while those slightly blue-shifted to 2146.9, 2145.7, and 2143.4 cm^{-1} are attributed to either CO perturbed by the impurity H_2O or to $(CO)_x$ species.[40,42] Isolated $C^{18}O$ gave rise to the weak bands at 2088.2 and 2086.6 cm^{-1}, while blue-shifted bands belonging to the analogous species, $^{18}OC\cdots H_2O$ or $(C^{18}O)_x$, occurred between 2093.6 and 2090.8 cm^{-1} (Table 6.3.4 and Figs. 6.3.3 and 6.3.4).

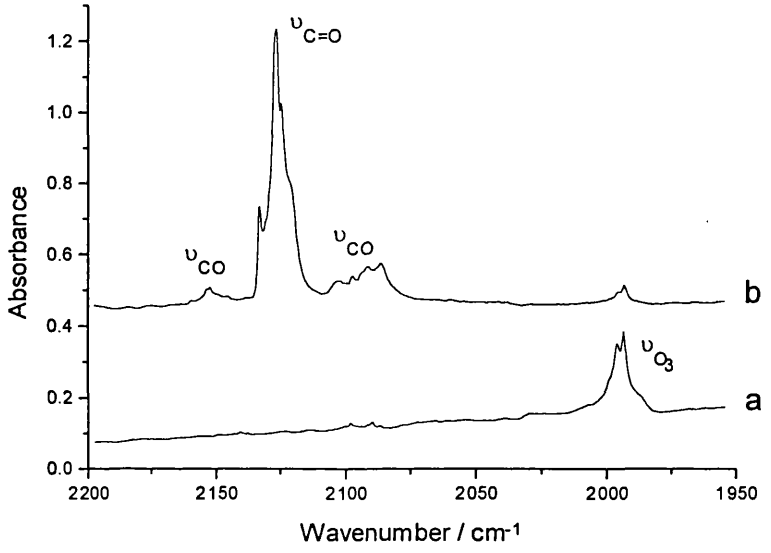

Figure 6.3.3. *Infrared spectra of a ClCH=CHCl/$^{18}O_3$/Ar matrix after (a) deposition and (b) quartz-filtered irradiation (λ > 240 nm). The spectra show the growth on irradiation of new bands in the $\nu_{C\equiv O}$ and $\nu_{C=O}$ (ClHC=C=O) region.*

The removal of electron density from the weakly antibonding orbital of CO by the Lewis acid (section 6.2.1), in this case HCl, leads to an increase in bond strength and in $\nu_{C\equiv O}$, whereas transfer of electron density into the HCl antibonding orbital leads to a decrease in bond strength and in ν_{H-Cl}. How the carbon monoxide species form after the photochemically induced reaction of ClCH=CHCl with O_3, is discussed in section 6.3.2.

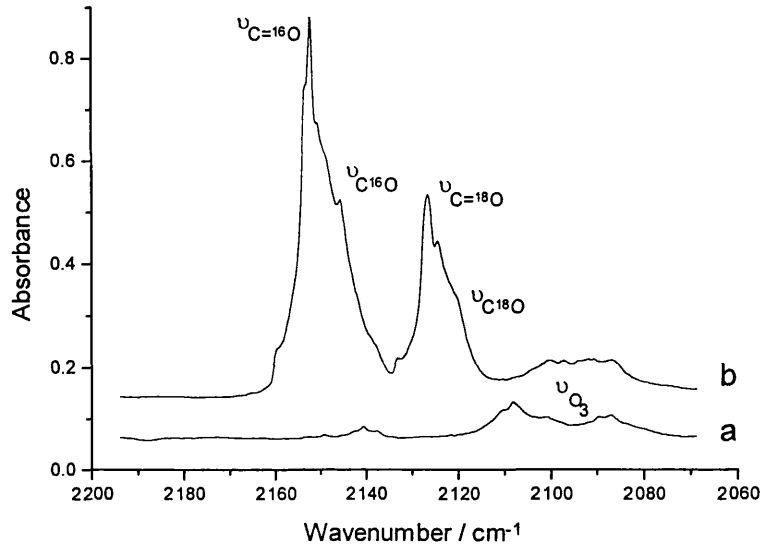

Figure 6.3.4. *Infrared spectra of a ClCH=CHCl/$^{16}O_{3-x}{}^{18}O_x$/Ar matrix after (a) deposition and (b) quartz-filtered irradiation ($\lambda > 240$ nm). New bands are assigned to $\nu_{C\equiv O}$ and $\nu_{C=O}$ (ClHC=C=O) of each isotopomer.*

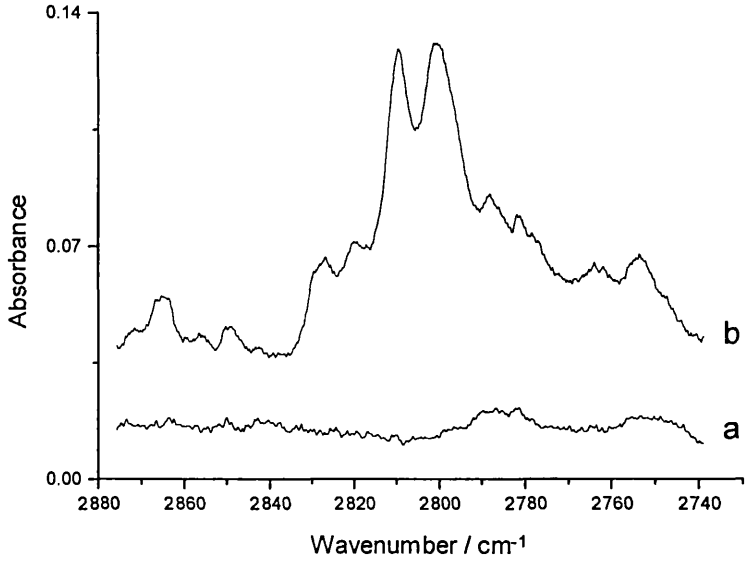

Figure 6.3.5. *Infrared spectra of a ClCH=CHCl/$^{18}O_3$/Ar matrix after (a) deposition and (b) quartz-filtered photolysis ($\lambda > 240$ nm) showing bands appearing in the ν_{H-Cl} region.*

Ketene. UV-vis photolysis of ClCH=CHCl/O_3/Ar matrices resulted in the appearance of new bands which are attributed to the ketene species ClHC=C=O (Table 6.2.5 and Figs. 6.3.3 and 6.3.4). The intensities of these bands increased after Pyrex- and quartz-filtered irradiation. Those at 2153.6 and 2152.4 cm^{-1} are assigned to $\nu_{C=O}$ while the ^{18}O counterpart bands occurred around 2126.8 cm^{-1} (bands belonging to both isotopomers were found in the mixed-ozone experiment). Bands belonging to the C=C stretch were detected in the $^{18}O_3$ and $^{16}O_{3-x}{}^{18}O_x$ experiments and occurred between 1110.9 and 1098.4 cm^{-1} and at 1108.1 and 1099.9 cm^{-1}, respectively. The $\nu_{C=O}$ and $\nu_{C=C}$ band wavenumbers detected here are similar to those observed for $H_2C=C=O$ studied elsewhere.[47,48]

Ozonide. After prolonged quartz-filtered irradiation, new bands appeared in the spectra which are attributed to the secondary ozonide species (SOZ) formed from the ozonolysis reaction between ClCH=CHCl and O_3 (Table 6.3.5).[2,20] The very weak band detected at 1218.3 cm^{-1} is assigned to δ_{CHCl}, while those appearing in the ^{18}O-enriched experiments near 1148 cm^{-1} are tentatively assigned to δ_{CHCl} as well. A very weak band at 1083.7 cm^{-1} and the ^{18}O counterpart bands occurring at 1067.7 and 1064.7 cm^{-1} are assigned to ν_{C-O}. In the mixed-ozone experiment bands that could be assigned to both $\nu_{C-^{16}O}$ and $\nu_{C-^{18}O}$ were detected. A band possibly resulting from the O–O stretch of the SOZ occurred at 796.4 cm^{-1} in the $^{16}O_{3-x}{}^{18}O_x$ experiment, while that resulting from the ^{18}O–^{18}O stretch occurred at 764.9 cm^{-1}. The fact that no bands result from the ^{16}O–^{18}O stretch makes these assignments speculative; some could, on the other hand, arise from a ring bending mode of the ozonide. The bands detected at 758.7 and 748.6 cm^{-1} are tentatively assigned to ν_{C-Cl} of the SOZ while the remaining bands in the 731–648 cm^{-1} region are tentatively attributed to ring bending modes of the ozonide (Table 6.3.5). Warming of the matrix had no effect on the intensities of these bands.

Other Species. Some of the bands previously assigned could equally be attributed to other species. The bands occurring near 1272, 1148, and 885 cm^{-1} (Table 6.3.5) could be attributed to an epoxide species because bands at 1265, 1165, and 865 cm^{-1} have been attributed to the epoxy group of ethene oxide by a number of groups.[26,36,49] Many bands occurred in the C≡C stretching region (Table 6.3.5) and

are thus assigned to $\nu_{C\equiv C}$, probably of C_2Cl_2 as no ≡C–H bands were detected and $\nu_{C\equiv C}$ of di-substituted alkynes occurs in the region of 2260–2190 cm^{-1}.[26] The matrix environment or the existence of a $C_2Cl_2\cdots$Lewis acid complex must have removed the symmetry of C_2Cl_2 for $\nu_{C\equiv C}$ to be infrared active. As in the $BrCH{=}CHBr/O_3$ experiments, no ν_{O-H} bands were detected, ruling out the formation of a carboxylic acid species.

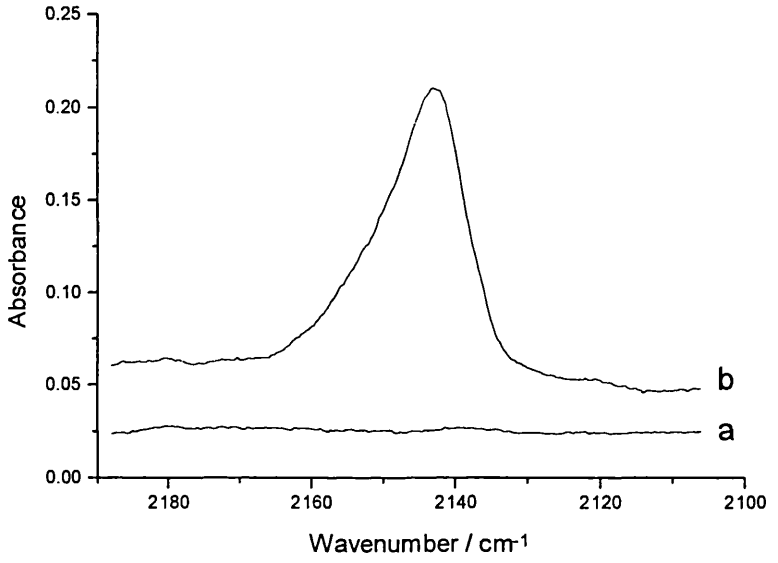

Figure 6.3.6. *Infrared spectra of a $ClCH{=}CHCl/O_2$ matrix after (a) deposition and (b) quartz-filtered photolysis ($\lambda > 240$ nm) for many hours showing the growth of $\nu_{C\equiv O}$ and $\nu_{C=O}$ (ClHC=C=O) bands.*

Solid Oxygen Matrices. Quartz-filtered photolysis for many hours of solid oxygen matrices containing ClCH=CHCl was required before any new bands could be detected. The new bands that formed resembled those detected in the analogous experiments utilising ozone and are thus assigned on this basis (Tables 6.3.3 and 6.3.4). As in section 6.2.1 no complex formed between the alkene and oxygen matrix resulting in the need for long photolysis times to initiate a reaction with ClCH=CHCl. The oxygen matrix therefore acts as an O atom source to produce the carbonyl, carbon monoxide, and ketene species (Fig. 6.3.6); the fact that these were detected but no SOZ species suggests that another photochemical pathway distinct from that of

Criegee is being followed. Warming of the matrix led to a slight decrease in the intensities of $\nu_{C=O}$ and $\nu_{C\equiv O}$ bands.

ClCH=CHCl and NO_2 Matrices

The infrared spectrum of 1,2-dichloroethene co-deposited with nitrogen dioxide in an argon matrix at 14 K has been recorded (Table 6.3.6), the band wavenumbers resembling those recorded for either precursor studied elsewhere (ClCH=CHCl[23–25] and NO_2 in the gas phase,[36,50] Appendix A2). Other bands belonging to traces of N_2O_4 and other nitrogen oxides were also detected. No bands were detected that could be attributed to a precursor complex. Photolysis of the matrix using quartz-filtered radiation ($\lambda > 240$ nm) led to the appearance of new bands which are listed in table 6.3.7. As in the BrCH=CHBr/O_3, BrCH=CHBr/NO_2, and ClCH=CH/O_3 experiments, bands detected are attributable to similar carbonyl, carbon monoxide, and ketene species.

6.3.2 PHOTOCHEMICAL PATHWAY

The photochemically induced reaction between ClCH=CHCl and ozone resulted in the formation of a number of new products (Scheme 6.3.1). Initially, upon deposition, a π complex is formed between O_3 and the double bond of ClCH=CHCl, as bands experiencing small wavenumber shifts from the fundamental bands of the precursors were observed and only UV-vis irradiation ($\lambda > 350$ nm) was required to start a reaction. This initial photo-induced reaction produced new bands belonging to the carbonyl and carbon monoxide species at the expense of bands of the complex, *cf.* section 6.2.1. Various carbonyl and carbon monoxide species were also detected in the halogenated alkane and ozone reactions (chapter 5), but in these situations no bands of a complex were detected and harsh UV photolysis for tens of hours was required to initiate the reactions.

Analogous to the ozonolysis reactions of alkenes studied in the gas and liquid phases,[1–18] the ozonolysis of ClCH=CHCl seems also to follow the Criegee mechanism whereby the initial π complex undergoes a 1,3-dipolar cycloaddition to

form the five-membered ring of the primary ozonide (POZ) which then cleaves to form the carbonyl oxide (Criegee intermediate) and HC(O)Cl. In these matrix experiments no bands were detected for the POZ[6] or the Criegee intermediate indicating that these species immediately undergo dissociation, whereas bands for HC(O)Cl were indeed detected. The carbonyl species HC(O)Cl then dissociates upon UV-vis irradiation to form the carbon monoxide species OC···HCl as seen for similar carbonyl species studied in chapter 5. Upon Pyrex- and quartz-filtered photolysis the relative intensities of bands belonging to HC(O)Cl remained approximately constant while those belonging to OC···HCl increased considerably. This greater concentration of CO species could result from the simultaneous dissociation of the carbonyl oxide intermediate.[7,11] Quartz-filtered photolysis for many hours gave rise to bands that resembled those of a secondary ozonide (SOZ),[2,20] which is formed by the recombination of any remaining carbonyl oxide and aldehyde species HC(O)Cl (Scheme 6.3.1).

The carbonyl and carbon monoxide species detected in the ozone experiments were also detected in the solid oxygen matrix experiments and nitrogen dioxide experiments; this and the fact that ClHC=C=O bands were detected but no SOZ bands, implies that a different pathway from that of ozonolysis is being followed. It is proposed that the different pathway involves the reaction of O atoms with ClCH=CHCl to give the same carbonyl and carbon monoxide species (Scheme 6.3.2). Therefore in the ClCH=CHCl/O_3 experiments, two possible reaction pathways may exist because ozone can either dissociate to give O atoms or remain as an O_3 molecule. As shown in scheme 6.3.2 (i)–(vi), there are many routes by which the O atom reaction can proceed,[20,51,60–62] producing intermediates that can react further. The exact pathway responsible for the production of the observed photoproducts is therefore difficult to clarify. The carbonyl HC(O)Cl and the carbon monoxide species OC···HCl, said to have formed from the ozonolysis reaction via the Criegee mechanism, could also have been produced from reaction (i) and (ii), respectively, (Scheme 6.3.2). The excited species CHClCHClO* represents several possible excited structures, including that of the epoxide (iii) which has been tentatively identified in these experiments. The species CHClCHClO* probably undergoes 1,1-HBr elimination to form the observed ketene species ClHC=C=O (iii). As in the

$BrCH{=}CHBr/O_3$ experiments, bands tentatively attributed to formaldehyde HC(O)H were detected, but 1,2-dichloroethene would first have to isomerise to form 1,1-dichloroethene so that HC(O)H could form via ozonolysis; the occurrence of this process without any photolysis seems doubtful. It is a possibility that 1,1-dichloroethene is present in the matrix as an impurity, but the fairly intense HC(O)H bands indicate that this reason is unlikely. Alternatively, rearrangements and recombination of fragments like those in pathway (iv) could give rise to HC(O)H. The most likely explanation is that the photolysis of complexed ClCH=CHCl in the matrix results in the elimination of H_2 or Cl_2 to form the alkyne ClC≡CCl or HC≡CH, respectively.[24,25] Some $\nu_{C\equiv C}$ bands were in fact detected and were attributed to ClC≡CCl only, as no ν_{C-H} bands were detected (v). Due to the symmetry constraints on the molecule, the $\nu_{C\equiv C}$ mode should be IR inactive; however the matrix environment or a complex of ClC≡CCl could effectively lower the symmetry and thus make this mode IR active. If ClC≡CCl is formed then the eliminated H_2 molecule could combine with the liberated CO as discussed above to form HC(O)H. Some of the $\nu_{C=O}$ bands could also belong to $\nu_{C=O}$ of the acyl chloride species $CH_2ClC(O)Cl$ formed from reaction pathway (vi), although at this stage there is insufficient evidence to identify this species. Other possible reactions could occur for the CHClCHClO* species and the diradical species formed in (i) and (ii), such as that shown in reaction pathway (vii), although no bands indicative of a cyclopropane species were detected.

Consequently the photochemical pathway of ClCH=CHCl with O_3 is not a trivial one as either O_3, O atoms or both participate in the photochemically induced reaction via different mechanisms. At this stage there is not enough evidence to distinguish between the two possibilities although it is probable that both pathways are followed in these experiments as each contributes to the production of the observed photoproducts.

Scheme 6.3.1

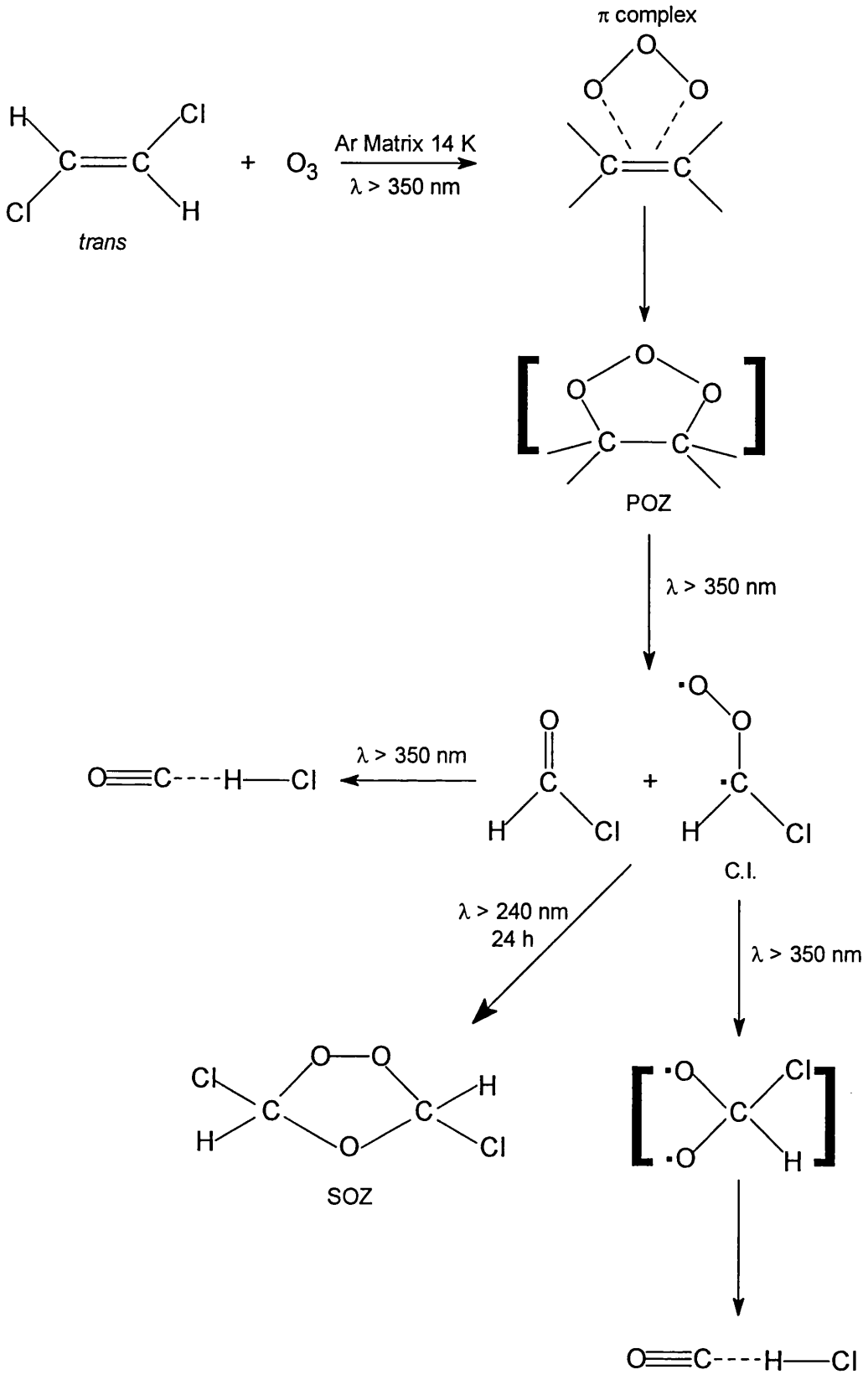
π complex
trans
Ar Matrix 14 K
λ > 350 nm
POZ
λ > 350 nm
λ > 350 nm
C.I.
λ > 240 nm
24 h
λ > 350 nm
SOZ

Scheme 6.3.2

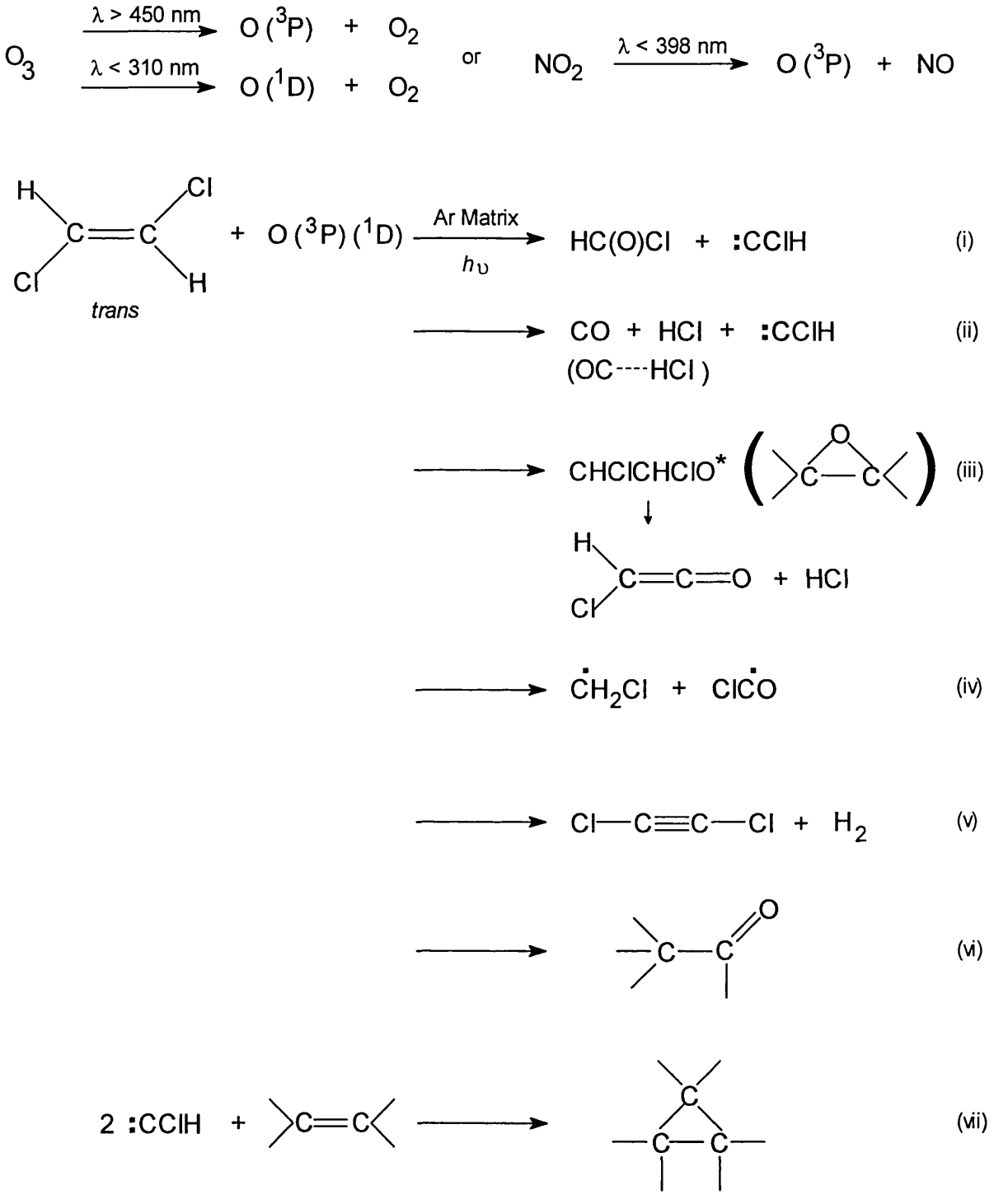
λ > 450 nm
λ < 310 nm
O(3P) + O2
O(1D) + O2
or
NO2
λ < 398 nm
O(3P) + NO
trans
Ar Matrix
hυ
HC(O)Cl + :CClH
(i)
CO + HCl + :CClH
(OC----HCl)
(ii)
CHClCHClO*
(iii)
HCl
CH2Cl + ClCO
(iv)
Cl—C≡C—Cl + H2
(v)
(vi)
2 :CClH +
(vii)

Table 6.3.1. *Infrared bands/cm^{-1} detected after deposition of trans-ClCH=CHCl in a variety of matrices at 14 K*

Ar	O_2	$^{16}O_3$/Ar	$^{18}O_3$/Ar	Assignment
3109.2m	3099.9ms	3109.8w	3109.6m	$\nu_{a\ C-H}$
3105.8mw, sh[a]	3090.6ms, sh[a]	3105.5vw, sh[a]	3105.4mw[a]	
3103.0w, sh[a]	3076.8mw[a]	3103.6vw, sh[a]		
3080.1w				$\nu_{s\ C-H}$
		2149.3w		$\nu_1 + \nu_3$ (O_3)
		2143.2vw[a]		
		2140.6vw		(CO···H_2O) ?
		2137.9vw[a]		
		2111.0vw[a]	1996.0mw[a]	
		2108.4w	1993.6mw	$3\nu_2$ (O_3)
1601.9mw[a]		1602.0mw[a]	1601.9mw[a]	
1599.4mw	1595.8ms	1599.4mw	1599.5mw	$\nu_{C=C}$[b]
			1598.0mw[c]	
1597.1w[a]			1597.0mw[a]	
		1595.7w[c]		
1593.4w[a]		1593.4w[a]	1593.4mw[a]	
1589.4w[a]		1590.5w[a]		
1211.3vw[a]				
1203.3mw, sh[a]	1204.9s[a]	1203.3w, sh[a]	1202.9m, sh[a]	
1201.8ms[a]	1203.6s, sh[a]	1202.0mw	1201.9ms[a]	
1200.5m, sh	1201.3s, sh		1200.4mw, sh	δ_{CHCl} (i-p)
		1046.8mw[a]		
		1040.6ms[a]		
		1039.4s	980s, br	ν_3 (O_3)
		1037.9m[a]	977.8s, sh[c]	
		1034.8mw, sh[c]		
		912.1w, sh		}
909.7s		910.2mw	909.8s	}
905.9ms	904vs, br	906.3w	906.0ms	} δ_{CHCl} (o-o-p)[a]
902.8m, sh			903.0m, sh	}
901.9m, sh	901.9vs, sh			}
	900.1vs, sh			}
851.2w	848.5mw			}
827.3vs		827.4m	827.2vs	}
824.4vs		824.4m	824.3vs	} $\nu_{a\ C-Cl}$[d]
821.5s		821.5mw	823.3vs	}
			821.6vs	}
818.9ms, sh	818vs, br	818.6mw, sh		}
		704.5vw		ν_2 (O_3)

[a] Bands due to aggregates or matrix site effects. [b] The $\nu_{C=C}$ stretch of *trans*-ClCH=CHCl is infrared inactive although the vibration does indeed appear in the spectrum due to the lowering of symmetry by the matrix. [c] Bands of complex. [d] Many bands may be due to isotopic splitting.

Table 6.3.2. Infrared bands/cm^{-1} assigned to ozone isotopomers after deposition of mixed-ozone ($^{16}O_{3-x}{}^{18}O_x$) and trans-ClCH=CHCl in argon at 14 K

ν_1	ν_2	ν_3	$3\nu_2$	Assignment[a]
1107.8vw, sh[b]	705.9w ,sh[b]		2110.4w, sh[b]	
1103.3vw	704.2w	1039.2s	2108.2w	16-16-16
	703.3w ,sh[c]	1037.8s[b]	2101.4vw, sh[c]	
		1034.7ms, sh[c]		
1091.2w, sh[b]	688.5w[b]		2089.6vw	
1090.0w	687.8w	1025.3ms	2087.0vw	16-16-18
		1022.8ms[b]	2083.9vw, sh[b]	
		1021.0m, sh[c]	2079.7vw, sh[c]	
			2059.2vw,sh[b]	
	672.0vw, sh	1016.4m	2057.1vw	18-16-18
d	670.5vw[b]	1015.2mw,sh[b]		
		1011.9mw, sh[c]		
	698.4vw[b]		2049.5vw, sh[b]	
1075.0vw	696.6vw	1005.8m	2046.5vw	16-18-16
		1004.5m,sh[b]	2040.0vw, sh[c]	
		1001.5mw, sh[c]		
1061.4vw, sh[b]	681.5vw,sh[b]		2026.7vwb	
1060.5vw	680.6vw	991.3m	2024.6vw	18-18-16
1056.5vw[c]		988.9m[b]	2019.0vw, sh[c]	
		987.1m, sh[c]		
			1995.7vw, sh[b]	
e	*f*	982.1m	1993.5vw	18-18-18
		981.1m, sh[b]	1986.8vw, sh[c]	
		977.7mw, sh[c]		

[a] Represents the isotopomer arrangement of ozone. [b] Bands due to matrix site effects. [c] Bands of complexed O_3. [d] Bands are too weak to be detected. [e] Bands are obscured by ν_3 bands of O_3. [f] Bands are obscured by CO_2 (663 cm^{-1}).

Table 6.3.3. *Infrared bands/cm^{-1} assigned to $\nu_{C=O}$ and detected after quartz-filtered ($\lambda > 240$ nm) photolysis of matrices containing trans-ClCH=CHCl at 14 K*[a]

$^{16}O_3$/Ar	$^{18}O_3$/Ar	$^{16}O_{3-x}{}^{18}O_x$/Ar	O_2	Species
		1831.0w		
		1819.2w		$CH_2ClC(O)Cl$?
		1808.8w, sh		
		1805.0w, sh		
		1802.6w, sh	1803 mw,br	$ClC(O)Cl$[b] ?
		1799.8w, sh		
		1796.2w, sh		
		1792.9w		?
		1788.5w		
		1787.3w		
		1782.6mw, sh		
		1780.6mw		$HC(^{16}O)Cl$
		1775.0 mw		
		1772.9mw		
		1771.5mw, sh		
		1768.1mw	1768.3mw, br	$(HC(O)Cl)_2$
		1765.3mw, sh		
		1763.1mw, sh		
1761.8vw		1760.2mw, sh		
1756.5vw		1756.2mw, sh	1757.3m, sh	$HC(^{16}O)Cl\cdots HCl$[c]
1751.5w		1751.8m	1752.2m	
		1749.4mw, sh	1748.7m, sh	
		1747.2mw, sh		
1746.5w, sh		1745.3m	1745.2m, sh	
1744.7w				
1741.6vw, sh		1741.6mw, sh		$HC(^{16}O)H$
	1751.5mw, sh			
	1748.8mw			
	1747.1mw, sh	1747.2mw, sh		
	1746.0mw, sh	1745.3m		
	1743.7mw, sh			
	1741.1w	1741.6mw, sh		$HC(^{18}O)Cl$
	1739.9mw			
	1734.5w	1734.9mw, sh	1735.2mw, sh	
1733.5vw	1733.5w	1733.6mw, sh		
	1730.0w		1730.3mw, sh	?
	1723.5mw, sh	1723.6mw, sh		
	1720.5mw	1720.6mw		
	1719.6mw	1719.6mw		
1718.4vw	1718.9mw, sh	1718.8mw, sh		$HC(^{16}O)H\cdots HCl$[c]
1717.2vw	1717.5mw			
1715.8vw, sh		1715.2mw		

continued

Table 6.3.3 continued

$^{16}O_3$/Ar	$^{18}O_3$/Ar	$^{16}O_{3-x}{}^{18}O_x$/Ar	O_2	Species
	1715.1mw	1715.2mw		
	1714.3mw, sh			
	1712.8mw			
	1711.3mw, sh			
	1710.0mw, sh			$HC(^{18}O)Cl\cdots HCl^c$
	1708.5mw	1708.6mw		$HC(^{18}O)H$
	1706.5mw	1706.8mw		
	1704.4m	1704.5mw		
	1700.9mw, sh			
	1700.0mw, sh	1699.3mw, sh		
	1697.9mw, sh	1698.1mw, sh		
	1696.0mw			$HC(^{18}O)H\cdots HCl^c$

[a] The large number of bands may be due to aggregates or to matrix site effects. [b] $\nu_{C=O}$ of ClC(O)Cl = 1803 cm^{-1}.[66] [c] Lewis acid HCl of the nearest neighbour.

Table 6.3.4. *Infrared bands/cm^{-1} assigned to $\nu_{C\equiv O}$ and detected after quartz-filtered ($\lambda > 240$ nm) irradiation of matrices containing trans-ClCH=CHCl at 14 K*

$^{16}O_3$/Ar	$^{18}O_3$/Ar	$^{16}O_{3-x}{}^{18}O_x$/Ar	O_2	Species
2160.2w[a]				
2157.7w		2159.3w, sh		$^{16}OC\cdots(HCl)_2$[b]
2155.5w, sh				$HCl\cdots C^{16}O\cdots HCl$[b]
2151.1w, sh[a]		2151.1m, sh[a]	2151.2w, sh[a]	$^{16}OC\cdots HCl$[b]
		2148.7m, sh		
2146.9w, sh		2146.2m		$^{16}OC\cdots H_2O$[c] or
2145.7w				$(CO)_x$
2143.4w		2142.1mw, sh	2142.5mw	
2138.5vw, sh		2138.0w, sh		$C^{16}O$
	2104.8w, sh[a]			
	2103.5w			$^{18}OC\cdots(HCl)_2$[b]
	2101.9w[a]	2100.3w[a]		
	2097.3w	2097.3w		$^{18}OC\cdots(HCl)$[b]
	2093.6w, sh	2094.4w, sh		$^{18}OC\cdots H_2O$[c] or
	2091.9w	2093.1w, sh		$(C^{18}O)_x$
	2090.8w	2092.0w		
	2088.2w, sh[a]	2090.8w[a]		
		2087.6w, sh		$C^{18}O$
	2086.6w[a]	2086.8w[a]		

[a] Bands due to aggregates or to matrix site effects. [b] HCl of the nearest neighbour. [c] H_2O impurity.

Table 6.3.5. *Infrared bands/cm^{-1} detected after quartz-filtered (λ > 240 nm) photolysis of a variety of matrices containing trans-ClCH=CHCl at 14 K*

$^{16}O_3$/Ar	$^{18}O_3$/Ar	$^{16}O_{3-x}{}^{18}O_x$/Ar	Assignment
a	2826.9w	2826.2vw	ν_{H-Cl}[c] $(HCl)_2$
	2819.5w[b]		
a	2809.4w	2809.4w	ν_{H-Cl}[d] (OC···HCl) or (OC···HCl···**HCl**)
a	2800.5w	2800.0w	ν_{H-Cl} (HCl···CO···HCl)
		2791.8w, sh[b]	
a	2788.2w	2788.0w, sh	ν_{H-Cl}[e] (OC···**HCl**···HCl)
		2784.8w, sh[b]	
	2764.2vw[b]		
	2753.7vw[b]		
	2735.8vw[b]		
	2261.6vw	2261.6vw	}
		2247.4vw	}
	2242.8vw	2242.5vw	} $\nu_{C\equiv C}$[f]
2230.8vw		2231.0vw	}
2227.7vw	2223.9vw	2224.4vw	}
2223.9vw, sh	2220.7w		}
2153.6w[b]		2153.6m, sh[b]	
2152.4w		2152.3ms	$\nu_{C=^{16}O}$ (ClHC=C=O)
	2133.2mw[b]	2132.9w, sh[b]	
	2130.5mw, sh[b]		
	2126.8ms	2127.0m	$\nu_{C=^{18}O}$ (ClHC=C=O)
	2124.7m[b]	2124.2mw, sh[b]	
	2121.3mw, sh[b]	2120.9mw, sh[b]	
	1288.7vw		}
1280.0vw	1287.0vw, sh		}
1272.0vw	1276.9vw		}
	1269.7vw	1269.5w	} δ_{CH}[b] (HC(O)H) or
	1265.3vw, sh		} epoxy group ?
1244.2vw	1240.7vw, sh	1244.1w	}
	1237.2vw		}
1218.3vw	1218.1vw	1218.3vw	δ_{CHCl} (SOZ)
		1168.9vw	}
a		1166.3vw	} δ_{CHCl}[b] (SOZ) or
	1148.5w	1148.3vw	} epoxy group ?
		1134.5vw	}
	1110.9vw		}
a	1106.1vw	1108.1vw	} $\nu_{C=C}$ (ClHC=C=O)[b]
	1098.4vw	1099.9vw	}
1083.7vw		1083.6w	$\nu_{C-^{16}O}$ (SOZ)
		1079.7w, sh[b]	

continued

Table 6.3.5 continued

$^{16}O_3$/Ar	$^{18}O_3$/Ar	$^{16}O_{3-x}{}^{18}O_x$/Ar	Assignment
	1067.7mw	1067.6w	$\nu_{C-^{18}O}$ (SOZ)
	1064.7w, sh	1064.6vw, sh[b]	
1053.2vw	1052.4w	1052.9vw	δ_{OCO} (SOZ) ?
a		889.3vw[b]	$\nu_{C-^{18}O}$ (SOZ) or
	885.5vw	885.5vw	epoxy group ?
a	796.4w[g]	796.4vw	$\nu^{16}{}_{O-}{}^{16}O$ (SOZ)[h] or
	784.5w[g]		Ring bend (SOZ) ?
	762.5w, sh	764.9w, sh	$\nu^{18}{}_{O-}{}^{18}O$ (SOZ)[h]
758.7vw	756.8mw	757.0mw, sh	} ν_{C-Cl}[b] (SOZ) ?
748.6vw	745.2mw, sh	748.4mw	}
731.0vw	731.0mw	731.0mw	}
		729.0mw	} Ring bend[b] (SOZ) or
728.7vw	728.7mw	723.5w, sh	} ν_{C-Cl}[i] (HC(O)Cl) ?
	716.8w	716.8w	}
		657.3mw	Ring bend (SOZ) ?
a	652.3mw	652.6mw, sh[b]	
	648.0mw[b]		

[a] Bands too weak to be detected. [b] Bands due to aggregates or to matrix site effects. [c] A very weak band detected at 2822.0 cm^{-1} in the O_2 matrix is assigned to ν_{H-Cl} $(HCl)_2$. [d] A very weak band detected at 2808.2 cm^{-1} in the O_2 matrix is assigned to ν_{H-Cl} (OC···HC). [e] Very weak bands detected at 2793.0, 2791.5, and 2787.2 cm^{-1} in the O_2 matrix are assigned to ν_{H-Cl} (OC···**HCl**···HCl). [f] Matrix environment or complex formation makes $\nu_{C\equiv O}$ IR active. [g] ^{16}O impurity? [h] No $^{16}O^{18}O$ isotopomer detected. [i] Bands due to isotopic splitting or to site effects.

Table 6.3.6. *Infrared bands/cm^{-1} recorded after deposition of trans-ClCH=CHCl and NO_2 in argon at 14 K*

Absorptions	Assignment[a]
3109.4m 3105.7m 3103.0m, sh	$\nu_{a\ C-H}$
2901.9mw 2897.0mw	$\nu_1 + \nu_3$ (NO_2)
1893.7mw	ν_1 (N_2O_2)
1852.6mw, sh 1844.9mw,br 1837.2mw, sh 1827.9m	ν_1 (*a*-N_2O_3)
1753.6mw 1739.0m 1716.9w	ν_9 (N_2O_4)
1688.8w 1675.9mw 1668.8mw 1663.4w, sh	ν_1 (*s*-N_2O_3)
1644.5ms 1639.8mw 1633.2m 1629.2m 1627.2m	ν_2 (*a*-N_2O_3)
1616.3s, sh 1609vs, br	ν_3 (NO_2)
1290.3m 1277.5m 1263.2ms 1256.5ms	ν_1 (NO_2)
1201.8s	δ_{CHCl} (i-p)
909.7vs 905.8vs 903.1vs, sh	δ_{CHCl} (o-o-p)
851.0mw 821vs, br	$\nu_{a\ C-Cl}$
786.4m	ν_4 (*a*-N_2O_3)
750.8mw, sh 748.7mw, sh	ν_2 (NO_2)
747.2mw	ν_{12} (N_2O_4)
646.8mw 639.9mw, sh 637.4mw, sh	ν_8 (N_2O_4)

[a] See Appendix A2 for reference to the band assignments used for the oxides of nitrogen.

Table 6.3.7. *Infrared bands/cm^{-1} recorded after quartz-filtered (λ > 240 nm) photolysis of trans-ClCH=CHCl and NO_2 in argon at 14 K*

Absorptions	Assignment
2147.5w, br	$\nu_{C\equiv O}$, $\nu_{C=O}$ (ClHC=C=O)
1876.5mw, sh 1871.9mw 1863.2mw	ν_{NO} (NO)
1771.0w, sh 1768.1w	$\nu_{C=O}$ (HC(O)Cl)
1761.8w, sh 1753.3mw 1751.1mw 1748.8mw, sh	$\nu_{C=O}$ (HC(O)Cl···HCl)
1739.8mw 1738.7mw	$\nu_{C=O}$ (HC(O)H)
1300.1mw	δ_{C-H} (HC(O)Cl)
1243.3w	δ_{C-H} (HC(O)H)
1120.7vw	$\nu_{C=C}$ (ClHC=C=O)
736.2w	
570.9w 569.2w	

6.4 CONCLUDING REMARKS

The two halogenated ethenes, 1,2-dibromoethene and 1,2-dichloroethene, have been co-deposited separately with ozone in argon matrices at 14 K and their subsequent photochemically induced reactions using different wavelength irradiation ($\lambda > 350$ nm, $\lambda > 290$ nm, and $\lambda > 240$ nm) have been examined. In each case ozonolysis occurs via the Criegee mechanism as the expected HC(O)X (X = Br or Cl) intermediate and related SOZ species have been detected. As seen previously in chapter 5, the carbonyl species can dissociate to form carbon monoxide species; OC···HX species (X = Br or Cl) are detected in these experiments. The ozonolysis reaction occurs after only UV-vis irradiation ($\lambda > 350$ nm) due to the formation of an ozone···XCH=CHX (X = Br or Cl) π complex upon deposition. This differs from previous studies in which the warming of N_2, Xe and CO_2 matrices was required to initiate ozonolysis of simple alkenes (no reaction took place after warming Ar matrices containing ozone and ethene).

Another reaction pathway is being followed in these XCH=CHX/O_3 matrix experiments as similar photoproducts were observed in the oxygen matrix and NO_2/Ar experiments. Therefore it is not only O_3 that reacts with XCH=CHX to produce the carbonyl and carbon monoxide species but atomic oxygen also.

These photolytic matrix experiments have shown halogenated ethenes to behave similarly with ozone to that of simple gas-phase alkenes, but the presence of the halogen substituents and O atom oxidation encourages the reaction to occur via alternative pathways.

6.5 REFERENCES

(1) Hull, L. A.; Hisatsune, I. C.; Heicklen, J., *J. Am. Chem. Soc.* **1972**, *94*, 4856–4864.

(2) Kuhne, H.; Gunthard, H. H., *J. Phys. Chem.* **1976**, *80*, 1238–1246.

(3) Nelander, B.; Nord, L., *Tetrahedron Lett.* **1977**, *32*, 2821–2822.

(4) Bailey, P. S. *Ozonation in Organic Chemistry*; Academic Press: New York, NY, 1978; Vol I.

(5) Harding, L.B.; Goddard, W. A., *J. Am. Chem. Soc.* **1978**, *100*, 7180–7188.

(6) Kohlmiller, C. K.; Andrews, L., *J. Am. Chem. Soc.* **1981**, *103*, 2578–2583.

(7) Atkinson, R.; Carter, W. P. L., *Chem. Rev.* **1984**, *84*, 437–470.

(8) McKee, M. L.; McMichael, R. C., *J. Am. Chem. Soc.* **1989**, *111*, 2497–2500.

(9) Samuni, U.; Fraenkel, R.; Haas, Y.; Fajgar, R.; Pola, J., *J. Am. Chem. Soc.* **1996**, *118*, 3687–3693.

(10) Horie, O.; Schafer, C.; Moortgat, G. K., *Int. J. Chem. Kinet.* **1999**, *31*, 261–269.

(11) Anglada, J. A.; Crehuet, R.; Bofill, J. M., *Chem. Eur. J.* **1999**, *5*, 1809–1822.

(12) Neeb, P.; Moortgat, G. K., *J. Phys. Chem.* **1999**, *103*, 9003–9012.

(13) Atkinson, R., *Atmos. Environ.* **1990**, *24A*, 1–41.

(14) Criegee, R., *Angew. Chem., Int. Ed. Engl.* **1975**, *14*, 745–752.

(15) Bailey, P. S.; Ward, J. W.; Hornish, R. E., *J. Am. Chem. Soc.* **1971**, *93*, 3552–3554.

(16) Bailey, P. S.; Ward, J. W.; Carter, T. P.; Neih, E.; Fischer, C. M.; Khashab, A. Y., *J. Am. Chem. Soc.* **1974**, *96*, 6136–6140.

(17) Jonnalagadda, S.; Chan, S.; Garrido, J.; Bond, J.; Singmaster, K. A., *J. Am. Chem. Soc.* **1995**, *117*, 562–563.

(18) Singmaster, K. A.; Pimentel, G. C., *J Phys. Chem.* **1990**, *94*, 5226–5229.

(19) Sanhueza, E.; Heicklen, J., *Int. J. Chem. Kinet.* **1975**, *7*, 589–604.

(20) Sanhueza, E.; Hisatsune, I. C.; Heicklen, J., *Chem. Rev.* **1976**, *76*, 801–826.

(21) Griesbaum, K.; Hayes, M. P.; Werli, V., *Can. J. Chem.* **1988**, *66*, 1366–1370.

(22) Hasson, A. S.; Smith, I. W. M., *J. Phys. Chem. A* **1999**, *103*, 2031–2043.

(23) Cartland, H. E.; Pimentel, G. C., *J. Phys. Chem.* **1986**, *90*, 5485–5491.

(24) Laursen, S. L.; Pimentel, G. C., *J. Phys. Chem.* **1989**, *93*, 2328–2333.

(25) Laursen, S. L.; Pimentel, G. C., *J. Phys. Chem.* **1990**, *94*, 8175–8182.

(26) Bellamy, L. J. *The Infrared Spectra of Complex Molecules;* Wiley: New York, NY; 1975.

(27) Cowieson, D. R.; Barnes, A. J.; Orville-Thomas, W. J., *J. Raman Spectrosc.* **1981**, *10*, 224–226.

(28) Rytter, E.; Gruen, D. M., *Spectrochim. Acta*, **1979**, *35A*, 199–207.

(29) Brosset, P.; Dahoo, R.; Gauthier-Roy, B.; Abouaf-Marguin, L.; Lakhlifi, A., *Chem. Phys.* **1993**, *172*, 315–324.

(30) Schriver-Mazzuoli, L.; de Saxce, A.; Lugez, C.; Camy-Peyret, C.; Schriver, A., *J. Chem. Phys.* **1995**, *102*, 690–701.

(31) Dimitrov, A.; Seppelt, K.; Scheffler, D.; Willner, H., *J. Am. Chem. Soc.* **1998**, *120*, 8711–8714.

(32) Lasson, E.; Nielsen, C. J., *Acta Chem. Scand.* **1997**, *51*, 1–7.

(33) Clark, R. J. H.; Dann, J. R., *J. Phys. Chem. A* **1997**, *101*, 2074–2082.

(34) Lugez, C.; Schriver, A.; Schriver-Mazzuoli, L.; Lasson, E.; Nielsen, C. J., *J. Phys. Chem.* **1993**, *97*, 11617–11624.

(35) Khoshkhoo, H.; Nixon, E. R., *Spectrochim. Acta* **1973**, *29A*, 603–612.

(36) Herzberg, G., *Infrared and Raman Spectra of Polyatomic Molecules*; Van Nostrand: NY; 1945.

(37) Nelander, B., *J. Chem. Phys.* **1980**, *73*, 1026–1033.

(38) Nelander, B., *J. Mol. Struct.* **1980**, *69*, 59–68.

(39) Solomons, T. W. G., *Organic Chemistry*; Wiley: NY, 1992.

(40) Dubost, H.; Abouaf-Marguin, L., *Chem. Phys. Lett.* **1972**, *17*, 269–273.

(41) Andrews, L.; Arlinghaus, R. T.; Johnson, G. L., *J. Chem. Phys.* **1983**, *78*, 6347–6352.

(42) Loewenschuss, A.; Givan, A.; Nielsen, C. J., *J. Mol. Struct.* **1997**, *408/409*, 533–537.

(43) Barnes, A. J.; Hallam, H. E.; Scrimshaw, G. F., *Trans. Faraday Soc.* **1969**, *65*, 3172–3178.

(44) Clark, R. J. H.; Dann, J. R.; Foley, L. J., *J. Chem. Soc. Dalton Trans.* **1999**, 73–78.

(45) Huo, W. M., *J. Chem. Phys.* **1965**, *43*, 624–628.

(46) Rosen, B., *Spectroscopic Data Relative to Diatomic Molecules*; Pergamon: NY, 1970.

(47) Hochstrasser, R.; Wirz, J., *Angew. Chem. Int. Ed. Engl.* **1990**, *29*, 411–413.

(48) Moore, C. B.; Pimentel, G. C., *J. Chem. Phys.* **1963**, *38*, 2816–2829.

(49) Lord, R. C.; Nolin, B., *J. Chem. Phys.* **1956**, *24*, 656–658.

(50) Laane, J.; Ohlsen, J. R., *Prog. Inorg. Chem.* **1980**, *27*, 465–513.

(51) Fitzmaurice, D. J.; Frei, H., *J. Phys. Chem.* **1992**, *96*, 10308–10315.

(52) Loison, J. C.; Dedonder-Lardeux, C.; Jouvet, C.; Solgadi, D., *J. Phys. Chem.* **1991**, *95*, 9192–9196.

(53) Begun, G. M.; Fletcher, W. H., *J. Mol. Spectrosc.* **1960**, *4*, 388–397.

(54) Bibart, C. H.; Ewing, G. E., *J. Chem. Phys.* **1974**, *61*, 1284–1292.

(55) Andrews, B.; Anderson, A., *J. Chem. Phys.* **1981**, *74*, 1534–1537.

(56) Fateley, W. G.; Bent, H. A.; Crawford, B., *J. Chem. Phys.* **1959**, *31*, 204–217.

(57) Busch, G. E.; Wilson, K. R., *J. Chem. Phys.* **1972**, *56*, 3626–3637.

(58) Zacharias, H.; Geilhaupt, M.; Meier, K.; Welge, K. H., *J. Chem. Phys.* **1981**, *74*, 218–225.

(59) Sander, W., *Angew. Chem., Int. Ed. Engl.* **1990**, *29*, 344–354.

(60) Bosch, E.; Kochi, J. K., *J. Am. Chem. Soc.* **1996**, *118*, 1319–1329.

(61) Nakata, M.; Frei, H.; *J. Phys. Chem.* **1989**, *93*, 7670–7677.

(62) Chatterjee, J.; Coombes, R. G.; Barnes, J. R.; Fildes, M. J., *J. Chem. Soc. Perkin Trans. 2* **1995**, 1031–1032.

(63) Strandman-Long, L.; Nelander, B.; Nord, L., *J. Mol. Struct.* **1984**, *117*, 217–233.

(64) Barnes, A. J.; Hallam, H. E.; Scrimshaw, G. F., *Trans. Faraday Soc.* **1969**, *65*, 3150–3158.

(65) Perchard, J. P.; Cipriani, J.; Silvi, B.; Maillard, D., *J. Mol. Struct.* **1983**, *100*, 317–339.

(66) Catalano, E.; Pitzer, K. S., *J. Am. Chem. Soc.* **1958**, *80*, 1054–1057.

Chapter 7

Photochemically Induced Reactions of Diiodomethane and 1,2-Diiodoethane

7.1 INTRODUCTION

The photochemically induced reactions of ozone with either diiodomethane or 1,2-diiodoethane in solid argon matrices are studied in this chapter. In the preceding chapters, a number of novel species have been produced and identified after treating ozone with a halogenated species and the photochemical pathways vary depending upon the type of halogenated species used. Using the results reported elsewhere and in this thesis, the photo-induced reactions of ozone with diiodoalkanes could proceed via two possible pathways: first, the reactions could proceed in a similar manner to those of ozone with mono-iodinated species, CH_3I,[1] ICl,[2] C_2H_5I,[3] CF_3I,[4] C_2F_5I,[5] CHClI,[6] and ICN[7] (chapter 3), producing an ozone···precursor complex, iodoso-, iodyl-, and hypoiodo-species, and second, they could proceed in a similar manner to those of ozone with other dihalomethanes, CH_2Br_2 and CH_2Cl_2,[8] producing carbonyl and carbon monoxide complexes. The presence of two large iodine atoms may give rise to an altogether new photochemical pathway, and so it is of interest to see how the CH_2I_2/O_3 and ICH_2CH_2I/O_3 reactions progress.

7.2 DIIODOMETHANE AND OZONE

The study of the photochemically induced reaction between CH_2I_2 and O_3 was chosen in order to compare it with the known reactions of ozone with mono-iodinated species, Z–I (CH_3I,[1] ICl,[2] C_2H_5I,[3] CF_3I,[4] C_2F_5I,[5] CHClI,[6] and ICN[7] (chapter 3)), as well as the known reactions of ozone with di- and tri-halomethanes, CH_mX_n, studied in this thesis[9] and elsewhere[6,8,10] (X = Br or Cl). The question of whether the CH_2I_2/O_3 reaction produces either $IH_2C–I\cdots O_3$, $IH_2C–IO$, $IH_2C–IO_2$, and $IH_2C–OI$ type species, as in the $Z–I/O_3$ reactions, or $HC(O)I\cdots HI$ and (CO)(HI)(HI) type species, as in the CH_2X_2/O_3 reactions (X = Br or Cl), is asked and investigated.

7.2.1 RESULTS AND DISCUSSION

Deposition of the Precursors, CH_2I_2 and O_3

The infrared spectrum of diiodomethane (CH_2I_2) isolated separately in an argon matrix (CH_2I_2/Ar = 1:500) has been recorded and a number of bands detected (Table 7.2.1) and assigned using the band assignments given elsewhere for $CH_2I_2^+$ and other dihalomethanes as guides.[6,8,11–14] Ultraviolet photolysis ($\lambda > 240$ nm) of the CH_2I_2/Ar matrix did not produce any new features in the spectrum. This differs from the results obtained by Maier *et al.*[12,13] whereby the photoisomerisation of diiodomethane (CH_2I_2) in an argon matrix formed iso-diiodomethane ($CH_2I\cdots I$). The characteristic C–H and C–I stretches of the $CH_2I\cdots I$ isomer were either too weak to be detected in these experiments or were hidden by precursor bands.

Upon co-deposition of CH_2I_2 with ozone in solid argon (CH_2I_2/O_3/Ar = 1:1:500) the infrared spectrum exhibited bands assignable to one or other precursor as the band wavenumbers matched those detected in the infrared spectrum of CH_2I_2 or ozone isolated separately in argon (Table 7.2.1).[15,16] Unlike the mono-iodinated species referred to in chapter 3, no bands were detected to support the formation of an $O_3\cdots I_2CH_2$ complex and only harsh photolysis with UV radiation ($\lambda > 240$ nm) led to the production of new bands. Even after many hours of quartz-filtered irradiation ($\lambda >$ 240 nm) the new bands remained weak. Irradiating the matrix during deposition made no difference to the intensities of the product bands. Isotopic ozone samples were also deposited with CH_2I_2 and the spectroscopic data are listed in Table 7.2.1.

Photolysis of CH_2I_2/O_3 Matrices

Pyrex- and quartz-filtered irradiation of CH_2I_2/O_3/Ar matrices gave rise to new weak absorptions in the infrared spectrum which are assigned in the following sections.

Carbonyl Species. Bands attributable to formaldehyde were detected after Pyrex- and quartz-filtered photolysis (Table 7.2.2 and Fig. 7.2.1) and resemble those detected in previous studies for HC(O)H in the gas phase[17] and in various

matrices.[17–19] The weak bands situated between 1741.8 and 1732.4 cm^{-1} are assigned to the carbonyl stretch of HC(O)H in its monomeric, dimeric, and higher polymeric forms,[17,19,20] while the weak bands at 1724.9 and 1721.6 cm^{-1} are assigned to the carbonyl stretch of HC(O)H perturbed by the remaining moiety of the precursor, I_2, *i.e.* the HC(O)H···I_2 complex is present. These wavenumbers can be compared with those of other formaldehyde···halogen complexes and thus show I_2 to be a stronger Lewis acid than Br_2 and Cl_2; HC(O)H···Br_2 (1727.7 cm^{-1})[8] and HC(O)H···Cl_2 (1734.5 and 1732.4 cm^{-1}).[8] Alternatively, the $\nu_{C=O}$ bands at 1724.9 and 1721.6 cm^{-1} could be attributed to the HC(O)H···HI complex on the basis that the $\nu_{C=O}$ bands detected elsewhere for HC(O)H···HI occurred at 1729.9 cm^{-1},[1] and 1728 cm^{-1}.[21] The wavenumber of the $\nu_{C=O}$ band at 1714.4 cm^{-1} suggests even greater perturbation of the carbonyl moiety, possibly due to the HC(O)H···$(HI)_2$ complex.

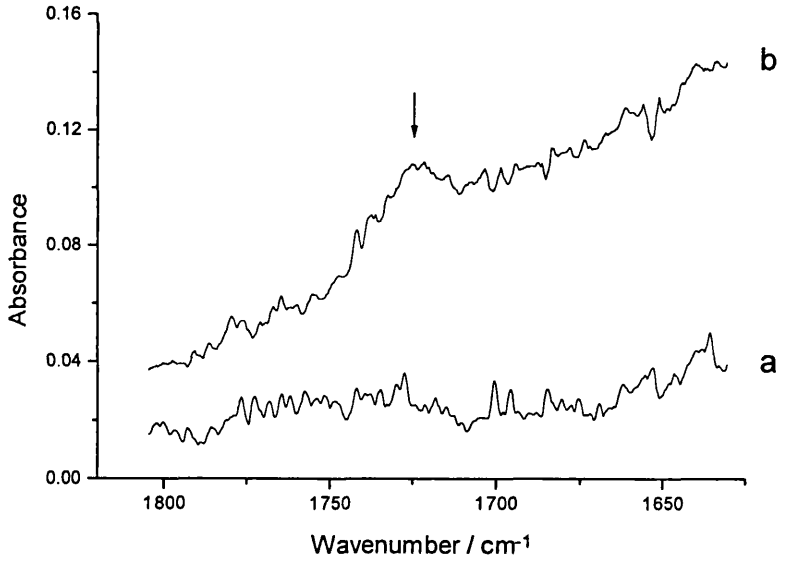

Figure 7.2.1. *Infrared spectra of a $CH_2I_2/^{16}O_3/Ar$ matrix after (a) deposition and (b) quartz-filtered photolysis (λ > 240 nm) showing new bands appearing in the $\nu_{C=O}$ region.*

The observation of very weak ν_{H-I} bands between 2234.4 and 2224.2 cm^{-1} (Fig. 7.2.2) provide further evidence to support the presence of HC(O)H···HI type complexes,

viz. ν_{H-I} = 2230.0 cm^{-1} (HI in the gas phase).[22,23] In the isotopic $^{18}O_3$ experiment $\nu_{C=O}$ bands appeared at 1706.3, 1702.1 and 1698.2 cm^{-1}, the first value belonging to isolated HC(^{18}O)H and the last two values to perturbed HC(^{18}O)H. The $\nu_{C=O}$ values obtained here compare well with those obtained for HC(^{18}O)H studied elsewhere.[1,8]

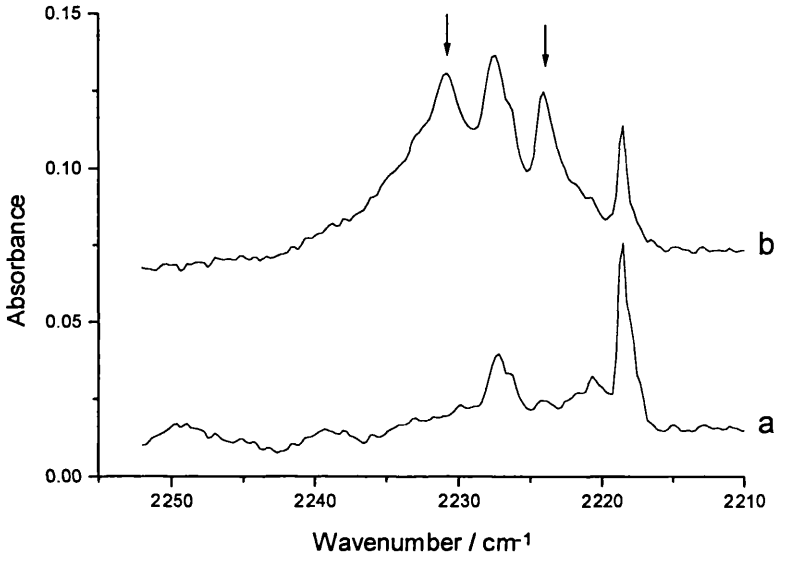

Figure 7.2.2. *Infrared spectra of a $CH_2I_2/^{16}O_3/Ar$ matrix after (a) deposition and (b) quartz-filtered photolysis ($\lambda > 240$ nm) showing new bands assigned to ν_{H-I}.*

Other bands that could be attributed to HC(O)H were detected; those at 1254.4 and 1243.4 cm^{-1} are assigned to ρ_{CH_2} while that at 1191.9 cm^{-1} is assigned to ω_{CH_2}. Remarkably no δ_{CH_2} bands appeared in the expected ~1500 cm^{-1} region of the spectrum; these bands may have been too weak or were shifted due to complexation and obscured by the precursor bands.

Carbon Monoxide Species. Pyrex- and quartz-filtered irradiation of $CH_2I_2/O_3/Ar$ matrices also led to the production of carbon monoxide bands, $\nu_{C\equiv O}$, (Table 7.2.2 and Fig. 7.2.3). The $\nu_{C\equiv O}$ bands appeared very weakly and were situated at 2138.4, 2138.0 and 2136.6 cm^{-1} and are attributed to CO isolated in argon.[24–26] A considerably weak $\nu_{C\equiv O}$ band at 2152.1 cm^{-1} is most likely attributed to the OC···HI species on the basis that H–I bands have indeed been detected, while the $\nu_{C\equiv O}$ band at

2142.9 cm^{-1} could possibly result from $OC\cdots I_2$. The ^{18}O counterparts appeared at 2093.9 and 2087.3 cm^{-1} and are assigned to $\nu_{C\equiv^{18}O}$ of $^{18}OC\cdots HI$ and CO, respectively.

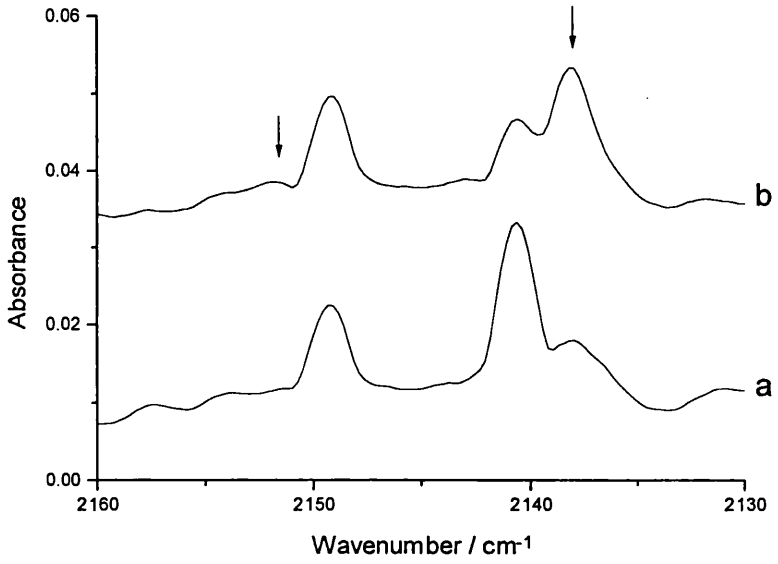

Figure 7.2.3. *Infrared spectra of a $CH_2I_2/^{16}O_3/Ar$ matrix after (a) deposition and (b) quartz-filtered photolysis ($\lambda > 240$ nm) showing the growth of new bands assigned to* $\nu_{C\equiv O}$.

Other Species. In the $^{16}O_3$ experiment a medium band at 3385.6 cm^{-1} appeared after photolysis and is indicative of an O–H stretching vibration. This band could possibly be attributed to the $I_2CH(OH)$ species which is analogous to the ICH_2OH species formed from the reaction between CH_3I and ozone.[1] Bands that could be assigned to ν_{C-O} and δ_{COH} of $I_2CH(OH)$ were also detected and occurred at 956.8 and 951.7 cm^{-1} and at 1151.4 cm^{-1}, respectively. These bands are listed in Table 7.2.2.

The reaction of CH_2I_2 with O_3 differs considerably from the reaction of mono-iodinated precursors, Z–I,[1-7] with O_3 such that UV irradiation for a few hours was required before any product bands were detected, unlike the Z–I/O_3 cases in which product bands were detected after near-infrared ($\lambda > 800$ nm) or visible ($\lambda > 650$ nm) photolysis for just 10 min. Another major difference is that the Z–I species formed a

complex with O_3 upon matrix deposition whereas, given the photochemical behaviour, CH_2I_2 did not. This is possibly due to some kind of steric hindrance imposed by the close proximity of the second iodine atom, although other Z–I species containing large functional groups ($-CH_3$ and $-CF_3$) still formed complexes with O_3. Ozone complexes are usually of the charge-transfer type and so it could be informative to look at the charge distribution of CH_2I_2 as an O_3 molecule approaches using theoretical calculations to find out why complex formation is not favoured. The absence of an $O_3\cdots I_2CH_2$ complex meant that no $IH_2C–IO$, $IH_2C–IO_2$, or $IH_2C–OI$ species were formed or detected.

7.2.2 PHOTOCHEMICAL PATHWAY

Co-deposition of CH_2I_2 with ozone in solid argon matrices followed by UV photolysis led to the formation of new species; the photochemical interconversion is illustrated in Scheme 7.2.1. Bands detected in the carbonyl stretching region are attributed to isolated HC(O)H and complexed HC(O)H. Although there were no $\nu_{C=O}$ bands that could be attributed to formyl iodide HC(O)I, the fact that HI was detected provides tentative evidence for its formation. The mechanism by which these carbonyl species form is probably via the insertion of an O atom (from photodissociated ozone) into a C–H or C–I bond, followed by hydrogen halide (HI) or halogen (I_2) abstraction. Bands belonging to the $I_2CH(OH)$ species, which presumably forms from the O atom insertion into a C–H bond of CH_2I_2, were also detected. In this case HI abstraction did not occur leaving $I_2CH(OH)$ stabilised by the matrix environment. An alternative pathway is one in which the C–I bond of CH_2I_2 dissociates and the CH_2I and I fragments go on to react with O atoms.[11,12,14,27] The fact that no resulting products were detected and neither was any iso-diiodomethane ($H_2C–I–I$)[13] rules this pathway out. The O atom insertion mechanism is therefore favoured in this study as well as in the analogous reactions of ozone with CH_2Br_2,[8] CH_2Cl_2,[8] $CHBr_2Cl$[9] (chapter 5), $CHBrCl_2$[9] (chapter 5), $CHCl_3$.[10] In the dichloro- and dibromomethane/O_3 study,[8] CH_2Cl_2 produced only HC(O)Cl and CH_2Br_2 produced both HC(O)Br and HC(O)H, while in the CH_2I_2/O_3 experiment it is clear that HC(O)H is the major carbonyl product; these results reflect the reduction in strength of the C–X and H–X bond as the halogen group is descended.

UV photolysis also led to the appearance of bands that are indicative of the C≡O stretch of carbon monoxide species. The small wavenumber shifts in $\nu_{C\equiv O}$ from that of isolated C≡O suggested that C≡O is perturbed either by HI or I_2. Thus OC···HI and OC···I_2 form from the photodissociation of either HC(O)H···I_2, HC(O)H···HI, or HC(O)I···HI. The photodissociation of carbonyl complexes to carbon monoxide complexes has also been observed in the CH_2Br_2/O_3 and CH_2Cl_2/O_3,[8] the $CHBr_2Cl/O_3$ and $CHBrCl_2/O_3$[9] (chapter 5), and the $BrCH{=}CHBr/O_3$ and $ClCH{=}CHCl/O_3$ (chapter 6) experiments. The photodecomposition of HC(O)H has been reported previously and the two major pathways produce either H and HCO or H_2 and CO species.[28]

Scheme 7.2.1

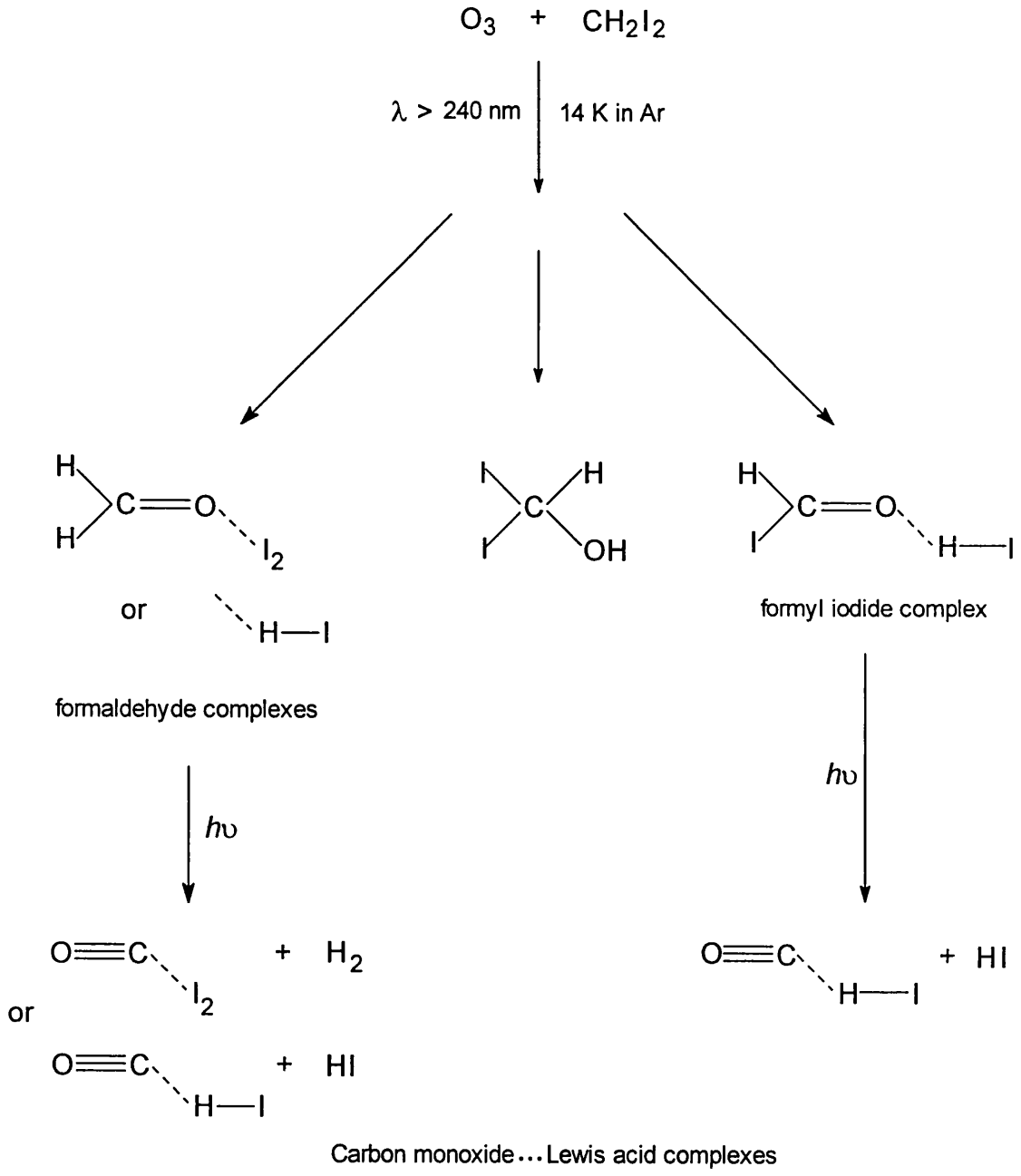
O3 + CH2I2
λ > 240 nm
14 K in Ar
or
formaldehyde complexes
formyl iodide complex
hυ
hυ
+ H2
+ HI
or
+ HI
Carbon monoxide...Lewis acid complexes

Table 7.2.1. *Infrared bands/cm^{-1} detected after deposition of CH_2I_2 in a variety of matrices at 14 K*

Ar	$^{16}O_3$/Ar	$^{18}O_3$/Ar	Assignment
3029.7mw	3029.4w	3028.2w	$\nu_{a\,CH_2}$
	2967.3mw	2967.5mw	$\nu_{s\,CH_2}$ [a]
	2950.4mw		
2944.1mw	2945.6mw, sh		
	2935.8mw, sh		
	2931.mw, sh		
2911.0w,sh	2912.2w, sh		ν_{CH_2} [a]
2902.8w,sh	2903.2w, sh		
2893.6w,sh	2881.7w, sh		$2\delta_{CH_2}$ [a]
2874.5mw	2868.5w, sh	2867.9w, sh	
2865.2mw	2864.5w	2864.7w	
2859.0mw			
2847.1w			
	2218.6vw		$2\nu_1$ (O_3)?
	2149.2vw		*b*
	2140.6vw		*b*
	2111.2w[a]	1996.3w[a]	
	2108.4w	1993.4w	$2\nu_3, 3\nu_2$ (O_3)?
	2101.4vw, sh[a]		
	1477.0vw, sh		δ_{CH_2} [a]
	1474.2w		
1466.9mw	1468.3w	1467.9w	
1462.1mw	1462.2w	1462.6w	
	1459.0w	1459.2w	
	1455.5w		
1452.0m	1451.6w	1452.0w	
1442.3mw	1442.2vw, sh		
	1382.5vw		δ_{CH_2} [a]
	1380.7vw	1381.1vw	
	1368.4vw		
1360.0w	1364.8vw	1365.0vw	
1355.7w			
1343.1w	1344.3vw		
1335.5w			
	1289.8vw		$\nu_{C-I} + \omega_{CH_2}$ [a]
	1285.8vw		
	1274.5vw, sh		
1271.0w	1271.6vw	1271.6vw	
1262.8w	1264.8vw		
1217.6w	1216.7vw		$2\omega_{CH_2}$
1187.2w		1188.7	CHI_2^+ [c] ?
1149.4w		1148.9	

continued

Table 7.2.1 continued

Ar	$^{16}O_3$/Ar	$^{18}O_3$/Ar	Assignment
	1106.4vw[a]		
	1104.8vw	1043.1vw	ν_1 (O_3)
	1102.7vw, sh[a]		
	1101.4vw, sh[a]		
	1046.5mw, sh[a]	998.8mw, sh[a]	
	1040.5s, sh[a]	989.0m[a]	
	1039.5s	983.1m	ν_3 (O_3)
	1037.9s, sh[a]	973.1w, sh[a]	
998.3mw	999.2w	999.2w	τ_{CH_2}[a]
995.9mw	997.8w, sh	992.1w	
890.9m	890.9w	890.7mw	$\nu_{C=I}$[d] ?
871.1mw	871.4vw,sh		
	870.1vw	870.6w	
864.8mw	862.3vw	864.2w, sh	
861.1mw	860.4vw	860.7w	
	859.0vw		
	854.2vw		
853.5w	852.5vw, sh	852.3w	
820.1m	821.4w	820.0mw	
808.7mw		808.4w	CHI_2^+[c] ?
804.5w			
	738.3w		ρ_{CH_2}[a]
734.2m	736.8w, sh	733.1w	
	729.5w		
720.8w		718.5w	CHI_2[c] ?
	704.0w	664.1w	ν_2 (O_3)
	690.3vw, sh[a]		
689.0m	689.1vw	681.3w	ω_{CH_2}
	687.8vw[a]		
648.2w, sh		652.8w	$\nu_{a\ C-I}$[a]
644.7mw	643.9vw		
		587.6w, sh[a]	
		582.0w[a]	
	564.6w	568.4w	$\nu_{s\ C-I}$

[a] The number of bands are due to aggregates or matrix site effects. [b] Bands are possibly due to impurities. [c] Bands are similar to those detected for CHI_2^+ and CHI_2.[14] [d] Bands are similar to those detected for $H_2C{=}I{-}I$.[12]

Table 7.2.2. *Infrared bands/cm^{-1} formed after quartz-filtered ($\lambda > 240$ nm) photolysis of CH_2I_2 deposited in $^{16}O_3$/Ar and $^{18}O_3$/Ar matrices at 14 K*

$^{16}O_3$/Ar	$^{18}O_3$/Ar	Assignment
3385.6m		ν_{O-H} ($I_2CH(OH)$)
2234.4vw[a]		
2230.7vw	2233.9vw	ν_{H-I} (HI)
2227.7vw		ν_{H-I} (···HI)[b]
2226.3vw, sh		
2224.2vw	2225.1vw	
2152.1vvw	2093.9vw	$\nu_{C\equiv O}$ (OC···HI)
2142.9vvw		$\nu_{C\equiv O}$ (OC···I_2)
2138.4vw[a]		
2138.0vw, sh	2087.3vw	$\nu_{C\equiv O}$ (CO)
2136.6vvw, sh[a]		
1741.8w	1706.3vw	$\nu_{C=O}$ (HC(O)H)
1737.5w, sh		*c*
1736.1w, sh		*c*
1732.4w, sh		*d*
1724.9w	1702.1vw	$\nu_{C=O}$ (HC(O)H···I_2) or
1721.6w	1698.2vw	$\nu_{C=O}$ (HC(O)H···HI)
1714.4w		$\nu_{C=O}$ (HC(O)H···$(HI)_2$)
1254.4vw[a]		
1243.4vw	1249.7vw	ρ_{CH_2} (HC(O)H)
1191.9vw	1166.3vw	ω_{CH_2} (HC(O)H)
1151.4vw		δ_{COH} ($I_2CH(OH)$)
1069.0vw, sh		?
1068.3vw		
956.8vw		ν_{C-O} ($I_2CH(OH)$)
951.7vw		

[a] Bands are due to aggregates or matrix site effects. [b] HI perturbed by either C=O or C≡O. [c] Dimer of HC(O)H. [d] Higher polymer of HC(O)H.

7.3 1,2-DIIODOETHANE AND OZONE

Following on from the diiodomethane and ozone photolytic experiments studied in section 7.2.1, the next step was to investigate a similar reaction using 1,2-diiodoethane, a longer chain alkane, and ozone in order to probe further the effect of an alkane containing two iodine atoms, rather than one. For example, should the photochemically induced reaction of 1,2-diiodoethane with ozone occur in the same way as that established for iodoethane with ozone,[3] producing an $O_3\cdots ICH_2CH_3$ complex and an array of I–O bonded intermediates upon visible irradiation or, in the same way as the CH_2I_2/O_3 system (section 7.2.1) in which no ozone complex or I–O bonded intermediates were detected after intense UV irradiation? It was expected that the reaction of ICH_2CH_2I and O_3 should occur similarly to that of ICH_2CH_3 and O_3 due to the functional group ICH_2– being present in both molecules.

7.3.1 RESULTS AND DISCUSSION

Deposition of the Precursors, ICH_2CH_2I and O_3

A matrix was formed from the gas deposition of a 1,2-diiodoethane and argon sample onto a CsI window held at 14 K (ICH_2CH_2I/Ar = 1:1200) and the subsequent IR spectrum was recorded (Table 7.3.1). The bands detected were assigned on the basis of assignments made previously for 1,2-dibromoethane[29] and iodoethane[3] in the liquid and matrix phase, respectively. Photolysis of the ICH_2CH_2I/Ar matrix with quartz-filtered irradiation ($\lambda > 240$ nm) did not result in the appearance of any new bands.

Co-deposition of ICH_2CH_2I/Ar and O_3/Ar samples (ICH_2CH_2I/O_3/Ar = 1:1:500) on to the cold CsI window led to the appearance of bands in the IR spectrum that could be assigned to either precursor (Table 7.3.1).[15,16] There were no bands that could be assigned to a $O_3\cdots ICH_2CH_2I$ complex, just as in the case of diiodomethane with O_3 (section 7.2.1). Again the difference in photochemical behaviour between mono- and di-iodoalkanes is apparent. Pyrex- or quartz-filtered photolysis cycles ($\lambda >$ 290 nm and 240 nm, respectively) for many hours produced new bands; for similar

photolysis times the Pyrex-filtered irradiation cycles produced weaker bands than those detected after quartz-filtered photolysis.

Photolysis of ICH_2CH_2I/O_3 Matrices

Pyrex- and quartz-filtered irradiation (λ > 290 nm and 240 nm, respectively) of ICH_2CH_2I/O_3/Ar matrices for many hours led to the appearance of weak bands in the infrared spectrum which are assigned as indicated below.

Carbonyl Species. Bands generated by UV photolysis of an argon matrix containing ICH_2CH_2I and O_3 are tentatively attributed to HC(O)H on the basis that similar bands were detected elsewhere for HC(O)H in the gas phase[17] and isolated in various matrices[17–20] (Table 7.3.2 and Fig. 7.3.1), although the breakage of the C–C bond would be required. The bands at 1741.8 and 1740.1 cm^{-1} are assigned to $\nu_{C=O}$, and those occurring at 1295.7, 1279.9, and 1272.6 cm^{-1} are assigned to ρ_{CH_2}; these values are indicative of those belonging to HC(O)H vibrations. If HC(O)H is indeed formed then the carbonyl bands occurring at lower wavenumbers are attributed to aggregates of HC(O)H and to HC(O)H perturbed by either I_2 or HI (Table 7.3.2). The $\nu_{C=O}$ values are comparable with those belonging to HC(O)H···Br_2 (1727.7 cm^{-1}),[8] HC(O)H···Cl_2 (1734.5 and 1732.4 cm^{-1}),[8] and HC(O)H···HI (1729.9 cm^{-1},[1] and 1728 cm^{-1})[21] species. The $\nu_{C=O}$ band at 1715.3 cm^{-1} suggests that HC(O)H is in an even greater perturbing environment such as HC(O)H···$(HI)_2$. Very weak ν_{H-I} bands detected at 2230.7 and 2224.1 cm^{-1} (Fig. 7.3.2) provide further evidence to support the presence of a HC(O)H···HI type complex, viz. ν_{H-I} = 2230.0 cm^{-1} (HI in the gas phase).[22,23] In the isotopic $^{18}O_3$ experiment $\nu_{C=O}$ bands appeared broadly at 1716 and 1690 cm^{-1} and are attributed to isolated HC(^{18}O)H and perturbed HC(^{18}O)H, respectively. The $\nu_{C=^{18}O}$ values obtained here also compare well with those obtained for HC(^{18}O)H studied elsewhere.[1,8] Alternatively, some of the carbonyl bands could belong to isolated $ICH_2C(O)H$ and perturbed $ICH_2C(O)H$···HI species.

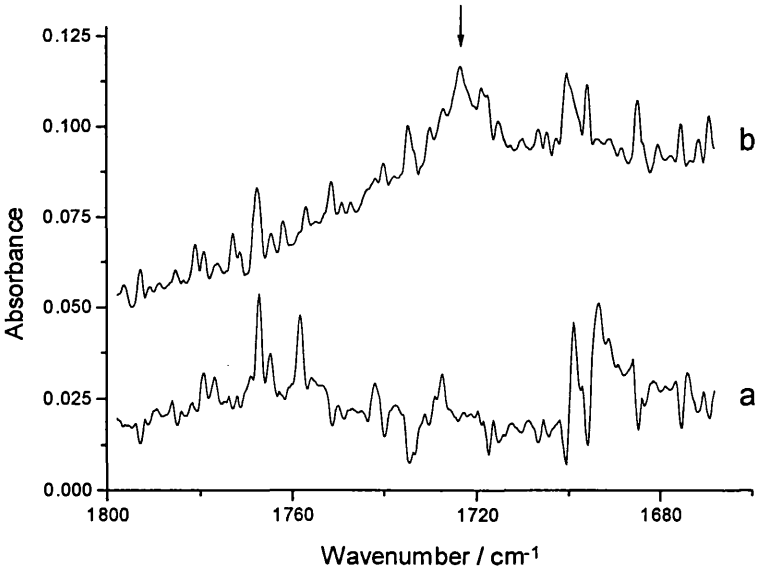

Figure 7.3.1. *Infrared spectra of an $ICH_2CH_2I/^{16}O_3/Ar$ matrix after (a) deposition and (b) quartz-filtered irradiation ($\lambda > 240$ nm) showing new bands appearing in the $\nu_{C=O}$ region.*

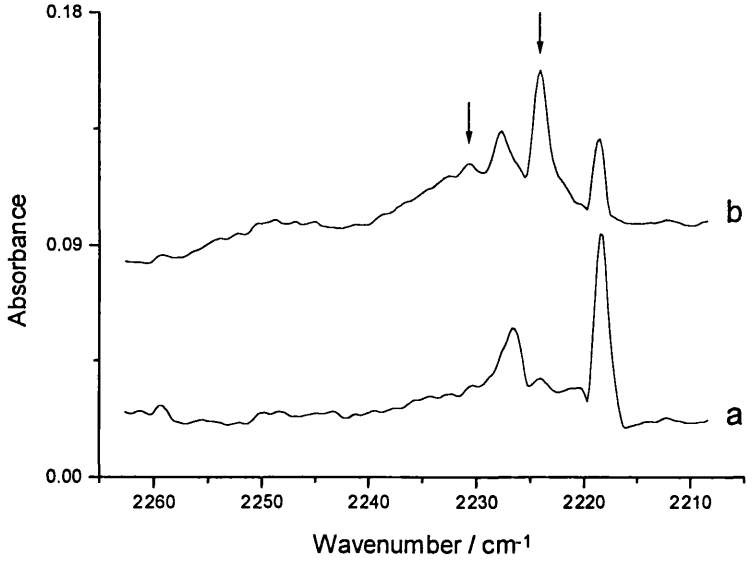

Figure 7.3.2. *Infrared spectra of an $ICH_2CH_2I/^{16}O_3/Ar$ matrix after (a) deposition and (b) quartz-filtered irradiation showing new bands occurring in the ν_{H-I} region.*

Carbon Monoxide Species. Bands appeared in the $\nu_{C\equiv O}$ region after UV irradiation of a $ICH_2CH_2I/O_3/Ar$ matrix and occurred at 2153.4 and 2138.0 cm^{-1} in the $^{16}O_3$ experiment and at 2098.0 and 2087.1 cm^{-1} in the $^{18}O_3$ experiment (Table 7.3.2). The $\nu_{C\equiv O}$ bands at 2138.0 and 2087.1 cm^{-1} are typical of CO isolated in argon,[24–26] while the other $\nu_{C\equiv O}$ bands at 2153.4 and 2098.0 cm^{-1} probably belong to a OC···HI species because perturbed ν_{H-I} bands were also detected.

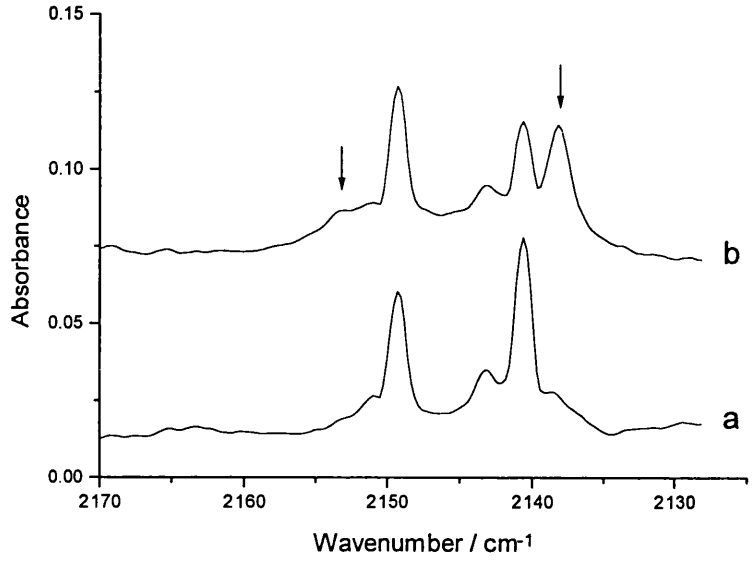

Figure 7.3.3. *Infrared spectra of an $ICH_2CH_2I/^{16}O_3/Ar$ matrix after (a) deposition and (b) quartz-filtered irradiation showing new bands growing in the $\nu_{C\equiv O}$ region.*

Other Species. A medium-weak band situated at 3385.5 cm^{-1} appeared after photolysis of an $ICH_2CH_2I/^{16}O_3/Ar$ matrix and is assigned to ν_{O-H} (Table 7.3.2). The species responsible for this absorption could arise from the insertion of an O atom into a C–H bond allowing $ICH_2CHI(OH)$ to form. Other bands detected at 960.9 and 946.5 cm^{-1}, assigned to ν_{C-O}, support $ICH_2CHI(OH)$ formation. An ICH_2OH species was formed after the analogous reaction between CH_3I and ozone.[1]

As noted in section 7.2.1 and in this section, the reaction of a diiodo-species with O_3 differs considerably from that using mono-iodinated precursors, Z–I.[1–7] Contrary to the initial expectation, ICH_2CH_2I does not react with O_3 in a similar

manner as ICH_2CH_3 does with O_3,[3] even though both molecules contain the same end group ICH_2–. The fact that ICH_2CH_2I is symmetrical and non-polar, while ICH_2CH_3 is unsymmetrical and polar, possibly accounts for the different photochemical behaviour, *i.e.* the non-polar character of ICH_2CH_2I reduces the chance of a charge-transfer complex forming ($O_3\cdots ICH_2CH_2I$) and consequently any iodoso-, iodyl- or hypoiodo species.

7.3.2 PHOTOCHEMICAL PATHWAY

The pathway of the photochemically induced reaction between 1,2-diiodoethane and ozone in an argon matrix is schematically shown in Scheme 7.3.1. As in the CH_2I_2/O_3 (section 7.2.1), CH_2Br_2/O_3,[8] CH_2Cl_2/O_3,[8] $CHBr_2Cl/O_3$ (chapter 5),[9] $CHBrCl_2/O_3$ (chapter 5),[9] and $CHCl_3$[10] reactions, the main mechanism established in this study is the insertion of an O atom, formed the photodissociation of O_3, into a C–H or C–X bond followed by HX abstraction to form the observed carbonyl products (HC(O)H and $ICH_2C(O)H$). The tentative attribution of carbonyl bands to HC(O)H species suggests that rupture of the C–C bond in ICH_2CH_2I must have occurred; the fact that carbon monoxide bands were also detected supports this assumption. The $ICH_2CHI(OH)$ species forms from the O atom insertion into a C–H bond of ICH_2CH_2I without HI abstraction occurring.

Some of the carbonyl species must photodissociate because bands attributed to carbon monoxide were detected. In cases where small wavenumber shifts in $\nu_{C\equiv O}$ occur, C≡O has been perturbed by some species, probably HI. Carbonyl complexes have been seen to photodissociate to form carbon monoxide complexes in other experiments, for example, CH_2Br_2/O_3,[8] CH_2Cl_2/O_3,[8] $CHBr_2Cl/O_3$[9] (chapter 5), $CHBrCl_2/O_3$[9] (chapter 5), $CHCl_3/O_3$,[10] BrCH=CHBr/O_3 (chapter 6), and ClCH=CHCl/O_3 (chapter 6). HC(O)H has been reported previously to dissociate upon photolysis via two major pathways, to produce either H and HCO or H_2 and CO species.[28] Bands belonging to ν_{C-I} of the precursor were seen to weaken upon photolysis, which supports the formation of HC(O)H and C≡O species.

Scheme 7.3.1

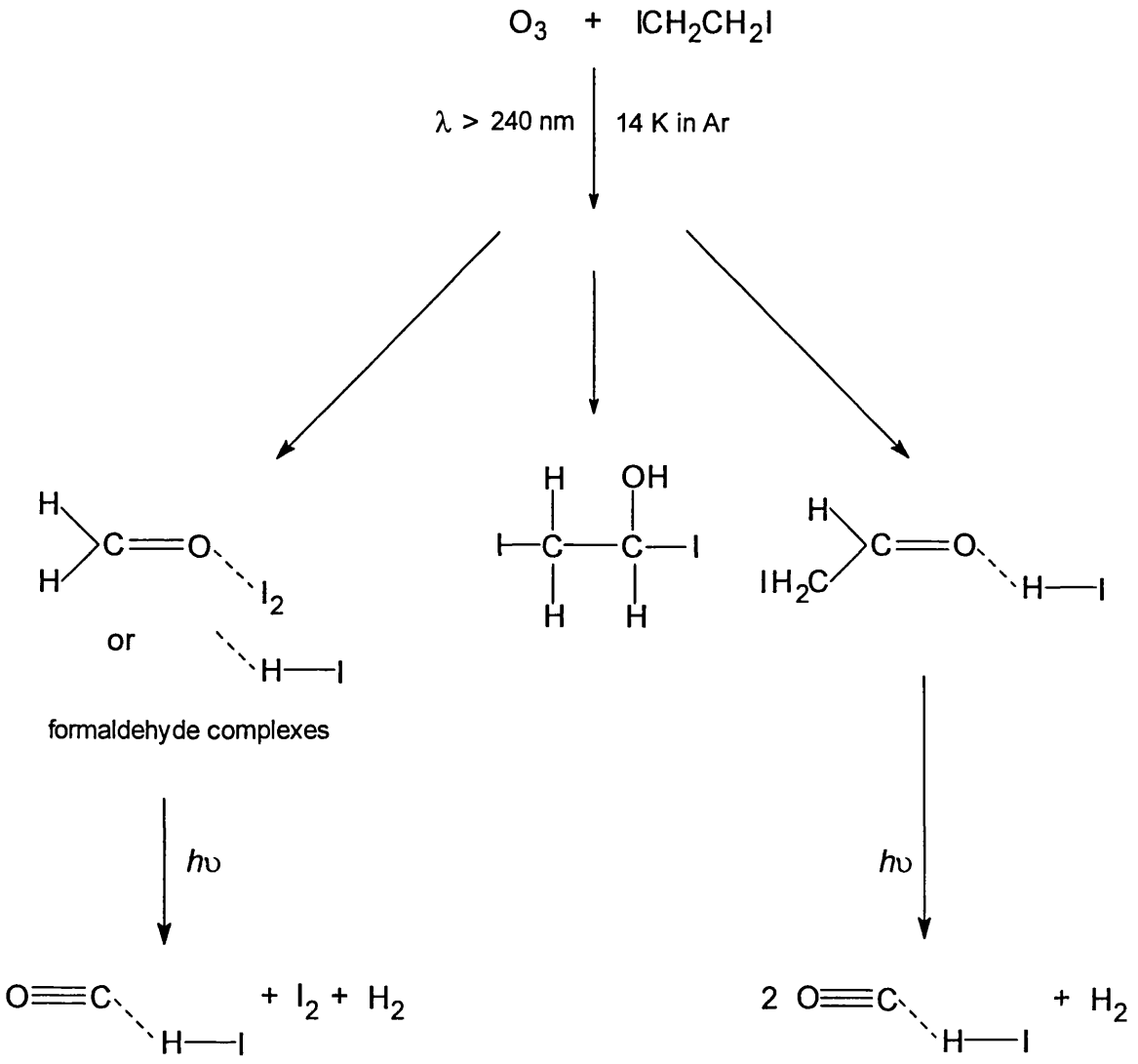
O3 + ICH2CH2I
λ > 240 nm
14 K in Ar
or
formaldehyde complexes
hυ
hυ
+ I2 + H2
2
+ H2
Carbon monoxide...Lewis acid complexes

Table 7.3.1 *Infrared bands/cm^{-1} detected after deposition of ICH_2CH_2I in a variety of matrices at 14 K*

Ar	$^{16}O_3$/Ar	$^{18}O_3$/Ar	Assignment
		3045.0vw[a]	
3040.5w	3041.4vw	3041.3vw	$\nu_{a\,CH_2}$
		2878.3vw	$2\delta_{CH_2}$[a]
		2861.1vw	
	2227.2vw, sh[a]		
	2226.3vw[a]		
	2218.6w		$2\nu_1$ (O_3)?
	2149.4w	2148.8vw	*b*
	2143.3vw		*b*
	2140.6w	2140.7vw	
	2114.5w, sh[a]		
	2111.2mw[a]	1995.1w[a]	
	2108.4mw	1993.3w	$2\nu_3$, $3\nu_2$ (O_3)?
1433.3w, sh	1440.0vw	1439.5vw	δ_{CH_2}[a]
1432.3w	1432.3w	1431.1vw	
1361.5vw	1343.6vw	1380.6w	δ_{CH_2}[a]
	1342.2vw	1347.3w	
	1341.3vw	1339.2w	
	1328.8w		
	1307.8w	1307.9vw	
	1305.1vw, sh		
1289.7vw	1285.7vw		$\rho_{CH_2} + \nu_{C-I}$[a] ?
	1283.8vw, sh		
	1282.8w		
1216.3vw			ω_{CH_2}[a]
1206.7w	1206.8vw	1206.8vw	
1146.1vw			
1144.8w			
1141.9vw		1142.4mw	
1140.2w, sh	1139.9w		
1137.9mw	1138.2w		
1136.8m	1136.9mw		τ_{CH_2}[a]
1134.1vw	1126.7vw		
	1106.4w[a]		
	1103.6w	1042.9w	ν_1 (O_3)
	1100.4vw[a]		
1053.2vw	1053.1vw, sh		?
	1046.1mw, sh[a]		
	1043.8m, sh[a]	991.4s[a]	
	1040.1s[a]	988.3ms, sh[a]	
	1039 s, br	981.9vs	ν_3 (O_3)
	1034.3m[a]	976.7m, sh[a]	

continued

Table 7.3.1 continued

Ar	$^{16}O_3$/Ar	$^{18}O_3$/Ar	Assignment
947.2vw	946.8vw	951.0vw	ν_{C-C}
729.4vw	726.9vw		ρ_{CH_2} [a]
726.6vw			
	707.9w[a]		
	705.4mw[a]		
	704.3mw	663.8vw	ν_2 (O_3)
515.4w[a]	515.4w[a]		
512.8m	512.9mw	511.2mw	ν_{C-I}
509.8w[a]	509.7mw[a]		

[a] Composite bands are due to aggregates or matrix site effects. [b] Bands are due to impurities.

Table 7.3.2. *Infrared bands/cm^{-1} formed after quartz-filtered (λ > 240 nm) irradiation of ICH_2CH_2I in a variety of matrices at 14 K*

$^{16}O_3$/Ar	$^{18}O_3$/Ar	Assignment
3385.5mw		ν_{O-H}
2230.7vw		ν_{H-I} (HI)
2224.1vw	2223.7vw	ν_{H-I} (···HI)[a]
2153.4vw, sh	2098.0vw	$\nu_{C\equiv O}$ (OC···HI)
2138.0vw	2087.1w	$\nu_{C\equiv O}$ (CO)
1741.8vw[b]		
1740.1vw, sh	1716w, br	$\nu_{C=O}$ (HC(O)H)
1735.6vw, sh		*c*
1731.2vw, sh		*d*
1727.2vw, sh	1690w, br	$\nu_{C=O}$ (HC(O)H···I_2) or
1723.7vw		$\nu_{C=O}$ (HC(O)H···HI)
1719.9vw, sh		
1715.3vw		$\nu_{C=O}$ (HC(O)H···$(HI)_2$)
1295.7w[b]		
1279.9w[b]	1271.9w[b]	
1272.6mw	1270.1w	ρ_{CH_2} (HC(O)H)
960.9vw		ν_{C-O}[b]
946.5vw		

[a] HI perturbed by either C=O or C≡O. [b] Bands are due to aggregates or matrix site effects. [c] Dimer of HC(O)H. [d] Higher polymer of HC(O)H.

7.4 CONCLUDING REMARKS

The photochemical study of diiodomethane and the longer chain alkane species, 1,2-diiodoethane, isolated separately with ozone in argon matrices, was carried out and reported in this chapter. The photochemical behaviour of both species with ozone was comparable, producing similar photoproducts via equivalent pathways. It was noticeable that the reactions between diiodo-species and ozone behaved very differently, photochemically, from those between monoiodo-species and ozone, while the reactions of ozone with dibromo- or dichloro-methane behaved similarly.

It would be worthwhile to look at the reaction of ozone with other diiodoalkanes in order to yield further information regarding the difference in photochemical behaviour between monoiodo- and diiodo-species. A true extension to the CH_2I_2/O_3 study would have been to investigate the reactions of 1,1-diiodoethane with ozone; this along with other 1,1-diiodoalkane/ozone experiments could complement these matrix studies. It would also prove informative to look at the CH_2BrI/O_3 matrix reaction in order to understand why the photochemistry for CH_2ClI/O_3[6] differs from that of CH_2I_2/O_3 (section 7.2.1) (CH_2BrI being intermediate between CH_2ClI and CH_2I_2).

7.5 REFERENCES

(1) Hawkins, M.; Andrews, L., *Inorg. Chem.* **1985**, *24*, 3285–3290.

(2) Hawkins, M.; Andrews, L.; Downs, A. J.; Drury, D., *J. Am. Chem. Soc.* **1984**, *106*, 3076–3082.

(3) Clark, R. J. H.; Dann, J. R., *J. Phys. Chem.* **1996**, *100*, 532– 538.

(4) Andrews, L.; Hawkins, M.; Withnall, R., *Inorg. Chem.* **1985**, *24*, 4234–4239.

(5) Clark, R. J. H.; Dann, J. R.; Foley, L. J., *J. Phys. Chem. A* **1997**, *101*, 9260– 9271.

(6) Clark, R. J. H.; Dann, J. R., *J. Phys. Chem. A* **1997**, *101*, 2074–2082.

(7) Clark, R. J. H.; Foley, L. J.; Price, S. D., *J. Phys. Chem. A* **2000**,

(8) Lugez, C.; Schriver, A.; Schriver-Mazzuoli, L.; Lasson, E.; Nielsen, C. J., *J. Phys. Chem.* **1993**, *97*, 11617–11624.

(9) Clark, R. J. H.; Dann, J. R.; Foley, L. J., *J. Chem. Soc. Dalton Trans.* **1999**, 73– 78.

(10) Schriver, L.; Gauthier-Roy, B.; Carrere, D.; Schriver, A.; Abouaf-Marguin, L., *Chem. Phys.* **1992**, *163*, 357–370.

(11) Zheng, X.; Phillips, D. L., *J. Phys. Chem. A* **2000**, *104*, 6880–6886.

(12) Maier, G.; Reisenauer, H. P., *Angew. Chem. Int. Ed. Engl.* **1986**, *25*, 819–822.

(13) Maier, G.; Reisenauer, H. P.; Hu, J.; Schaad, L. J.; Hess, B. A., *J. Am. Chem. Soc.* **1990**, *112*, 5117–5122.

(14) Andrews, L.; Prochaska, F. T.; Ault, B. S., *J. Am. Chem. Soc.* **1979**, *101*, 9–15.

(15) Dimitrov, A.; Seppelt, K.; Scheffler, D.; Willner, H., *J. Am. Chem. Soc.* **1998**, *120*, 8711–8714.

(16) Brosset, P.; Dahoo, R.; Gauthier-Roy, B.; Abouaf-Marguin, L.; Lakhlifi, A. L., *Chem. Phys.* **1993**, *172*, 315–324.

(17) Khoshkhoo, H.; Nixon, E. R., *Spectrochim. Acta* **1973**, *29A*, 603–612.

(18) Harvey, K. B.; Ogilvie, J. F., *Canad. J. Chem.* **1962**, *40*, 85–91.

(19) Nelander, B., *J. Chem. Phys.* **1980**, *73*, 1026–1033.

(20) Nelander, B., *J. Chem. Phys.* **1980**, *73*, 1034–1039.

(21) Bach, S. B. H.; Ault, B. S., *J. Phys. Chem.* **1984**, *88*, 3600–3604.

(22) Barnes, A. J.; Hallam, H. E.; Scrimshaw, G. F., *Trans Faraday Soc.* **1969**, *65*, 3159–3171.

(23) Barnes, A. J.; Hallam, H. E.; Scrimshaw, G. F., *Trans. Faraday Soc.* **1969**, *65*, 3150–3158.

(24) Lasson, E.; Nielsen, C. J., *Acta Chem. Scand.* **1997**, *51*, 1–7.

(25) Loewenschuss, A.; Givan, A.; Nielsen, C. J., *J. Mol. Struct.* **1997**, *408/409*, 533–537.

(26) Dubost, H.; Abouaf-Marguin, L., *Chem. Phys. Lett.* **1972**, *17*, 269–273.

(27) Baughcum, S. L.; Leone, S. R., *J. Chem. Phys.* **1980**, *72*, 6531–6545.

(28) Thomas, S. G.; Guillory, W. A., *J. Phys. Chem.* **1973**, *77*, 2469–2473.

(29) Brown, J. K.; Sheppard, N., *Discussions Faraday Soc.* **1950**, *9*, 144–154.

Chapter 8

Conclusions and Further Work

8.1 CONCLUSIONS

In this thesis the photochemically induced reactions of ozone with a variety of halogenated species have been studied using the matrix isolation technique. The properties of low temperature matrices, discussed in chapter 2, enabled weak complexes and reactive intermediates to be observed, as well as the determination of several photochemical reaction pathways. The themes linking the five research chapters (3–7) have already been discussed in chapter 1. Chapters 3 and 7 involved the study of ozone with iodine-containing precursors while chapters 4, 5, and 6 involved the study of ozone with bromine- and chlorine-containing precursors, or other non iodine-containing precursors. Ozone···precursor complexes were detected for the iodine cyanide and haloethene species in chapters 3 and 6, respectively, and resulted in the detection of numerous intermediates after photolysis of the matrix using radiation of several different wavelengths; the photochemical reaction pathways were thus complex in nature. The species studies in chapters 4, 5, and 7 did not form any complexes with ozone and so harsh UV photolysis was required to initiate any kind of reaction. In chapters 5, 6, and 7 various carbonyl and carbon monoxide Lewis acid complexes were reported. The species detected in chapters 3–7 are summarised in Table 8.1.1.

The original aim of this thesis was to conduct a series of experiments investigating the unknown reactions of ozone with several halogenated precursors. The driving force was to reveal and characterise a number of novel species that form from the reactions under investigation using FT-IR matrix isolation spectroscopy and to determine fitting mechanisms for such reactions. It was also hoped that the current research would extend on and complement the previous studies of ozone photochemistry.

Of the ozone and halogenated precursor systems investigated, novel species and new photochemical routes were indeed discovered. It is hoped therefore that the results presented in this thesis will benefit research workers at present and in the future by providing information and insight regarding the photochemical behaviour of reactions between ozone and halogenated species.

8.2 SUGGESTIONS FOR FURTHER WORK

Improvements to Current Apparatus

There are a number of improvements that can be made to the present apparatus in order to enhance current operations. The Bruker IFS 113v spectrometer dates from 1982 and is controlled by the out-of-date Aspect computer; this is in urgent need of being upgraded so that the spectrometer is controlled by a much faster PC operating system. It would be advantageous to re-design the sample chamber to allow the sample matrix to be probed using UV-vis or Raman spectroscopy so that increased electronic and vibrational information about the sample could be collected. Upgrade of the two-stage Displex closed-cycle He refrigerator to a three-stage one (Heliplex) would allow the base temperature to reach 6.5 K allowing neon to be used as the matrix material. The use of neon, as opposed to argon,[1] significantly improves the optical quality and non-perturbing nature of the matrix and therefore neon matrices are especially suited to studies of very weak complexes. Various improvements could be made to the vacuum system and layout of the gas handling manifolds. In particular the replacement of the current oil-based diffusion pump and rotary pump by a turbo-pumped system would lead to increased pumping speeds and a cleaner vacuum system, while if the gas handling lines were wider and shorter the pumping efficiency would be improved even further.

Future Experiments

For the immediate future there are several studies that require investigation and which would complement those reported in this thesis. Referring to chapters 3 and 4, the studies of the reaction of ozone with the halogen cyanides, ICN and BrCN, could be extended to involve the similar reaction of ozone with chlorine cyanide, ClCN, in order to compare the photochemistry and reaction pathways of each. It would also be interesting to look at the reaction of ozone with ICH_2CN as the reaction of O atoms and CH_3CN in matrices has been shown to produce CH_3CNO and $HOCH_2CN$ as the major photoproducts and the isocyanate CH_3NCO as the minor photoproduct.[2] It would also prove informative to repeat the reactions discussed in chapters 3 and 4

using ^{15}N enriched samples, $IC^{15}N$ and $BrC^{15}N$, so as to reinforce the existing band assignments. As an extension to the reactions studied in chapter 6, the photochemically induced reaction of ozone with some fluoroalkenes (*e.g.* CH_2=CHF, CH_2=CF_2, CF_2=CF_2, and CH_2=$CFCF_3$) could be investigated. The fact that fluoroalkenes are the most likely impurities in HFC production and that there is currently very limited information on their reactions, makes these an ideal group to investigate using the matrix isolation technique.[3] As mentioned before in reference to chapter 7, the reaction of ozone with CH_2BrI and separately with 1,1-diiodoethane, would complete the study of the diiodoalkanes, although these compounds are currently commercially unavailable and would need to be prepared in the laboratory. The reaction of ozone with CHI_3 would also provide additional information to this study.

All the experiments in this thesis have involved the reaction of O atoms, which were produced by the photodecomposition of ozone, oxygen or nitrogen dioxide, with a variety of halogenated species. The hydroxyl radical has also been shown to be a dominant species in initiating the oxidation of a variety of species in the atmosphere, and so it would be worthwhile to study the reactions of OH• with some halogenated species in the matrix. The reaction between OH• and the HFCs and HCFCs is of particular interest since the HFCs and HCFCs were developed in order to replace the damaging CFCs since they have a reactive C–H bond which would allow their chemical removal from the troposphere before transport into the stratosphere;[4–6] moreover, the hydroxyl radical (OH•) is known to abstract H atoms. A matrix study of this kind would provide information about the structure and connectivity of any intermediates produced and whether any complexes existed, as well as understanding of the photochemistry of the reaction and hence details about the processes involved in the tropospheric chemistry of the HFCs and HCFCs.

The study of photochemically induced reactions of sulfur atoms, instead of O atoms, could also be an interesting route to follow. In previous matrix studies, OCS has been used as a source of S atoms[7] in the reactions of NO,[8] PF_3,[9] PCl_3,[9] CH_4,[9] C_2H_4,[9] and C_2H_2,[9] while CS_2 has also been used as a source in the reaction with H atoms.[10] Another investigation worth pursuing is the study of the reactions of

halogenated silanes and germanes, for comparison with that of the carbon analogues studied in this thesis.[11–14]

Table 8.1.1. *Species detected after photo-induced reactions of ozone with various halogenated precursors in solid argon matrices*

Precursor	Species Detected	λ
Chapter 3 – ICN	O_3···ICN	(deposition)
	OICN	> 650 nm
	INCO	> 410 nm
	IC(O)NCO	> 290 nm
	$I_2NC(O)NCO$[a]	> 240 nm
	O_2ICN	> 240 nm
Chapter 4 – BrCN	BrNCO	> 240 nm
	BrC(O)NCO	> 240 nm
Chapter 5 – $CHBr_2Cl$	HC(O)Cl···Br_2	> 240 nm
	HC(O)Br···BrCl	> 240 nm
	BrC(O)Cl···HBr	> 240 nm
	(OC)(HCl)(Br_2)	> 240 nm
	(OC)(BrCl)(HBr)	> 240 nm
– $CHBrCl_2$	HC(O)Cl···BrCl	> 240 nm
	HC(O)Br···Cl_2	> 240 nm
	BrC(O)Cl···HCl	> 240 nm
	ClC(O)Cl···HBr	> 240 nm
	(OC)(HCl)(BrCl)	> 240 nm
	(OC)(HBr)(Cl_2)	> 240 nm
Chapter 6 – BrCH=CHBr	O_3···BrCH=CHBr	(deposition)
	HC(O)Br···HBr	> 350 nm
	HC(O)H···HBr	> 350 nm
	(OC)(HBr)	> 350 nm
	BrHC=C=O	> 350 nm
	SOZ[b] species	> 240 nm
– ClCH=CHCl	O_3···ClCH=CHCl	(deposition)
	HC(O)Cl···HCl	> 350 nm
	HC(O)H	> 350 nm
	(OC)(HCl)	> 350 nm
	ClHC=C=O	> 350 nm
	SOZ[b] species	> 240 nm
Chapter 7 – CH_2I_2	HC(O)H···I_2	> 240 nm
	HC(O)H···HI	> 240 nm
	HC(O)I···HI[a]	> 240 nm
	(OC)(HI)	> 240 nm

continued

Table 8.1.1 continued.

Precursor	Species Detected	λ
Chapter 7 – CH_2I_2	$I_2CH(OH)$	> 240 nm
– ICH_2CH_2I	$HC(O)H\cdots I_2$	> 240 nm
	$HC(O)H\cdots HI$	> 240 nm
	$HC(O)CH_2I\cdots HI$[a]	> 240 nm
	(OC)(HI)	> 240 nm
	$ICH_2CHI(OH)$	> 240 nm

[a] Detection remains tentative. [b] Secondary ozonide.

8.3 REFERENCES

1. Hallamasek, D.; Babka, E.; Knözinger, E., *J. Mol. Struct.* **1997**, *408/409*, 125–132.
2. Mielke, Z.; Hawkins, M.; Andrews, L., *J. Phys. Chem.* **1989**, *93*, 558–564.
3. Orkin, V. L.; Huie, R. E.; Kurylo, M. J., *J. Phys. Chem.* **1997**, *101*, 9118–9124.
4. Crutzen, P. J., *Angew. Chem., Int. Ed. Engl.* **1996**, *35*, 1758–1777.
5. Molina, M. J., *Angew. Chem., Int. Ed. Engl.* **1996**, *35*, 1778–1785.
6. Baird, C., *Environmental Chemistry*; Freeman: NY, 2nd ed; 1999.
7. Gunning, H. E.; Strausz, O. P., *Adv. Photochem.* **1966**, *4*, 143–149.
8. Hawkins, M.; Downs, A. J., *J. Phys. Chem.* **1984**, *88*, 3042–3047.
9. Hawkins, M.; Almond, M. J.; Downs, A. J., *J. Phys. Chem.* **1985**, *89*, 3326–3334.
10. Bohn, R. B.; Andrews, L.; Brabson, G. D., *J. Phys. Chem.* **1992**, *96*, 1582–1589.
11. Khabashesku, V. N.; Kudin, K. N.; Tamas, J.; Boganov, S. E.; Margrave, J. L.; Nefedov, O. M., *J. Am. Chem. Soc.* **1998**, *120*, 5005–5016.
12. Withnall, R.; Andrews, L., *J. Am. Chem. Soc.* **1986**, *108*, 8118–8119.
13. Withnall, R.; Andrews, L., *J. Phys. Chem.* **1990**, *94*, 2351–2357.
14. Withnall, R.; Andrews, L., *J. Phys. Chem.* **1988**, *92*, 594–602.

Appendix

A1 Ozone, O_3

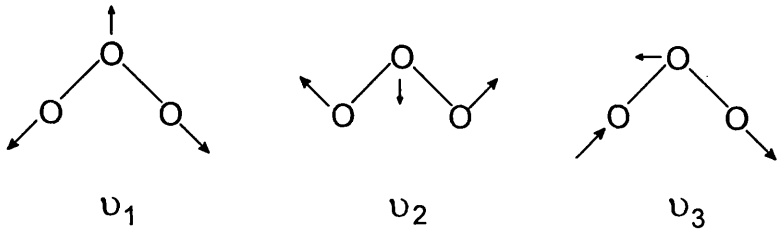

Figure A1.1. *The normal vibrations of ozone (C_{2v}),[1] symmetric stretching mode, ν_1, bending mode, ν_2, and antisymmetric stretching mode, ν_3.*

Table A1.1. *Vibrational wavenumbers/cm^{-1} for IR bands (one matrix site) of ozone isolated in argon matrices*[a]

$^{16}O_3$	$^{18}O^{16}O^{16}O$	$^{18}O^{16}O^{18}O$	$^{16}O^{18}O^{16}O$	$^{18}O^{18}O^{16}O$	$^{18}O_3$	Assignment
2108.4	2087.6	2057.5	2047.4	2024.7	1993.5	$3\nu_2$ or $\nu_1 + \nu_3$
1104.5	1090	–	–	1060.4	1042.7	ν_1
1039.8	1025.8	1016.7	1006.3	991.6	982.5	ν_3
703.6	687.2	670.9	696.2	680.2	664.0	ν_2

[a] From reference 2.

Table A1.2. *Vibrational wavenumbers/cm^{-1} for IR bands (two matrix sites) of ozone isolated in argon matrices*[a]

$^{16}O_3$	$^{18}O^{16}O^{16}O$	$^{18}O^{16}O^{18}O$	$^{16}O^{18}O^{16}O$	$^{18}O^{18}O^{16}O$	$^{18}O_3$	Assignment
2111.2	2090.2	2060.2	2050.0	2027.5	1996.2	$3\nu_2$ or
2108.5	2087.6	2057.5	2047.3	2024.9	1993.7	$\nu_1 + \nu_3$
1106.3	1091.7	1075.6	–	1061.9		ν_1
1104.9	1090.1	1074.5	–	1060.5	*b*	
1040.4	1026.6	1017.6	1007.0	992.5	983.3	ν_3
1039.5	1025.5	1016.6	1006.1	991.5	982.3	
705.2	688.8	672.2	697.5	681.6	665.5	ν_2
704.3	688.0	671.4	696.5	680.7	664.7	

[a] This work. [b] Bands obscured by ν_3 mode.

(1) Herzberg, G. *Infrared and Raman Spectra of Polyatomic Molecules*;Van Nostrand: NY; 1945.
(2) Dimitrov, A.; Seppelt, K.; Scheffler, D.; Willner, H., *J. Am Chem. Soc.*, **1998**, *120*, 8711–8714.

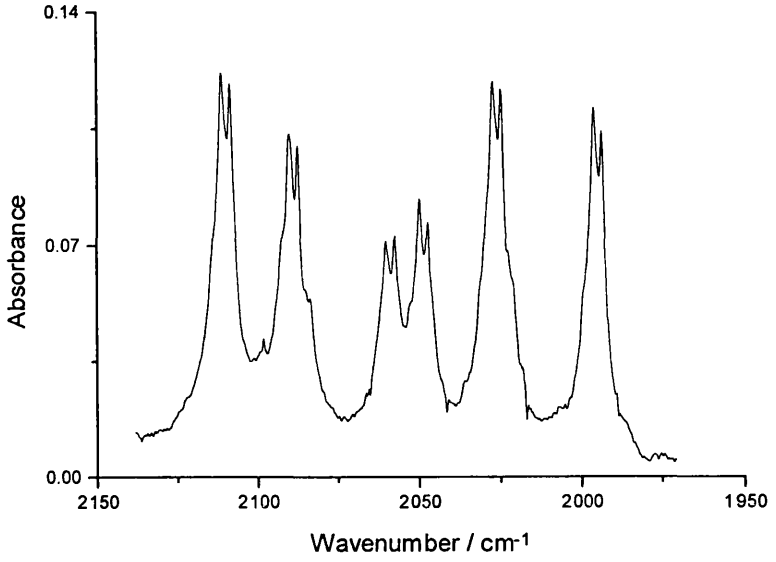

Figure A1.2. *Infrared spectrum of a $^{16}O_{3-x}{}^{18}O_x$/Ar matrix after deposition showing ^{16}O and ^{18}O isotopomer bands assigned to $3\nu_2$ or to $\nu_1 + \nu_3$.*

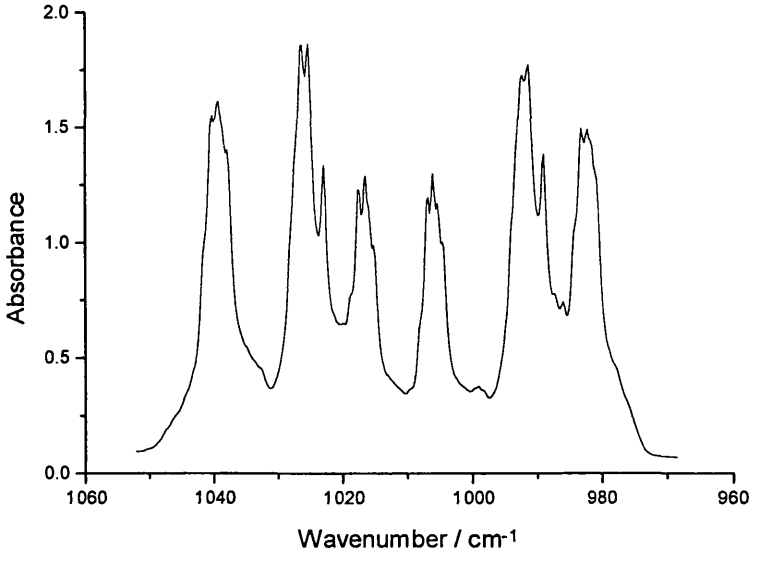

Figure A1.3. *Infrared spectrum of a $^{16}O_{3-x}{}^{18}O_x$/Ar matrix after deposition showing ^{16}O and ^{18}O isotopomer bands assigned to ν_3. The relative intensity ratio is approximately 1:2:1:1:2:1 which matches the probability distribution of isotopic ozone.*

A2 Nitrogen Dioxide, NO_2

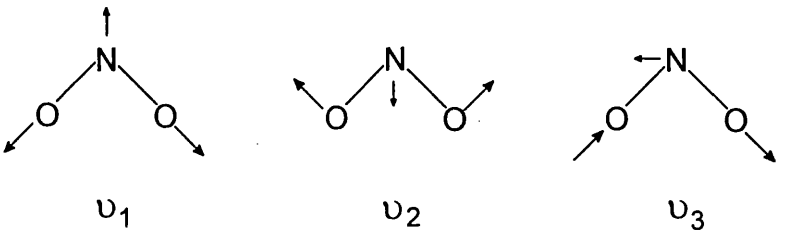

Figure A2.1. *The normal vibrations of nitrogen dioxide (C_{2v}),[1] symmetric stretching mode, v_1, bending mode, v_2, and antisymmetric stretching mode, v_3.*

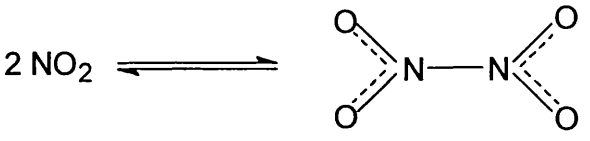

Figure A2.2. *NO_2 exists in a temperature-dependent equilibrium with N_2O_4 (D_{2h}) in the gaseous and liquid states.*

Table A2.1. *Vibrational wavenumbers/cm^{-1} for IR bands of nitrogen dioxide isolated in argon matrices*[a]

Bands	Assignment[b]
2903.9m	$v_1 + v_3$ (NO_2)
2902.2ms	
2893.5w	
2218.6vw	$v_2 + v_3$ (NO_2)
1893.9w	
1871.9w	v_1 (N_2O_2)
1844.3w	v_1 (*a*-N_2O_3)[c]
1836.3mw	
1833.3m	
1831.5ms	
1828.3s	
1796.9vw	
1776.3vw	v_5 (N_2O_2)

continued

Table A2.1 continued

Bands	Assignment[b]
1750.3w	
1738.7vw	ν_9 (N_2O_4)
1688.7mw	ν_1 (s-N_2O_3)[c]
1644vs, br	ν_2 (a-N_2O_3)[c]
1633.3m	
1630.3m	
1616.3ms, sh	
1612.6vs, sh	
1611.0vs	ν_3 (NO_2)
1300.4mw	
1298.6mw	ν_1 (NO_2)
1296.3m	
1291.0s	
1290.3s	
1287.2m	
1277.9mw	
1270.2mw	
1265.5mw	
1256.2mw	ν_{11} (N_2O_4)
917.8vw	
903.4mw	
881.0vw	ν_2 (s-N_2O_3)[c]
786.8m	
781.6mw, sh	ν_4 (a-N_2O_3)[c]
769.4mw	
753.6w	
750.9mw	
749.4mw, sh	ν_2 (NO_2)
746.0w	ν_{12} (N_2O_4)
645.5w	ν_8 (N_2O_4)
640.2m	
636.7m	

[a] Bands belonging to other nitrogen oxides were also detected. [b] Assignments based on those made in references 1 and 2. [c] *a* – asymmetric arrangement of N_2O_3, *s* – symmetric arrangement of N_2O_3.

(1) Herzberg, G. *Infrared and Raman Spectra of Polyatomic Molecules*;Van Nostrand: NY; 1945.
(2) Laane, J.; Ohlsen, J. R., *Prog. Inorg. Chem.* **1980**, *27*, 465–513.